# Smoke Explosion in Severally Ventilation Limited Compartment Fires

**By**

**Nick Z.J. Chen**

Supervised by

Dr Charles M. Fleischmann

And

Dr Michael J. Spearpoint

Fire Engineering Research
January 2012

A thesis submitted in partial fulfillment of the requirements for the degree of
Master of Engineering in Fire Engineering

Department of Civil Engineering
University of Canterbury
Private Bag 4800
Christchurch, New Zealand

For a full list of reports please visit http://www.civil.canterbury.ac.nz/fire/fe_resrch_reps.shtml

# Abstract

A smoke explosion is generally considered as a deflagration of the accumulated unburned fuel inside a closed compartment. However, the term smoke explosion has been widely misused for decades with a great deal of confusion, and very little research has been done towards this topic. The purpose of this research is to study the smoke explosion phenomenon in much more detail through the development of a fire scenario under various experimental conditions including ventilation size, fuel elevation and fuel mass, so that a more comprehensive understanding of this phenomenon can be achieved.

A total of twenty experiments are carried out including both exploratory and final experiments. Thirteen experiments result in smoke explosions, among which there are five experiments result in more than one smoke explosion. A phenomenon referred as smoldering decay is observed in all experiments with smoke explosions, making it one of the precursors of the smoke explosion phenomenon. The smoldering decay is often indicated by an exponential decay of the temperature and is caused by the low oxygen concentration within the compartment.

Based on the analysis, it is found that the vent size must be at least 50 mm in diameter in order for smoke explosions to occur. The fuel elevation has no influence on the occurrence of the smoke explosion. However when the fuel is placed near the ceiling, the temperature, the mass flow rate and the heat release rate are all lowered significantly. The size of the fuel also has no significant influence except for the duration of the experiment. The concentration of CO is scattered in the range of 1.9% and 4.3% when explosions occur. Hence, the accumulation of CO is considered not to be the direct cause for the smoke explosion. The triggering factor for smoke explosions is believed to be the flammable limit formed by the mixture of hydrocarbon and CO. The pressure difference caused by the explosion inside the compartment has to be at least 27 Pa for it to be considered as a smoke explosion.

# Acknowledgments

I would like to sincerely show appreciation to the following persons who have helped me completing this research.

First of all, I am extremely thankful for my supervisor Dr. Charles Fleischmann for his persistence with continued support and direction. His friendly encouragement and technical guidance at all stages have been a driving force of the progress throughout this research. His teachings challenged my mind in both academic and daily life, which are demanding and educational. It will certainly benefit me in my future career and life.

Sincere gratitude also goes to Dr. Michael Spearpoint for his time and advice all the way through both techniques in fire engineering and computer skills.

Appreciation must go to New Zealand Fire Service Commission for their financial support throughout this research and to the ME Fire program at the University of Canterbury.

Thanks Grant Dunlop for his expertise and help with setting up the Cone Calorimeter, Phi-Meter and the help throughout the research, and Bob Wilsea-Smith for helping preparing the wood cribs.

Lastly, I would like to thank my wife and parents for their understanding and support, which make all this possible.

# Table of Contents

**ABSTRACT** ..... **II**

**ACKNOWLEDGMENTS** ..... **III**

**TABLE OF CONTENTS** ..... **IV**

**LIST OF FIGURES** ..... **VII**

**LIST OF TABLES** ..... **XVII**

**CHAPTER 1 INTRODUCTION** ..... **1**

1.1 Research Impetus ..... 1

1.2 Research Objectives ..... 3

1.3 Research Outlines ..... 4

**CHAPTER 2 LITERATURE REVIEW** ..... **5**

2.1 Introduction ..... 5

2.2 The Development of Compartment Fires ..... 5

2.3 Characteristics of Smoldering Combustion ..... 8

2.4 Flammability Diagram ..... 9

**CHAPTER 3 EXPERIMENTAL SETUP AND PROCEDURE** ..... **12**

3.1 Introduction ..... 12

3.2 Preliminary Setup ..... 12

*3.2.1 Constructions* ..... *15*

*3.2.2 Ventilations* ..... *17*

*3.2.3 Pressure Relief Panel* ..... *18*

*3.2.4 Observation Window* ..... *18*

3.3 Experimental Measurements ..... 20

*3.3.1 Data Acquisition* ..... *20*

*3.3.2 Temperature* ..... *21*

*3.3.3 Compartment Pressure* ..... *23*

*3.3.4 Vent Flow* ..... *23*

*3.3.5 Burning Rate* ..... *25*
*3.3.6 Gas Species* ..... *28*
3.4 Final Setup and Procedures ..... 33
*3.4.1 Experimental Setup* ..... *33*
*3.4.2 Experimental Preparations* ..... *35*
*3.4.3 Experimental Procedures* ..... *36*
**CHAPTER 4 EXPLORATORY EXPERIMENTS ..... 37**
4.1 Introduction ..... 37
4.2 Detailed Smoke Explosion Scenario ..... 39
4.3 Specific Experimental Results ..... 52
*4.3.1 10 kg Crib At Floor Elevation* ..... *52*
*4.3.2 10 kg Crib At Middle Elevation* ..... *55*
*4.3.3 5 kg Crib At Middle Elevation* ..... *58*
**CHAPTER 5 FINAL DETAILED EXPERIMENTS ..... 61**
5.1 Introduction ..... 61
5.2 Experiment 10-M-100 ..... 64
*5.2.1 Ignition and Growth* ..... *64*
*5.2.2 Smoldering Decay* ..... *68*
*5.2.3 Smoke Explosions* ..... *69*
*5.2.4 Post Smoke Explosion* ..... *72*
5.3 Experiments With Middle Elevation ..... 73
5.4 Experiments With 71 mm Vent ..... 76
5.5 Experiments With 50 mm Vent ..... 80
**CHAPTER 6 CONCLUSIONS ..... 82**
**CHAPTER 7 FUTURE RECOMMENDATIONS ..... 85**
**REFERENCES ..... 86**
**APPENDIX A BURNING REGIMES OF CRIBS ..... 89**
**APPENDIX B THE DEVELOPMENT OF THE PHI-METER ..... 91**

**B.1 THE CONCEPT OF PHI-METER ..... 91**

**B.2 THE THEORY OF PHI-METER ..... 92**

**B.3 THE CONSTRUCTION OF PHI METER ..... 96**

**B.4 THE CALIBRATION OF PHI METER ..... 99**

**APPENDIX C EXPLORATORY EXPERIMENTS DATA ..... 103**

**APPENDIX D FINAL EXPERIMENTS DATA ..... 114**

# List of Figures

Figure 2.1: Fully enclosed space with developed growing upper layer (Cooper 2002)..... 7

Figure 2.2: Fully enclosed space with developed growing upper layer..... 7

Figure 2.3: A typical flammability diagram showing all the flammable gases compositions within the envelope..... 10

Figure 2.4: A typical flammability diagram showing 5 different mixture compositions when ventilation is introduced..... 11

Figure 3.1: Schematic diagram of the exploded compartment (All dimensions in mm)... 13

Figure 3.2: Photograph showing the front view of the compartment ..... 14

Figure 3.3: Photograph showing the layout of thermal insulations ..... 15

Figure 3.4: Photograph of the compartment hatch with both upper and lower ventilation openings (Ø 100 mm) and the clamping system..... 16

Figure 3.5: Schematic diagram for layout of the thermal insulations within the compartment ..... 17

Figure 3.6: Photograph of the compartment wall with and without the pressure relief panel ..... 18

Figure 3.7: Photograph of the observation window ..... 19

Figure 3.8: Schematic diagram of the Main Fire Lab and the Control Room showing the position of the compartment and the video camera..... 19

Figure 3.9: The screen capture of the UDL software interface ..... 20

Figure 3.10: Photograph of the protecting steel tube extended out of the compartment... 22

Figure 3.11: Schematic diagrams showing the location of thermocouple trees: (a) Front view of the compartment (b) Vertical view of the compartment (All dimensions are in mm) ..... 22

Figure 3.12: Sketch of the compartment showing the positions of three pressure transducers: (a) Probe of the 100 Torr pressure transducer (b) & (c) Probe of the 10 Torr pressure transducer (All units are in mm) ..... 24

Figure 3.13: Photograph of the compartment showing three pressure transducers ..... 25

Figure 3.14: Photograph for the 10 kg wood crib ..... 26

Figure 3.15: Photograph of the loading table inside the compartment ..... 26

Figure 3.16: Photograph of the load cell under the compartment ..... 27

Figure 3.17: Side view of the schematic diagram for three different crib locations (All dimensions are measured from the middle of the crib to the bottom of the compartment)27

Figure 3.18: Schematic diagram of the compartment showing sampling tubes in plan view (All dimensions in mm) ..... 28

Figure 3.19: Schematic diagram of the compartment showing sampling tubes at three different heights in side view (All dimensions in mm) ..... 29

Figure 3.20: Photograph for the back of the compartment showing wrapped sampling tubes ..... 30

Figure 3.21: Photograph of both gas analysers (a) room analyser on the left (b) furnace analyser on the right ..... 32

Figure 3.22: Photograph of the hood analyser ..... 32

Figure 3.23: Schematic diagram of the compartment in front view (all units in mm) ..... 33

Figure 3.24: Schematic diagram of the compartment in top view (all units in mm) ..... 34

Figure 3.25: Schematic diagram of the compartment in side view (all units in mm) ..... 34

Figure 3.26: Schematic diagram of the final gas sampling system ..... 35

Figure 4.1: Temperature histories from the rear top (950 mm) thermocouple for experiment 10-F-71 and experiment 10-F-50..... 40

Figure 4.2: Temperature histories from the rear top (950 mm) thermocouple for experiment 10-M-100 and experiment 10-M-71 ..... 40

Figure 4.3: Video captures of experiment 10-M-100 showing the ghosting fire period: The flame starts to detach from the crib at 0 second and then migrates to both sides of the crib. Flames start to appear at the bottom left corner at 20 seconds. As the ghosting fire develops, the intensity of the flame keeps diminishing until it self-extinguishes at 50 seconds. (All images are taken from the video camera placed under the compartment) .. 43

Figure 4.4: Video captures of experiment 10-M-100 showing the flame and the smoke shooting out through the top vent ..... 46

Figure 4.5: Video captures of experiment 10-F-71 showing the flame filling up the entire compartment ..... 49

Figure 4.6: Flow chart diagram for the process of multi-explosion scenario ..... 50

Figure 4.7: Temperature histories from the rear thermocouple tree for experiment 10-F-100..... 52

Figure 4.8: Mass loss histories for experiment 10-F-100, 10-F-71 and 10-F-50..... 53

Figure 4.9: Heat release rate curve for experiment 10-F-100, 10-F-71 and 10-F-50 with a 10-point moving average ..... 54

Figure 4.10: Temperature histories from the rear top (950 mm) thermocouple for experiment 10-M-100, 10-M-71 10-M-50, 10-M-36 and 10-M-25 ..... 56

Figure 4.11: Mass loss histories for experiment 10-M-100, 10-M-71 10-M-50, 10-M-36 and 10-M-25 ..... 56

Figure 4.12: Heat release rate curve for experiment 10-M-100, 10-M-71 10-M-50, 10-M-36 and 10-M-25 with a 10-point moving average ..... 57

Figure 4.13: Temperature histories from the rear top (950 mm) thermocouple for experiment 5-M-100, 5-M-71 and 5-M-50..... 59

Figure 4.14: Mass loss histories for experiment 5-M-100, 5-M-71 and 5-M-50..... 60

Figure 4.15: Heat release rate curve for experiment 5-M-100, 5-M-71 and 5-M-50 with a 10-point moving average ..... 60

Figure 5.1: Temperature histories from the rear thermocouple tree for experiment 10-M-100..... 65

Figure 5.2: Heat release rate history for experiment 10-M-100 with a 10-point moving average..... 66

Figure 5.3: $O_2$, $CO_2$ and CO molar concentrations for experiment 10-M-100 ..... 66

Figure 5.4: Temperature profile constructed from the rear thermocouple tree for experiment 10-M-100 ..... 67

Figure 5.5: Mass flow rate through both opening vents for experiment 10-M-100 ..... 67

Figure 5.6: Mass loss history for experiment 10-M-100 ..... 68

Figure 5.7: A simplified flow chart diagram for the multi-explosion scenario describing the corresponding changes in the gas concentrations ..... 69

Figure 5.8: Short histories of mass flow rates and the mass loss for experiment 10-M-100 ..... 71

Figure 5.9: Video captures of experiment 10-M-100 at 28 minutes showing the ignition moment (Video camera is placed under the fire compartment) ..... 72

Figure 5.10: Temperature histories comparison between experiment 10-M-100, 10-M-71 and 10-M-50 using data from the rear top thermocouple (Each asterisk designates a smoke explosion) ..... 74

Figure 5.11: Mass loss histories comparison between experiment 10-M-100, 10-M-71 and 10-M-50 (Each asterisk designates a smoke explosion) ..... 75

Figure 5.12: Mass flow rates comparison between experiment 10-M-100, 10-M-71 and 10-M-50 ..... 75

Figure 5.13: Heat release rate histories comparison between experiment 10-M-100, 10-M-71 and 10-M-50 ..... 76

Figure 5.14: Temperature histories comparison between experiment 10-C-71, 10-M-71 and 10-F-71 ..... 78

Figure 5.15: Mass loss histories comparison between experiment 10-C-71, 10-M-71 and 10-F-71 ..... 78

Figure 5.16: Mass flow rates comparison between experiment 10-C-71, 10-M-71 and 10-F-71 ..... 79

Figure 5.17: Heat release rate histories comparison between experiment 10-C-71, 10-M-71 and 10-F-71 ..... 79

Figure 5.18: Temperature histories from the rear thermocouple tree for experiment 10-C-50..... 81

Figure B.1: Schematic diagram of the Phi meter layout showing the sample line and instrumentations in conjunction with the compartment gas analyser layout..... 97

Figure B.2: Photograph of the furnace showing the quartz glass tube with its cap and connector ..... 98

Figure B.3: A comparison of the experimental and theoretical equivalence ratio..... 102

Figure C.1: Temperature histories for experiment 10-F-100 at the front of the compartment ..... 103

Figure C.2: Temperature histories for experiment 10-F-100 at the rear of the compartment ..... 103

Figure C.3: Temperature histories for experiment 10-F-71 at the front of the compartment ..... 104

Figure C.4: Temperature histories for experiment 10-F-71 at the rear of the compartment ..... 104

Figure C.5: Temperature histories for experiment 10-F-50 at the front of the compartment ..... 105

Figure C.6: Temperature histories for experiment 10-F-50 at the rear of the compartment ..... 105

Figure C.7: Temperature histories for experiment 10-M-100 at the front of the compartment ..... 106

Figure C.8: Temperature histories for experiment 10-M-100 at the rear of the compartment ..... 106

Figure C.9: Temperature histories for experiment 10-M-71 at the front of the compartment ..... 107

Figure C.10: Temperature histories for experiment 10-M-71 at the rear of the compartment ..... 107

Figure C.11: Temperature histories for experiment 10-M-50 at the front of the compartment ..... 108

Figure C.12: Temperature histories for experiment 10-M-50 at the rear of the compartment ..... 108

Figure C.13: Temperature histories for experiment 10-M-36 at the front of the compartment ..... 109

Figure C.14: Temperature histories for experiment 10-M-36 at the rear of the compartment ..... 109

Figure C.15: Temperature histories for experiment 10-M-25 at the front of the compartment ..... 110

Figure C.16: Temperature histories for experiment 10-M-25 at the rear of the compartment ..... 110

Figure C.17: Temperature histories for experiment 5-M-100 at the front of the compartment ..... 111

Figure C.18: Temperature histories for experiment 5-M-100 at the rear of the compartment ..... 111

Figure C.19: Temperature histories for experiment 5-M-71 at the front of the compartment ..... 112

Figure C.20: Temperature histories for experiment 5-M-71 at the rear of the compartment ..... 112

Figure C.21: Temperature histories for experiment 5-M-50 at the front of the compartment ..... 113

Figure C.22: Temperature histories for experiment 5-M-50 at the rear of the compartment ..... 113

Figure D.1: Temperature histories for experiment 10-C-100 at the front of the compartment ..... 114

Figure D.2: Temperature histories for experiment 10-C-100 at the rear of the compartment ..... 114

Figure D.3: Temperature profile constructed from the rear thermocouple tree for experiment 10-C-100 ..... 115

Figure D.4: $O_2$, $CO_2$ and CO molar concentrations for experiment 10-C-100 ..... 115

Figure D.5: Mass flow rate through both opening vents for experiment 10-C-100..... 116

Figure D.6: Mass loss history and pressure history for experiment 10-C-100..... 116

Figure D.7: Heat release rate history for experiment 10-C-100 with a 10-point moving average..... 117

Figure D.8: Temperature histories for experiment 10-C-71 at the front of the compartment ..... 117

Figure D.9: Temperature histories for experiment 10-C-71 at the rear of the compartment ..... 118

Figure D.10: The compartment pressure and the temperature history compiled from the top rear thermocouple for experiment 10-C-71 ..... 118

Figure D.11: Temperature profile constructed from the rear thermocouple tree for experiment 10-C-71..... 119

Figure D.12: $O_2$, $CO_2$ and CO molar concentrations for experiment 10-C-71..... 119

Figure D.13: Mass flow rate through both opening vents for experiment 10-C-71..... 120

Figure D.14: Mass loss history for experiment 10-C-71 ..... 120

Figure D.15: Heat release rate history for experiment 10-C-71 with a 10-point moving average..... 121

Figure D.16: Temperature histories for experiment 10-C-50 at the front of the compartment ..... 121

Figure D.17: Temperature histories for experiment 10-C-50 at the rear of the compartment ..... 122

Figure D.18: Temperature profile constructed from the rear thermocouple tree for experiment 10-C-50..... 122

Figure D.19: $O_2$, $CO_2$ and CO molar concentrations for experiment 10-C-50..... 123

Figure D.20: Mass flow rate through both opening vents for experiment 10-C-50..... 123

Figure D.21: Mass loss history for experiment 10-C-50 ..... 124

Figure D.22: Heat release rate history for experiment 10-C-50 with a 10-point moving average..... 124

Figure D.23: Temperature histories for experiment 10-M-71 at the front of the compartment ..... 125

Figure D.24: Temperature histories for experiment 10-M-71 at the rear of the compartment ..... 125

Figure D.25: Temperature profile constructed from the rear thermocouple tree for experiment 10-M-71..... 126

Figure D.26: $O_2$, $CO_2$ and CO molar concentrations for experiment 10-M-71..... 126

Figure D.27: Mass flow rate through both opening vents for experiment 10-M-71..... 127

Figure D.28: Mass loss history for experiment 10-M-71 ..... 127

Figure D.29: Heat release rate history for experiment 10-M-71 with a 10-point moving average..... 128

Figure D.30: Temperature histories for experiment 10-M-50 at the front of the compartment ..... 128

Figure D.31: Temperature histories for experiment 10-M-50 at the rear of the compartment ..... 129

Figure D.32: Temperature profile constructed from the rear thermocouple tree for experiment 10-M-50..... 129

Figure D.33: $O_2$, $CO_2$ and CO molar concentrations for experiment 10-M-50..... 130

Figure D.34: Mass flow rate through both opening vents for experiment 10-M-50..... 130

Figure D.35: Mass loss history for experiment 10-M-50 ..... 131

Figure D.36: Heat release rate history for experiment 10-M-50 with a 10-point moving average..... 131

Figure D.37: Temperature histories for experiment 10-F-100 at the front of the compartment ..... 132

Figure D.38: Temperature histories for experiment 10-F-100 at the rear of the compartment ..... 132

Figure D.39: Temperature profile constructed from the rear thermocouple tree for experiment 10-F-100 ..... 133

Figure D.40: $O_2$, $CO_2$ and CO molar concentrations for experiment 10-F-100 ..... 133

Figure D.41: Mass flow rate through both opening vents for experiment 10-F-100 ..... 134

Figure D.42: Mass loss history for experiment 10-F-100..... 134

Figure D.43: Heat release rate history for experiment 10-F-100 with a 10-point moving average (The large increase at 28 minutes is caused by the pressure relief panel being blown out)..... 135

Figure D.44: Temperature histories for experiment 10-F-71 at the front of the compartment ..... 135

Figure D.45: Temperature histories for experiment 10-F-71 at the rear of the compartment ..... 136

Figure D.46: Temperature profile constructed from the rear thermocouple tree for experiment 10-F-71 ..... 136

Figure D.47: $O_2$, $CO_2$ and CO molar concentrations for experiment 10-F-71 ..... 137

Figure D.48: Mass flow rate through both opening vents for experiment 10-F-71 ..... 137

Figure D.49: Mass loss history for experiment 10-F-71..... 138

Figure D.50: Heat release rate history for experiment 10-F-71 with a 10-point moving average..... 138

Figure D.51: Temperature histories for experiment 10-F-50 at the front of the compartment ..... 139

Figure D.52: Temperature histories for experiment 10-F-50 at the rear of the compartment ..... 139

Figure D.53: Temperature profile constructed from the rear thermocouple tree for experiment 10-F-50 ..... 140

Figure D.54: $O_2$, $CO_2$ and CO molar concentrations for experiment 10-F-50 ..... 140

Figure D.55: Mass flow rate through both opening vents for experiment 10-F-50 ..... 141

Figure D.56: Mass loss history for experiment 10-F-50..... 141

Figure D.57: Heat release rate history for experiment 10-F-50 with a 10-point moving averageh..... 142

# List of Tables

Table 3.1: Summary of descriptions and objectives for all three analyser sets ..... 31

Table 4.1: Summary data for exploratory experiments showing the experimental conditions; time and temperature at the smoldering decay; time of the first smoke explosion and the temperature (before and after) the first smoke explosion; GF = the occurrence of the ghosting fire; SD = the occurrence of the smoldering decay, and SE = total numbers of explosions (N/A = Not applicable since no explosions occurred) ..... 38

Table 4.2: The division of heat release rate curves for experiment 4 to 8 10-M-100, 10-M-71 10-M-50, 10-M-36 and 10-M-25 ..... 57

Table 5.1: Experimental matrix summarises experimental conditions of final nine detailed experiments ..... 61

Table 5.2: Summary data from final experiments showing the experimental conditions; time and temperature at the smoldering decay; fuel mass, mass flow rates, gas concentrations, time, temperature (before and after) and pressure and at the first smoke explosion; ME = the total mass ejected at the first smoke explosion; GF = the occurrence of the ghosting fire; SD = the occurrence of the smoldering decay, and SE = total number of explosions (N/A = data not available or no explosion occurred) ..... 63

Table B.3: Summary of various flow rates for calculating the theoretical equivalence ratio ..... 101

# Chapter 1 Introduction

## *1.1 Research Impetus*

In the event of fire, typically high temperatures and flames are not the direct cause of death. Rather, it is the smoke containing toxic compounds and flammable gases that has the major impact on building occupants and fire fighters. In an under-ventilated condition, a room full of fuel rich smokes can ignite without any warnings causing a deflagration, which results in significant damage and even threatens people outside the building. Such incidents are referred as smoke explosions, which rarely occur in fires and have been very poorly documented or researched. One example of the smoke explosion phenomenon is an explosion from a warehouse fire at the Chatham Dockyards investigated and reported by Wooley and Ames (1975). The fire causes the death of two fire fighters and injures four others. Prior to the explosion, the fire fighters find no flame, but cool, dense smoke forming a layer half-meter above the floor in the main storeroom containing 178 foam mattresses. Smoke is also observed leaking out through windows of the main storeroom. Suddenly, an unexpected explosion occurs when the fire fighters try to open the door to ventilate the smoke. The explosion is large enough to break windows but no structural damages to the building. The uniqueness of this event is that the burning conditions prior to the explosion are unchanged and gave no indication of what is to come.

Despite the previous studies done in the past (Bowyer and Wertman 2008; Steward 1914; Sutherland 1999; Wooley and Ames 1975), there is still very limited understanding of smoke explosion phenomena. Not only is the smoke explosion phenomenon being falsely described as a delayed flashover (Grimwood 2007), the name smoke explosion is also used synonymously with backdraft (Fleischmann 1993), which assumes a fire develops in a room where the leakage exists in the bounding surfaces. The hot layer descends over the fire as the oxygen concentration is reduced and the fire becomes under-ventilated. Excess pyrolysates accumulate in the upper layer forming a fuel rich mixture with low oxygen concentration. Suddenly, a new opening is introduced and cold, oxygen rich, air enters the compartment and propagates across the floor mixing with the hot, fuel rich, upper layer. When the mixing zone between hot and cold layers is within the flammable range and

contacts with an ignition source, a large deflagration can propagate through the compartment ending in a large fire ball outside the compartment as the unburned fuel ejecting from the opening. Although, many studies (Abbasi and Abbasi 2007; Fleischmann 1993; Gottuk et al. 1999) and training have been done on the topic of backdraft within both academic and fire fighting community, researchers are still unable to fully characterise backdraft phenomena.

A preliminary study of smoke explosion is done by Sutherland (1999) at University of Canterbury. He creates a series of smoke explosions within a fire compartment, based on which, it is concluded that the smoke explosion is a result of smouldering combustion. Unfortunately, researches on the smoke explosion are not sufficient to fully reveal its mechanism. A comprehensive literature review is done by Croft (1980) covering a total of 127 fires in a seventy-year period ending in 1976, from which a conclusion is drawn that the most hazardous explosive conditions come from smouldering fires with low heat release rate. Moreover, low temperature and non-flaming situation can no longer be treated as relatively safe conditions for the entry of fire fighting personnel.

The smoke explosion scenario presented in this research assumes a fire within a compartment where the only ventilation is through a small window or the leakage in the building envelop. Initially, the fire is considered to burn in an over-ventilated condition given the oxygen level is sufficient in the early development. As the fire grows, the upper layer containing combustion products descends down over the burning object. The diminishing level of oxygen in the upper layer inhibits the combustion and results in large amounts of unburned fuel in the upper layer. Meanwhile, the scale and intensity of the flame keeps declining until the flaming combustion stops and the fire goes into smoldering combustion where a large quantity of pyrolysates are produced due to the limited oxygen supply. Glowing embers still remain as the fuel smolders. Once the gas mixture surrounding the fuel falls within the flammable range, it may be ignited by the glowing ember. The flame then rapidly grows into a large fire ball that pressurises the compartment driving some of the excess pyrolysates out of the compartment to burn outside the openings and in certain cases the over-pressure may be sufficient to cause structural damage. As one can see backdrafts and smoke explosions share many commonalities in terms of limited oxygen supply, high quantities of unburned fuel in the

upper layer, and deflagration of the flammable gases, but there exists one primary difference, that is the ventilation condition. In a backdraft, the compartment is filled with fuel rich combustible gases but very little oxygen. In order for there to be a backdraft, there has to be a change in the ventilation, which allows oxygen-rich air to flow into the compartment mixing with combustible gases in the upper layer and proceeding to a backdraft upon contact with an ignition source. Such change of ventilation is not required for a smoke explosion where the combustible gases inside the compartment are pre-mixed with oxygen and the gas mixture is within the flammable range prior to the explosion. Unfortunately, the details of the smoke explosion and the backdraft have not been fully identified and studied. Hence, it is important to develop a fundamental physical understanding of the nature of smoke explosion phenomena.

## *1.2 Research Objectives*

This research expands on the previous study by Sutherland (1999) to quantify the conditions within the compartment prior to the explosion under various experimental conditions including fuel elevations, vent sizes and fuel mass, in order to characterise the smoke explosion phenomenon. The main objective of this research is to develop a fundamental physical understanding of conditions that lead to a smoke explosion. The practical application of this study is to help fire fighters be more aware of the potential hazards of smoke explosions. A total of 20 experiments are to be conducted in a fire compartment at the Main Fire Lab at the University of Canterbury, New Zealand. Particular aims of this research are:

- To provide a qualitative analysis of the smoke explosion phenomenon including a detailed fire scenario.

- To investigate the impact of vent size, fuel height and fuel mass on the burning characteristics of the fuel and the occurrences of smoke explosions.

- To discover the conditions that lead to the smoke explosion based on flammable limits and species concentrations.

## 1.3 Research Outlines

This report consists of seven chapters,

**Chapter 2 Literature Review:**

Provides a review of the literature of compartment fires and related phenomenon including the smoldering combustion and pyrolysis. Also gives description of a flammable gas prior to the explosion using flammability diagrams.

**Chapter 3 Experimental Setup and Procedure**:

Describes the construction of the fire compartment used in this research and the apparatus used to acquire all the data, including fuel mass, temperature, pressure, mass flow rate and heat release rate. Finally, it provides a detailed description of the final experimental set up and procedures.

**Chapter 4 Exploratory Experiments:**

Presents the phenomena observed during the exploratory experiments and discuss the findings obtained from the experiments. The data acquired includes the upper layer temperature, mass loss and heat release rate.

**Chapter 5 Final Detailed Experiments:**

Provides a discussion on additional experiments to explore the impact of vent sizes, fuel elevations on the burning process, and the occurrence of smoke explosions.

**Chapter 6 Conclusions:**

Describes conclusions drawn from this research.

**Chapter 7 Future Recommendations:**

Provides recommendations for potential further researches.

# Chapter 2 Literature Review

## 2.1 Introduction

A literature review has been undertaken before any analysis or laboratory experiments are carried out. This section gives a summary of the literature review. It provides essential background of compartment fires including gas temperatures and related outcomes. The section also describes the nature and characteristics of the smoldering combustion, which is thought to be the essential step to produce smoke explosions. Finally, it discusses the change of the gas composition and the formation of a flammable gas prior to the explosion using flammability diagrams.

## 2.2 The Development of Compartment Fires

Fires controlled by any confined spaces are referred as compartment fires. The fuel first vaporises and rises due to the buoyancy, and then reacts with oxygen creating a flame above. The fuel move upward in the flame due to the convective flow and react there with oxygen (Karlsson and Quintiere 2000). Since the fire is confined within a compartment, this mixture of hot gas and cold air will impinge on the ceiling and then spread across as a momentum-driven circular jet forming a layer of hot gases and a layer of cold air. Figure 2.1 is an example of a compartment fire showing the smoke layer and heat transfer. If the compartment is over-ventilated, the development of the fire follows a typical growth scenario as shown by Line A in Figure 2.2 where two idealised heat release rate curves are constructed for both over-ventilated and under-ventilated condition. The fire goes into a steady growth until it reaches the condition for flashover, which makes the fire rapidly transit from a growing fire on a single item to a fully developed fire involving all combustible materials with flames burning outside the compartment. One of the criteria to determine the flashover is based on the temperature at which the radiation from the hot gases in the compartment will ignite all of the combustible contents. Generally speaking, flashover occurs when the temperature is above the range between 500 to 600 ℃ in the smoke gas layer. With no intervention after the flashover, all the fuel is to be consumed and finally the fire drops into a decay phase until the fuel is depleted.

When the ventilation of the compartment is limited, instead of growing along Line A, the fire development follows Line B in Figure 2.2, which qualitatively indicates the fire starts off with the same growth. However, as the fire develops, the available oxygen becomes less given the air flow is limited, so the heat release rate diminishes as the burning rate decreases. The flame may even self-extinguish and under the right condition, the fire goes into the smoldering phase instead of flashover. During smoldering, large quantities of unburned fuel are discharged into the upper layer forming a mixture of combustible gases. Once the concentration of the gas mixture enters the flammable range, an explosion may occur upon contact with an ignition source.

When the fire is limited by the ventilation, the fire may go into the smoldering phase prior to the smoke explosion and the associated temperatures are much below the flashover and fully-developed temperature. In Sutherland's case, the temperatures within the compartment range between 300 to 400 ℃ with the exception of much higher temperature when the smoke explosion occurs, but typically the overall temperature is much lower when the fire is limited by the ventilation. Other researches on compartment fires with limited ventilations (Fleischmann 1993; Gottuk et al. 1999; Sutherland 1999) shown that the temperature of the hot gas layer prior to the explosion are all well below the criterion for flashover.

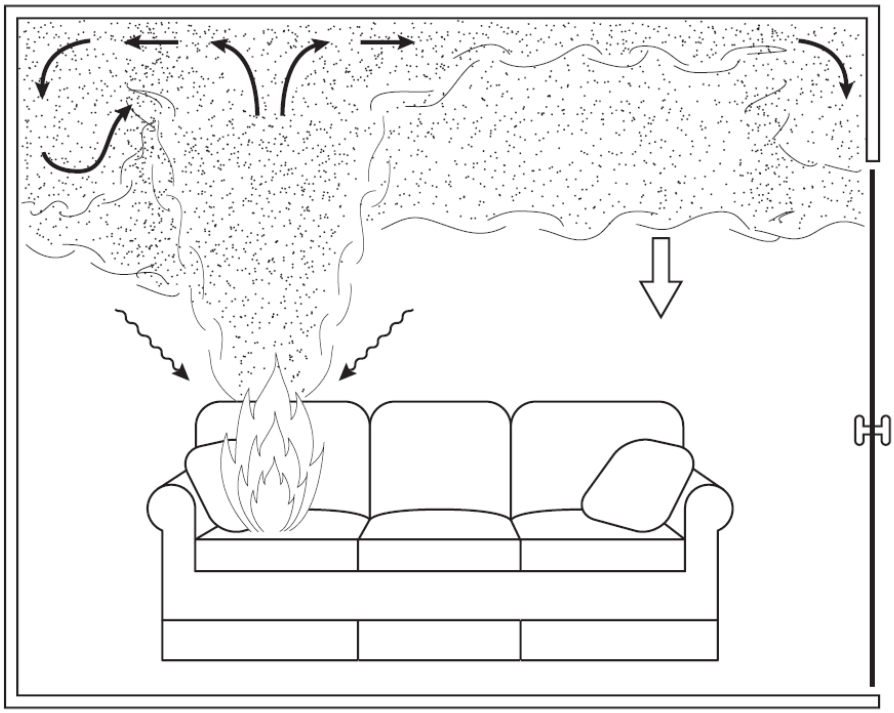

**Figure 2.1: Fully enclosed space with developed growing upper layer (Cooper 2002)**

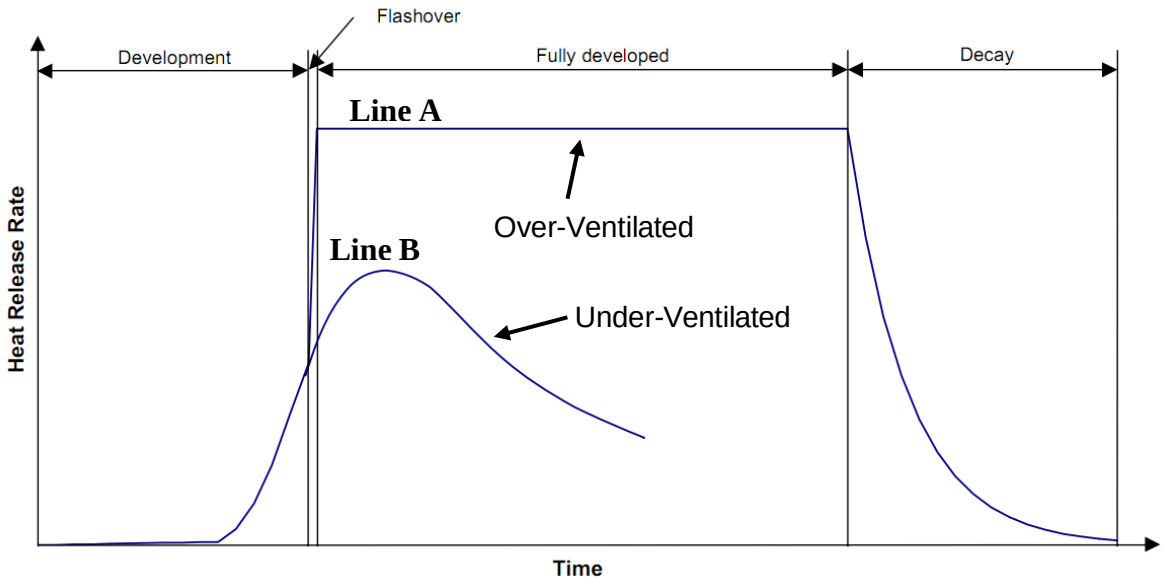


**Figure 2.2: Fully enclosed space with developed growing upper layer**

## 2.3 Characteristics of Smoldering Combustion

Smoldering combustion is a slow, low temperature and flameless form of combustion. Examples of smoldering include a lighted cigarette and glowing embers of coal, where the combustion is self-sustained by the heat generated when oxygen contacts the surface of a condensed-phase fuel. Although smoldering combustion can occur under many conditions, only those relevant to compartment fires are covered below. The following characteristics are identified to provide insights in the development of smoke explosion scenario; low oxygen environment, high yield of combustible gases and low yield of heat.

Consider a fire developing within a ventilation-limited compartment, as the fire evolves, the available oxygen is reduced. The flame self-extinguishes as the fire goes into smoldering under the right condition. The cause of the smoldering combustion is believed to be oxygen depletion in compartment fires as reported by Quintiere (1997). Similar findings are reported in Sutherland's research (1999), the fire always go through the smoldering phase in order to generate large quantity of combustible gases including unburned fuel and CO. Purser (2002) also reports that a high yield of unburned fuel and CO are expected for smoldering fires. The unburned fuel comes from the pyrolysis reactions, which is a process of thermal decomposition of the fuel as described by Madrzykowski and Stroup (2008), because there is not enough oxygen and the post flame compartment temperature is significantly low to sustain the oxidation of most of the fuel. The CO is an intermediate product of the incomplete combustion.

Although oxygen depletion is believed to cause the smoldering combustion, the oxygen is still needed to support smoldering combustion and it is consumed at a much lower rate than in flaming combustion. The corresponding heat release rate and compartment temperature all decrease significantly as the burning rate is limited by the available oxygen as suggested by Ohlemiller (2002). Although the compartment temperature is low, enough heat is retained in the reaction zone to maintain the temperature needed to sustain the reaction as the porous materials on the smoldering surface are poor conductors of heat (Friedman 2003).

## 2.4 Flammability Diagram

Flammability diagram is a useful tool in analysing fuel/air mixtures. The qualitative description using flammability diagram provides valuable insights into explaining the development of the smoke explosion scenario. There exist composition limits of fuel/air mixture, within which flames can propagate during combustion (Beyler 2002). Those composition limits are referred as flammable limits which are determined experimentally by igniting a combustible gas with known concentration inside a vertical tube. If the flame propagates at least half way through the tube, the gas is considered flammable. The upper flammable limit (UFL) is the maximum gas concentration at which the flame propagates at least half way through the tube. Likewise, the lower flammable limit (LFL) is the minimum gas concentration that results in flame propagation. Based on an extensive series of tests with a range of mixture compositions, a flammability diagram can be constructed incorporating all possible combinations of fuel/oxidant/diluent mixture concentrations (by volume) that can propagate a flame. Figure 2.3 shows the flammability diagram with both UFL and LFL for methane. Three axes represent three gases respectively ranging from 0% to 100% (by volume). The flammability mixture is the area within the envelope. The air line indicates where the ratio of oxygen to nitrogen is the same as in air. For example, the LFL of methane in air is 5% by volume and the UFL is 15 % by volume. As such, only the methane/air mixture between 5% to 15% methane concentrations has the potential to propagate flame. The 5% point represents a gas mixture with 5% methane, 20% oxygen and 75% nitrogen.

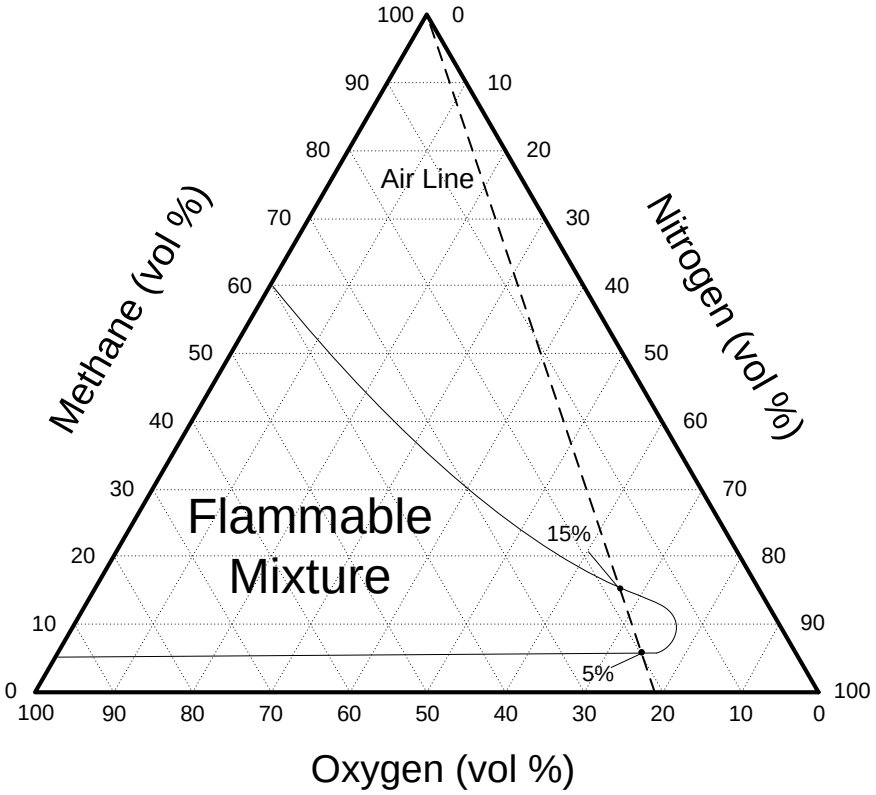


**Figure 2.3: A typical flammability diagram showing all the flammable gases compositions within the envelope**

Figure 2.4 is the zoom-in version of a flammability diagram with a shaded area representing the possible condition that can result in a smoke explosion. This flammability diagram is used here for explanatory purposes only, because the composition of the gas mixture is not known. The Point A simply represents fresh air which contains 21% of oxygen, 79% of nitrogen and 0% fuel, by volume. Line A-B-C shows the varying mixture compositions that may be created for a smoke explosion experiment. All mixtures within the designated envelope are flammable, which are predominantly determined by the concentration of unburned fuel. However, the exact details of the flammability envelope are not known nor is it necessary for this qualitative discussion.

Consider a fire developing inside a compartment with limited ventilations, at first the fire is considered to burn in an over-ventilated condition given the oxygen level is sufficient in the early development. The mixture composition starts to shift towards Point B, as the diminishing level of oxygen in the upper layer inhibits the combustion and results in increasing amount of unburned fuel to accumulate in the compartment. Meanwhile, the

scale and intensity of the flame keeps declining until the flaming combustion stops and the fire goes into smoldering combustion where a large quantity of pyrolysates are produced due to the limited oxygen supply. The smoldering phase can be represented by shift from Point B to Point C. Once the gas mixture surrounding the fuel reaches Point C, it may be ignited upon contact with an ignition source. Line A-D represents another possible scenario where a smoke explosion may occur at an earlier stage of the fire development. Anywhere beyond Point D indicates a flammable gas composition.

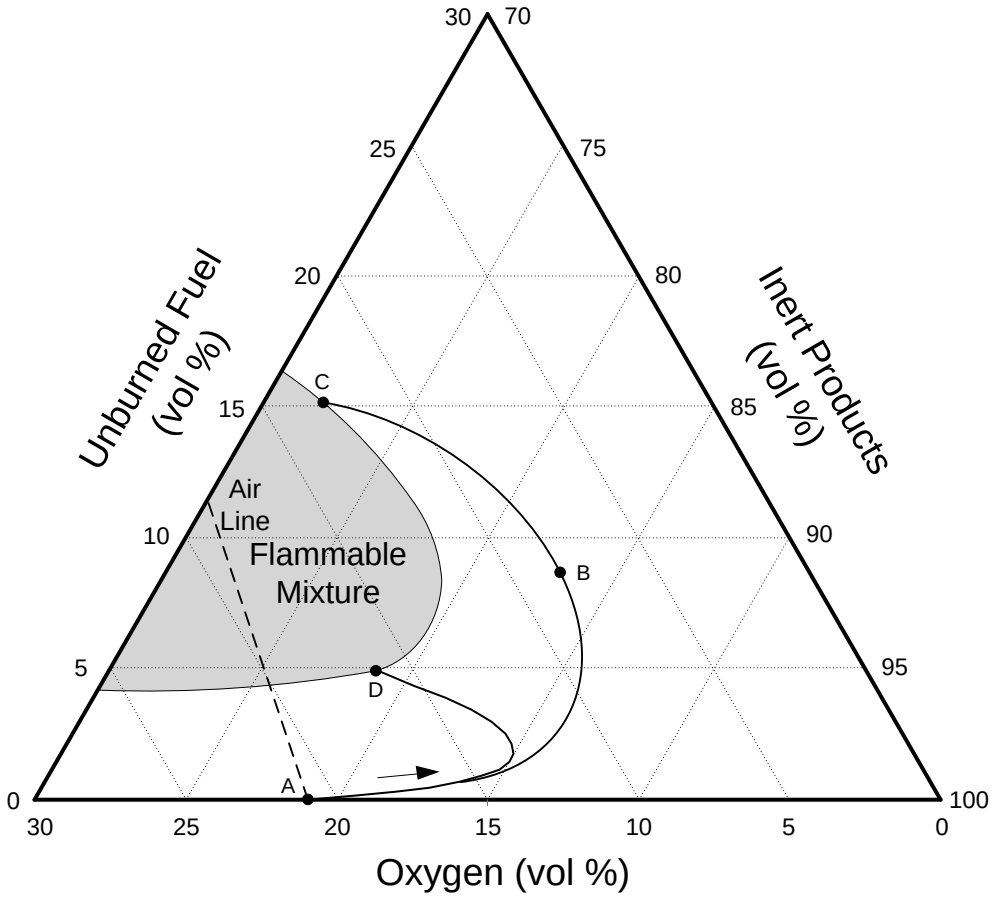


**Figure 2.4: A typical flammability diagram showing 5 different mixture compositions when ventilation is introduced**

# Chapter 3 Experimental Setup and Procedure

## 3.1 Introduction

Due to the complexity of the smoke explosion phenomenon, well controlled experiments inside a fire compartment were required in a reproducible and safe manner, in order to study the smoke explosion. By the nature of a smoke explosion, a potential hazard might occur during the experiment. Therefore, a purposely designed pressure reliving compartment was built. Experiments were carried out in the fire research lab at the University of Canterbury. The compartment was placed underneath the hood of the furniture calorimeter with a large exhaust to reduce the potential hazard. This chapter described the details of the construction and setup of the compartment and the experimental measurements that are used for analysis.

## 3.2 Preliminary Setup

For this particular research, the size of the compartment was designed to a half residential scale at 1.5m × 1 m × 1 m. A 3m × 3m hood next to the opening of the compartment was utilised to collect all the combustion gases and had an instrumented duct capable of measuring several exhaust parameters, including oxygen consumption (from which heat release rate can be determined), major gas concentrations, temperatures and pressures. In order to fully characterise the smoke explosion phenomenon, the position and the size of the fuel were investigated to provide insights of any significant impacts on the fire behaviour and the occurrence of the smoke explosion.

Figure 3.1 shows the detailed layout of the compartment including the dimension of compartment, the positioning of the relevant experimental measurements and the relative location of the vents. Figure 3.2 shows the front view of the fire compartment and the blackened area on the thermal insulation was the soot from exploratory experiments. Thermocouples, pressure transducers, sampling tubes were highlighted in the photograph.

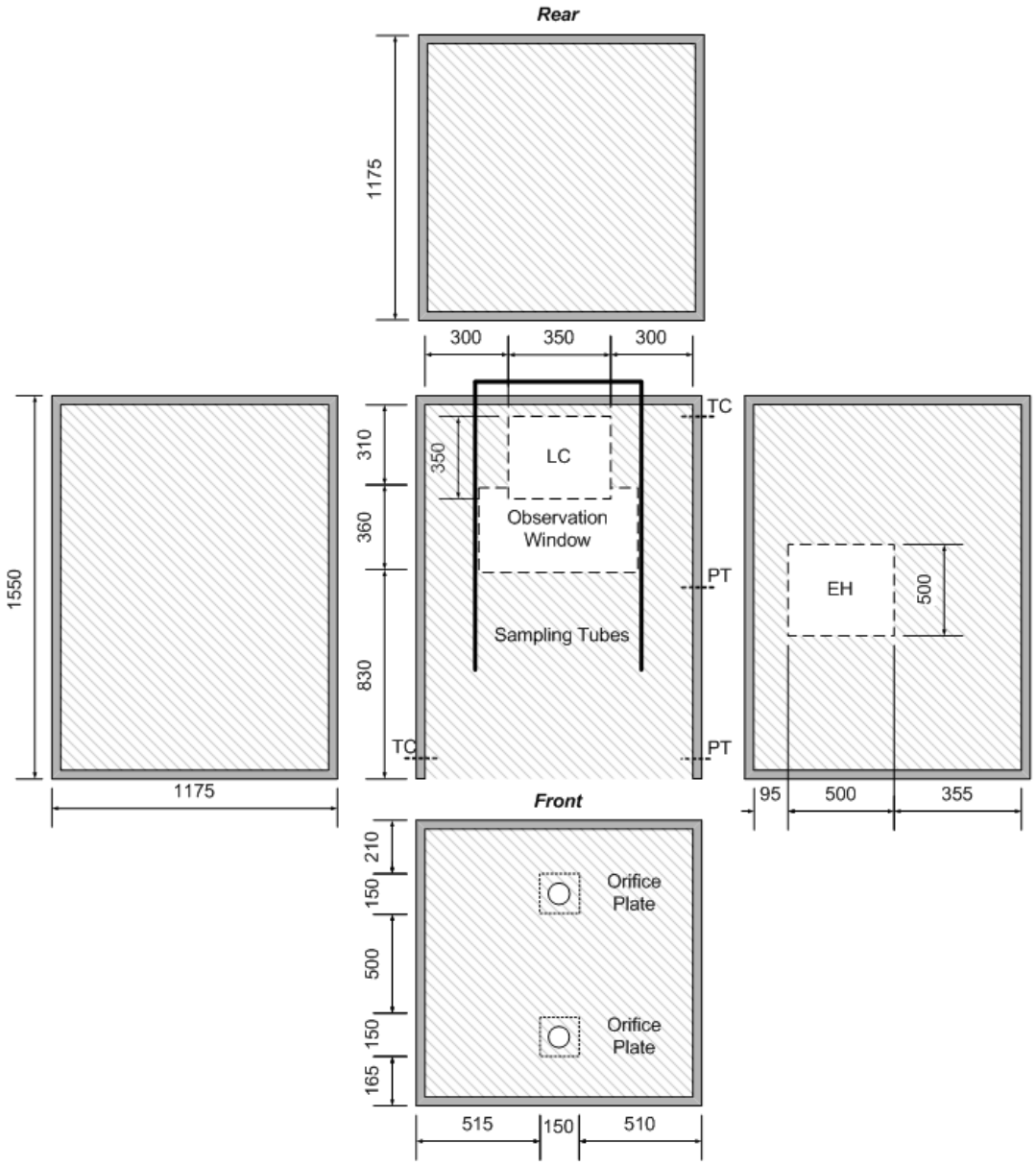


| | | | |
|---|---|---|---|
| | Thermal Insulation | LC | Loading Cell |
| EH | Pressure Relief Panel | PT | Pressure Transducer |
| TC | Thermocouple | | |

**Figure 3.1: Schematic diagram of the exploded compartment (All dimensions in mm)**

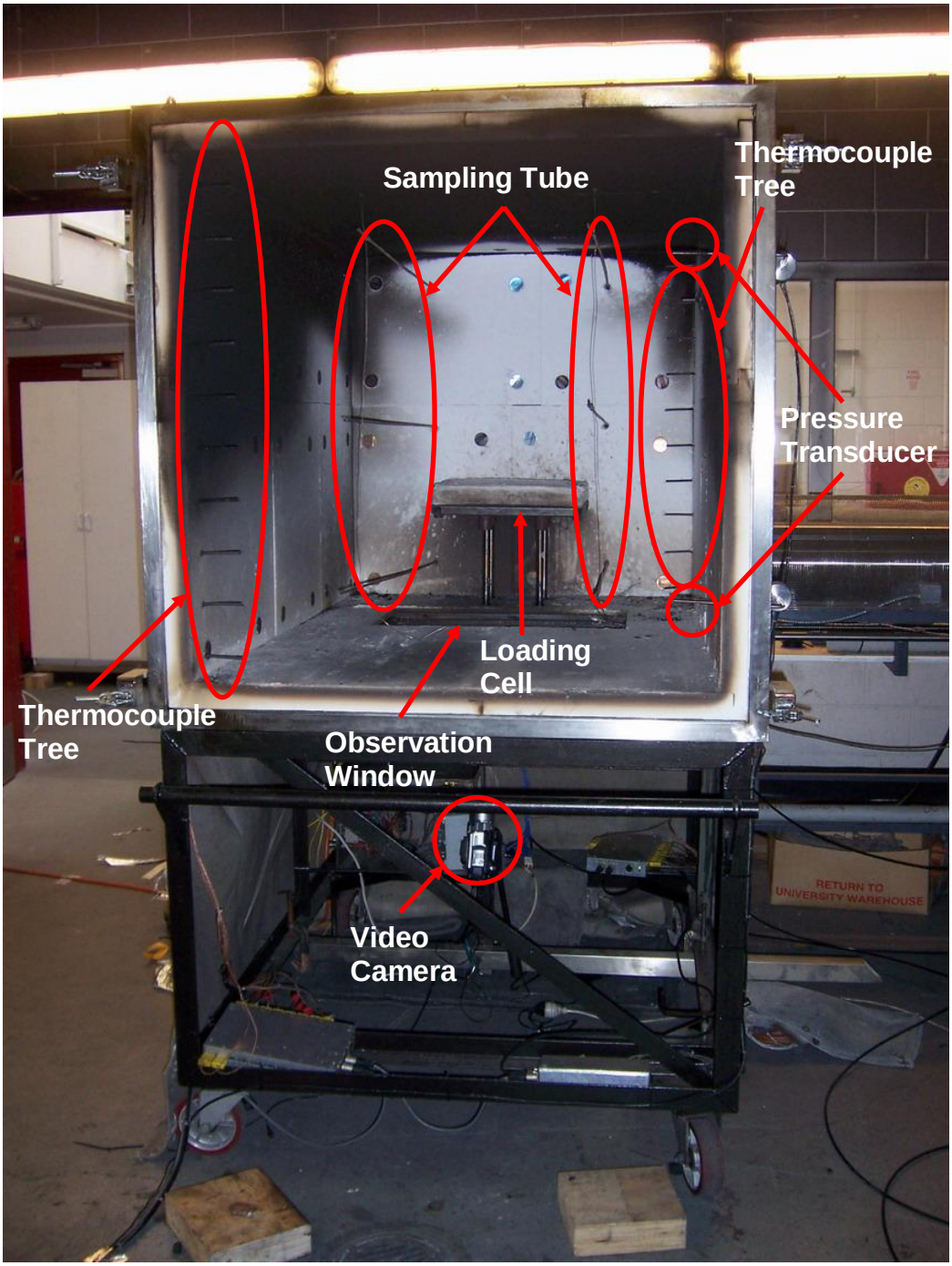


**Figure 3.2: Photograph showing the front view of the compartment**

### 3.2.1 Constructions

One of the first tasks of this research was to rebuild the fire compartment, as the previous one constructed by Sutherland was no longer usable. The finished compartment measured at 1.5 m deep, 1.2 m high and 1.2 m wide. The compartment was constructed from grade 305 stainless steel members and sheets because of their durability and sustainability under high temperature and pressure conditions. The main frame was made of 40 mm × 40 mm rectangular hollow sections spaced at approximately 500 mm apart from each other. All sections were welded together to form the main frame, then a 2 mm thick grade 305 stainless steel was used as the wall sheeting, which was welded to the inside of the frame.

The floor, walls, ceiling were lined with a single layer of Kaowool ceramic fiber vacuum board as thermal insulations. The lining measured 50 mm thick and positioned to overlap the adjacent jointing section as shown in the photograph of the partially insulated compartment in Figure 3.3. Such layout was to prevent direct exposure of the inner steel sheet to the high temperature. All thermal insulation sections were fastened to the steel structure by metal studs instead of using high temperature adhesive, given the insufficient adhesion between thermal insulation and steel lining from previous compartment experiments when using high temperature adhesive (Sutherland 1999).

**Figure 3.3: Photograph showing the layout of thermal insulations**

The hatch had dimensions of 1.2 m × 1.2 m with similar construction procedures. The hatch frame was made up with 50 mm × 50 mm L-shaped steel bars welded together and a single stainless steel sheet was fastened to the inside of the steel-bar frame using rivets as shown in the photograph of the hatch in Figure 3.4. The thermal insulation was fastened to the steel sheet with metal studs. A toggle clamping system, as shown in the inset image of Figure 3.4, was adapted for holding the hatch firmly shut during experiments, because hinges inevitably provide unwanted leakage between the hatch and the frame of the compartment. The compartment sat on a steel-frame stand whose height measured at 750 mm. The stand provided space for experimental apparatus, which will be described in more details later this chapter. Four wheels were attached to the stand for easy transportation.

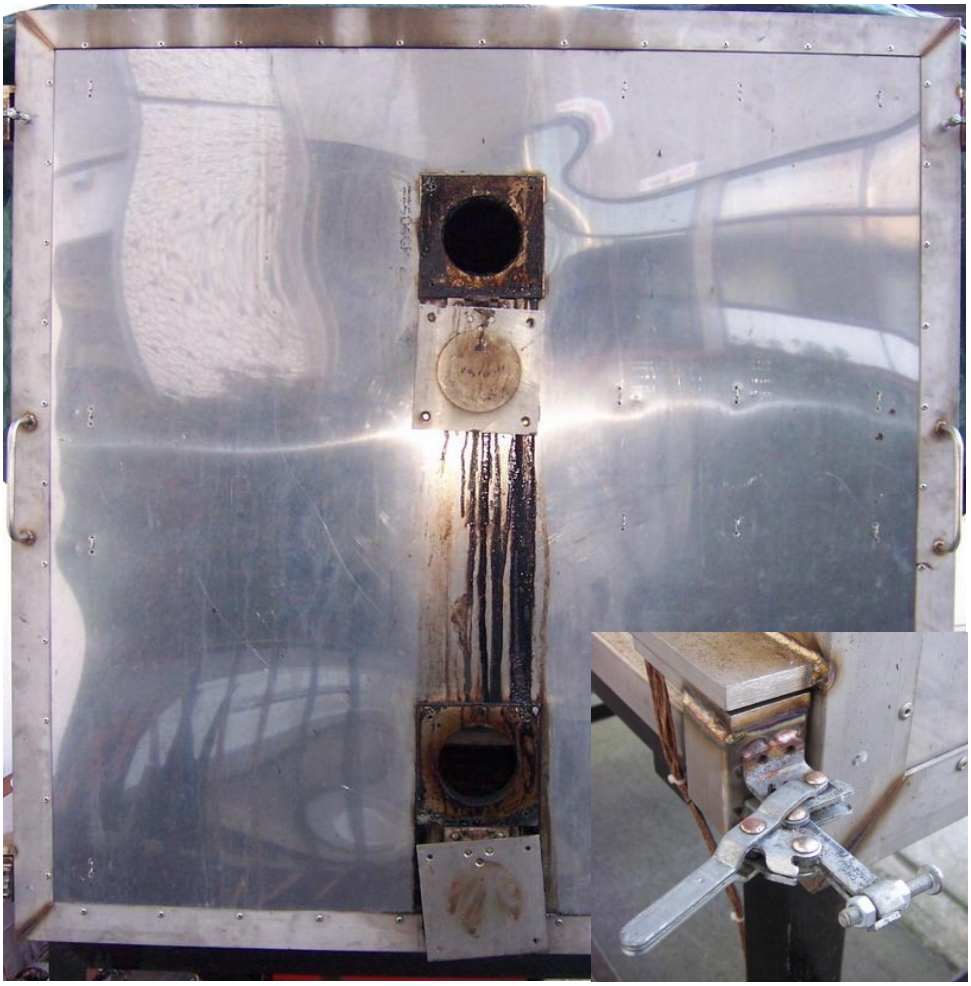

**Figure 3.4: Photograph of the compartment hatch with both upper and lower ventilation openings (Ø 100 mm) and the clamping system**

### 3.2.2 Ventilations

In order to fulfil the aim of this research, which was to investigate the compartment conditions that lead to a smoke explosion under various sizes of vent openings, the ventilation for the compartment was designed to be adjustable by using removable steel orifice plates. Four steel plates were cut and ready to be screwed onto the base plate (Ø 100 m) to give a variety of ventilation conditions. Two base plates were welded onto the hatch and hinged with covers so that openings can be shut to terminate the experiment. Total of five different sizes of vents were designed for this research. Figure 3.5 shows a sketch of the hatch with the location and size of the orifice plates. The vent area was halved by replacing a smaller set of orifice plates as indicated by the calculated area in Figure 3.5.

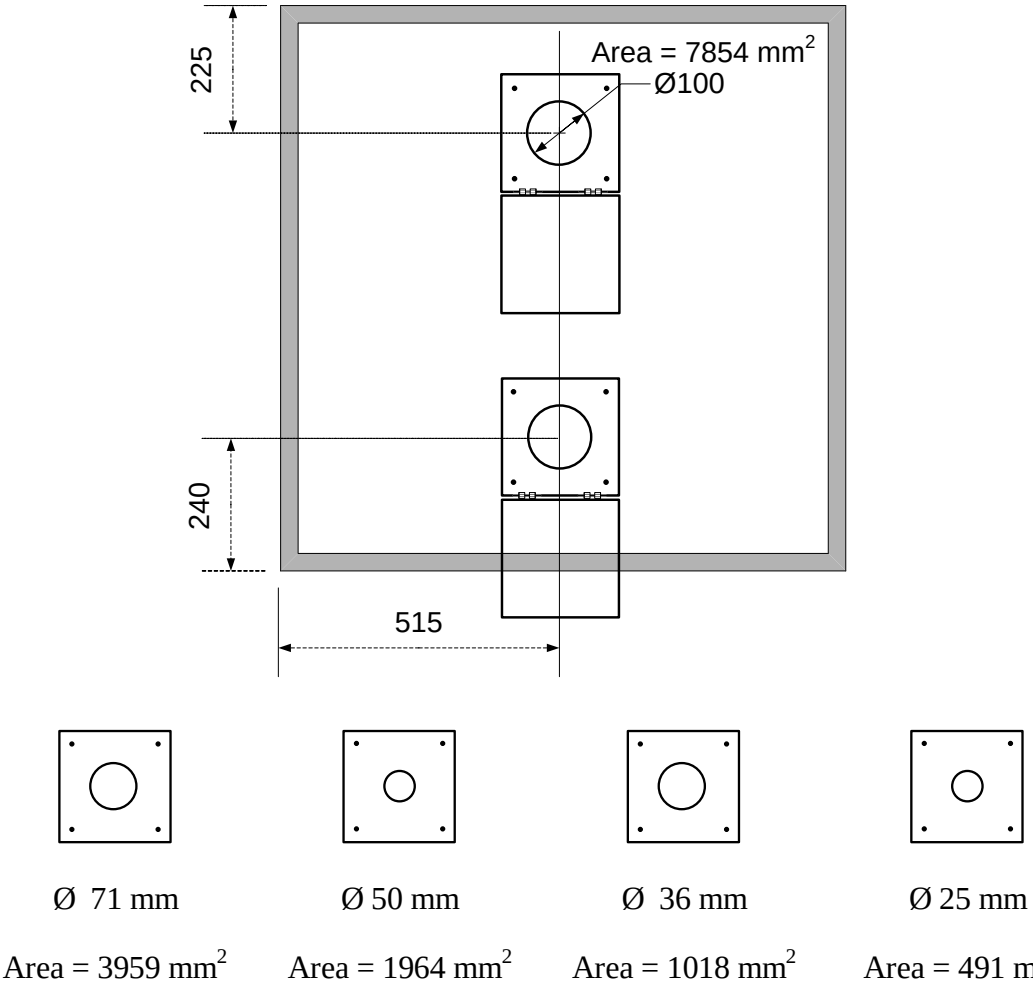


**Figure 3.5: Schematic diagram for layout of the thermal insulations within the compartment**

### 3.2.3 Pressure Relief Panel

A pressure relief panel (400 mm × 400 mm) was embedded to the outer steel frame of the compartment as shown in Figure 3.6. The frame of the pressure relief panel itself was made of 20 mm × 20 mm rectangular hollow sections with 2 mm thick 305 stainless steel sheeting welded to the inside of the frame. A 50 mm thick single layer of Kaowool ceramic fiber vacuum board was positioned onto the steel lining as thermal insulations and fastened to the steel lining by metal studs. Four clips with spring-loaded ball catch provide the securing mechanism for the panel. The maximum design pressure of the panel is 2 kPa. The panel was to provide relief for excessive pressure produced when the smoke explosion occur, in order to maintain safety for both lab personnel and equipments.

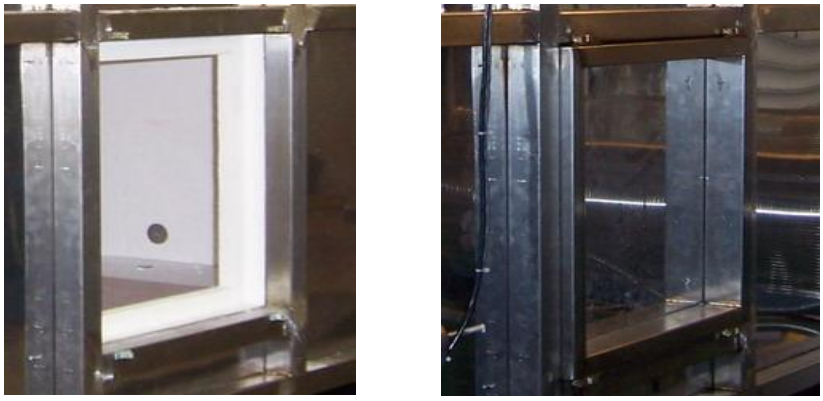

**Figure 3.6: Photograph of the compartment wall with and without the pressure relief panel**

### 3.2.4 Observation Window

In order to observe the fire behaviour during the experiment, a window was constructed and placed right below the loading table as shown in Figure 3.7. The dimension was 620mm × 640 mm and the glazing was consisted of 5 mm FireLite® ceramic glass. High temperature adhesive was used to secure the glass within the steel frame. One video camera was placed approximately 60 ° against the observation window to record the full duration of all experiments. The other camera was placed at an angled view pointing at the compartment vents within the control room as illustrated in Figure 3.8. It should be noted that since the first camera was located very close to the compartment, after certain time through the experiment, the radiative heat affects the CMOS sensors of the camera resulting in discoloured images.

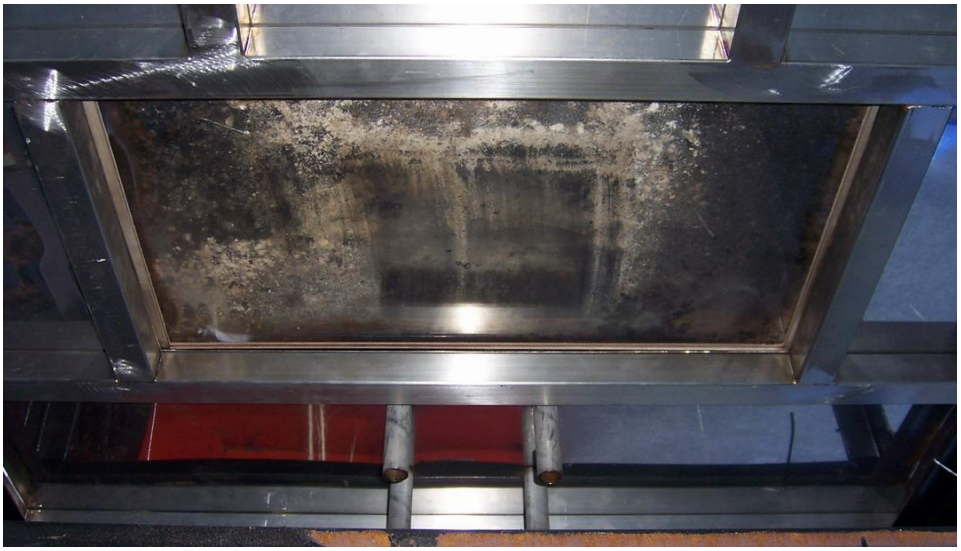

**Figure 3.7: Photograph of the observation window**

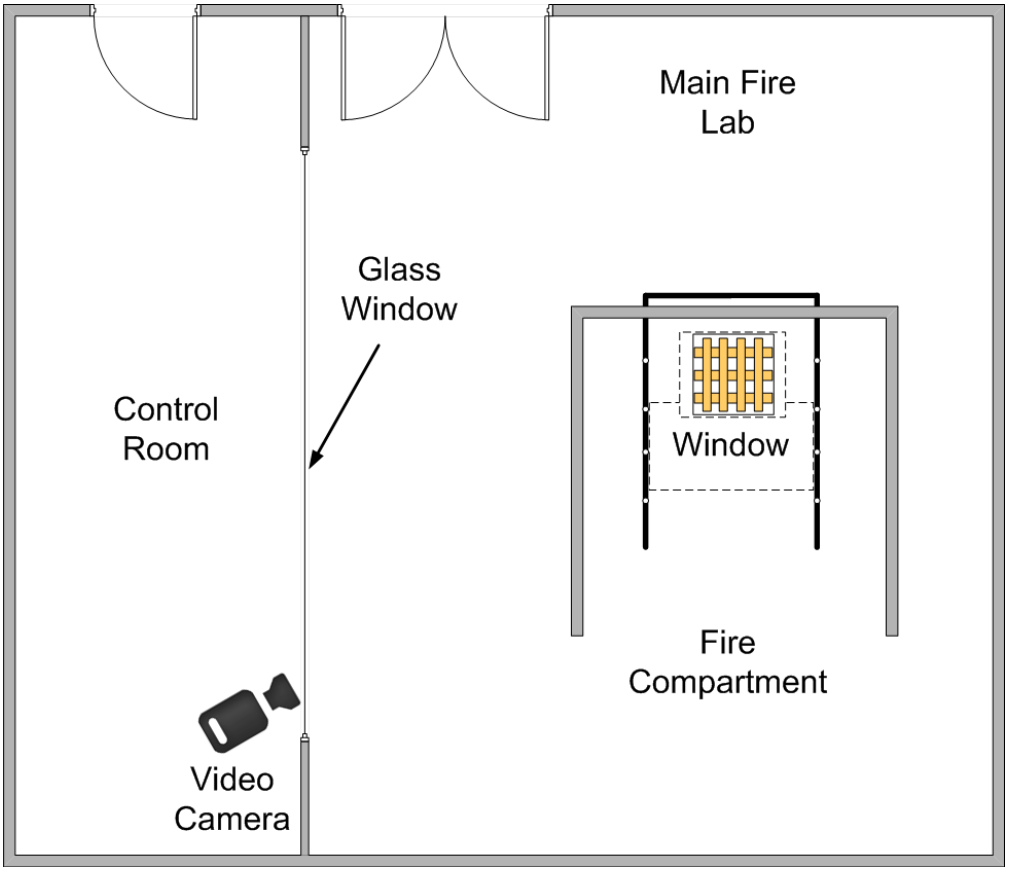


**Figure 3.8: Schematic diagram of the Main Fire Lab and the Control Room showing the position of the compartment and the video camera**

# 3.3 Experimental Measurements

## 3.3.1 Data Acquisition

All data were logged using the Universal Data Logging (UDL) system developed by University of Canterbury, which included both software and hardware interfaces. A total of forty-seven channels were monitored and logged using a Pentium 4 computer running Windows XP professional operating system. The system logged voltage at one sample per second from a wide range of measuring devices including temperature measuring thermal couples, pressure transducers, mass flow controller and gas analysers, and consists of both hardware and software interface. Figure 3.9 shows an example of the UDL software interface. The software could achieve live monitoring on a total of 10 channels. The upper five channels were set to monitor the desired thermocouples and the lower five channels were set to monitor the desired gas species from analysers for this particular research.

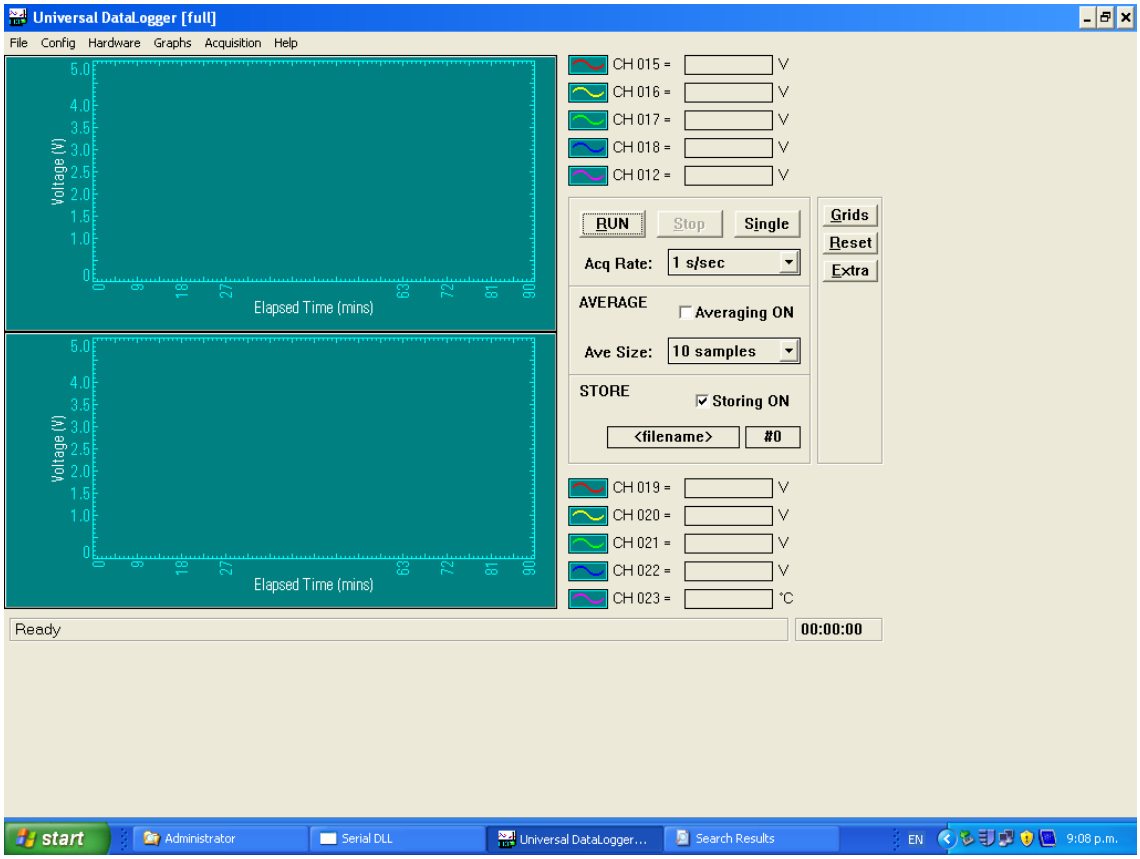


**Figure 3.9: The screen capture of the UDL software interface**

The change in voltage for each measuring device was buffered inside a serial box and transferred back to the computer. Subsequently, the UDL was used to both monitor and store the data into a CSV file, which could be further processed using a spreadsheet program. Temperatures were monitored and logged directly in ℃. Other measured variables such as pressure and gas concentrations were monitored and logged as a raw voltage.

### 3.3.2 Temperature

A total of twenty thermocouples were used to monitor the temperature within the compartment, so that a comprehensive temperature distribution across the height of the compartment could be obtained. Based on the analysis of the temperature data, the position of the neutral plane and the movements of the smoke layer could be estimated. All thermocouples were standard type K bare bead 24 gauge with glass insulation and protected within a 6 mm thick 316 stainless steel tube and sealed by RTV heat resistant silicone sealant, leaving only the bead exposed to the compartment environment. Thermocouples were designed to measure the temperature of the surrounding atmosphere, but in reality, it was the temperature of the thermocouple itself being measured. In order to reduce any errors caused by measurements being too close to the surface nearby, all thermocouples were placed 100 mm away from the boundaries. Finally, a metal flange was used to fasten the steel tube to the compartment as shown in the photograph of the compartment in Figure 3.10. Two thermocouple trees were placed vertically at the front and rear corner between ceiling and floor respectively. Figure 3.11 shows a schematic diagram of the compartment with the location of both front and rear thermocouple trees.

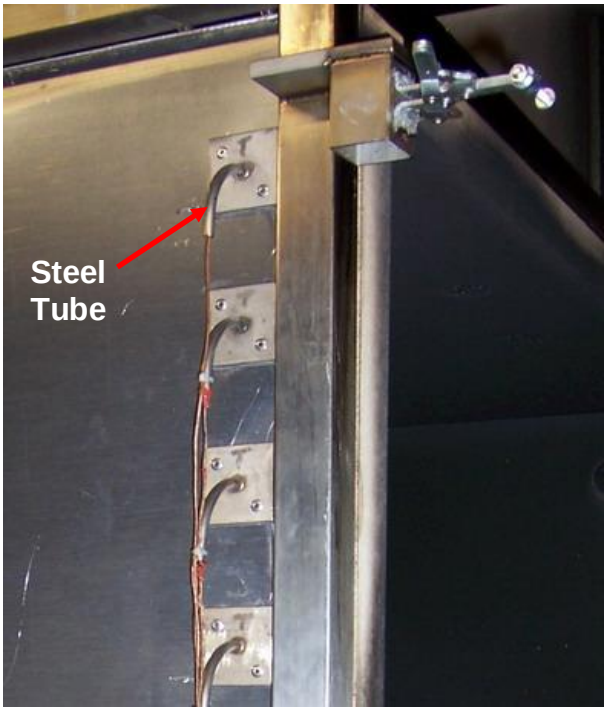


**Figure 3.10: Photograph of the protecting steel tube extended out of the compartment**

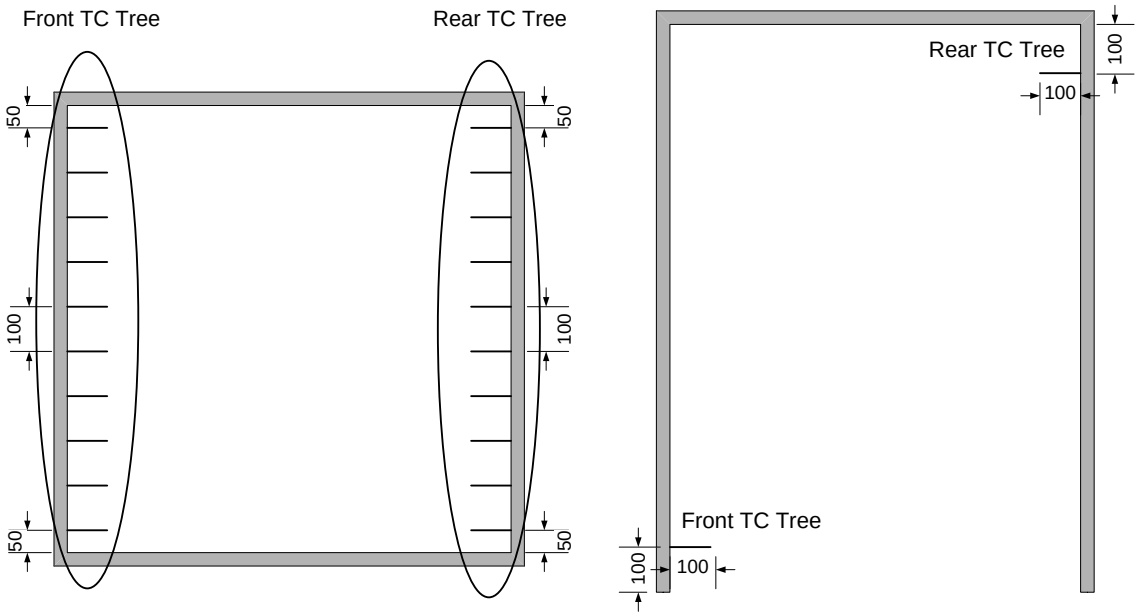


**(a)** **(b)**

**Figure 3.11: Schematic diagrams showing the location of thermocouple trees: (a) Front view of the compartment (b) Vertical view of the compartment (All dimensions are in mm)**

### 3.3.3 Compartment Pressure

In order to characterise the smoke explosion in terms of the pressure, a differential pressure transducer was installed to monitor the pressure in the upper layer, to capture the pressure of the explosion. It had an output range from 0 – 1V which corresponds to 0 – 100 Torr. One end of the differential pressure transducer was located inside the compartment with a length of 100 mm from the wall. The probe was located 750 mm from the back wall and 225 mm from the ceiling as shown in the schematic diagram of the compartment in Figure 3.12. The other end of the differential pressure transducer was connected directly to the ambient with a glass-fiber filter to reduce fluctuation of ambient conditions.

### 3.3.4 Vent Flow

Two differential pressure transducers were installed to monitor the pressure at both upper and lower vents. They had an output range from 0 – 1V which corresponds to 0 – 10 Torr. Again, one end of the differential pressure transducer was located inside the compartment, and the other end was connected directly to the ambient with a glass-fiber filter. Two probes were both 100 mm long and 100 mm away from the hatch. The probe in the upper layer was 225 mm from the ceiling, while the probe in the lower layer was 240 mm from the floor. Probes were placed at the same height as the center of two vent openings, so that pressures would be measured on an isobaric plane with respect to the vents. Figure 3.13 shows a photo of the compartment with three pressure transducers mounted on the outside of the compartment. The temperature and pressure were available to calculate the vent flow velocity by applying the following equations presented by Emmons (2002),

$$\dot{V} = 0.93\sqrt{\frac{2\Delta p}{\rho}} \qquad \textbf{Equation 3.1}$$

where Δp is the pressure difference (Pa) across the vent and ρ is the density of the flow gas in $kg/m^3$,

$$\rho = \frac{352.8}{T} \qquad \textbf{Equation 3.2}$$

where T is the temperature in Kelvin.

To convert the volumetric flow to the mass flow,

$$\dot{m} = CA\dot{V}\rho \qquad \textbf{Equation 3.3}$$

where C is the flow coefficient (0.6 for an orifice), A is the area of the orifice in $m^2$.

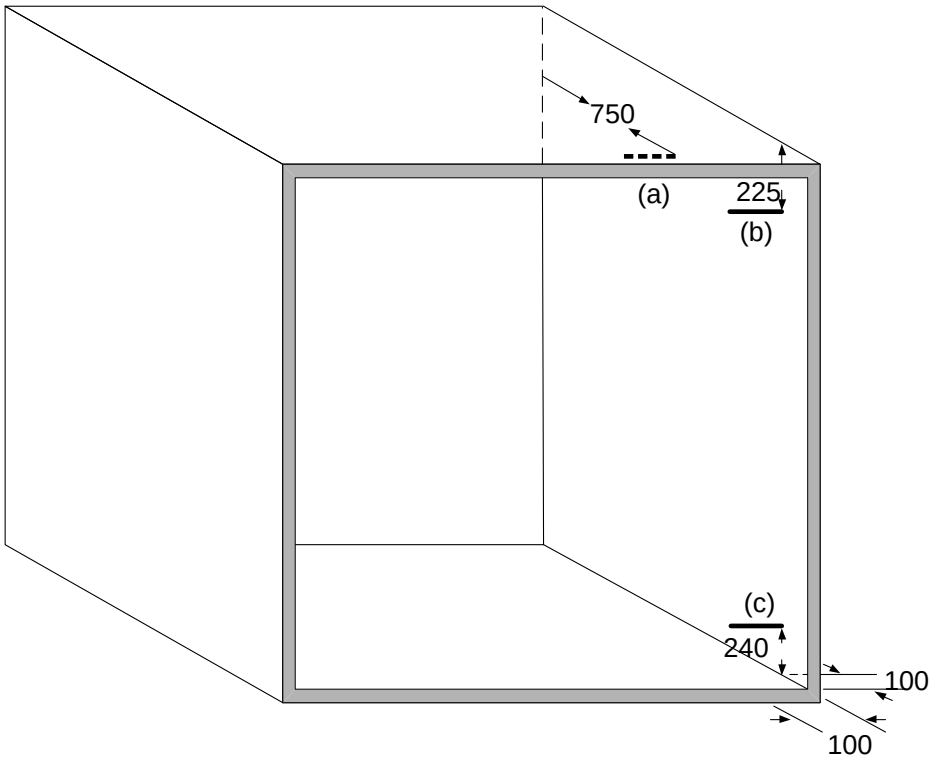


**Figure 3.12: Sketch of the compartment showing the positions of three pressure transducers: (a) Probe of the 100 Torr pressure transducer (b) & (c) Probe of the 10 Torr pressure transducer (All units are in mm)**

**Figure 3.13: Photograph of the compartment showing three pressure transducers**

### 3.3.5 Burning Rate

Wood was chosen to be the fuel for this particular research because firstly it was considered to be the most common building material widely used in New Zealand and it was found to be responsible for 74% of the explosions in fires (Croft 1980). Secondly, wood could produce a large amount of CO and unburned hydrocarbons under limited oxygen environment. Finally, it was essential to maintain the consistency between previous and present researches, because the first goal of this research was to reproduce smoke explosions given the experimental environment that was as identical as possible to the previous study. Hence, medium density fiber board (MDF) was chosen to be the fuel throughout the experiments, because the property of engineered wood product is homogenous and uniform comparing to unprocessed timbers.

A 30 mm thick MDF board was cut into 30 mm × 30 mm × 300 mm square sticks and nailed together at 30 mm spacing in a crisscross pattern. The ventilation within the wood crib was kept at minimum while still providing as much surface area as possible to produce a high level of carbon monoxide and unburned hydrocarbon. To be consistent with Sutherland's research, two sizes of cribs were chosen: 10 kg (300 mm × 300 mm × 300 mm) as shown in Figure 3.14 and 5 kg (300 mm × 300 mm × 150 mm) respectively. All cribs were conditioned under 25 ± 2 ℃ and 50% relative humidity environment for at

least two weeks prior to testing. The burning rate of the wood crib was calculated to be ventilation controlled. Detailed calculations were included in Appendix A.

**Figure 3.14: Photograph for the 10 kg wood crib**

The crib was located at the rear of the compartment (50 mm from the back wall) sitting on a loading table which could be placed at three different heights according to the requirement. The loading table was made of a 20 mm thick steel frame having dimensions of 350 mm × 350 mm × 20 mm, on top of which is a layer of 80 mm thick Kaowool ceramic fiber vacuum board as shown in the photograph of the loading table in Figure 3.15. The whole table was supported by four steel bars that extended through holes to the bottom of the compartment. Steel bars were replaceable making it possible to lower or raise the loading table. The other end of the bars sat on a Mettler Toledo load cell, as shown in Figure 3.16, in order to precisely monitor the mass loss history. The load cell was calibrated with two 5 kg weights since the experiments were designed to have two sizes of cribs (5 kg and 10 kg). The accuracy of the load cell was ±0.0005 kg.

**Figure 3.15: Photograph of the loading table inside the compartment**

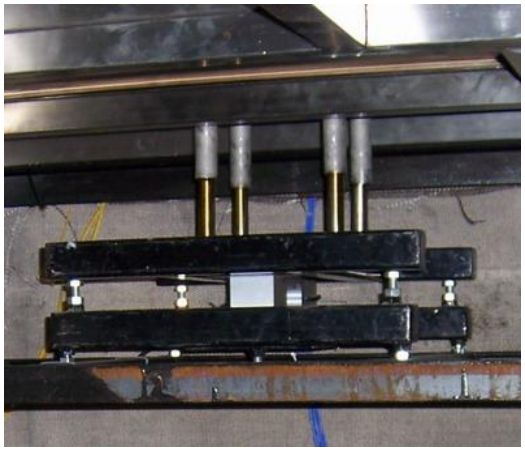

**Figure 3.16: Photograph of the load cell under the compartment**

The crib sat in a steel meshed cage to avoid wood falling off the loading table during experiments. In order to investigate the impact of fuel positions on crib burning behaviours, the transition between smoldering and flaming, and the time taken for explosions to occur, the loading table was designed to be adjustable with three heights as shown in the elevation view of the compartment in Figure 3.17. All locations were along the centerline and 50 mm away from the back of the compartment.

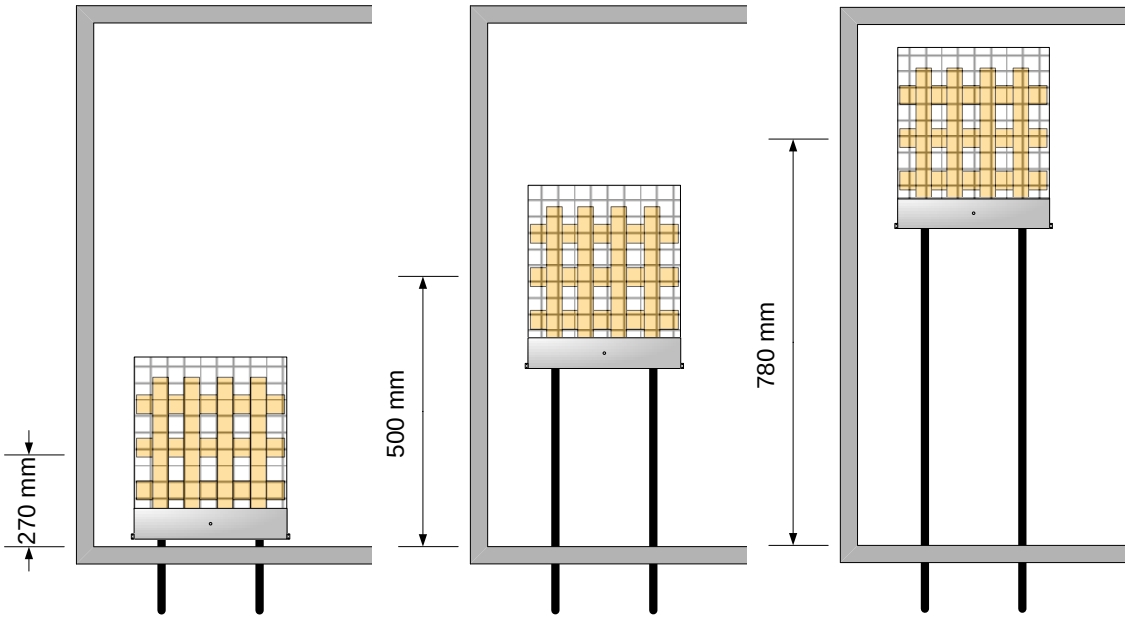


**Figure 3.17: Side view of the schematic diagram for three different crib locations (All dimensions are measured from the middle of the crib to the bottom of the compartment)**

### 3.3.6 Gas Species

Originally, three sampling tubes were made and located at three different heights to sample the gas mixture from upper layer, lower layer and middle of the compartment, so that a comprehensive gas concentration data at various locations could be obtained. They were constructed using 2 mm thick 316 stainless steel tube with five holes on each side of the u-shaped tube. Tubes had an internal diameter of 6 mm and each hole had a diameter of 1.5 mm (later increased to 2.5 mm to prevent blockage). The sampling tube spanned the depth of the compartment and was equally spaced from either side of the wall by 230 mm as shown in the schematic diagram of the compartment in both Figure 3.18 and Figure 3.19.

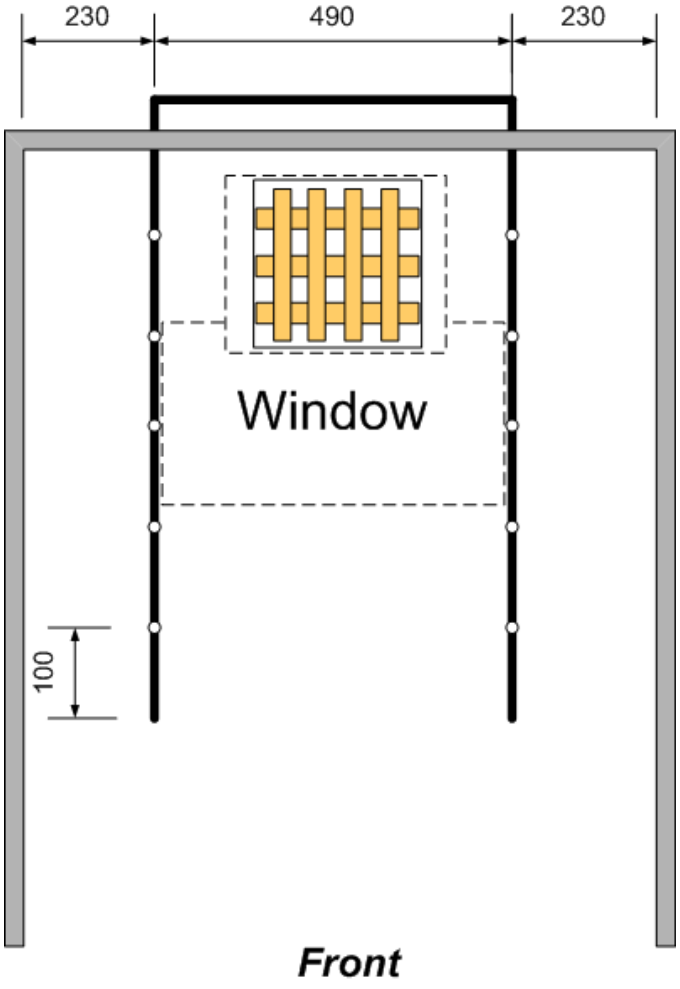


**Figure 3.18: Schematic diagram of the compartment showing sampling tubes in plan view (All dimensions in mm)**

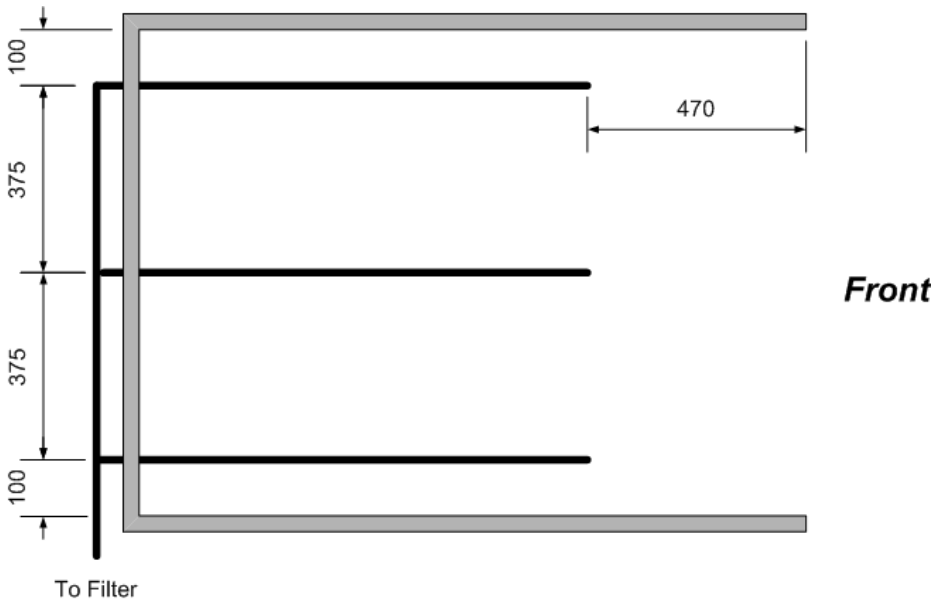


**Figure 3.19: Schematic diagram of the compartment showing sampling tubes at three different heights in side view (All dimensions in mm)**

Since the sampling tubes extended outside the compartment, holes going through the compartment boundary were sealed with RTV heat resistant silicone sealant. Tubes were wrapped with electric heating elements covered with reinforced glass fiber as thermal insulation to maintain the temperature of the sample gas as high as possible before being processed. Danco® 830 pure aluminium foil was used to secure the heating element and thermal insulation. Figure 3.20 shows the sampling tubes outside the compartment wrapped with thermal insulations.

The compartment gas was sampled at three different heights effectively creating three sample lines, but only one gas analyser could be dedicated for measuring all processed sample gases. The practical solution was to put a valve at the very end of sample lines. The valve was manually adjusted every 5 minutes switching from one sample line to another during experiments. Such method was proven to be tedious and inefficient but still served its purpose. The main disadvantage was that the valve became blocked up by the soot and tar as the experiment progressed, which provided insufficient mass flow for the gas analyser to work properly. Hence, the valve was discarded leaving only the upper layer gas concentrations being monitored during final experimental setup in order to prevent inaccurate measurements.

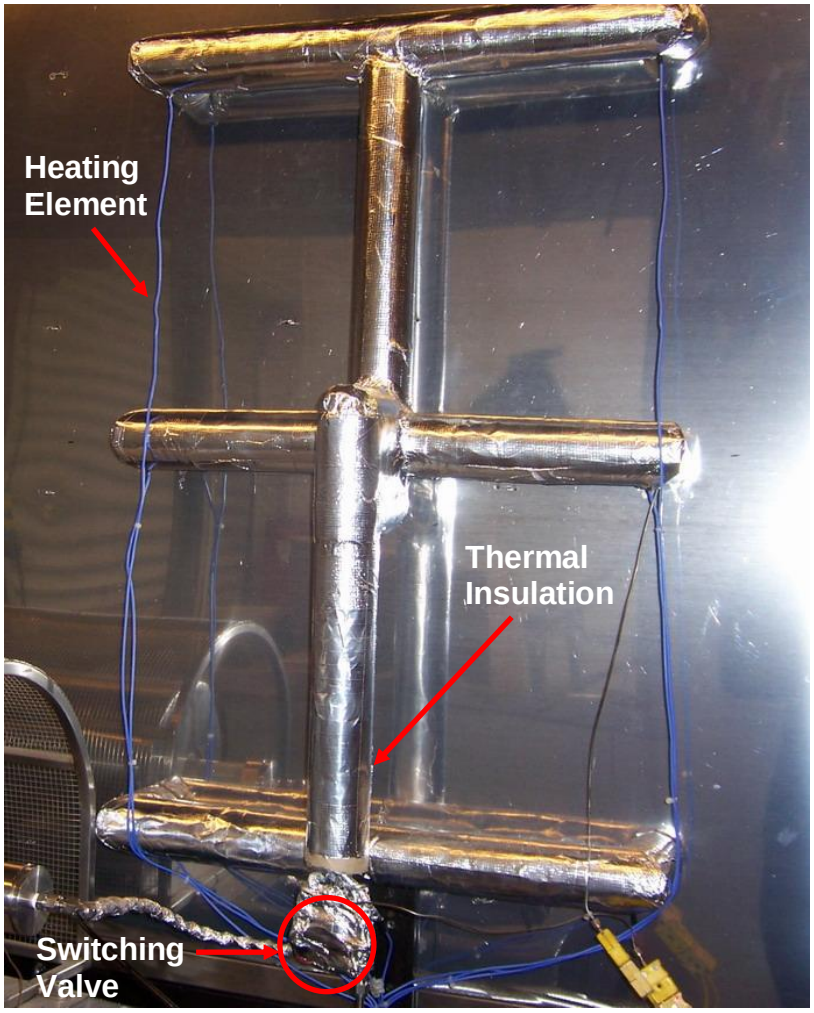


**Figure 3.20: Photograph for the back of the compartment showing wrapped sampling tubes**

Three sets of gas analysers were used to monitor concentrations of various gas species including CO, $CO_2$ and $O_2$. The first set was used to analyse the gas concentration on the samples directly taken out of the compartment and the second set was used to monitor the gas species after the sampled gas run through the furnace. The details of the furnace setup were included in section B.3. Figure 3.21 shows the first and second set of analyser. The third set was used to measure gas concentrations from furniture calorimeter as shown in Figure 3.22.

| Analyser Set | Apparatus | Gas Species | Objective |
|---|---|---|---|
| Furnace Analyser | Servomex 540A | $O_2$ | Monitor the gas species coming out of the furnace |
| | Siemens Ultramat 6 | CO, $CO_2$ | |
| Room Analyser | Siemens Ultramat 6 and Oxymat 6 | CO, $CO_2$ and $O_2$ | Monitor the gas species within the compartment |
| Hood Analyser | Siemens Ultramat 6 and Oxymat 6 | CO, $CO_2$ and $O_2$ | Calculate the heat release rate of each experiment |

**Table 3.1: Summary of descriptions and objectives for all three analyser sets**

All gas analyser sets had a similar hardware configuration. The main components of the gas sampling system included:

1. A 12V DC diaphragm pump to draw gas sample
2. A filter to block the soot
3. A cold trap that condenses the water from the gas sample
4. Drierite desiccant crystals that absorb the remaining water passed through the cold trap

All gas analysers were calibrated prior to the start of the first experiment of that day to ensure the experimental results were valid. The calibration was carried out using gases of known concentrations. The gases used are 99.99% Nitrogen and a combination of 16% $O_2$, 4.51% $CO_2$ and 0.794% CO (7940 ppm). Firstly, the $O_2$, $CO_2$ and CO analysers were all "zeroed" using 99.99% Nitrogen. Secondly, the analysers were calibrated using atmospheric $O_2$ to ensure that the oxygen analyser gave a voltage corresponding to 20.95% atmospheric $O_2$. Lastly, the $CO_2$ and CO analyser span was calibrated using the combined gases 16% $O_2$, 4.51% $CO_2$ and 0.794% CO (7940 ppm) to ensure that instrument readings gave correct corresponding gas percentages.

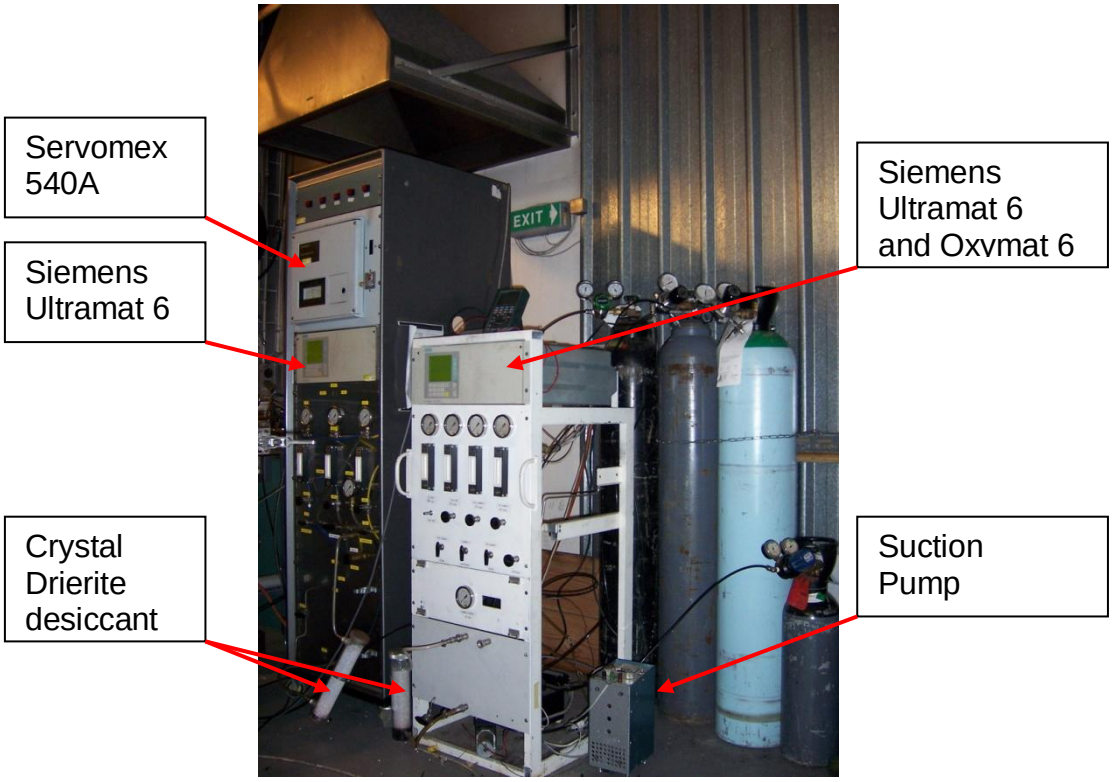


**Figure 3.21: Photograph of both gas analysers (a) room analyser on the left (b) furnace analyser on the right**

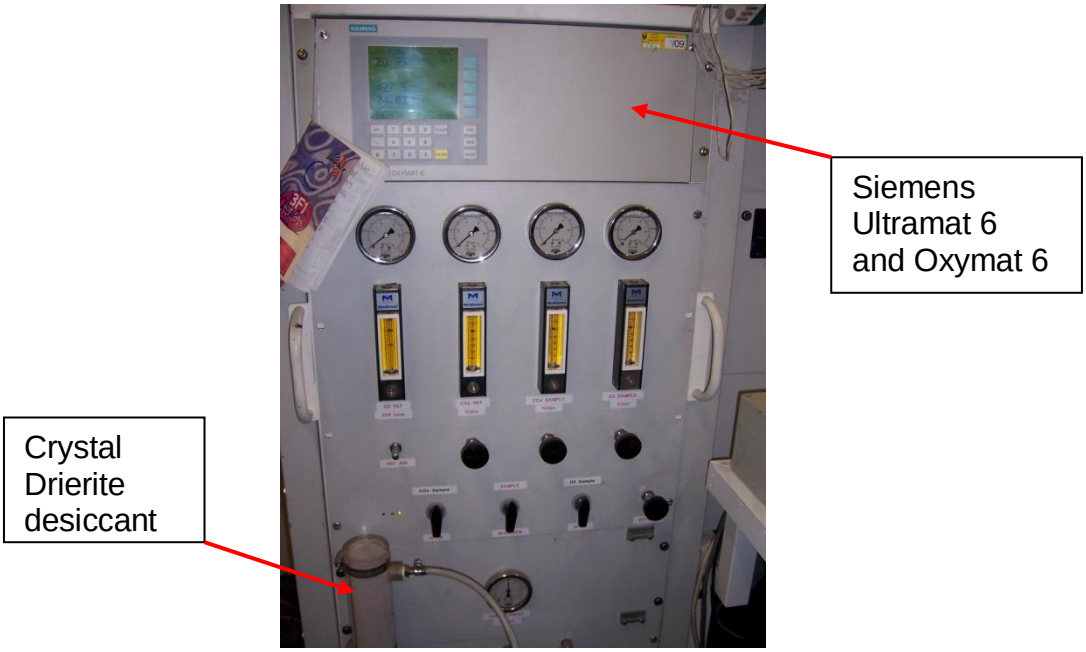


**Figure 3.22: Photograph of the hood analyser**

# 3.4 Final Setup and Procedures

## 3.4.1 Experimental Setup

All instruments discussed above, including the compartment gas analyser, loading scale, thermocouples, pressure transducers and data logging system were all incorporated into the final setup. The Phi-Meter system was originally constructed to measure the unburned fuel, however there were errors found within the Phi-Meter system during the calibration. Although attempts had been made to resolve the issue, ultimately time pressure on the equipment and laboratory space prevented the possibility of pursuing the Phi-Meter system any further. The detailed development of the Phi-meter system was included in Appendix B. The following figures include schematic diagrams of the compartment layout with all the measuring components and detailed dimensions, followed by an updated schematic diagram of the gas sampling system.

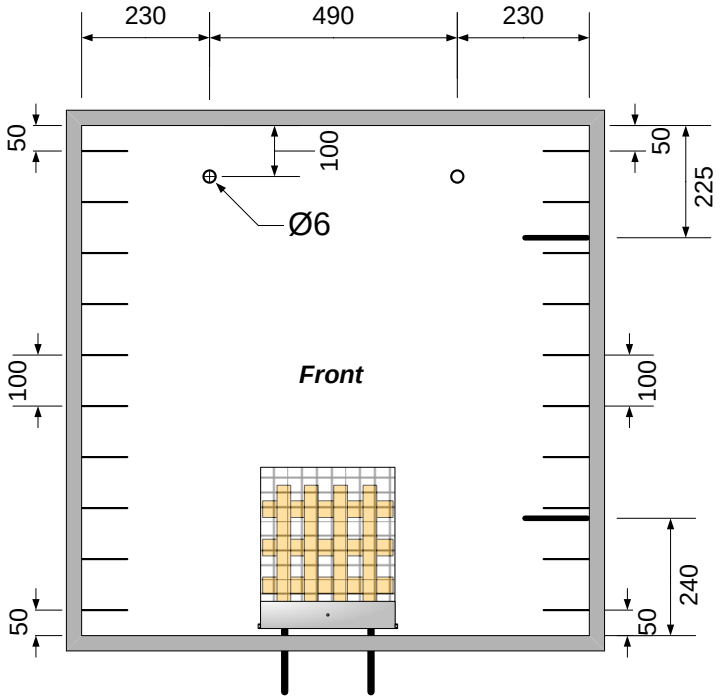


**Figure 3.23: Schematic diagram of the compartment in front view (all units in mm)**

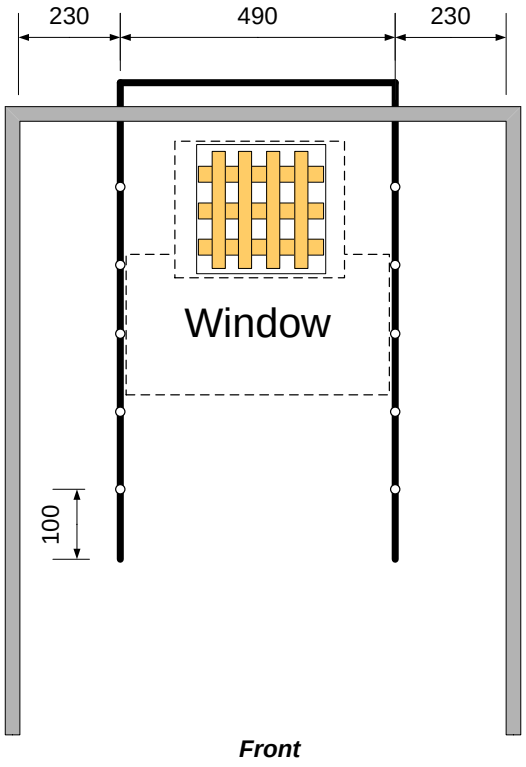


**Figure 3.24: Schematic diagram of the compartment in top view (all units in mm)**

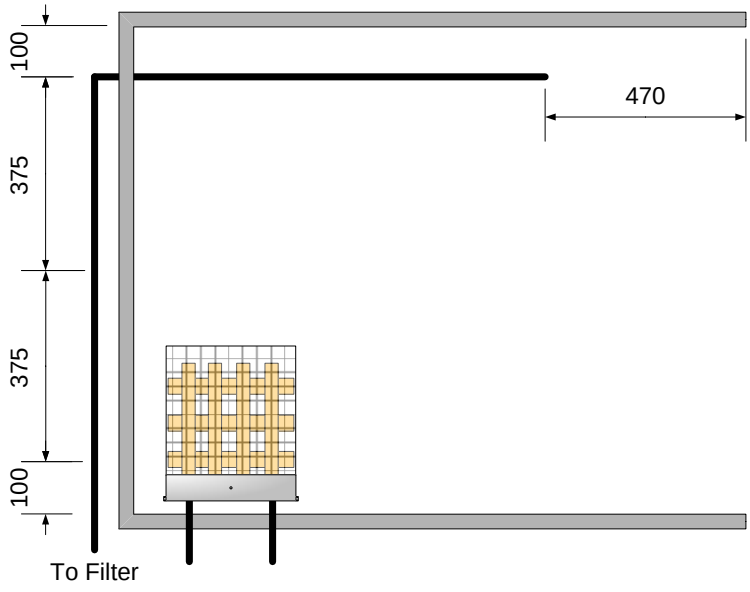


**Figure 3.25: Schematic diagram of the compartment in side view (all units in mm)**

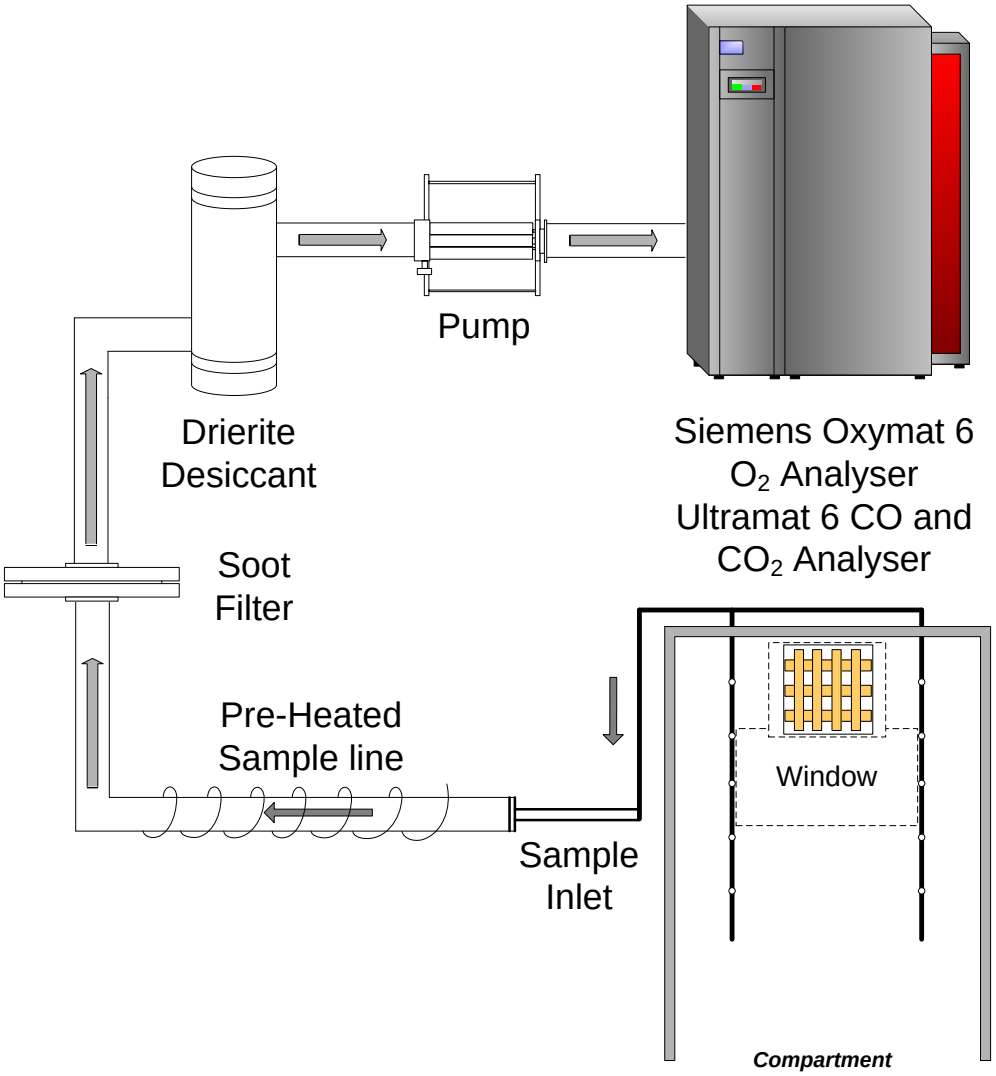


**Figure 3.26: Schematic diagram of the final gas sampling system**

## 3.4.2 Experimental Preparations

Each experiment started with the calibration of the UC Furniture Calorimeter and the gas analyser. The calibration procedures had been specifically designed for the University of Canterbury Furniture Calorimeter. Refer University of Canterbury Fire Lab Furniture Calorimeter Calibration and Testing Procedure (1999) for all the detailed calibration procedures. While the calibration was in progress, the wood crib was weighed and recorded. Ambient temperature and humidity of the day prior to the experiment were recorded. Filter papers were changed and the sampling tubes were cleaned thoroughly prior to the experiment.

### 3.4.3 Experimental Procedures

1. A 3-minute baseline of the ambient condition was logged before the ignition of the wood crib. The video camera placed under the compartment was turned on after the 3-minute baseline. The second video camera inside the control room was turned on after the compartment was shut.

2. Once the crib was in position, a cup of 200 ml methylated spirits was poured into the cage and lit up to stimulate the combustion of the wood crib. Generally, a minute was needed for the fire to be become established before closing the compartment hatch. The elapsed time of each experiment varied from 45 minutes to 3 hours depending on the ventilation condition and the fuel size.

3. The end of the experiment was declared when no visible smoke was ventilating from the upper opening vent and/or the mass of the remaining fuel was less than 20%. Once it reached the end of experiment, the compartment hatch was removed and the crib would re-ignite from the fresh air, extra cautions needed to be taken at that time. The burning crib was extinguished with a water spray to the front and side of the crib to ensure re-ignition would not happen again. Due to the high temperature of those experiments, the compartment needed to be cool down prior to the next experiment.

# Chapter 4 Exploratory Experiments

## 4.1 Introduction

A total of eleven exploratory experiments were carried out prior to the final set of experiments. The first three experiments were carried out to reproduce smoke explosion phenomena based on the study done by Sutherland. The remaining 8 experiments were carried out to explore the impact of fuel height and fuel mass, in order to develop the final experimental matrix for a more thorough investigation of the smoke explosion phenomena.

The fuel mass and vent size was used to examine both the impact on the room temperature, mass loss, heat release rate and the impact on the smoke explosion. In experiment 10-F-100, 10-F-71 and 10-F-50, a 10-kg wood crib was placed 270 mm above the floor with the vent diameter varying from 100 mm to 50 mm. In experiment 10-M-100, 10-M-71, 10-M-50, 10-M-36, and 10-M-25, a 10-kg wood crib was placed 500 mm above the floor with the vent diameter varying from 100 mm to 25 mm. In experiment 5-M-100, 5-M-71 and 5-M-50, a 5-kg wood crib was placed 500 mm above the floor with the vent diameter varying from 100 mm to 50 mm, excluding 36 mm and 25 mm, because experiments with vent diameter less than 50 mm took excessively long time and the filters became saturated with water, therefore affecting the final measurements. Additionally, the smoke explosion never occurred in the 10-kg experiments with 36 mm and 25 mm vents.

The eleven experiments are summarised in Table 4.1, where column 1 is the code for each experiment consists of fuel mass, fuel elevation and vent size, column 2 is the mass of the fuel, column 3 is the elevation of the crib measured from the floor level of the compartment to the geometric center of the crib, column 4 is the size of vents on the compartment hatch, column 5 and 6 are the time and temperature when the smoldering decay occurred, column 7 is the time when the first smoke explosion occurred, column 8 and 9 are the temperature before and after the smoke explosion, column 10 indicates the occurrence of smoke explosions, column 11 indicates the occurrence of the ghosting fire and column 12 indicates whether smoldering occurs during prior to the smoke explosion.

| Experiment Code | Fuel mass (kg) | Fuel Elevation (mm) | Vent Size (mm) | $t_D$ (min) | $T_D$ (℃) | $t_E$ (min) | $T_{E_0}$ (℃) | $T_{E_1}$ (℃) | GF | SD | SE |
|---|---|---|---|---|---|---|---|---|---|---|---|
| 10-F-100 | 10 | 270 | 100 | N/A | N/A | N/A | N/A | N/A | YES | YES | 0 |
| 10-F-71 | 10 | 270 | 71 | 35 | 550 | 72 | 420 | 610 | YES | YES | 1 |
| 10-F-50 | 10 | 270 | 50 | 21 | 220 | 138 | 355 | 490 | YES | YES | 1 |
| 10-M-100 | 10 | 500 | 100 | 24 | 610 | 37 | 500 | 560 | YES | YES | 22 |
| 10-M-71 | 10 | 500 | 71 | 25 | 500 | 43 | 300 | 620 | YES | YES | 2 |
| 10-M-50 | 10 | 500 | 50 | N/A | N/A | N/A | N/A | N/A | YES | YES | 0 |
| 10-M-36 | 10 | 500 | 36 | N/A | N/A | N/A | N/A | N/A | NO | NO | 0 |
| 10-M-25 | 10 | 500 | 25 | N/A | N/A | N/A | N/A | N/A | NO | NO | 0 |
| 5- M -100 | 5 | 500 | 100 | N/A | N/A | N/A | N/A | N/A | YES | NO | 0 |
| 5- M -71 | 5 | 500 | 71 | N/A | N/A | N/A | N/A | N/A | YES | NO | 0 |
| 5- M -50 | 5 | 500 | 50 | 92 | 305 | 99 | 280 | 500 | YES | YES | 4 |

**Table 4.1: Summary data for exploratory experiments showing the experimental conditions; time and temperature at the smoldering decay; time of the first smoke explosion and the temperature (before and after) the first smoke explosion; GF = the occurrence of the ghosting fire; SD = the occurrence of the smoldering decay, and SE = total numbers of explosions (N/A = Not applicable since no explosions occurred)**

## 4.2 Detailed Smoke Explosion Scenario

The smoke explosion scenario presented in this research was described as a rapid deflagration of accumulated flammable gases including excess pyrolysates and carbon monoxide inside a ventilation limited compartment. The explosion was often accompanied by flames shooting out through the openings. The smoke explosion was also identified by a sudden increase in the compartment temperature history. Heat release rate was not used as an indicator for the smoke explosion as the measured data was too noisy and outside range of accurate measurement for the furniture calorimeter.

Experiments 10-F-71, 10-F-50, 10-M-100, 10-M-71 and 5-M-50 resulted in smoke explosions judging from the video footage and temperature increase. Among all five experiments where smoke explosions occurred, experiments 10-F-71, 10-F-50, 10-M-100, and 10-M-71 all shared a common trend of the fire development as shown in the temperature histories in Figure 4.1 and Figure 4.2. The temperature readings from the top (950 mm) rear thermocouple were utilised only as an illustration of a typical temperature history. A complete set of temperature histories for all thermocouples were listed in Appendix C. The fire development could be generally divided into five phases. Each phase would be described separately in the following section, in order to provide a better insight of the smoke explosion phenomenon. Experiment 5-M-50 would be discussed separately in section 4.3.3.

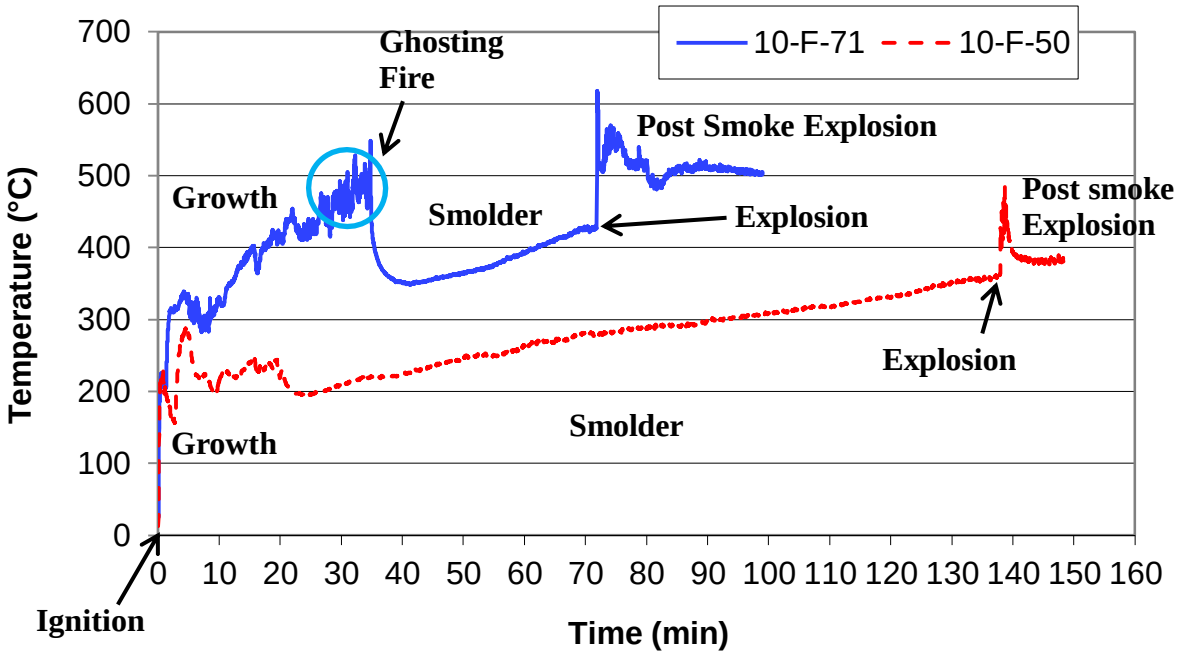


**Figure 4.1: Temperature histories from the rear top (950 mm) thermocouple for experiment 10-F-71 and experiment 10-F-50**

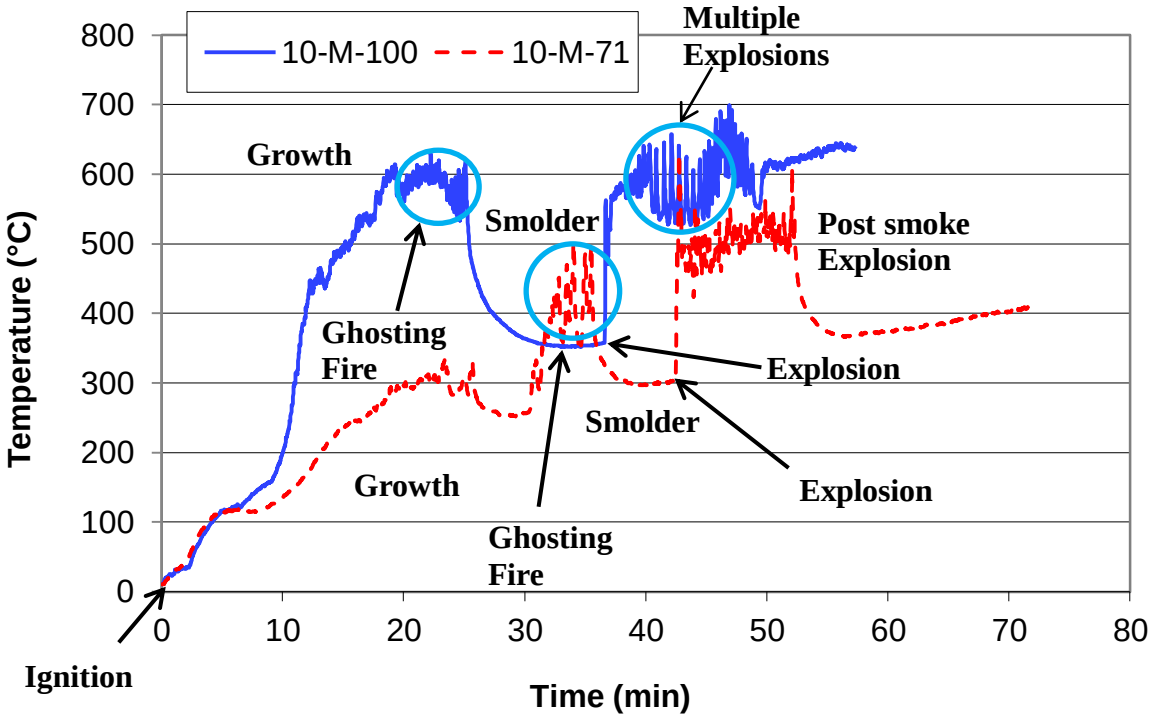


**Figure 4.2: Temperature histories from the rear top (950 mm) thermocouple for experiment 10-M-100 and experiment 10-M-71**

### *Phase I: Ignition*

200 ml methylated spirits was poured on top of the crib. Once the methylated spirits was ignited, the compartment was left open to allow the fire to become established over the crib. The methylated spirits gave a rapid development of the fire in terms of a sudden increase in the temperature from the ambient condition to around 200 ℃ as shown in Figure 4.1. During that period of time, only light smoke was seen as hot gases flew out of the compartment. The compartment hatch was closed at 60 seconds after the ignition.

### *Phase II: Growth*

Once the compartment hatch was shut, only two opening vents were left for combustion gas to flow out and ambient air to flow in. During phase II, the compartment environment was transitioning from oxygen rich to oxygen lean, because the air inlet was severely limited by the bottom vent. At the beginning of Phase II, only clear hot gases were observed exciting from the top vent suggesting near complete combustion. As the experiment progress, the intensity of the flame decreased as the methylated spirits was consumed. Meanwhile, smoke might be visible at the top vent depending on the fuel elevation and vent opening sizes. After a period of time, light grey smoke starts to flow out of the top vent. Experiments with larger vent openings had a longer waiting time before the smoke being visible, as compared to the smaller vent openings. Subsequently, the smoke changed from light grey to thick grey.

As the fire developed, the compartment temperature started a steady growth as the fire in the crib became established until the temperatures rose to the first peak as seen in Figure 4.1 at 8 minutes and Figure 4.2 at 20 minutes. The temperature rise was proportional to the size of the vent. The peak temperature values were quite diverse ranging from 300 ℃ to 600 ℃ due to the availability of the oxygen supply coming from the bottom vent opening and the position of the fuel.

At the end of phase II, the fire started to detach from the crib once the temperature reached the first peak. As the intensity of the flame increased, the flame slowly migrated from the center of the crib to the surrounding space of the crib. The phenomenon regarding the detached flame was referred as ghosting fires and had been observed by

Sugawa et al. (1991) in their experiments. They referred this detached flame as ghosting fires, where flame completely detached from the fuel and burnt alone in the upper layer. The oxygen starvation was believed to be one of the causes for ghosting fires, but the mechanism of ghosting fires was yet to be fully understood. The ghosting fire was often accompanied with smoke shooting out of the compartment during smoke explosion experiments. When the flame propagated and spread out, the volume of the burning gas increased, which generated a positive pressure. Then, the smoke was forced out through the top vent due to the positive pressure. As the temperature decreased, a negative pressure was created in the lower layer, so that the cool air was drawn into the lower layer through the bottom vent. This in and out movement of the smoke was referred as pulsation. When enough oxygen mixed with the upper layer, the flaming combustion occurred, hence going into another cycle of ghosting fires. Such cycle was observed and repeated before the combustion transitioned to smoldering. Not only was the ghosting fire evidenced by the pulsation of the smoke, it was also seen from the fluctuation of the temperature profile as highlighted in Figure 4.1 and Figure 4.2. However, the ghosting fire did not necessarily lead to smoke explosions. A brief development of the ghosting fire using video captures from experiment 10-M-100 was included in Figure 4.3.

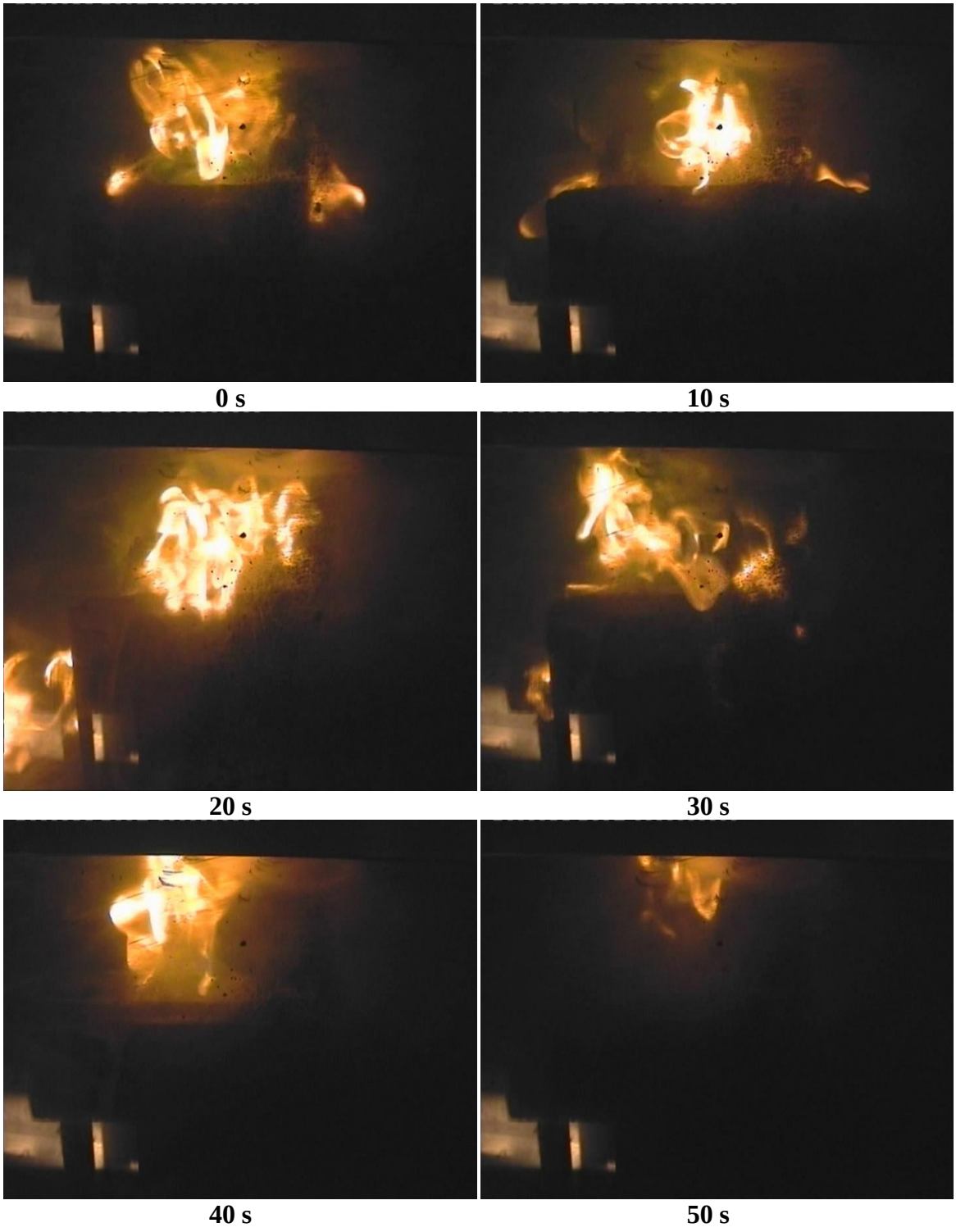


**Figure 4.3: Video captures of experiment 10-M-100 showing the ghosting fire period: The flame starts to detach from the crib at 0 second and then migrates to both sides of the crib. Flames start to appear at the bottom left corner at 20 seconds. As the ghosting fire develops, the intensity of the flame keeps diminishing until it self-extinguishes at 50 seconds. (All images are taken from the video camera placed under the compartment)**

### *Phase III: Smolder*

The beginning of phase III could be easily identified by the disappearance of the flame. The oxygen depletion was believed to cause the transition from flaming to smoldering, but the amount of oxygen at which the smoldering started to develop was very case-dependent. Once the flame self-extinguished, the crib started to smolder with glowing embers on the surface and all the fuel vapors would go directly into the atmosphere (compartment). Usually, the glowing embers started to appear a few minutes after the flame self-extinguished. Then the intensity and the size of the glowing region gradually increased as the experiment progressed until the explosion occurred. It was observed that the flame resumed in some cases during smoldering combustion, which occurred in experiments with the vent size less than 50 mm. Such smoldering and flaming transition often cycled several times before it settled. The glowing embers on the crib were believed to be the cause for both the smoke explosion and crib re-ignition. The smoldering phase was projected as an exponential decay in the temperature profile indicated in Figure 4.1 and Figure 4.2. The decay phase continued until the smoke explosion occurred or the experiment was terminated. Larger vents did not necessarily lead to a longer smoldering decay. In experiment 10-F-71 and 10-F-50, where the crib was placed near the floor level, the smoldering decay lasted longer for a smaller vent. The smoldering decay was only observed in experiment 10-F-71, 10-F-50, 10-M-100, 10-M-71, and 5-M-50 where smoke explosion were present. Detailed analysis from the video footage and gas concentrations were presented in Chapter 5.

## *Phase IV: Smoke Explosion*

The time when smoke explosions occurred was very case dependent and unpredictable, which was one of the hazardous smoke explosion characteristics. Smoke explosions were observed in experiment 10-F-71, 10-F-50, 10-M-100, 10-M-71 and 5-M-50. The increase of temperature in experiment 10-F-71, 10-F-50, 10-M-100, and 10-M-71 at the smoke explosion varied between 150 ℃ to 300 ℃, and the peak temperature after the smoke explosion varied between 500 ℃ to 600 ℃. These temperature rises were only indicative since the thermocouples were not capable of responding fast enough to truly capture the full intensity of the smoke explosion.

Figure 4.4 included a series of video images showing the development of the smoke explosion as the flame and smoke shoot out through the openings for experiment 10-M-100. The video camera was placed in the control room and the video time started from ignition of the smoke explosion at the crib. The images were taken at an interval of 0.3 second. The smoke explosion always started with a large quantity of smoke discharged through the top vent, due to the thermal expansion from the explosion inside the compartment, followed by a meter-long flame shooting out of the compartment through the top vent as shown in Figure 4.4. The smoke was pushed out of the compartment with a very high velocity impinging on the wall of the lab 3.5 meters from the front of the compartment. The structure of the flame was known as a jet flame confined by the orifice plate. It was a premixed flame where fuel and air were mixed prior to the ignition compared to a non-premixed flame where the fuel and air were separate prior to the ignition. In the fourth image of Figure 4.4, the flame started to recede as the premixed combustible gases were consumed. After 0.3 second, another stream of smoke, shorter in length, shot out of the bottom vent right after the upper flame receded, followed by a short flame. The discharge of smoke and flame at the bottom was believed to be caused by the flame expansion.

**0.0 s**

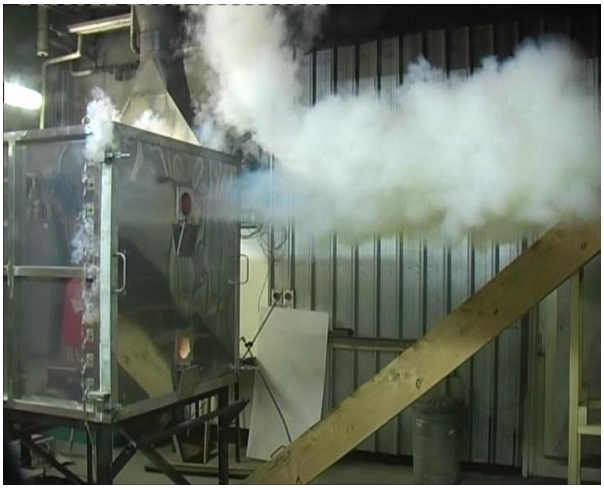

**0.3 s**

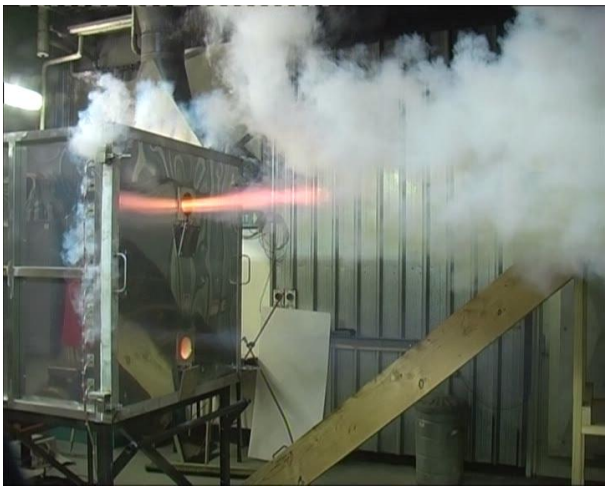

**0.6 s**

**0.9 s**

**1.2 s**

**1.5 s**

**Figure 4.4: Video captures of experiment 10-M-100 showing the flame and the smoke shooting out through the top vent**

Figure 4.5 included a series of 16 video images showing the development of the explosion for experiment 10-F-71. The video camera was placed under the compartment, which provided more insight into the development of smoke explosions in terms of how the flame propagated. The images were taken at an interval of 0.1 second. As previously mentioned, the glowing ember on the crib was believed to be the ignition source of the explosion, which could be supported by the video footage best seen in experiment 10-F-71. Immediately before the explosion, the wood crib was smoldering with glowing embers on the surface. Without any warning signs, a flame suddenly appeared in the center of the crib as seen in Figure 4.5 at 0.1 second. The flame then spread through the surrounding combustible gases. The ignition started as a small flame inside the crib and expanded to a large fireball filling the entire compartment in 1.8 seconds. From the video images, it could be seen that, the majority of the fireball was located in the upper layer, although the wood crib was placed at 270 mm above the compartment floor. Because, the flame expanded upwards due to buoyancy, the built up pressure forced the combustible gases out through the top vent burning the gases outside the compartment. The expansion forced the gases below the flame downward through the lower opening. As the flame propagated, the gases below the flame were ignited as seen in Figure 4.4 at 1.2 seconds.


**0.0 s**

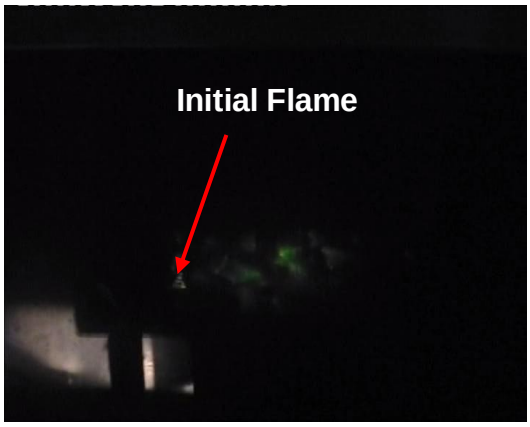


**0.1 s**

**0.2 s**

**0.3 s**

**0.4 s**

**0.5 s**

**0.6 s**

**0.7 s**

**0.8 s** **0.9 s**

**1.0 s** **1.1 s**

**1.2 s** **1.3 s**

**1.4 s** **1.5 s**

**Figure 4.5: Video captures of experiment 10-F-71 showing the flame filling up the entire compartment**

For those experiments with a single explosion, the wood crib often re-ignited after the first explosion and eventually burned out. However, in experiment 10-M-100 and 10-M-71, in which multiple smoke explosions were observed, especially in experiment 10-M-100, the subsequent explosions were repetitive with the same pattern for each explosion. The video footage of the bottom camera showed that the whole system went into the cycle of patterns as illustrated in Figure 4.6. The explosion created a gas expansion and temperature rose, which pressurised the whole compartment forcing a large amount of smoke out of the compartment. However, the temperature within the compartment quickly fell down to pre-explosion level, creating a negative pressure within the compartment relative to the surrounding environment. Fresh air was drawn into the compartment through the bottom vent due to the negative pressure. Once the ventilation was re-established, the compartment went back to the buoyancy driven regime. Meanwhile, the smoldering combustion continued to develop until another explosion occurred. Ultimately, the combustion broke out of the multi-explosion cycle and the wood crib switched back to flaming combustion until it burned out.

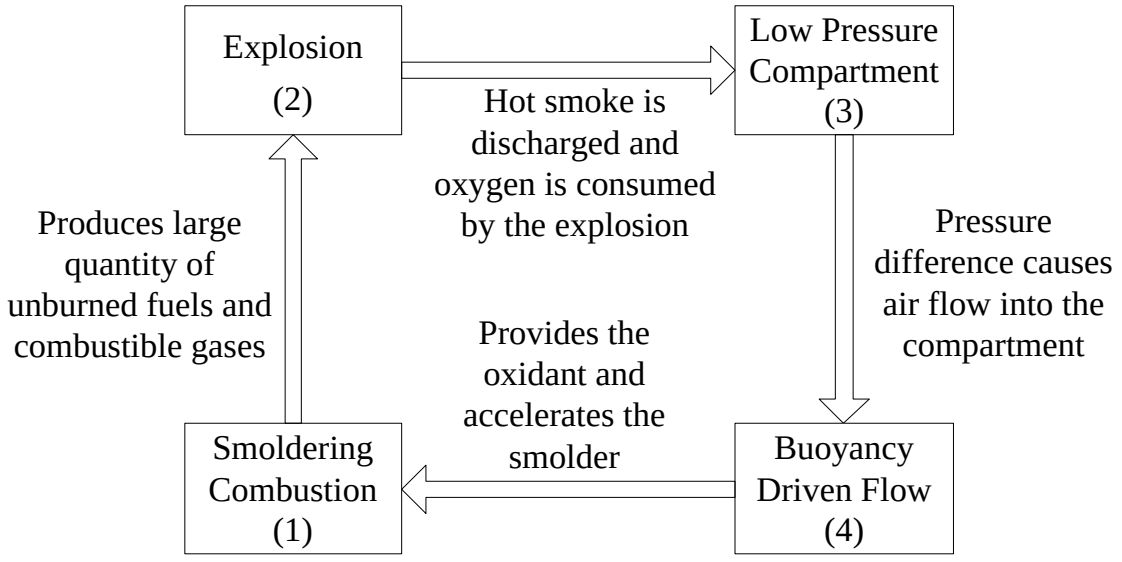


**Figure 4.6: Flow chart diagram for the process of multi-explosion scenario**

### *Phase V: Post Smoke Explosion*

All experiments were terminated according to pre-set criteria described in section 3.4.3, which led to a situation that the temperature might still be very high. Depending on a particular experiment, there were basically three types of post smoke explosion scenarios observed in all experiments. The first scenario was that the flame self-extinguished after the explosion as suggested in the temperature history of experiment 10-F-71 and 10-F-50. The video footage showed that there was no flame associated with the temperature decay. The second scenario was that the flame self-extinguished after the explosion, but the flame quickly came back with less intensity, usually referred as lazy flames. These lazy flames danced around the crib until the fire went into the smoldering decay as shown in the temperature history of experiment 10-M-71 in Figure 4.2. The third scenario was observed in experiments with multiple explosions. The flame self-extinguished after the explosion, and the flame quickly came back as in scenario two. But instead of going into the decay, the fire turned into a cycle of smoke explosions as shown by the temperature history of experiment 10-M-100 in Figure 4.2. Finally, the lazy flame became established and remained until the fire was completely extinguished.

## 4.3 Specific Experimental Results

### 4.3.1 10 kg Crib At Floor Elevation

As previously mentioned, the data collected during the exploratory period of the research were limited to temperature, mass loss history and heat release rate. Only temperature history for experiment 10-F-100 would be discussed in this section. Experiment 10-F-71 and 10-F-50 had already been discussed in section 4.2. The temperature histories from the rear thermocouple tree for experiment 10-F-100 are shown in Figure 4.7. The complete set of temperature histories could be found in Appendix C. It could be seen from Figure 4.7 that the data from the top rear thermocouple best reflected the value and the dynamic change of the compartment temperature. For the benefit of discussion in this research, the temperature data from the top rear thermocouple would be used to outline the complete temperature histories for all experiments. The ignition started at time 0. After the compartment was shut at 1 minute, the temperature quickly went up until it reached 13 minutes where the temperature changed from a rapid increase to a steady and slow increase. At 26 minutes, a spike appeared in the temperature histories as a result of the ghosting fire. As seen on the video footage, the flames on the crib suddenly detached and spread onto the floor. Not until 45 minutes, a small flame restored on the crib. The fire kept burning for the rest of the experiment without noticeable change of the flame.

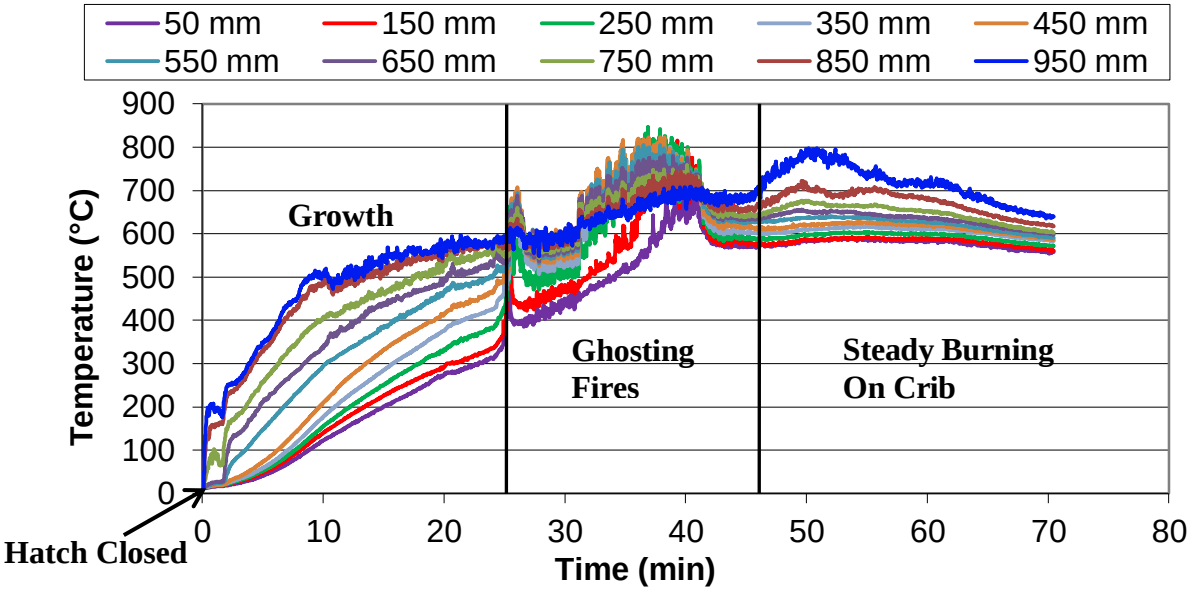


**Figure 4.7: Temperature histories from the rear thermocouple tree for experiment 10-F-100**

The mass loss histories for experiment 10-F-100, 10-F-71 and 10-F-50 are shown in Figure 4.8, and the corresponding heat release rate histories are shown in Figure 4.9. The mass loss curves were quite distinguishable in terms of their slopes, although experiment 10-F-100 and 10-F-71 had a similar slope at the beginning and towards the end of the experiment. For experiments with smaller vents, the whole burning process lasted longer because smaller vents provided less oxygen and the crib burned slower. For the 100 mm opening, the whole experiment lasted approximately 70 minutes. The mass loss curve started off very smoothly until around 23 minutes when the ghosting fires started to appear. The point of discontinuity at 57 minutes was caused by pieces of crib falling off the loading table. There was no smoke explosion for the 100 mm opening experiment. For the 71 mm opening, the experiment took approximately 100 minutes to finish, during which time a smoke explosion occurred at 72 minutes. For the 50 mm opening, the experiment took more than twice as long as the 100-mm experiment, to consume the fuel until it reached 20% of its original mass. The smoke explosion occurred at 127 minutes broke the crib as indicated in Figure 4.8.

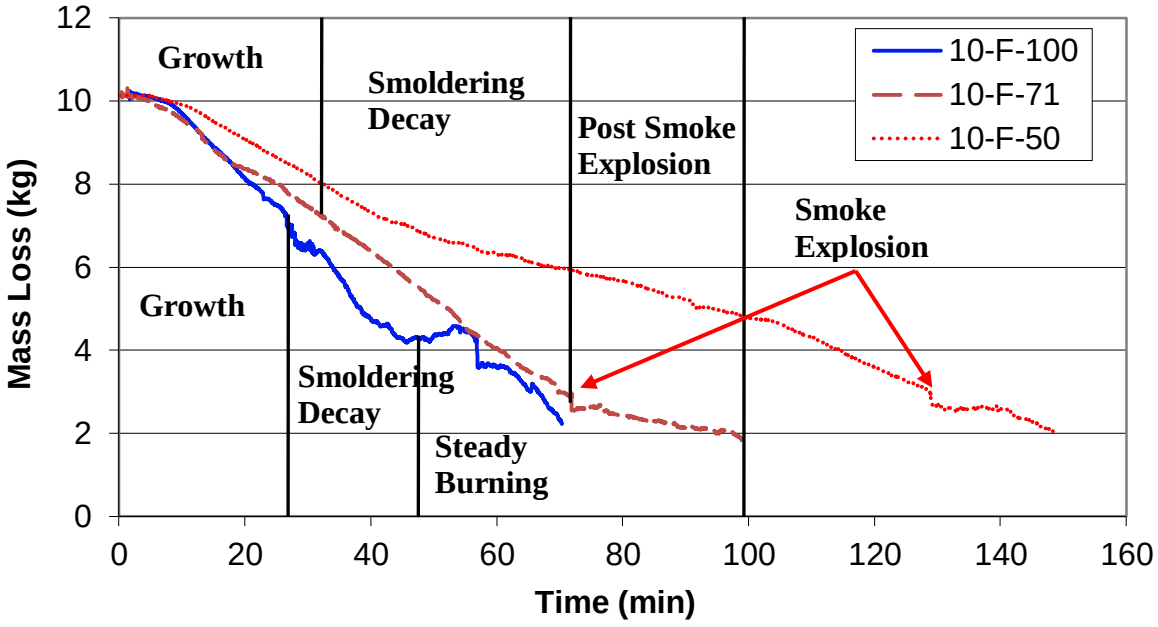


**Figure 4.8: Mass loss histories for experiment 10-F-100, 10-F-71 and 10-F-50**

The heat release rate histories for experiment 10-F-100, 10-F-71 and 10-F-50 are shown in Figure 4.9. The nature of the noise (fluctuations) on the heat release rate curve was a result of the limitation of the oxygen depletion calorimetry. Unlike other large scale (MW) fire experiments, the smoke explosion experiments were carried out under severely

ventilation limited conditions creating small scale (KW) fires. Hence, the resolution of the furniture calorimeter became inevitably low and the relative uncertainty (fluctuations of the heat release rate value) was large. Due to such nature of the heat release rate data, all data collected for this research was smoothed with a 10-point moving averaging. The heat release rate curves all started off with a rapid increase due to the first minute of free burn. After that, the heat release rate curves decreased substantially as the compartment hatch was sealed and the burning rate decreased significantly. As the fire developed, the heat release rate curves followed the same trend as the temperature histories. It could be seen from Figure 4.9 that experiments with large vents led to higher rate of heat release, since the combustion was ventilation controlled, and the burning rate was governed by the level of available oxygen.

For experiment 10-F-50, the heat release rate curve followed the trend of the temperature history as previously discussed in Figure 4.1. However, the second half starting from 107 minutes experienced a more rapid growth with a relatively constant rate. The explosion occurred at 137 minutes was not explicitly shown given the noisy nature of the heat release rate data.

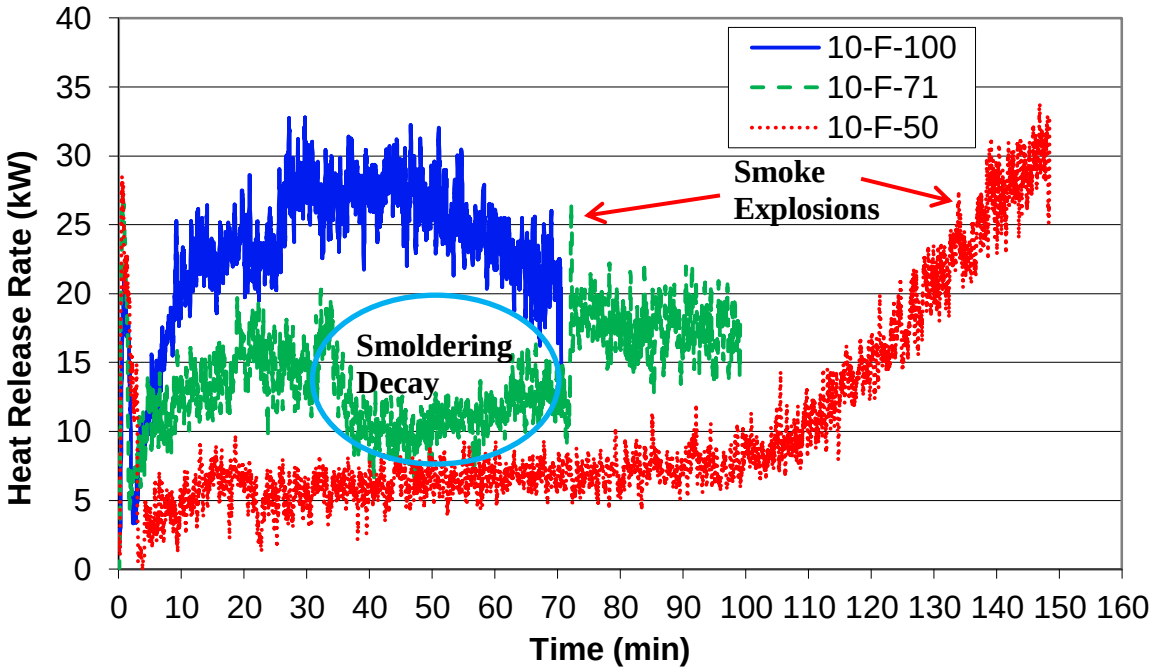


**Figure 4.9: Heat release rate curve for experiment 10-F-100, 10-F-71 and 10-F-50 with a 10-point moving average**

### 4.3.2 10 kg Crib At Middle Elevation

In this section, the discussion would focus on the impact of different ventilation conditions on the combustion through descriptions of experiment 10-M-100, 10-M-71 10-M-50, 10-M-36 and 10-M-25., where the 10 kg crib was fixed at mid-height. Figure 4.10 shows the plot of the data of top rear thermocouple for experiment 10-M-100, 10-M-71 10-M-50, 10-M-36 and 10-M-25. The complete set of temperature histories could be found in Appendix C. Within the first 8 minutes, the temperature quickly rose up to approximately 110 ℃ with a similar trend for all three experiments. After that, the temperature stayed at around 110 ℃ level as the fire developed. At 20 minutes, the fire entered into the smoldering combustion for all three experiments. The flame either self-extinguished or extinguished by the flame expansion as a result of the ghosting fire within the compartment, as noted in Figure 4.10. The change of slope in the temperature histories during the smoldering phase, as previously seen, corresponded to the size of the vent. Experiment 10-M-50 had a higher overall temperature given that the vent size was the biggest among all three experiments. However, the impact of the vent size on the combustion started to diminish as the vent size became smaller and smaller. Similar fire development trend could be found in the floor height experiments. Correspondingly, the mass loss curves shown in Figure 4.11 confirmed that the burning rate was proportional to the vent size, and was governed by the level of available oxygen within the compartment. Smoke explosions were indicated as either a point of discontinuity or a change of slope along the mass loss curve in Figure 4.11. Experiment 10-M-50, 10-M-36 and 10-M-25 were terminated earlier than expected due to the filter saturation and blockage of the sampling tube.

Figure 4.12 shows the heat release rate data for experiment 10-M-100, 10-M-71 10-M-50, 10-M-36 and 10-M-25. The heat release rate curves followed the same trend as the temperature history including the ignition, hatch closed, growth, smoldering decay, (smoke explosion) and (post smoke explosion). Further analysis showed that above heat release rate curves could be divided into three blocks to characterise the heat release rate data, as illustrated in Table 4.2. An interesting phenomenon occurred in experiment 10-M-100 where a series of 21 smoke explosions were recorded after the first explosion

took place. During the multiple-explosion period, each event was 40 seconds apart and the average temperature rise was approximately 130 ℃.

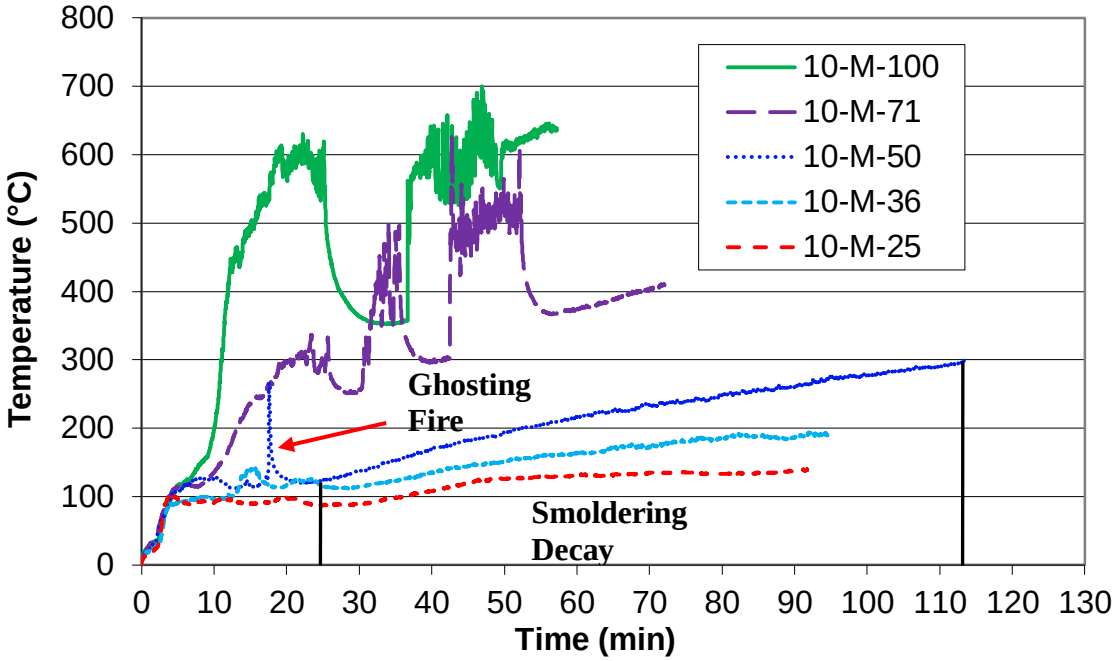


**Figure 4.10: Temperature histories from the rear top (950 mm) thermocouple for experiment 10-M-100, 10-M-71 10-M-50, 10-M-36 and 10-M-25**

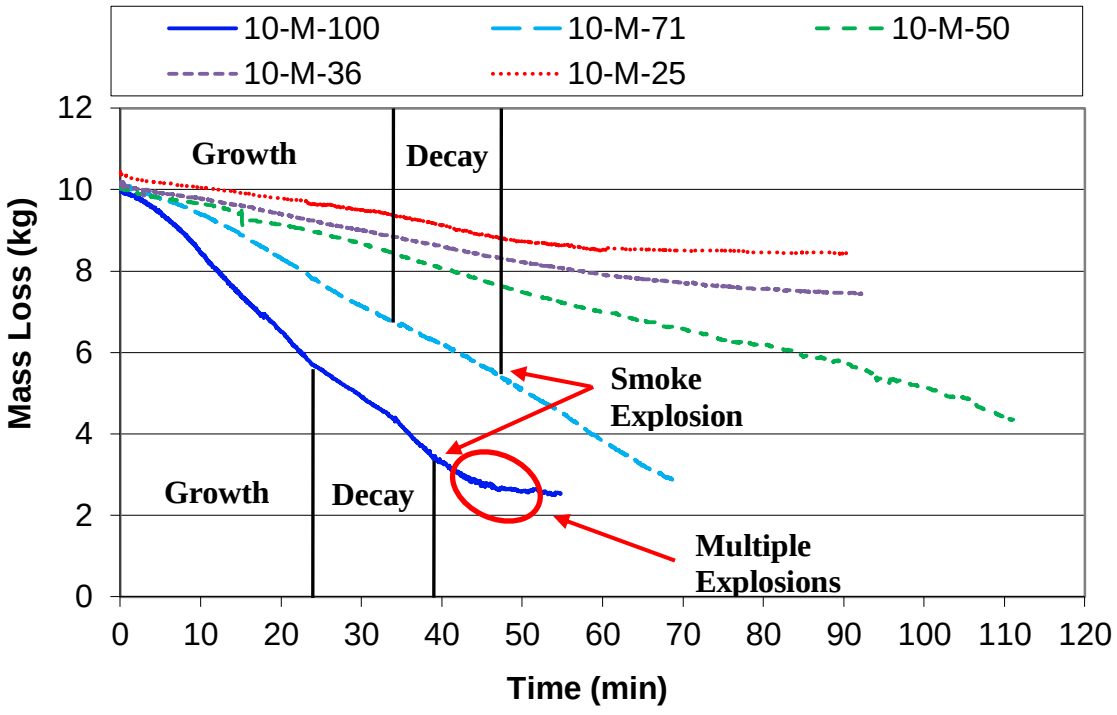


**Figure 4.11: Mass loss histories for experiment 10-M-100, 10-M-71 10-M-50, 10-M-36 and 10-M-25**

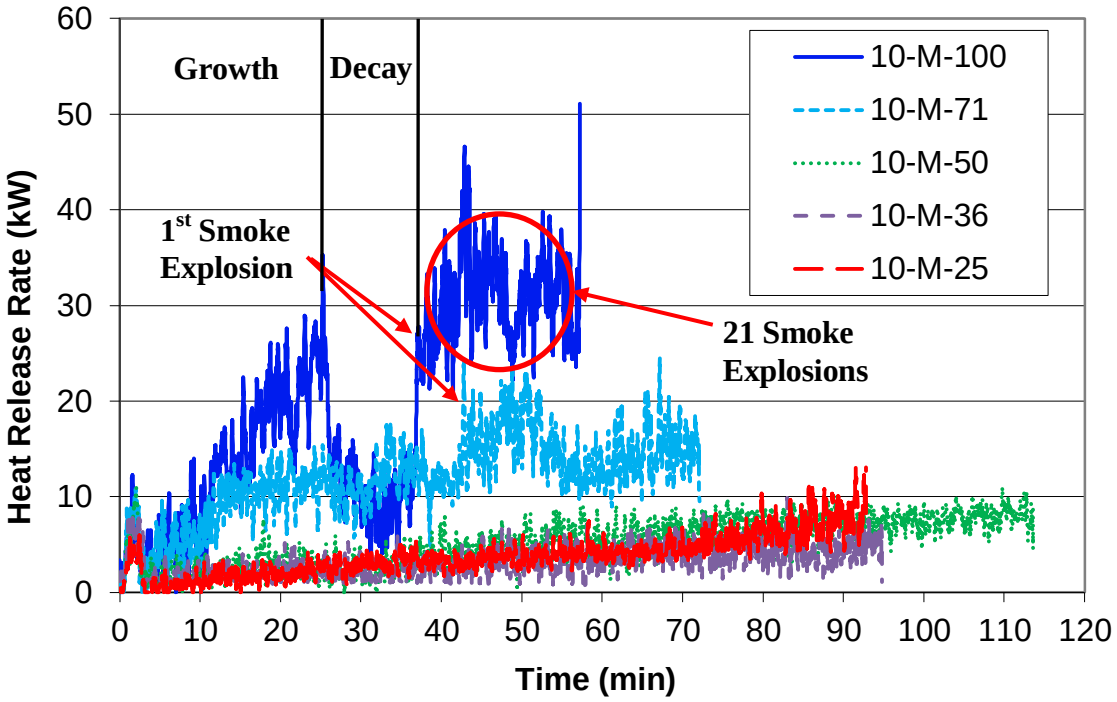


**Figure 4.12: Heat release rate curve for experiment 10-M-100, 10-M-71 10-M-50, 10-M-36 and 10-M-25 with a 10-point moving average**

| HRR Range (kW) | Vent Diameter (mm) | Smoke Explosion | Descriptions |
|---|---|---|---|
| 0 – 10 | 50, 36, 25 | None | The heat release rate slowly rose up to 10 kW. The length of the experiment was considerably longer due to limited air flow rate. |
| 10 – 20 | 71 | 1 | The fluctuation of the heat release rate curve was moderate. The general trend of the temperature history was followed. |
| 20 – 50 | 100 | 21 | The heat release rate varied severely due to the higher burning rate and high intensity of the smoke explosions |

**Table 4.2: The division of heat release rate curves for experiment 10-M-100, 10-M-71 10-M-50, 10-M-36 and 10-M-25**

### 4.3.3 5 kg Crib At Middle Elevation

In this section, the discussion would focus on the impact of different ventilation conditions on the combustion through descriptions of experiment 5-M-100, 5-M-71 and 5-M-50, where the 5 kg crib was fixed at mid-height. Experiment 5-M-100 and 5-M-71 followed the same trend as shown in the temperature histories constructed from the top rear thermocouple in Figure 4.13. The complete set of temperature histories could be found in Appendix C. The ignition started at time zero and the compartment was shut at 1 minute. The fire then built up with a steady growth phase, followed by a steady burning phase accompanied by ghosting fires. The smoke explosions were highlighted on the temperature histories shown in Figure 4.13. Experiment 5-M-100 and 5-M-71 did not result in any smoke explosions, because these two experiments did not go into the smoldering phase. It was believed that the fire always went into the smoldering phase before the smoke explosion occurred, during which time, a large amount of unburned fuel and combustible gases were produced and mixed with oxygen. For experiment 5-M-50, the fire did go into the smoldering phase at around 17 minutes. However, the ghosting fire started to appear at around 22 minutes, which forced the temperature to rise and depleted the oxygen within the compartment leading the fire go into the smoldering again. The cycle between smoldering and ghosting fire were observed throughout the experiment until the first smoke explosion occurred at 98 minutes. By comparing with the 10-kg experiment 10-M-100, 10-M-71 and 10-M-50, it can be seen that the temperature history had the same range from 150 ℃ to 300 ℃ for experiment 10-M-50 and 5-M-50. Experiments with 100 mm (10-M-100 and 5-M-100) and 71 mm (10-M-71 and 5-M-71) openings had almost identical trend in their fire development. The only difference was that the fire did not turn into smoldering for experiment 5-M-100 and 5-M-71. Hence, the mass of the fuel had a significant impact on the occurrence of the smoldering decay. Furthermore, detailed analysis showed that for experiments with larger vents, the whole burning process was shortened because larger vents provided more air flow. For the 100 mm opening, the whole experiment lasted approximately 50 minutes, whereas for the 71 mm opening, the experiment took approximately 70 minutes to finish. For the 50 mm opening, the experiment took more than 140 minutes to consume the fuel until it reached 20% of its original mass. Correspondingly, the mass loss histories in Figure 4.14 showed that burning rate was higher for experiments with larger vents as indicated by a steeper

slope of the curve. For experiment 5-M-100 and 5-M-71, the point of discontinuity occurred at approximately 15 minutes were direct results of the ghosting fires.

The heat release rate history for experiment 5-M-100, 5-M-71 and 5-M-50 are shown in Figure 4.15. All heat release rate curve followed the same trend suggested by the temperature history. Not only did the experiment last longer, the burning rate was also smaller for experiments with smaller vents, because the level of available oxygen within the compartment determined the burning rate of the crib. However, the peak heat release rates of all three experiments were approximately at the same level.

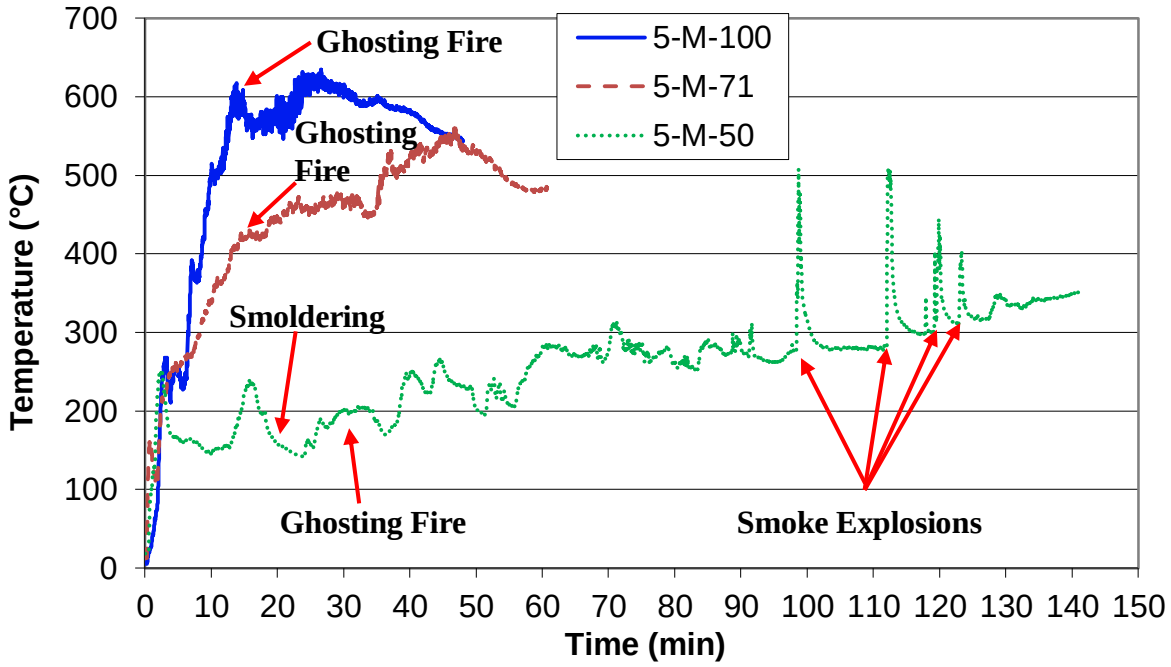


**Figure 4.13: Temperature histories from the rear top (950 mm) thermocouple for experiment 5-M-100, 5-M-71 and 5-M-50**

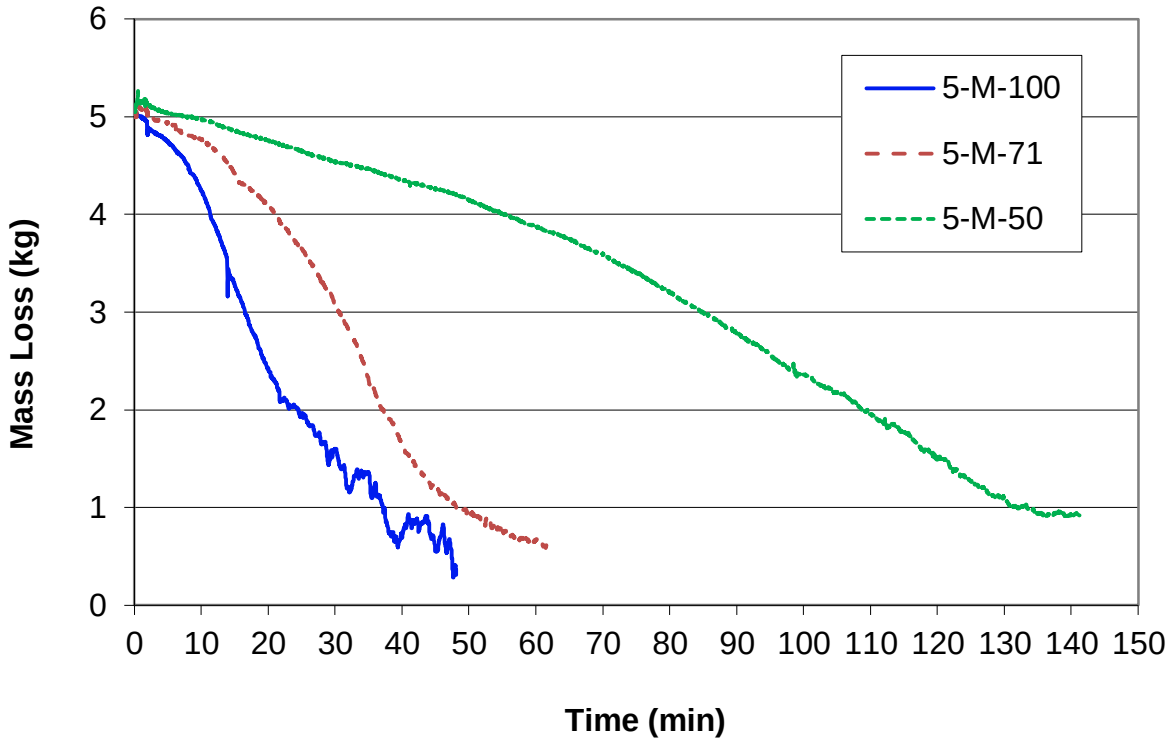


**Figure 4.14: Mass loss histories for experiment 5-M-100, 5-M-71 and 5-M-50**

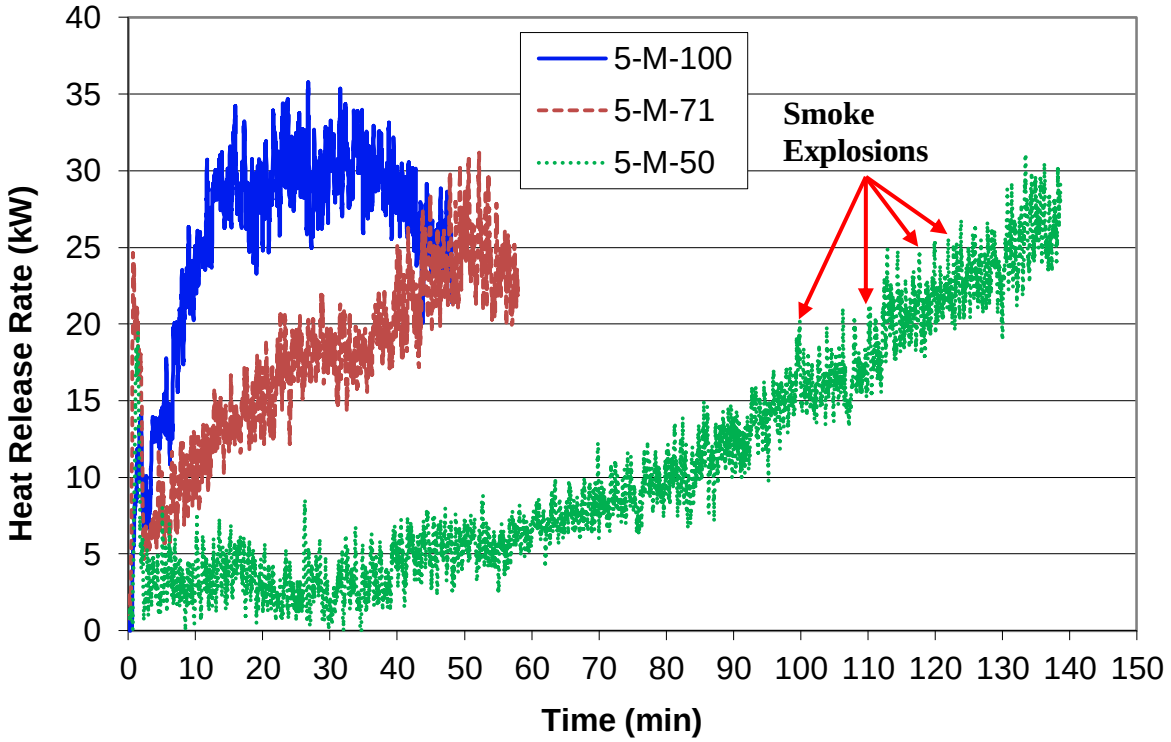


**Figure 4.15: Heat release rate curve for experiment 5-M-100, 5-M-71 and 5-M-50 with a 10-point moving average**

# Chapter 5 Final Detailed Experiments

## 5.1 Introduction

Based on the preliminary study and exploratory experimental results, final nine experiments were chosen in order to further study the smoke explosion phenomenon in detail. The fuel mass was fixed at 10 kg along with the vent size varying between 100 mm, 71 mm and 50 mm. Vents sizes smaller than 50 mm were not included because the results from exploratory experiments suggested that experiments with vents less than 50 mm did not produce smoke explosions and caused instability and inaccuracy in the gas analyser, and blockage of the system. Similar issues were noted in experiments done by Sutherland (1999). The elevation of the fuel was still kept as a variable so that the impact of the fuel position could be investigated.

In this chapter, discussions would focus on experiment 10-M-100 to present the important details of the smoke explosion scenario in order to characterise the smoke explosion phenomenon. A complete set of experimental results for all nine experiments including the heat release rate history, temperature profiles, temperature histories, compartment pressure, mass flow rate through vent openings, mass loss, and $O_2$, $CO_2$ and CO concentrations could be found in Appendix D. Table 5.1 is a matrix of all nine experiments showing the experimental variables and number of smoke explosions.

| | Vent Size | | |
|---|---|---|---|
| Fuel Elevation | 100 (mm) | 71 (mm) | 50 (mm) |
| Ceiling (780 mm) | 1 | 25 | 0 |
| Middle (500 mm) | 3 | 1 | 1 |
| Floor (270 mm) | 1 | 1 | 0 |

**Table 5.1: Experimental matrix summarises experimental conditions of final nine detailed experiments**

In this section, only data prior to the first smoke explosion is presented, since the first explosion would not be affected by any previous explosions and more accurately reflected the conditions within the compartment prior to the smoke explosion. It was expected that smoke explosions in real buildings would result in failure of windows or some form of structural damage which could change the ventilation and prevented subsequent smoke explosion. In these experiments, the compartment was specially built to resist the over-pressure up to at least 5 kPa which would normally be sufficient to cause failure of the windows, as reported by Mannan and Lees (2005).

Table 5.2 shows a summary of all the important data for 9 final experiments. Column 1 is the experiment code that consists of fuel mass, fuel elevation and vent size. Column 2 and 3 are the fuel elevations and vent sizes. Columns 4 and 5 are the time and temperature when the smoldering decay started. Column 6 is the fuel mass when the smoke explosion occurred. Columns 7 to 9 are the gas concentrations from the upper layer at the first smoke explosion. Column 10 is the time when the first smoke explosion occurred. Columns 11 and 12 are the temperature before and after the first smoke explosion respectively. Column 13 is the compartment pressure when the first smoke explosion occurred. Column 14 indicates the occurrence of the ghosting fire. Column 15 indicates the occurrence of the smoldering decay. Lastly, column 16 shows the number of smoke explosions.

| Experiment Code | Fuel Elevation (mm) | Vent Size (mm) | Smoldering Decay | | $m_F$ (kg) | $Y_{O_2}$ (%) | $Y_{CO_2}$ (%) | $Y_{CO}$ (%) | $t_E$ (min) | $T_{E_0}$ (℃) | $T_{E_1}$ (℃) | $P_E$ (Pa) | GF | SD | SE |
|---|---|---|---|---|---|---|---|---|---|---|---|---|---|---|---|
| | | | $t_D$ (min) | $T_D$ (°C) | | | | | | | | | | | |
| 10-C-100 | 780 | 100 | 38 | 415 | 5.79 | 12.9 | 6.9 | 3.8 | 67 | 336 | 482 | 990 | YES | YES | 1 |
| 10-C-71 | 780 | 71 | 42 | 378 | 6.47 | 11.1 | 8.3 | 4.3 | 68 | 330 | 501 | 4934.4 | YES | YES | 25 |
| 10-C-50 | 780 | 50 | N/A | N/A | N/A | N/A | N/A | N/A | N/A | N/A | N/A | N/A | NO | YES | N/A |
| 10-M-100 | 500 | 100 | 19 | 573 | 7.03 | 13.7 | 6.7 | 3.1 | 28 | 362 | 531 | N/A | YES | YES | 3 |
| 10-M-71 | 500 | 71 | 36 | 602 | 3.37 | 6.5 | 16.8 | N/A | 68 | 433 | 657 | N/A | YES | YES | 1 |
| 10-M-50 | 500 | 50 | N/A | N/A | N/A | N/A | N/A | N/A | N/A | N/A | N/A | N/A | NO | YES | N/A |
| 10-F-100 | 270 | 100 | 21 | 579 | 6.85 | 14.9 | 6.1 | 2.5 | 27 | 367 | 567 | N/A | YES | YES | 2 |
| 10-F-71 | 270 | 71 | 39 | 501 | 1.95 | 7.7 | 9.9 | 3.5 | 90 | 418 | 585 | N/A | YES | YES | 1 |
| 10-F-50 | 270 | 50 | N/A | N/A | N/A | N/A | N/A | N/A | N/A | N/A | N/A | N/A | NO | YES | N/A |

**Table 5.2: Summary data from final experiments showing the experimental conditions; time and temperature at the smoldering decay; fuel mass, mass flow rates, gas concentrations, time, temperature (before and after) and pressure and at the first smoke explosion; ME = the total mass ejected at the first smoke explosion; GF = the occurrence of the ghosting fire; SD = the occurrence of the smoldering decay, and SE = total number of explosions (N/A = data not available or no explosion occurred)**

## 5.2 Experiment 10-M-100

### 5.2.1 Ignition and Growth

Ignition started at time zero using 200 ml methylated spirits which was poured into the tray under the crib prior to the experiment. For the first minute, the compartment was left open to allow the fire to become established on the crib. Once the compartment was shut, the temperature and the heat release rate decreased temporarily. As the crib started to become more involved in the burning process, the temperature and the heat release rate started to increase again and enter a steady growth period as shown in the temperature history constructed from the rear thermocouple tree in Figure 5.1 and heat release rate history in Figure 5.2. The general trend of temperature and heat release rate for the growth period was observed in all final detailed experiments. The complete set of data for the final detailed experiments could be found in Appendix D. After the compartment was shut, the concentration of $O_2$ in the upper layer decreased from 10% to 2.5% during the growth period. As a result of the incomplete combustion, the production of CO increased to 4% as shown in the gas concentration plot in Figure 5.3. Figure 5.4 shows the temperature profile at a 10-minute interval throughout the experiment. The unburned fuel, soot and other intermediate combustion products continuously discharged from the fire plume into the upper layer, which descended to around 600 mm above the compartment floor at the beginning of the growth phase. The smoke layer height was estimated based on the temperature profile constructed from the rear thermocouple tree within the compartment. The mass flow rate through both vents shown in Figure 5.5 suggested that the smoke flowing out of the compartment followed a steady growth, whereas the air flowing into the compartment stayed at around 2 g/s. (Positive values of the mass flow rate indicated the out-flow and negative values of the mass flow rate indicated the in-flow). According to the conservation of mass, the amount of mass flowing in should equal to the amount of mass flowing out of the compartment. The discrepancy between the two mass flow rates was because the burning rate of the crib itself had not yet been incorporated. The burning rate of the crib would have been trivial if the vent opening was large enough. However, for this particular research, given the ventilation was relatively small, the burning rate of the crib became significant when considering the conservation of mass. Figure 5.6 shows

the mass loss history for the timber crib in experiment 10-M-100, where the growth phase was divided into two stages judging by the slope of the curve. Stage II was used to illustrate the derivation of the conservation of mass. During stage II of the growth phase, the average in-flow mass was at 2 g/s and the average out-flow mass was calculated to be 4.75 g/s. The mass decreased from 10 kg to 8.6 kg in 10 minutes, the burning rate of the crib could be estimated as the mass loss dividing by time, which gives 2.3 g/s. Hence, the mass flow rate through the bottom vent plus the burning rate of the crib was approximately equal to the mass flow rate through the top vent. The fluctuation indicated in the mass flow rate in Figure 5.5 was caused by ghosting fires and associated pulsation effect mentioned in section 4.2. When the cool oxygen mixed with the fuel in the upper layer, the mixture could be ignited by the existing flame causing an increase in the mass flow rate through the top vent, which created a negative pressure allowing oxygen flow into the compartment and mixing with the fuel again.

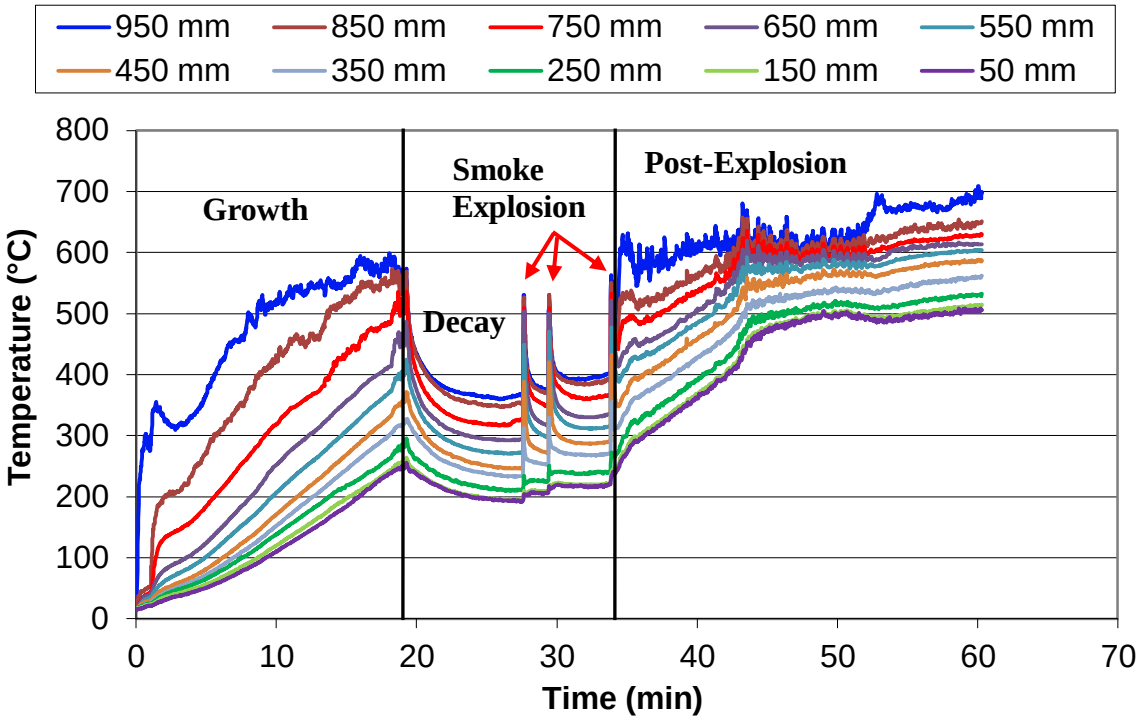


**Figure 5.1: Temperature histories from the rear thermocouple tree for experiment 10-M-100**

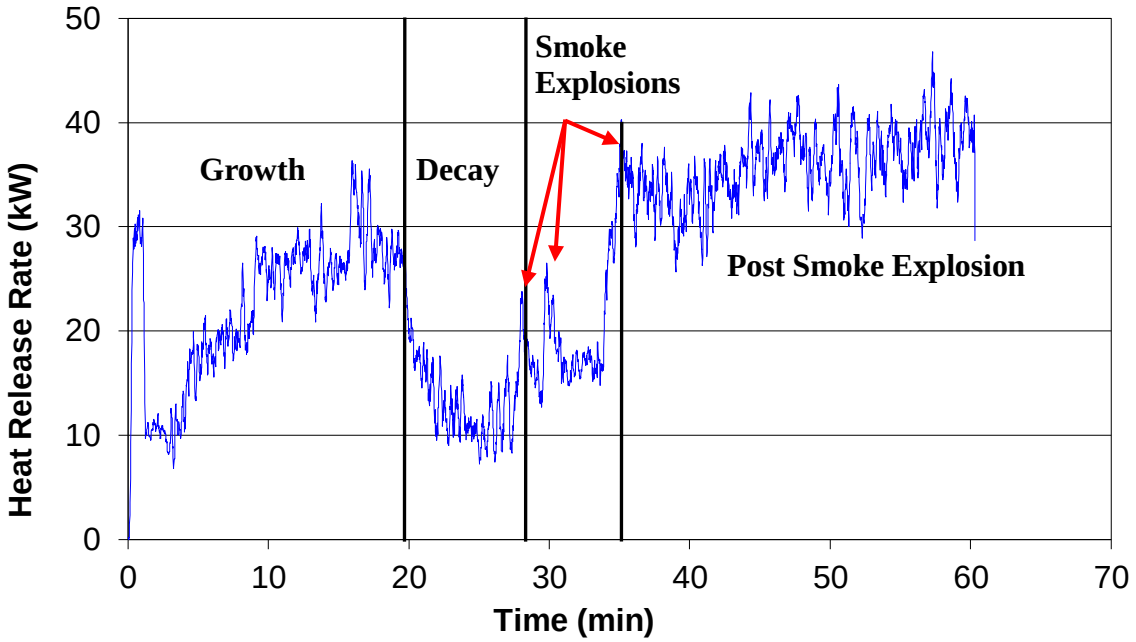


**Figure 5.2: Heat release rate history for experiment 10-M-100 with a 10-point moving average**

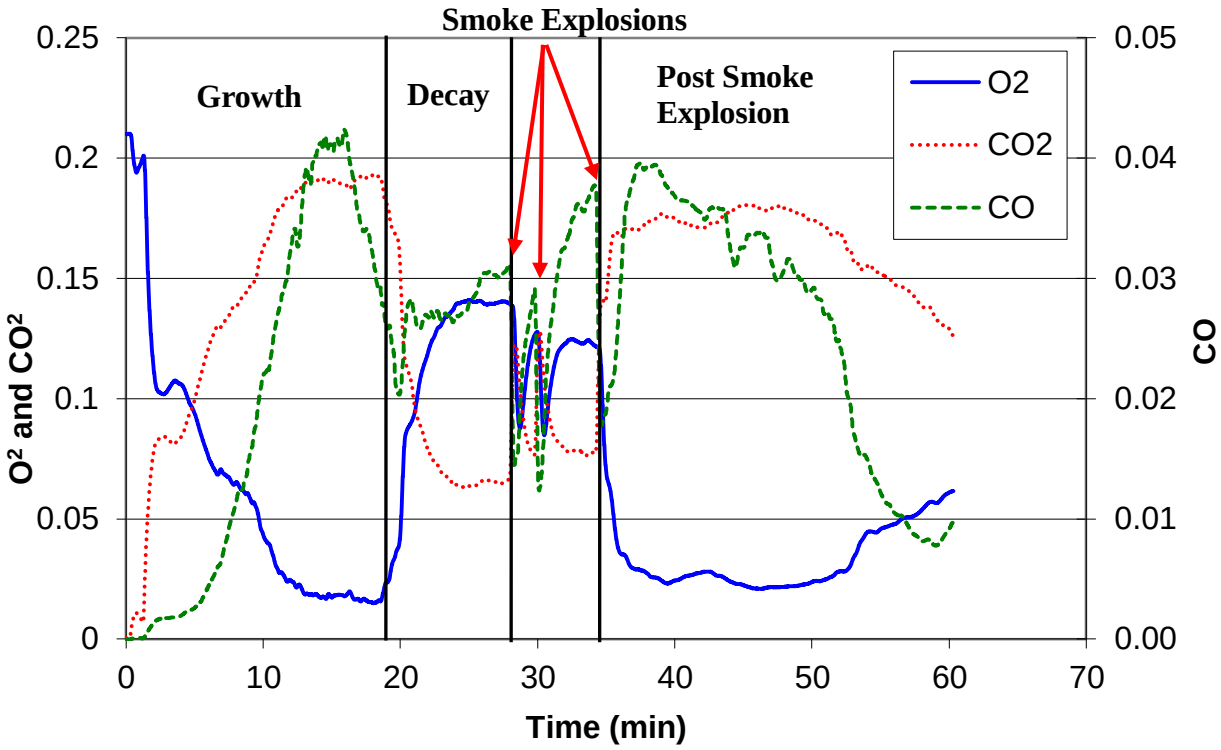


**Figure 5.3: $O_2$, $CO_2$ and CO molar concentrations for experiment 10-M-100**

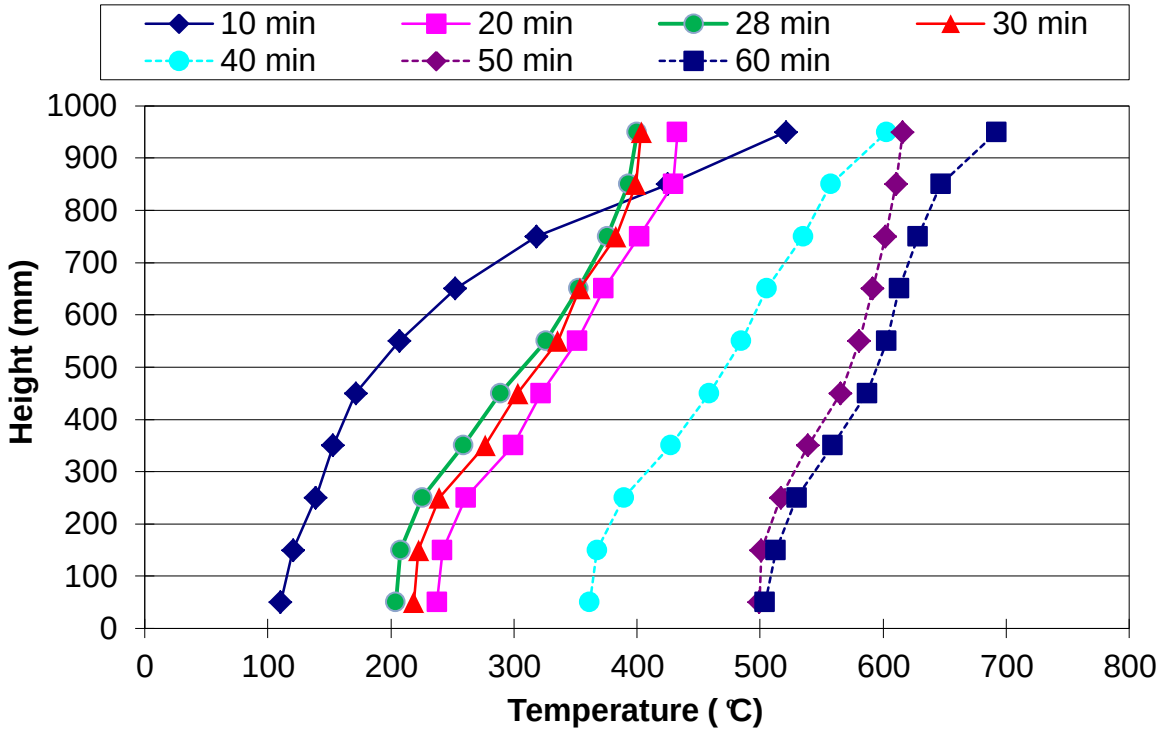


**Figure 5.4: Temperature profile constructed from the rear thermocouple tree for experiment 10-M-100**

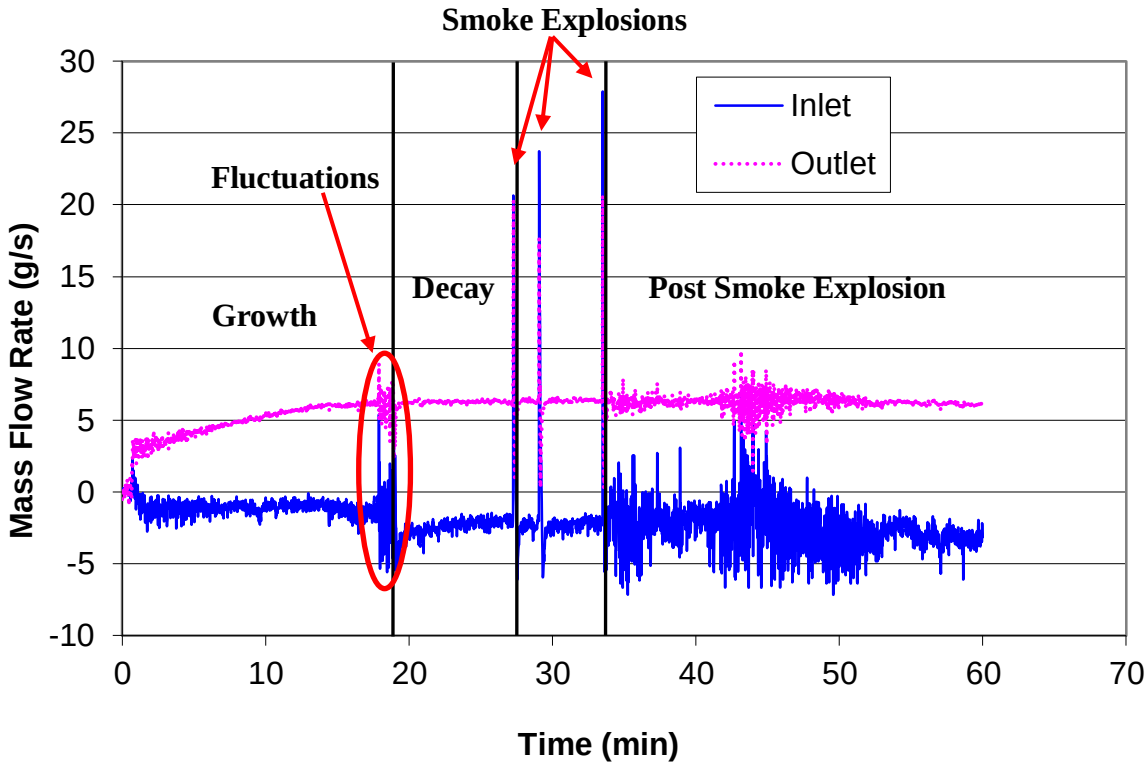


**Figure 5.5: Mass flow rate through both opening vents for experiment 10-M-100**

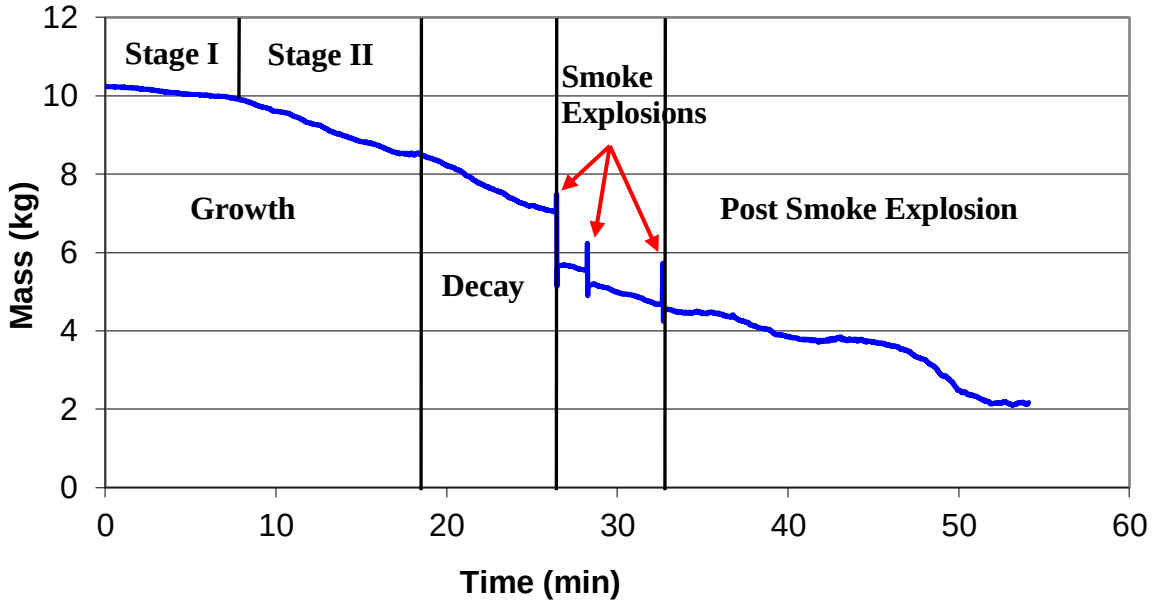


**Figure 5.6: Mass loss history for experiment 10-M-100**

### 5.2.2 Smoldering Decay

At 19 minutes, the flame extinguished completely suggesting the start of the smoldering decay. The glowing embers became visible and gradually spread out over the surface of the crib. The temperature history showed an exponential decay from 580 ℃ at 19 minutes to 380 ℃ at 27 minutes during the smoldering combustion phase and the heat release rate started to decrease following the same trend. The general trend of temperatures for the smoldering decay period was observed in all final experiments. Prior to the explosion at 28 minutes, the smoke layer had already descended down to approximately 350 mm above the floor. The temperature profile did not change significantly after the smoke explosion as seen in Figure 5.4, indicating that the height of the smoke layer stayed unchanged. Since less oxygen was consumed in the smoldering combustion, the concentration of $O_2$ started to increase during the smoldering phase and levelled off at 14% as the concentration of $CO_2$ dropped and levelled off at 6%. As a result of the smoldering combustion, the concentration of CO increased and plateaued at 3%. The mass flow rate shown in Figure 5.5 suggested that the smoke flowing out of the compartment was averaged at 6 g/s for the rest of the experiment, whereas the air flowing into the compartment stayed at approximately 3 g/s. The mass loss history in Figure 5.6 showed that the mass decreased from 8.6 kg to 7.2 kg in 8.2 minutes, the burning rate of

the crib was estimated at approximately 2.85 g/s. By checking the conservation of mass, the mass flow rate through the bottom vent plus the burning rate of the crib (5.85 g/s) was approximately equal to the mass flow rate through the top vent (6 g/s).

### 5.2.3 Smoke Explosions

The first explosion occurred at 28 minutes as indicated in Figure 5.1 to Figure 5.6. The temperature rapidly increased from 380 ℃ to 530 ℃. The amount of temperature rise and the trend of the smoke explosion are consistent for all three smoke explosions that occurred in this experiment. At the end of the third explosion, the heat release rate had increased from ~10 kW to ~35 kW. The upper layer concentration of $O_2$ decreased from 14% to 8.5% and CO decreased from 3% to 1.5% due to the explosion, while the level of $CO_2$ increased from 6.5% to 12% because of the combustion. The crib returned to smoldering immediately after the first and second explosion with an increasing level of $O_2$ and CO against a decreasing level of $CO_2$. However, after the third explosion, the flame was re-established at the center of the crib along with ghosting fires around the crib. The concentration of $O_2$ was at low level of 2.5%, which was not usual prior to a smoke explosion. In order to have a smoke explosion, the crib always went into the smoldering combustion with an increasing level of $O_2$ until the smoke explosion occurred. Hence, the amount of $O_2$ was not considered as a major component within the gas mixture that determined the occurrence of the smoke explosion. The cycle for each explosion in terms of changes in gas species was explained in the following flow chart in Figure 5.7.

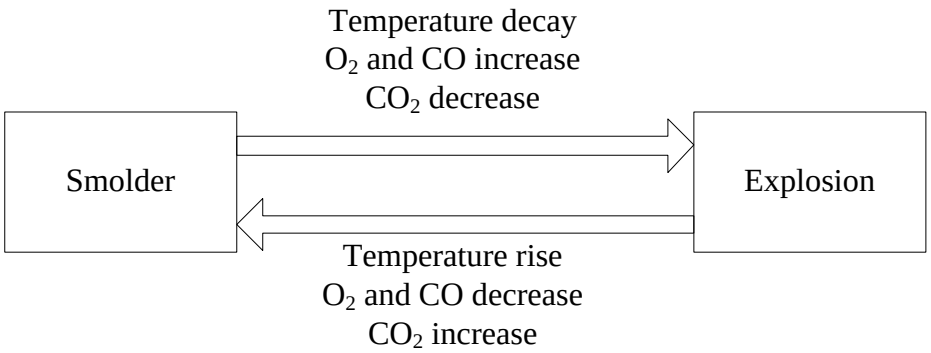


**Figure 5.7: A simplified flow chart diagram for the multi-explosion scenario describing the corresponding changes in the gas concentrations**

Figure 5.8 featured the impacts from the explosions of experiment 10-M-100 in terms of the mass loss and mass flow rate. The time started at 26 minutes and showed an 8- minute period where three explosions took place. All three explosions occurred with the same outcomes in terms of the spike in the mass flow rate out of the compartment and the decrease of the fuel mass. The mass loss history showed an instant increase at the smoke explosion followed by a sudden drop. The rapid change was believed to be the result of mechanical disturbance of the loading cell. The mass flow rate for both vents consistently returned to a quasi-steady state with a constant value of 6 g/s out-flow and 3 g/s in-flow. The fuel mass gradually decreased from 7 kg to 5.5 kg and then to 5 kg, as the experiment progressed.

In order to quantify the intensity of the smoke explosion, the following factors were considered: temperature rise, compartment pressure, peak mass flow rate, and the total mass ejected from the compartment. However, only the compartment pressure was chosen as a relatively reliable factor. Although the amount of temperature rise after each smoke explosion was similar, and the average temperature rise was calculated as 160 ℃, thermocouples still experienced delays due to the response time and difficulties in representing the flame temperature using single point measurement. The compartment pressure at the smoke explosion for this experiment was not available because the pressure transducer malfunctioned after the second experiment 10-C-71, but the pressure transducer used to measure the mass flow rate still functioned properly. The range for the pressure transducer was 0.2 Torr (27 Pa) / 1V. The compartment pressure at the smoke explosions all exceeded 0.2 Torr (27 Pa), and the exact value was unknown except for the first two experiments where the maximum pressure went up to 4934 Pa, which was more than the designed pressure (2 kPa) of the pressure relief panel. However, the pressure relief panel was still intact after the smoke explosion. The compartment pressure for the ghosting fire though often sat in the range between 0.6 - 0.8 V (16 - 21 Pa) of the pressure transducer. Hence, for this discussion, a pressure difference of at least 27 Pa was chosen as one of the criteria for a smoke explosion along with the video observation. Nevertheless, there was still a reasonable amount of uncertainties around the measurements, therefore the above criterion needed to be further investigated for any future researches. The peak mass flow rate had already exceeded the maximum value that the pressure transducer can measure. Likewise, the calculation of the total mass ejected

from the compartment when the smoke explosion occurred became non-applicable, since it only captured part of the mass ejected.

Figure 5.9 is a video image showing the ignition moment for experiment 10-M-100. It could be seen that the ignition appeared to be instantaneous and caused directly by the ember of the crib. Prior to the explosion, the wood crib was smoldering with green glowing embers on the surface. A flame suddenly appeared at the back of the crib as seen by the video image. The flame then ignited the surrounding combustible gases and expanded to a large fireball filling the entire compartment.

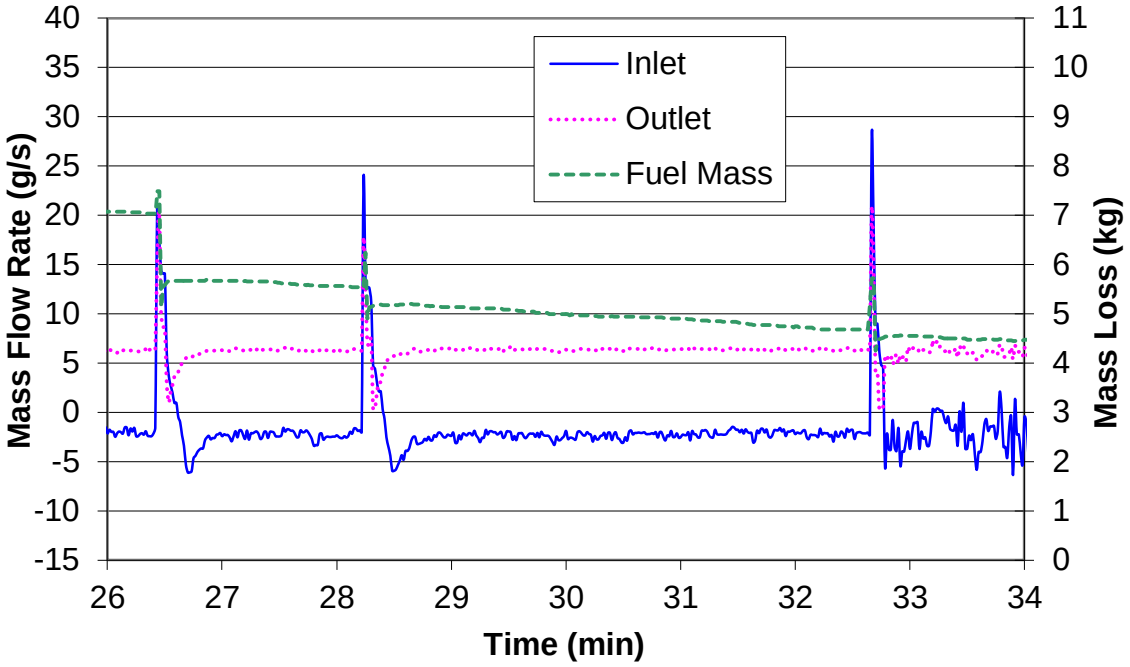


**Figure 5.8: Short histories of mass flow rates and the mass loss for experiment 10-M-100**

**Figure 5.9: Video captures of experiment 10-M-100 at 28 minutes showing the ignition moment (Video camera is placed under the fire compartment)**

### 5.2.4 Post Smoke Explosion

At the end of the third explosion, the crib started to burn with only few flames around the bottom of the crib and ghosting fires located below the loading table. The compartment temperature followed a slow growth as the crib burned. At 45 minutes, the ghosting fire completely disappeared leaving only minor flames on the crib. Later, the crib transitioned to a well established steady burning phase where temperatures evenly distributed between 500 ℃ to 700 ℃. The heat release rate history correspondingly showed a steady burning phase ranging from 30 kW to 40 kW during the post smoke explosion phase. The general trend of $O_2$ started to increase whereas that of CO and $CO_2$ progressively decreased towards the end of experiment where the fuel mass levelled off at 2 kg and no visible smoke could be seen from the vent.

## 5.3 Experiments With Middle Elevation

In this section, the discussion would focus on the impact of different ventilation conditions on the combustion through descriptions of experiment 10-M-100, 10-M-71 and 10-M-50, where the elevation of the fuel was fixed at mid-height. All three experiments followed the typical trend described in section 4.2 as shown in the temperature histories constructed from the top rear thermocouple in Figure 5.10. The complete set of temperature histories could be found in Appendix D. The fires built up with a steady growth phase, followed by a decay phase until the smoke explosion occurred when the concentration of the combustible mixture was within the flammable range upon contact with the embers on the crib. The stars on the temperature histories indicated when the smoke explosions occurred. Experiment 10-M-50 did not result in any smoke explosions. Unfortunately, the parameters used to characterise the smoke explosion did not provide an obvious explanation for why the smoldering phase did not transition into a smoke explosion. Detailed analysis showed that for experiments with larger vents, the whole burning process was shortened because larger vents provided more air flow. Since the fuel concentration was fixed, the crib burned faster when the vent was larger. For the 100 mm opening, the whole experiment lasted approximately 60 minutes, whereas for the 71 mm opening, the experiment took approximately 90 minutes to finish. For the 50 mm opening, the experiment took more than twice as long as the 100-mm experiment, to consume the fuel until it reached 20% of its original mass. Correspondingly, the mass loss histories in Figure 5.11 showed that burning rate was higher for experiments with larger vents as indicated by a steeper slope of the curve. The mass flow rate shown in Figure 5.12 suggested that the vent flow through the top vent decreased from 6 g/s to 3 g/s, and to 1.5 g/s as the vent sizes were varied from 100 mm to 71 mm to 50 mm. The concentration of $O_2$ and CO prior to the smoke explosion ranged between 6.65% to 14% and 2.9% to 3.7% respectively as shown in the summary Table 5.2. The production of CO was dependent on the size of the vent, i.e., the smaller the vent, the lower the burning rate, and hence a higher level of CO was expected. The detail of gas concentrations for each experiment was included in Appendix D. The heat release rate curves shown in Figure 5.13 confirmed that the same trends of the fire development. Following the initial growth, the heat release rate quickly dropped after the compartment was shut. As the fire developed, the heat

release rate started a steady growth as the fire in the crib became established. The increase in heat release rate was proportional to the size of the vent. Experiment 10-M-100 and 10-M-71 went into the smoldering phase suggested by the decay of heat release rate curves and temperature histories. During the smoldering combustion, a large quantity of unburned fuel was discharged into the atmosphere and mixed up with the fresh air. Once inside the flammable range, the combustible gases were ignited by the glowing ember. All smoke explosions were highlighted in Figure 5.13 and could be seen from the sudden increase of the heat release rate curves.

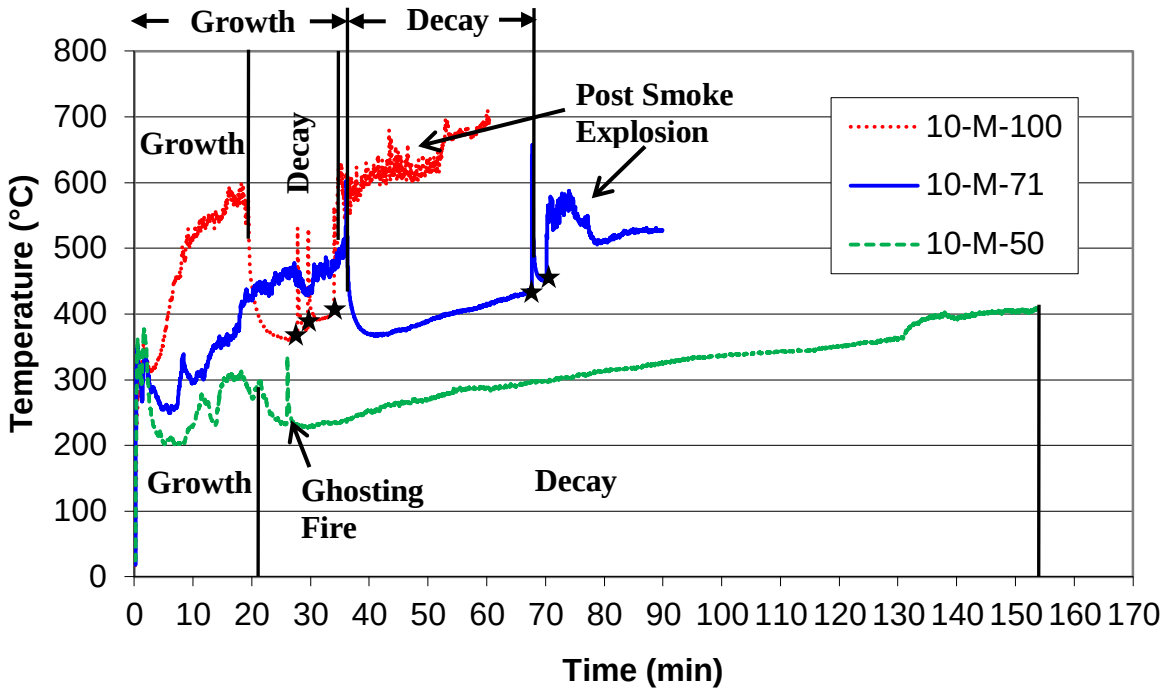


**Figure 5.10: Temperature histories comparison between experiment 10-M-100, 10-M-71 and 10-M-50 using data from the rear top thermocouple (Each asterisk designates a smoke explosion)**

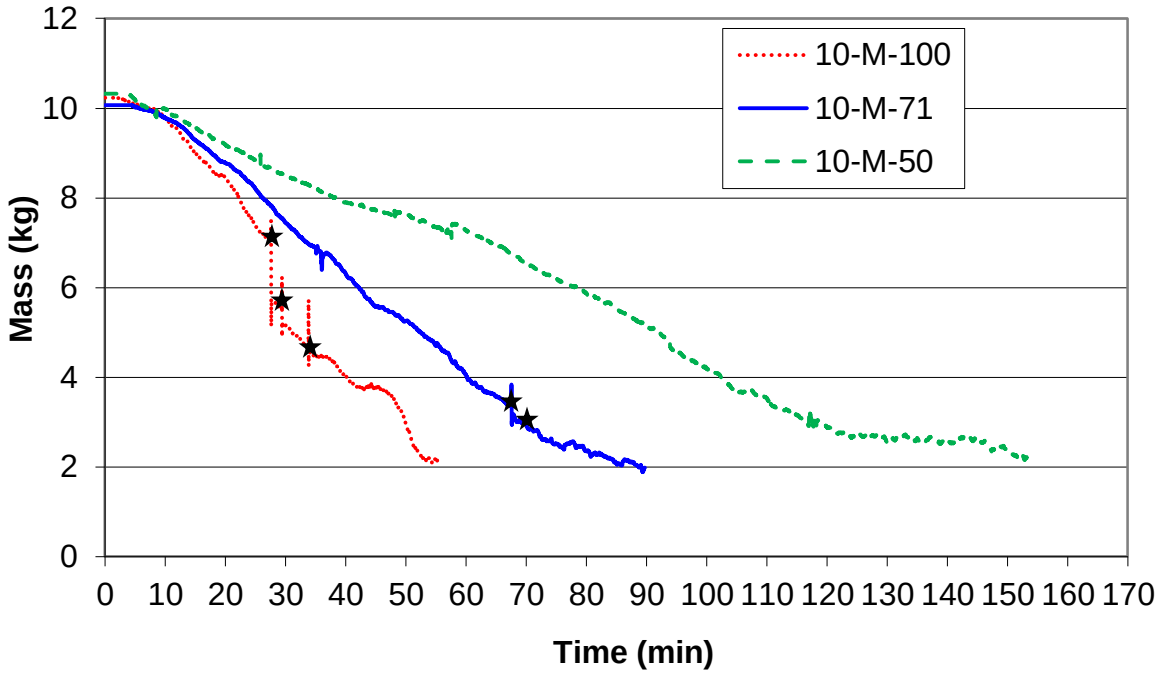


**Figure 5.11: Mass loss histories comparison between experiment 10-M-100, 10-M-71 and 10-M-50 (Each asterisk designates a smoke explosion)**

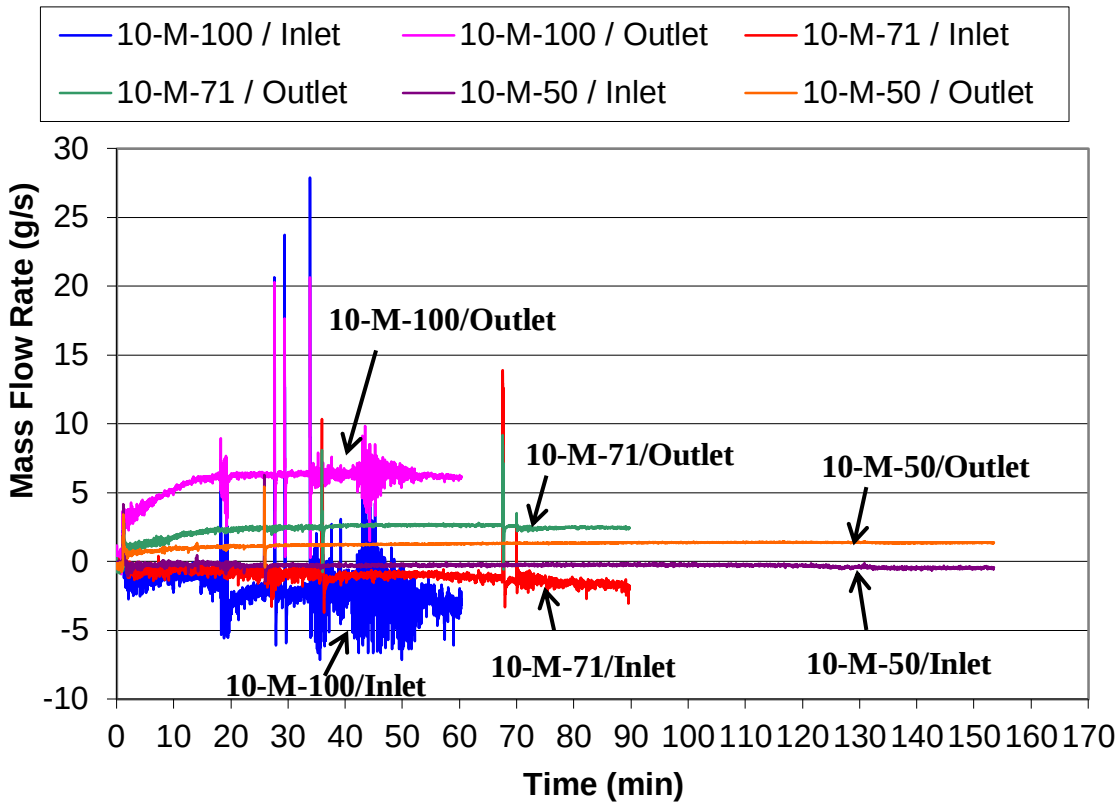


**Figure 5.12: Mass flow rates comparison between experiment 10-M-100, 10-M-71 and 10-M-50**

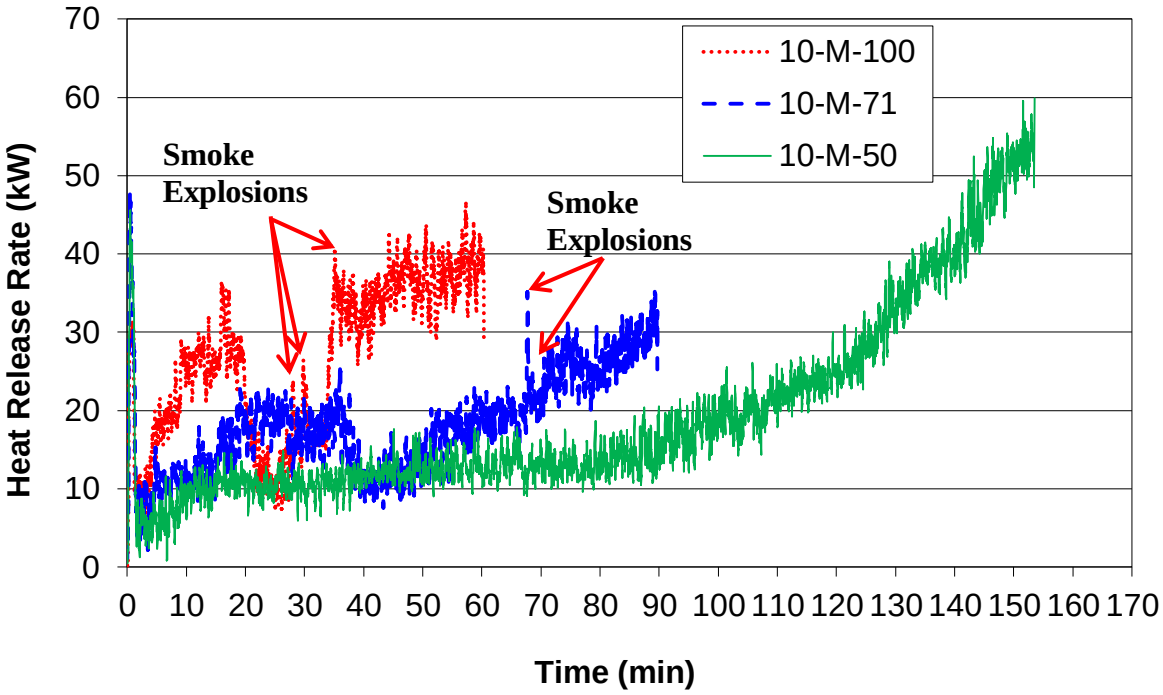


**Figure 5.13: Heat release rate histories comparison between experiment 10-M-100, 10-M-71 and 10-M-50**

## 5.4 Experiments With 71 mm Vent

This section provides further details on the impact of the fuel elevation by comparing the results for experiment 10-C-71, 10-M-71 and 10-F-71, given the same vent opening size. All three experiments followed the typical fire development trend mentioned in section 4.2 including growth, decay and post smoke explosion, as shown in the temperature histories constructed from the top rear thermocouple in Figure 5.14. The complete set of temperature histories could be found in Appendix D. The temperature followed a steady growth, followed by the smoldering decay until the smoke explosion occurred. The stars on the temperature histories indicated the smoke explosions. The temperature within the growth phase for experiment 10-C-71 was relatively low compared to the other two experiments, because the burning rate was limited by the availability of oxygen, which was reduced when the fuel was placed within the oxygen depleted upper layer. However, the temperatures during the decay phase were quite closely distributed. It was worth mentioning that, for experiment 10-C-71 and 10-M-71, the first smoke explosion all occurred at 68 minutes, suggesting that the time taken for the

combustible gases to mix and fall into the flammable range was almost identical. However a scientific explanation was not available given the available data at that time. All experiments had a similar mass loss rate regardless of where the fuel was located, as seen in Figure 5.15. The concentration of $O_2$ and CO prior to the smoke explosion ranged between 3.7% to 11.6% and 1.9% to 4.3% respectively. The detail of gas concentrations for each experiment was included in Appendix D. The mass flow rate histories for experiment 10-C-71, 10-M-71 and 10-F-71 could be found in Figure 5.16. The difference between vent flows for all three experiments was relatively small, which agreed with the fact that the vent size were all chosen as 71 mm. For experiment 10-C-71, the fire turned into a series of 24 smoke explosions after the first explosion, which could be explained by the following mechanism: The explosion created a gas expansion and temperature rise, which pressurised the whole compartment forcing a large amount of smoke out of the compartment. However, the temperature within the compartment almost immediately fell back to pre-explosion level, creating a negative pressure within the compartment relative to the surrounding environment. Fresh air was drawn into the compartment through the bottom vent due to the negative pressure. Once the ventilation was re-established, the compartment went back to the buoyancy driven regime. Meanwhile, the smoldering combustion continued to develop until another explosion occurred. Ultimately, the combustion broke out of the multi-explosion cycle and the wood crib switched back to flaming combustion until it burned out. The multiple smoke explosions were indicated by the evenly distributed spikes in Figure 5.16. The mass out-flow rate for experiment 10-M-71 had the highest flow rate of 2.6 g/s which was 1 g/s higher than the other two experiments. The heat release rate curves shown in Figure 5.17 confirmed that the same trend of the fire development applied. Followed by the initial growth, the heat release rate quickly dropped after the compartment was shut. As the fire developed, the compartment temperature started a steady growth as the fire in the crib became established. The crib went into the smoldering phase as seen from the decay of the heat release rate curves. All smoke explosions were highlighted in Figure 5.17 and could be seen from the sudden increase of the heat release rate curves.

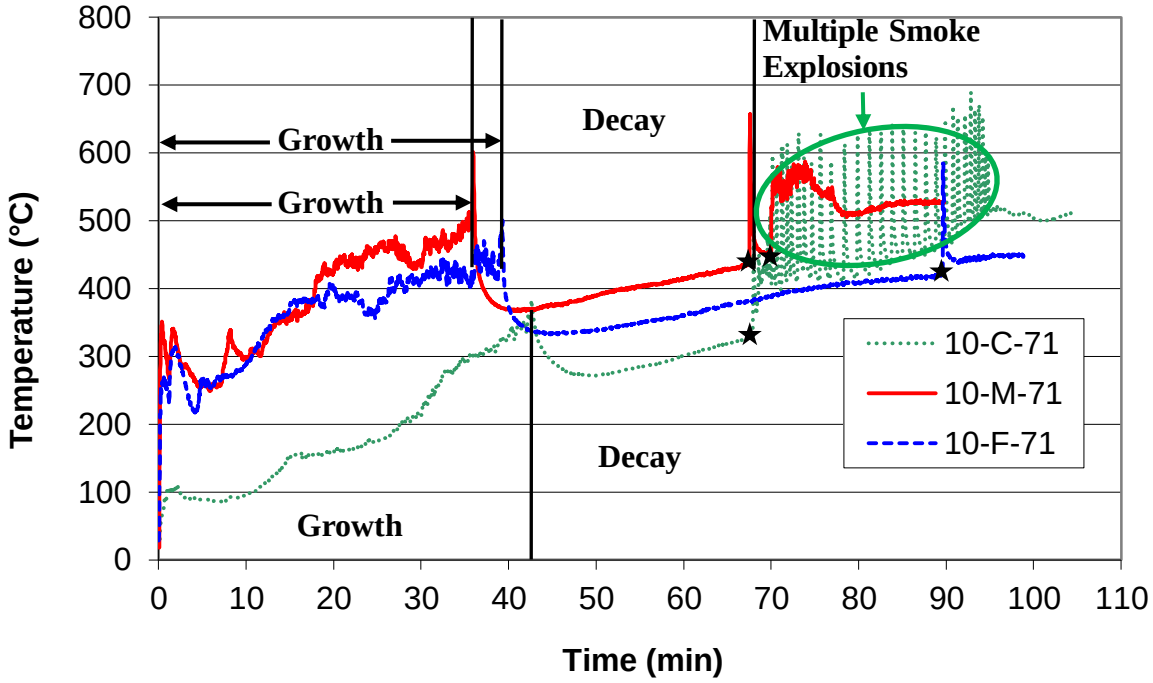


**Figure 5.14: Temperature histories comparison between experiment 10-C-71, 10-M-71 and 10-F-71**

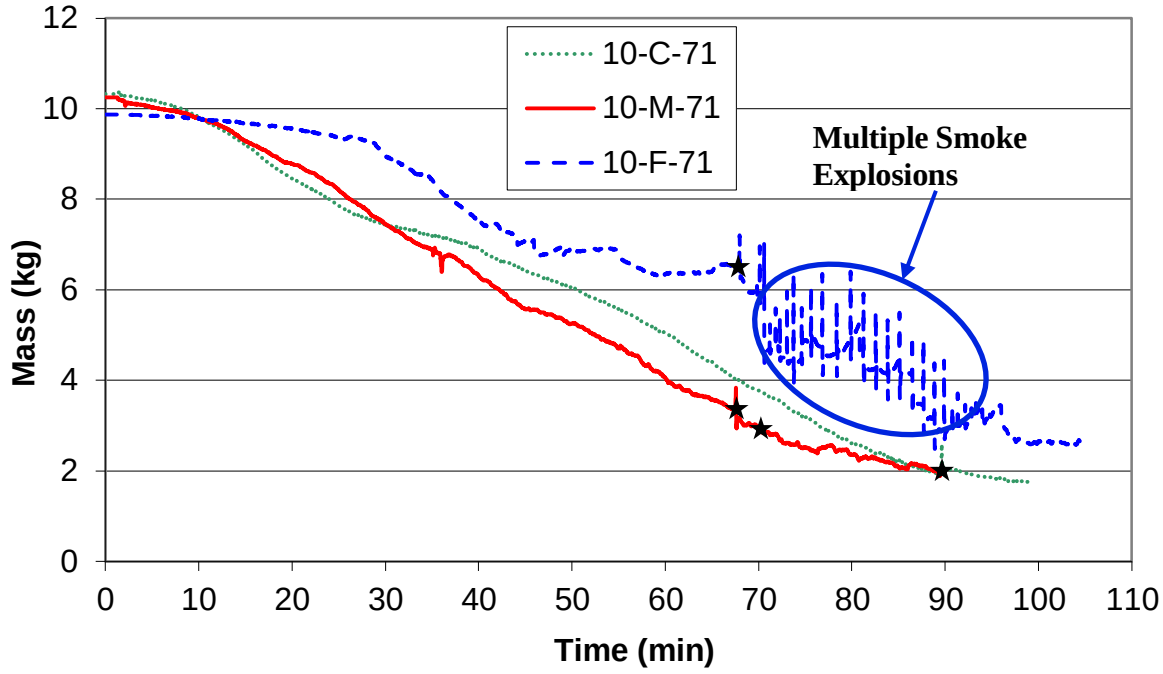


**Figure 5.15: Mass loss histories comparison between experiment 10-C-71, 10-M-71 and 10-F-71**

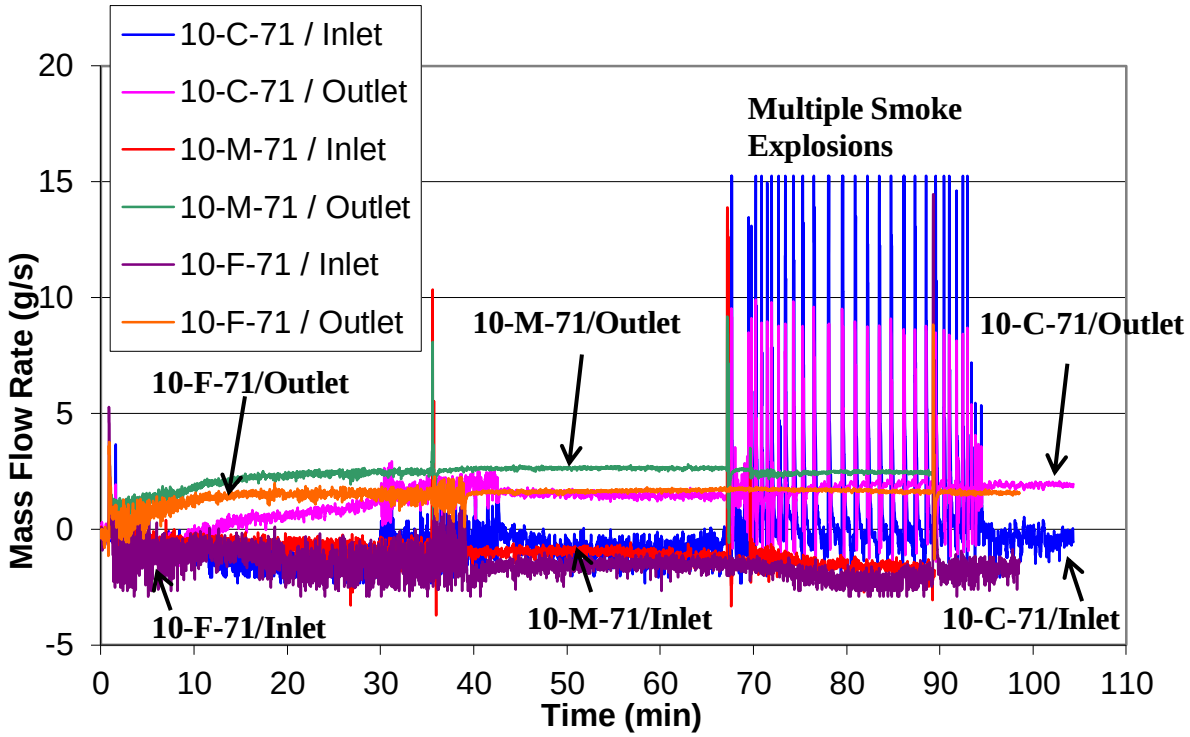


**Figure 5.16: Mass flow rates comparison between experiment 10-C-71, 10-M-71 and 10-F-71**

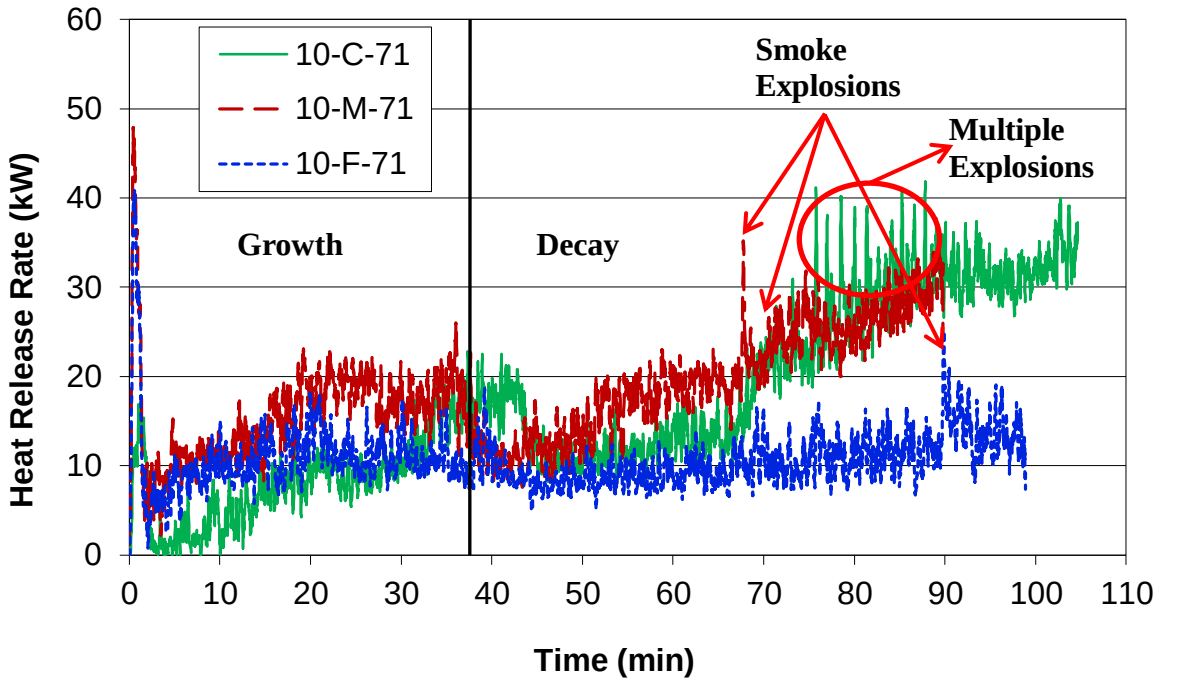


**Figure 5.17: Heat release rate histories comparison between experiment 10-C-71, 10-M-71 and 10-F-71**

## 5.5 Experiments With 50 mm Vent

For all three experiments with the 50 mm vent opening, it was not as easy to characterise a smoke explosion as for the experiments with 71 mm and 100 mm vent opening. The fire development of those experiments did not fit the typical trend of a smoke explosion. The complete set of data for experiments with the 50 mm vent opening could be found in Appendix D.

In experiment 10-C-50, the fire went through a steady growth from 100 ℃ at 5 minutes to 300 ℃ at 106 minutes, followed by a series of ghosting fires that caused some sudden increases of temperature between 106 and 112 minutes. The ghosting fire depleted the available oxygen and forced the fuel to go into the smoldering combustion. A smoke explosion possibly occurred at 175 minutes judging from the temperature history constructed from the rear top (950 mm) thermocouple in Figure 5.18. Further analysis showed that there was a small puff of flame "dancing" on top of the crib. After that, the crib went back into the flaming combustion. The temperature rise at 175 minutes was measured of only 27 ℃, which was quite low compared to the average temperature rise of 180 ℃ at the smoke explosion calculated from other six experiments with 100 mm and 71 mm vent openings. The pressure history was not available for this experiment. However, the peak mass flow rate did not exceed its maximum, meaning the compartment pressure did not reach the 27 Pa criterion established in section 5.2.3, Therefore, it confirmed that the incident at 26 minutes was not energetic enough to be categorised as a smoke explosion.

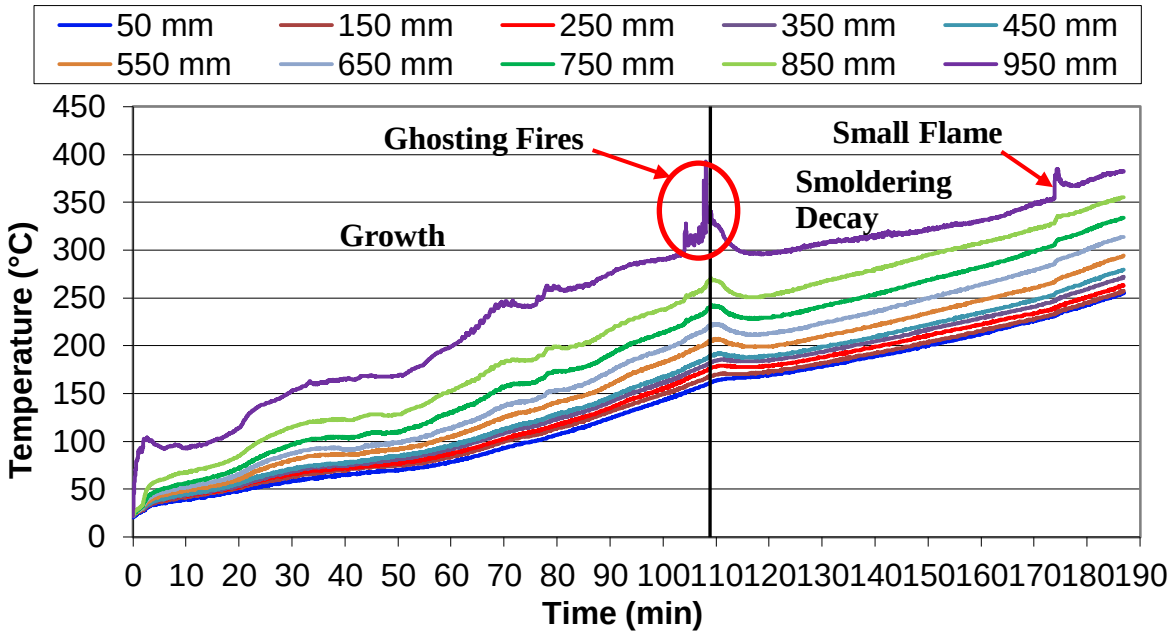


**Figure 5.18: Temperature histories from the rear thermocouple tree for experiment 10-C-50**

In experiment 10-M-50, it would appear that there might be a smoke explosion at 26 minutes upon the initial investigation. Further analysis showed that it was a series of ghosting fire. Followed by a temperature growth from 200 ℃ at 5 minutes to 300 ℃ at 21 minutes, the fire went into the smoldering phase at 21 minutes once the flame self-extinguished. At 26 minutes, there were two small flames appeared on the crib 2 seconds apart prior to the flame expansion, which was thought to be a sudden ignition of the combustible smoke around the crib. After that, the crib quickly went back into the smoldering phase and maintained in that situation until 131 minutes when the flame re-established on the crib. The temperature rise at 26 minutes was measured of only 95 ℃, which was relatively low compared to the average temperature rise of 180 ℃ at the smoke explosion. The compartment pressure did not reach 27 Pa, which confirmed that the incident at 26 minutes was not energetic enough to be categorised as a smoke explosion.

In experiment 10-F-50, the fire went into smoldering at 20 minutes and stayed in the smoldering phase till the end of the experiment. No smoke explosions were recorded in the video footage for this experiment, nor did the temperature history, mass flow rates or the gas concentrations suggest otherwise. Unfortunately, the parameters used to characterise the smoke explosion did not provide an obvious explanation for why the smoldering phase did not transition into a smoke explosion.

# Chapter 6 Conclusions

A reduced scale fire compartment with high durability and sustainability was constructed for the purpose of smoke explosion experiments. Experimental measurements including temperature, pressure, mass loss history, mass flow rate, gas concentration and heat release rate were recorded to help gain valuable insights in smoke explosion phenomena. A Phi-meter was set up to monitor the equivalence ratio in the combustion system so that the level of hydrocarbon within the compartment could be calculated based on the chemical reaction equation. However, due to irresolvable technical issues with the Phi-meter during the calibration process, the level of unburned hydrocarbon was unable to be measured.

A total of twenty experiments were completed including both exploratory and final experiments. Eleven exploratory experiments were carried out prior to final set of experiments, in order to reproduce smoke explosions and develop the final experimental matrix for a more thorough investigation of the smoke explosion phenomenon. Final nine experiments were designed and conducted in order to further study the smoke explosion phenomenon in detail. Both qualitative and quantitative analysis and comparisons were made against the combustion and explosion under various experimental conditions including three vent opening sizes (100 mm, 71mm and 50 mm) and three fuel elevations (780 mm, 500 mm and 270 mm). The experimental data used in the analysis were temperature, pressure, layer height, gas concentration, fuel mass loss, mass flow rate through the vents and heat release rate.

Based on the observations and the experimental results, the following scenario was developed to describe the smoke explosion phenomenon. When a fire developed in a closed compartment, initially there was sufficient oxygen for the fire to become established. As the fire evolved, the upper layer temperature increased while the oxygen within the compartment decreased forcing the combustion to slow down. Under the right conditions, the fire could turn into smoldering combustion with a large quantity of unburned fuel being discharged into the atmosphere and the gas concentrations reaching a quasi-steady level. Once the combustible gas mixture entered its flammable range, the

combustible mixture could ignite and turned into a large fire ball occupying the whole compartment.

Based on the analysis of the smoke explosion experiments, the following characteristics and commonalities were discovered.

1. The temperature rise for all smoke explosions ranged between 146 ℃ to 224 ℃.
2. The pressure difference inside the compartment had to be at least 27 Pa for it to be considered as a smoke explosion.
3. The maximum pressure recorded for a single smoke explosion was 4934 Pa.
4. No change in ventilation conditions were made throughout any smoke explosion experiment.
5. The smoldering phase was believed to be a necessary condition for the smoke explosion to occur.

The results from the experiments also showed that the vent size and the fuel elevation all had impact on the fire development and the occurrence of the smoke explosion. It was found that the vent size must be $\geq$ 50 mm in order for smoke explosion to occur. When the vent size was < 50 mm, the crib still entered into the smoldering combustion, but the ventilation was so limited that the quantity of gasified hydrocarbon was insufficient for a smoke explosion to occur. The fuel elevation had no influence on the occurrence of the smoke explosion. However when the fuel was placed near the ceiling, the temperature, the mass flow rate and the heat release rate were all lowered. Only minor difference was observed between the case where fuel was placed in the middle and on the floor.

Neither CO nor $O_2$ was considered as the sole triggering factor for the smoke explosion for the following reasons:

1. The ignition of a gas mixture within a confined space was determined by the overall flammable limit calculated from each combustible gas component from the mixture. The concentration of CO had already plateaued at a quasi-steady level below its lower flammable limit prior to the smoke explosion. Additionally, the level of CO when smoke explosions occurred scattered within a range of 1.9% to 4.3%. Therefore, the CO was not considered as a dominant component within the gas mixture.

2. The concentration of $O_2$ and $CO_2$ always plateaued at a quasi-steady level prior to smoke explosions. Experiments with larger vents had a longer smoldering decay, i.e., the quasi-steady state maintained for a longer period of time than it did in those experiments with smaller vents. One possible explanation was that the amount of excess pyrolysates needed to reach a critical value so that the fuel/air mixture was within the desired flammable range for the smoke explosion to occur.

3. Similar values of CO and $O_2$ concentrations that created smoke explosions were also seen in the experiments without any smoke explosions.

The concentration of CO ranged between 1.9% and 4.3% when the smoke explosion occurred, which was below the lower flammable limit of CO, therefore it was theorised that the unburned hydrocarbons made up a significant amount of portion in determining the flammable range of the combustible gas mixture. Although the level of CO was not considered as the sole triggering factor for the smoke explosion, it still played an important role in terms of predicting the smoke explosion.

# Chapter 7 Future Recommendations

It is recommended that the future researchers should include the following work and improvements.

- The lower layer gas concentrations need to be monitored along with the upper layer to create a gas species profile within the compartment.
- The amount of unburned hydrocarbons inside the compartment needs to be continuously monitored in order to estimate the flammable limit of the combustible mixture in the upper layer.
- More experiments involving higher/lower fuel mass and other vent sizes such as > 100 mm and < 50 mm are recommended to examine the threshold conditions for a smoke explosion to occur.
- The pressure in the compartment should be characterised using a pressure transducer with at least a range of 5 kPa, as part of the investigation for smoke explosion phenomena.
- The impact of the crib height on the mass loss rate and the time when smoke explosion occurs needs to be studied by varying the heights while fixing the weight.
- The location of the fuel needs to be further investigated to understand its impact on the mixing of the combustible gases and oxygen. Having located the fuel at the rear of the compartment, the possible locations for any future research should include front and middle of the compartment, or corners of the compartment.
- The mesh of the cage needs to be finer while still being capable of providing sufficient air flow, so that the fuel will not fall off the loading table at the smoke explosion causing inaccurate measurement.

# References

"University of Canterbury Furniture Calorimeter Calibration Procedure." (1999).

"University of Canterbury Furniture Calorimeter Test Procedure." (1999).

Abbasi, T., and Abbasi, S. A. (2007). "Dust explosions-Cases, causes, consequences, and control." *Journal of Hazardous Materials*, 140(1-2), 7-44.

Babrauskas, V. (2002). "Heat Release Rates." SFPE handbook of fire protection engineering, P. J. DiNenno, ed., National Fire Protection Association; Society of Fire Protection Engineers, Quincy, Mass. Bethesda, MD., 3-14.

Babrauskas, V., Parker, W. J., Mulholland, G., and Twilley, W. H. (1994). "The Phi Meter - a Simple, Fuel-Independent Instrument for Monitoring Combustion Equivalence Ratio." *Review of Scientific Instruments*, 65(7), 2367-2375.

Beyler, C. (2002). "Flammability Limits of Premixed and Diffusion Flames." SFPE handbook of fire protection engineering, P. J. DiNenno, ed., National Fire Protection Association; Society of Fire Protection Engineers, Quincy, Mass. Bethesda, MD., 2-172 to 2-187.

Bowyer, M., and Wertman, S. (2008). "Nine Fire Fighters Injured in an Explosion at a Restaurant Fire." The National Institute for Occupational Safety and Health, http://www.cdc.gov/niosh/fire/pdfs/face200803.pdf Accessed November 11,2010.

Cooper, L. Y. (2002). "Compartment Fire-Generated Environment and Smoke Filling." SFPE handbook of fire protection engineering, P. J. DiNenno, ed., National Fire Protection Association; Society of Fire Protection Engineers, Quincy, Mass. Bethesda, MD., 3-246.

Croft, W. M. (1980). "Fires involving explosions -- A literature review." *Fire Safety Journal*, 3(1), 3-24.

Emmons, H. W. (2002). "Vent Flows." SFPE handbook of fire protection engineering, P. J. DiNenno, ed., National Fire Protection Association; Society of Fire Protection Engineers, Quincy, Mass. Bethesda, MD., 2-32, 2-35.

Fleischmann, C. M. (1993). "Backdraft Phenomena," University of California at Berkeley, CA 94720, USA.

Friedman, R. (2003). "Theory of Fire Extinguishment." Fire Protection Handbook, A. E. Cote, ed., National Fire Protection Association, Quincy, Massachusetts, 2-84.

Gottuk, D. T., Peatross, M. J., Farley, J. P., and Williams, F. W. (1999). "The development and mitigation of backdraft: a real-scale shipboard study." *Fire Safety Journal*, 33(4), 261-282.

Grimwood, P. (2007). "Smoke Burns." http://www.firetactics.com/SMOKE_BURNS.htm Accessed November 11, 2010.

Karlsson, B., and Quintiere, J. G. (2000). *Enclosure fire dynamics*, CRC Press, Boca Raton, FL.

Madrzykowski, D., and Stroup, D. W. (2008). "Flammability Hazard of Materials." NFPA Fire Protection Handbook, A. E. Cote, ed., National Fire Protection Assoc, Quincy, MA, 2-31 to 2-48

Mannan, S., and Lees, F. P. (2005). *Lee's loss prevention in the process industries: hazard identification, assessment, and control*, Elsevier Butterworth-Heinemann.

Ohlemiller, T. J. (2002). "Smoldering Combustion." SFPE handbook of fire protection engineering, P. J. DiNenno, ed., National Fire Protection Association; Society of Fire Protection Engineers, Quincy, Mass. Bethesda, MD., 2-200 to 2-210.

Parkes, A. R. (2009). "The impact of size and location of pool fires on compartment fire behaviour," Civil and Natural Resources Engineering, University of Canterbury, Christchurch.

Purser, D. A. (2002). "Toxicity Assessment of Combustion Products." SFPE handbook of fire protection engineering, P. J. DiNenno, ed., National Fire Protection Association; Society of Fire Protection Engineers, Quincy, Mass. Bethesda, MD., 2-123.

Quintiere, J. G. (1997). "Fire Investigation An Analysis of the Waldbaum Fire, Brooklyn, NY August 3, 1978." *Fire Science and Technology*, Vol. 17, pp.10-14.

Steward, P. D. C. (1914). "Dust and smoke explosions." *National Fire Protection Association Quarterly*(7), 424 - 428.

Sugawa, O., Kawagoe, K., and Oka, Y. (1991). "Burning Behavior in a Poor-Ventilation Compartment Fire - Ghosting Fire." *Nuclear Engineering and Design*, 125(3), 347-352.

Sutherland, B. J. (1999). "Smoke Explosions," School of Engineering University of Canterbury, Christchurch, N.Z.

Wooley, W. D., and Ames, S. A. (1975). "The explosive risk of stored foamed rubber." *Building Research Establishment*, current page 36/75.

# Appendix A Burning Regimes of Cribs

For cribs ignited uniformly overall, it is observed that the burning rate can be governed by one of three conditions. The least of following three equations is to be taken as the governing rate.

1. Fuel Surface Control: This limit applies to cribs with wide inter-stick spacings,

$$\dot{m} = \frac{4}{D} m_o v_p \left(1 - \frac{2 v_p t}{D}\right) \qquad \textbf{Equation A.1 (2002)}$$

Where,

D = stick thickness (m)

$m_o$ = initial mass of the crib (kg)

$v_p = 2.2 \times 10^{-6} D^{-0.6}$ (regression velocity)

2. Crib Porosity Control: This governs for tightly packed cribs,

$$\dot{m} = 4.4 \times 10^{-4} \left(\frac{s}{h_c}\right)\left(\frac{m_o}{D}\right) \qquad \textbf{Equation A.2 (2002)}$$

Where,

S = stick spacing (m)

$h_c$ = crib height (m)

D = stick thickness (m)

$m_o$ = initial mass of the crib (kg)

3. Room Ventilation Control: This is based on the maximum oxygen that can be supplied to the room,

$$\dot{m} = 0.12 A_v \sqrt{h_v}$$ **Equation A.3 (2002)**

Where,

$A_v$ = ventilation opening area ($m^2$)

$h_v$ = ventilation opening height (m)

| 10 kg Crib | | Wood Stick (m) | |
|---|---|---|---|
| Length | 0.3 m | Thickness | 0.03 m |
| Width | 0.3 m | Spacing | 0.02 m |
| Height | 0.3 m | Vent Diameter | 0.1 m |
| Weight | 10 kg | Vent Height | 0.2 m |
| $v_p$ | 0.000018 | Vent Area | 0.0157 m2 |
| $\dot{m}_{fuel}$ | 24.02 g/s | | |
| $\dot{m}_{porosity}$ | 9.78 g/s | | |
| $\dot{m}_{ventilation}$ | 0.84 g/s | | |

| 5 kg Crib | | Wood Stick (m) | |
|---|---|---|---|
| Length | 0.3 m | Thickness | 0.03 m |
| Width | 0.3 m | Spacing | 0.02 m |
| Height | 0.2 m | Vent Diameter | 0.1 m |
| Weight | 5 kg | Vent Height | 0.2 m |
| $v_p$ | 0.000018 | Vent Area | 0.0157 m2 |
| $\dot{m}_{fuel}$ | 12.01 g/s | | |
| $\dot{m}_{porosity}$ | 9.78 g/s | | |
| $\dot{m}_{ventilation}$ | 0.84 g/s | | |

# Appendix B The Development of The Phi-Meter

The Phi meter is first introduced by Babrauskas et al (1994) as a simple fuel-independent apparatus measuring the equivalence ratio $\phi$, which is defined as the ratio between the available fuel and air/oxygen of the sample gas, divided by the stoichiometric fuel to air/oxygen ratio.

$$\phi = \frac{\left(\dot{m}_f / \dot{m}_o\right)_{sample}}{\left(\dot{m}_f / \dot{m}_o\right)_{stoichiometric}} \qquad \textbf{Equation B.1}$$

The denominator is usually denoted as r and has a constant value corresponding to each combustible gas, which leaves two variables in the numerator that affects the value of $\phi$. When $\phi$=1, it is referred as stoichiometry, where all reactants are converted to products with no remaining reactants in the combustion process. When $\phi$<1, the fire is considered to be over-ventilated, where the amount of oxygen is more than needed to fully combust the fuel. A typical example of an over-ventilated fire is a free-burn fire. On the contrary, when $\phi$>1, the fire is considered to be under-ventilated, where the amount of oxygen is inadequate for the fuel to fully combust, creating a fuel rich environment.

## B.1 The Concept of Phi-Meter

Not only is the equivalence ratio a parameter that indicates the level of ventilation during a fire, whether it is oxygen rich or fuel rich, it can be utilized to calculate the amount of unburned fuel left in the combustion products, given the equivalence ratio is known from the equation derived by Babrauskas et al (1994). The idea of the original Phi meter is to sample the gas from the compartment and inject oxygen/air into the furnace tube where the sampled gas is re-combusted, so that all carbon atoms a reduced to $CO_2$ and all hydrogen atoms are reduced to $H_2O$. However, only $O_2$ can be measured from the gas mixture, due to the simplicity and portability of the original Phi meter. The $CO_2$ is removed by Ascarite chemical sorbant (NaOH) and $H_2O$ is removed by Drierite desiccant

($CaSO_4$). The basic principle of the original Phi meter is simply maintaining complete combustion no matter how much unburned gas is in the gas mixture. In the case of oxygen rich/fuel lean case, where $\phi$ <1, excessive oxygen has already presented in the gas mixture, so that the remaining combustible gas will be easily reduced down to $CO_2$ and $H_2O$, but in the case of oxygen lean/fuel rich case, where $\phi$ >1, insufficient oxygen will lead to an incomplete combustion, so that an extra fixed amount of oxygen is essential to maintain a complete combustion.

For this particular research, the original Phi meter is further developed and modified to measure all necessary gas species such as $O_2$, $CO_2$ and CO. However, $H_2O$ iss still excluded in the measurement, because the gas analyser is not capable of handling water. The water is filtered by cooling the combusted gas mixture then passing through the Drierite desiccant. Since the equations for calculating the equivalence ratio has been derived based on the usage of the original Phi meter, now by measuring both $O_2$, $CO_2$ and CO, a new set of equations is required to address the additional gas species.

## B.2 The Theory of Phi-Meter

All the equations in this section are modified based on Parkes' research. One can refer the original work for detailed explanation (2009). The basic relationship of the equivalence ratio i expressed in Equation B.2. Under the situation where sampled gas is led into the furnace tube with no added oxygen, the equivalence ratio is considered to be less than 1 and complete combustion is expected. Therefore, the mass flow of the fuel in the sample must equal to the stoichiometric fuel flow, $\left(\dot{m}_f\right)_{sample} = \left(\dot{m}_f\right)_{stoichiometric}$ thus,

$$\phi = \frac{\left(\dot{m}_o\right)_{stoichiometric}}{\left(\dot{m}_o\right)_{sample}} \qquad \textbf{Equation B.2}$$

where $\left(\dot{m}_o\right)_{sample}$ is the oxygen molar flow from the sampled gas and $\left(\dot{m}_o\right)_{stoichiometric}$ is the oxygen molar flow required for stoichiometric combustion, which can be expressed as,

$$\left(\dot{m}_o\right)_{stoichiometric} = \left(\dot{m}_o\right)_{sample} - \left(\dot{m}_o\right)_{exhaust} \qquad \textbf{Equation B.3}$$

$$= \dot{m}^{o}_{O_2} - \dot{m}_{O_2}$$

Where $(\dot{m}_o)_{exhaust}$ is the exhaust oxygen molar flow (the molar flow of un-reacted oxygen). Substitute Equation B.3 into Equation B.2 gives,

$$\phi = \frac{\dot{m}^o_{O_2} - \dot{m}_{O_2}}{\dot{m}^o_{O_2}} \qquad \textbf{Equation B.4}$$

Since the amount of nitrogen is conserved during the burning process in the furnace tube, thus divide Equation B.4 by the molar flow of nitrogen where $\dot{m}^o_{N_2} = \dot{m}_{N_2}$, which gives

$$\phi = \frac{\frac{\dot{m}^o_{O_2}}{\dot{m}^o_{N_2}} - \frac{\dot{m}_{O_2}}{\dot{m}_{N_2}}}{\frac{\dot{m}^o_{O_2}}{\dot{m}^o_{N_2}}} \qquad \textbf{Equation B.5}$$

It is known that the ratio of the molar flow equals the ratio of the mole fraction, hence

$$\phi = \frac{\frac{X^o_{O_2}}{X^o_{N_2}} - \frac{X_{O_2}}{X_{N_2}}}{\frac{X^o_{O_2}}{X^o_{N_2}}} \qquad \textbf{Equation B.6}$$

For any given conditions, the sum of the mole fraction for each gas species must equal to 1, which gives

$$X^o_{N_2} = X_{N_2} = 1 - X_{O_2} - X_{CO_2} - X_{CO} \qquad \textbf{Equation B.7}$$

Substituting Equation B.7 back into Equation B.6 gives,

$$\phi = 1 - \frac{X_{O_2}}{X^o_{O_2}}\left(\frac{1 - X^o_{O_2} - X^o_{CO_2} - X^o_{CO}}{1 - X_{O_2} - X_{CO_2} - X_{CO}}\right) \quad \textbf{when } \phi < 1 \qquad \textbf{Equation B.8}$$

To account for the oxygen lean/fuel rich situation, extra oxygen must be added to the total flow. Therefore Equation B.3 and Equation B.5 become,

$$\left(\dot{m}_o\right)_{stoichiometric} = \left(\dot{m}_o\right)_{added} + \left(\dot{m}_o\right)_{sample} - \left(\dot{m}_o\right)_{exhaust}$$

$$= \dot{m}^a_{O_2} + \dot{m}^o_{O_2} - \dot{m}_{O_2}$$

**Equation B.9**

And

$$\phi = \frac{\frac{\dot{m}^a_{O_2}}{\dot{m}_{N_2}} + \frac{\dot{m}^o_{O_2}}{\dot{m}^o_{N_2}} - \frac{\dot{m}_{O_2}}{\dot{m}_{N_2}}}{\frac{\dot{m}^o_{O_2}}{\dot{m}^o_{N_2}}}$$

**Equation B.10**

The first term of Equation B.10 is the add oxygen equivalence ratio term and can be expressed separately as follows:

$$\phi^a_{O_2} = \frac{\frac{\dot{m}^a_{O_2}}{\dot{m}_{N_2}}}{\frac{\dot{m}^o_{O_2}}{\dot{m}^o_{N_2}}}$$

**Equation B.11**

The added oxygen flow and nitrogen flow in the numerator can be expressed in terms of volumetric flow by using ideal gas law.

$$\dot{m}^a_{O_2} = \frac{\dot{V}_{added} \cdot \dot{P}_{added}}{R\dot{T}_{added}}$$

**Equation B.12**

$$\dot{m}_N = \frac{\dot{V}_N \cdot \dot{P}}{R\dot{T}} = \frac{(1 - X_{O_2} - X_{CO_2} - X_{CO})\dot{V} \cdot \dot{P}}{R\dot{T}}$$

**Equation B.13**

The ambient oxygen and nitrogen flow in the denominator can be expressed as follows:

$$\frac{\dot{m}^o_{O_2}}{\dot{m}^o_{N_2}} = \frac{X^o_{O_2}}{1 - X^o_{O_2} - X^o_{CO_2} - X^o_{CO}}$$

**Equation B.14**

Thus the added oxygen equivalence term can be expressed as follows:

$$\phi_{O_2}^{a} = \frac{(1 - X_{O_2}^{o} - X_{CO_2}^{o} - X_{CO}^{o})\dot{V}_{added} \cdot \dot{P}_{added}\dot{T}}{X_{O_2}^{o}(1 - X_{O_2} - X_{CO_2} - X_{CO})\dot{V} \cdot \dot{P}\dot{T}_{added}} \qquad \textbf{Equation B.15}$$

Since the temperature at both upstream and downstream of the sample line is relatively unchanged and the pressure stays unchanged as long as the total flow rate remains constant, above equation becomes,

$$\phi_{O_2}^{a} = \frac{(1 - X_{O_2}^{o} - X_{CO_2}^{o} - X_{CO}^{o})\dot{V}_{added}}{X_{O_2}^{o}(1 - X_{O_2} - X_{CO_2} - X_{CO})\dot{V}} \qquad \textbf{Equation B.16}$$

And the final equation for calculating the equivalence ratio when $\phi > 1$ can be expressed as follows:

$$\phi = 1 - \frac{X_{O_2}}{X_{O_2}^{o}}\left(\frac{1 - X_{O_2}^{o} - X_{CO_2}^{o} - X_{CO}^{o}}{1 - X_{O_2} - X_{CO_2} - X_{CO}}\right) + \frac{(1 - X_{O_2}^{o} - X_{CO_2}^{o} - X_{CO}^{o})\dot{V}_{added}}{X_{O_2}^{o}(1 - X_{O_2} - X_{CO_2} - X_{CO})\dot{V}} \qquad \textbf{Equation B.17}$$

**when** $\phi > 1$

Where,

$X_{O_2}^{o}$ = baseline oxygen mole fraction at ambient air

$X_{CO_2}^{o}$ = baseline carbon dioxide mole fraction at ambient air

$X_{CO}^{o}$ = baseline carbon monoxide mole fraction at ambient air

$X_{O_2}$ = oxygen mole fraction during the combustion

$X_{CO_2}$ = carbon dioxide mole fraction during the combustion

$X_{CO}$ = carbon monoxide mole fraction during the combustion

$\dot{V}_{added}$ = volumetric flow of the added oxygen (l/s)

$\dot{V}$ = total volumetric flow to the furnace analyser (l/s)

## B.3 The Construction of Phi Meter

As part of this research, a more robust Phi meter is developed based on the idea of the original model, yet the basic principle stays the same. The combustion gas is sampled and fed into the furnace tube where unburned gas species are re-combusted. An extra steam of oxygen is injected into the furnace to assist the re-combustion. The combustion gas is drawn into the system using two 12V pumps. One pump is required for the room analyser by which the compartment gas are directly measured and monitored. The other pump is required for the furnace analyser by which the re-combusted gas species are measured. The sample line is wrapped with electric heating elements and covered with reinforced glass fiber as thermal insulation to prevent sampled gas from condensation. Since extra oxygen is needed to achieve a complete combustion, a constant stream of 1 l/s oxygen is provided and controlled by a MFC (Mass Flow Controller). Equation B.1 shows a schematic diagram of a complete layout of the phi meter, in addition to that, a schematic diagram of the second sample line leading to the room analyser is also included.

The main component of the Phi meter is the furnace. It is 1000 mm long, 250 mm wide and 250 mm high as shown in Figure B.2. It consists of a furnace tube, heating elements, ceramic fiber insulations, temperature control unit and a safety mesh. The furnace tube is made of high temperature proof quartz glass. It measures 1500 mm long, 60 mm in diameter with both ends extended out of the furnace for observation. Both ends are sealed by a two-part metal screw cap, with a high temperature rubber gasket. Each metal cap is fitted with a stainless steel tube with a two-way connector on top for connection of the sample line as shown in Figure B.2.

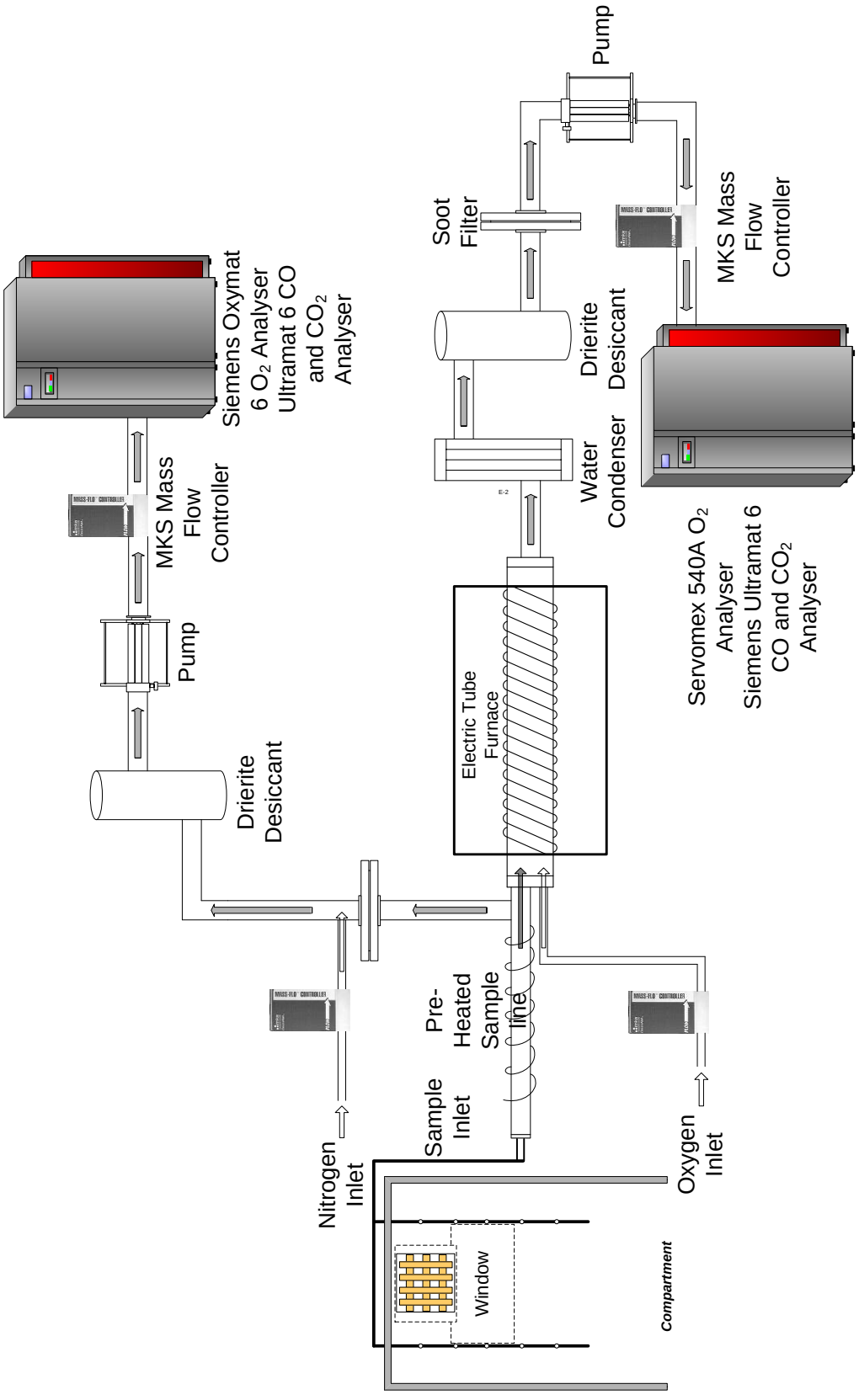


**Figure B.1: Schematic diagram of the Phi meter layout showing the sample line and instrumentations in conjunction with the compartment gas analyser layout**

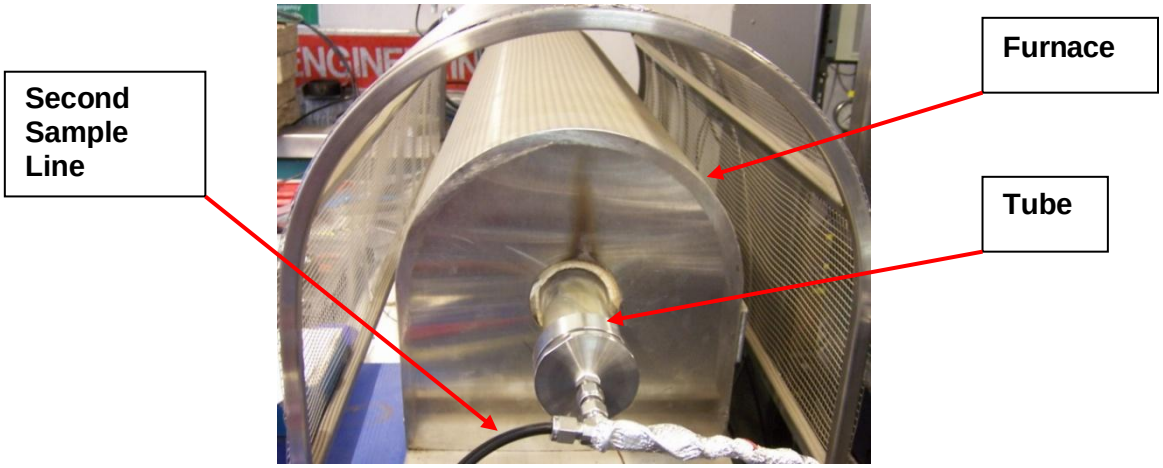


**Figure B.2: Photograph of the furnace showing the quartz glass tube with its cap and connector**

The tube is wrapped with two electric heating elements providing a working temperature up to 1000 ℃. In order to get the highest possible temperature out of the furnace while keep it under stable condition, 900 ℃ is chosen as the operating temperature for all experiments. The temperature is adjusted manually from room temperature to 900 ℃ at a 100 ℃ interval, because the automatic temperature ramping often ended in over-heating the tube and it is much harder for the furnace to cool down to a desired level than to heat it up. The furnace quartz tube is muffled with ceramic fiber insulation to maintain a high temperature environment.

Subsequently, the re-combusted gas mixture is passed through a condenser and Drierite to remove all the water first, and then it went through a soot filter to remove any remaining soot particle. By the time the gas mixture leaving the furnace tube, there ought to be no solid particle left, but for conservative purposes, a soot filter is still placed in the sample line. The amount of sampled gas is precisely controlled by another MFC working at 6 l/s, before entering the gas analysers. The $O_2$ is measured using a Servomex 540A Paramagnetic Oxygen Analyser. The CO and $CO_2$ are measured using a Siemens Ultramat 6 NDIR (Non Dispersive Infra Red) Analyser.

A second set of analysers are used to measure the sampled gas mixture directly from the compartment, in order to monitor the gas species within the compartment immediately prior to the smoke explosion. At the inlet of the furnace tube, the sample line is split using

a T-connector as shown in Figure B.2. A soot filter is the first appliance along that sample line, because the sample gas from the compartment contains large amounts of soot and pyrolysed fuel. During exploratory experiments, the filters are unable to sustain the whole experiment session due to the length of experiments. Not only is the filter saturated with condensed water, and blocked by soot and sticky tar, the sampling tubes inside the compartment are also blocked. To solve the problem, a filter with much bigger area is utilised to minimise the negative impacts from water saturation and soot clogging. The sampling tubes within the compartment are increased from 1.5 mm to 2.5 mm to prevent further blockage. Before and after each experiment session, the sampling tubes are cleaned to make sure there is no residual left.

Due to the constraint of operating capacity of analysers, the sample gas is diluted with $N_2$, which is controlled by a MFC working at 1.8 l/s. Again, Drierite desiccant is placed in the sample line to get rid of most of the water following by a 12 V pump and a MFC drawing a total of 2.5 l/s gas mixture into the compartment analysers.

## B.4 The Calibration of Phi Meter

Ten runs are performed in order to calibrate the Phi meter. The process of the calibration is to pass through propane and oxygen into the furnace at a pre-calculated ratio of flow rates, which are controlled by two MFCs. The theoretical equivalence ratio is determined from the combustion equation of Propane ($C_3H_8$) and the readings of MFCs, whereas the experimental equivalence ratio is calculated from gas measurements of the analyser using Equation B.8 and Equation B.17. Finally, by comparing the calculated and experimental equivalence ratio, the validation of the Phi meter can be confirmed.

The reason to choose Propane as the calibration gas is its ready availability. The following equation shows the combustion equation of Propane,

$$C_3H_8 + 5O_2 \rightarrow 3CO_2 + 4H_2O \qquad \textbf{Equation B.18}$$

The stoichiometric ratio of fuel and oxygen ratio r can be calculated using equation 9.5 given by Karlsson and Quintiere (2000).:

$$r = \frac{m_{fuel}}{m_{O_2}} = \frac{3\times 12 + 8\times 1}{5\times(16\times 2)} = 0.275$$

Therefore,

$$\phi = \frac{\dot{m}_{fuel} / \dot{m}_{O_2}}{r} = \frac{\dot{m}_{fuel} / \dot{m}_{O_2}}{0.275}$$

During initial experiments, three MFCs are used to control the flow of added oxygen, flow of the fuel and the total flow. The MFC controlling the added oxygen has a maximum capacity of 20 l/s. The MFC controlling the fuel has a maximum capacity of 5 l/s. The MFC controlling the total flow has a maximum capacity of 10 l/s. All MFCs are operating on a percentage basis. The added oxygen is fixed at 4 l/s and the total flow is fixed at 6 l/s. Thus,

$$\dot{m}_{fuel} + \dot{m}_{air} + \dot{m}_{O_2} = \dot{m}_{total} = 6 \text{ l/s}$$

An equivalence ratio range from 0 to 4 is examined against the experimental values.
Table B.3 summarises all the desired flow rates regarding each level of equivalence ratio. Column 1 is the desired equivalence ratio. Column 2 is the amount of fuel passing through the 2 l/s mass flow controller. Column 3 and 4 are the required amount of oxygen and its corresponding level of air passing through the 2 l/s mass flow controller. Column 5 is the fixed oxygen supply for the phi-meter. Column 6 is the percentage value of the fuel calculated for the mass flow controller including the gas factor of propane.

| $\phi$ | Fuel (l/s) | Oxygen in Air (l/s) | Ambient Air (l/s) | Added Oxygen (l/s) | Fuel MFC* (% of 5 l/s ) |
|---|---|---|---|---|---|
| 0.1 | 0.011 | 0.417 | 1.989 | 4.000 | 0.61% |
| 0.5 | 0.056 | 0.407 | 1.944 | 4.000 | 3.10% |
| 1 | 0.109 | 0.396 | 1.891 | 4.000 | 6.04% |
| 1.5 | 0.159 | 0.386 | 1.841 | 4.000 | 8.81% |
| 2 | 0.207 | 0.376 | 1.793 | 4.000 | 11.45% |
| 2.5 | 0.252 | 0.366 | 1.748 | 4.000 | 13.95% |
| 3 | 0.295 | 0.357 | 1.705 | 4.000 | 16.33% |
| 3.5 | 0.336 | 0.349 | 1.664 | 4.000 | 18.59% |
| 4 | 0.375 | 0.341 | 1.625 | 4.000 | 20.75% |
| A gas factor of 2.77 must be applied to propane according to the MKS mass flow controller operational manual | | | | | |

**Table B.3: Summary of various flow rates for calculating the theoretical equivalence ratio**

Figure B.3 shows a result of the phi meter calibration, the experimental equivalence ratio is not matching with the theoretical one, However, in the range of 0 and 2, the gap between two graphs gradually became smaller and smaller. Conversely, in the range of 2 and 4, two graphs are in a quite good agreement.

In order to try to fix the issue, another MFC with maximum capacity of 2 l/s is placed in the sample line to strictly control the flow of air. All the flows are known and controlled before entering the furnace. The calibration is re-performed under the same combinations of fuel and oxygen flow rates to minimise the possibility of errors. However, the calibration results are still unsuccessful with similar profiles previously stated.

The suspected error is believed lying within the MFC itself, after only ambient air is fed into the furnace, the $O_2$ reading from the gas analyser is less than to 21%. Additionally, the whole sample system is checked for leakage but with no success in finding the error.

Therefore, the experiments have to be paused and postponed when the MFCs are returned to the manufacturer for further investigations.

After the MFCs are recalibrated and returned to us, the attached calibration sheet shows no faults or errors of those four MFCs. However, the issue is still present during the later calibration. Finally, due to the time constraint, we decide to discard the Phi meter, and use one set of gas analyser to measure the gas concentration directly from the compartment during experiments. By doing that, at least another major combustible gas CO can be monitored, which is also considered to be a triggering gas species for smoke explosions.

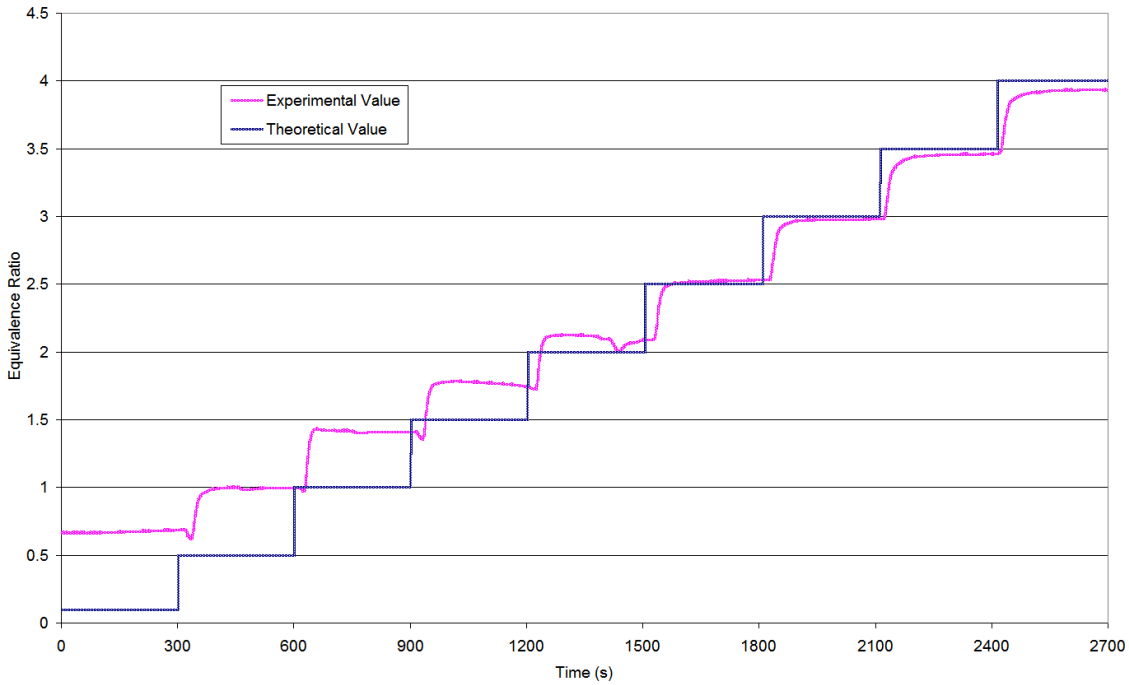


**Figure B.3: A comparison of the experimental and theoretical equivalence ratio**

# Appendix C Exploratory Experiments Data

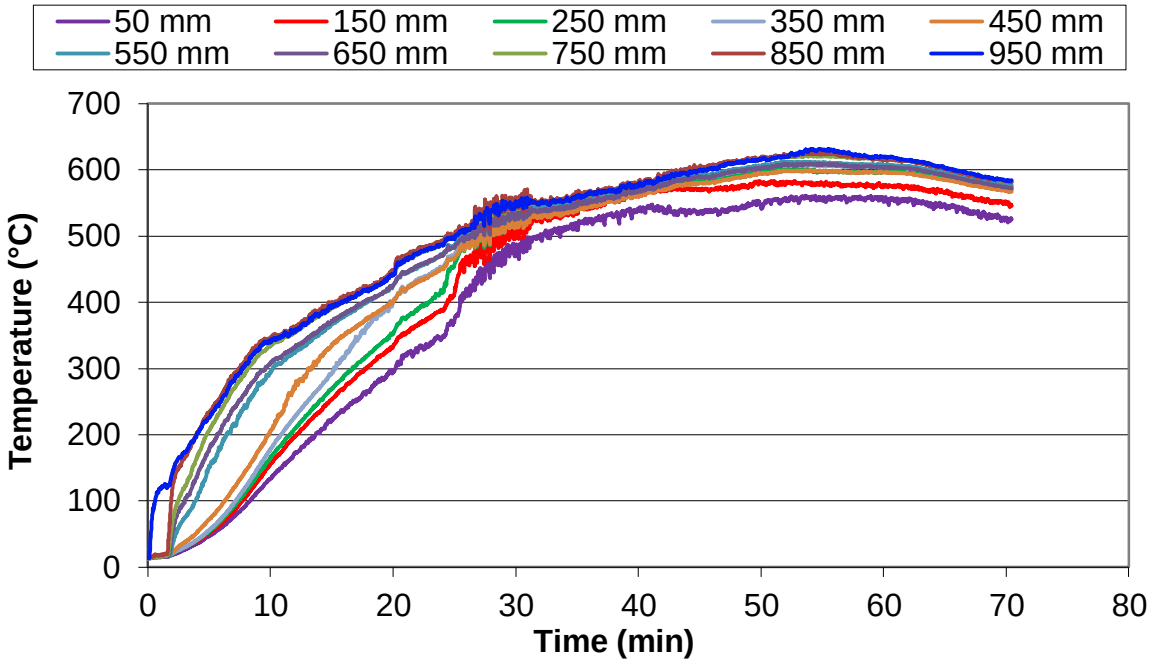


**Figure C.1: Temperature histories for experiment 10-F-100 at the front of the compartment**

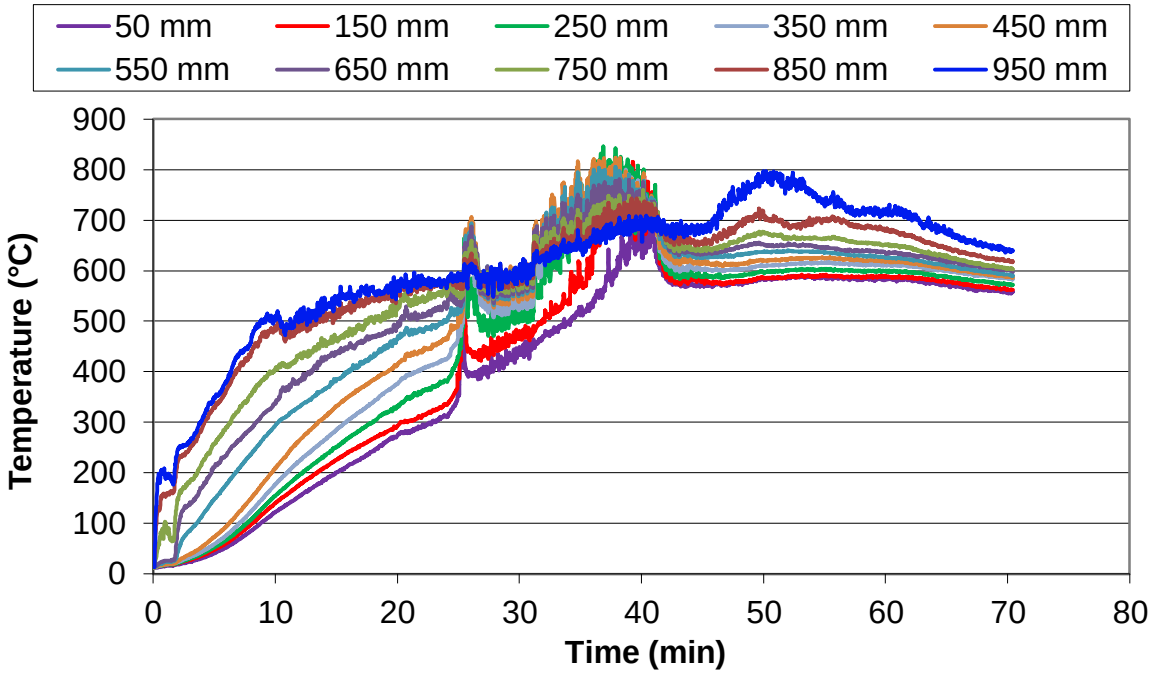


**Figure C.2: Temperature histories for experiment 10-F-100 at the rear of the compartment**

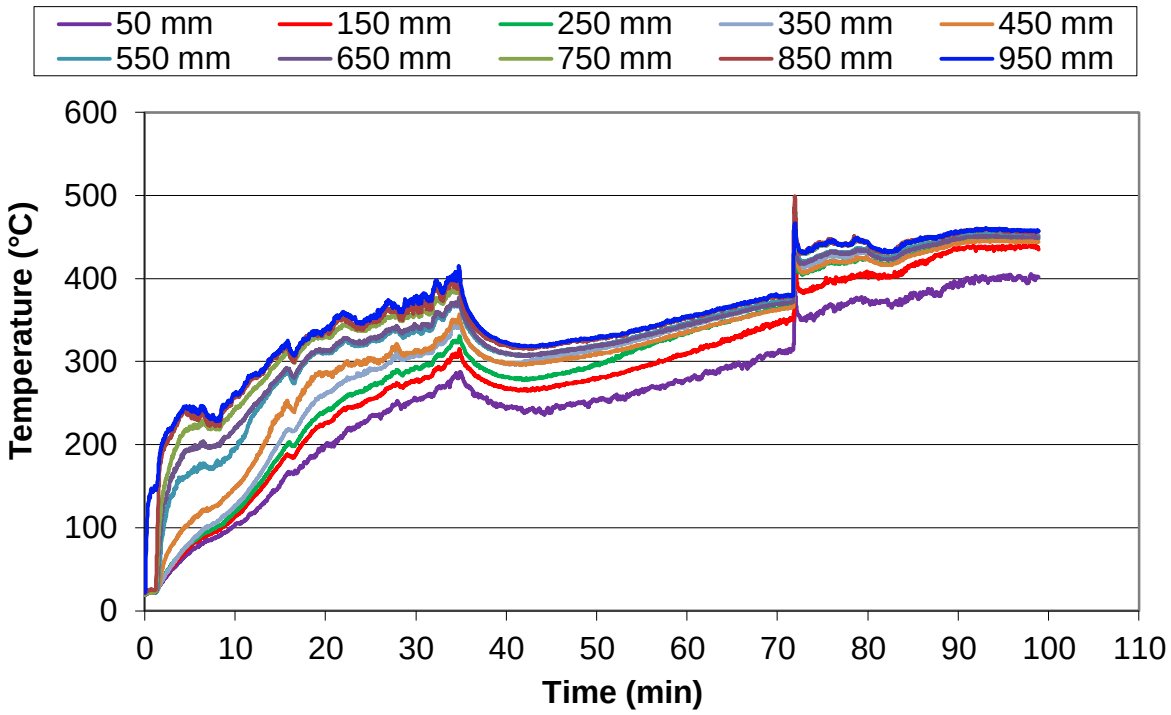


**Figure C.3: Temperature histories for experiment 10-F-71 at the front of the compartment**

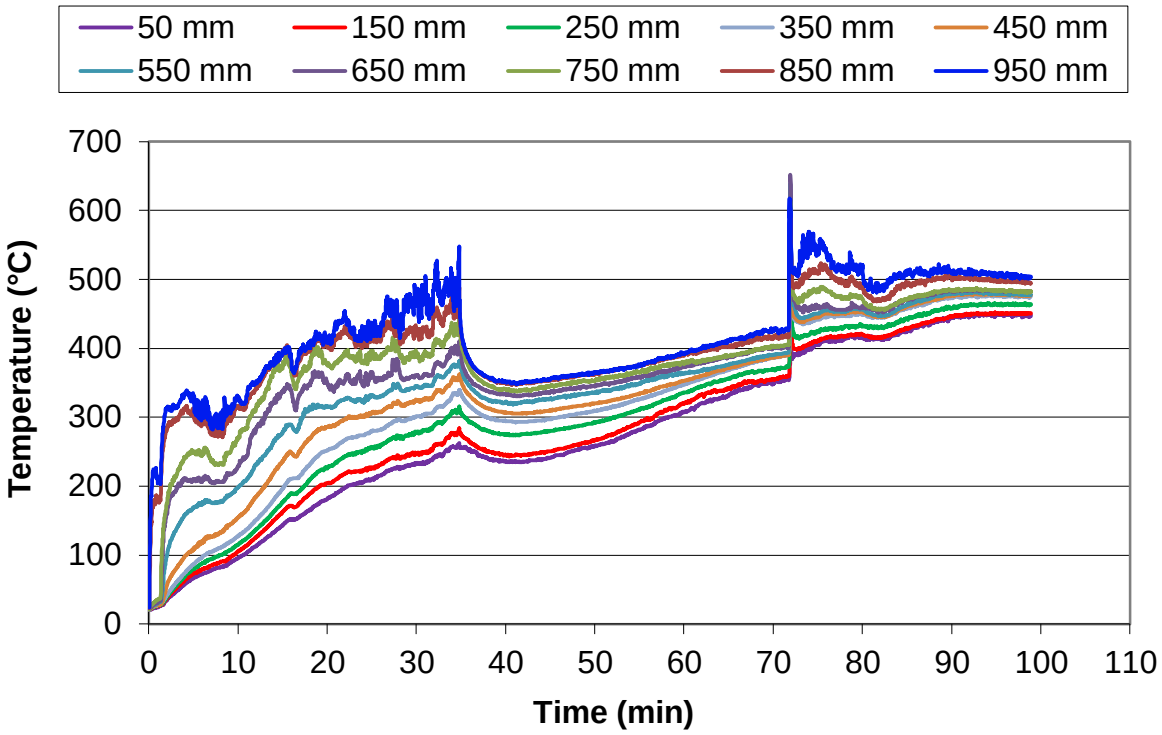


**Figure C.4: Temperature histories for experiment 10-F-71 at the rear of the compartment**

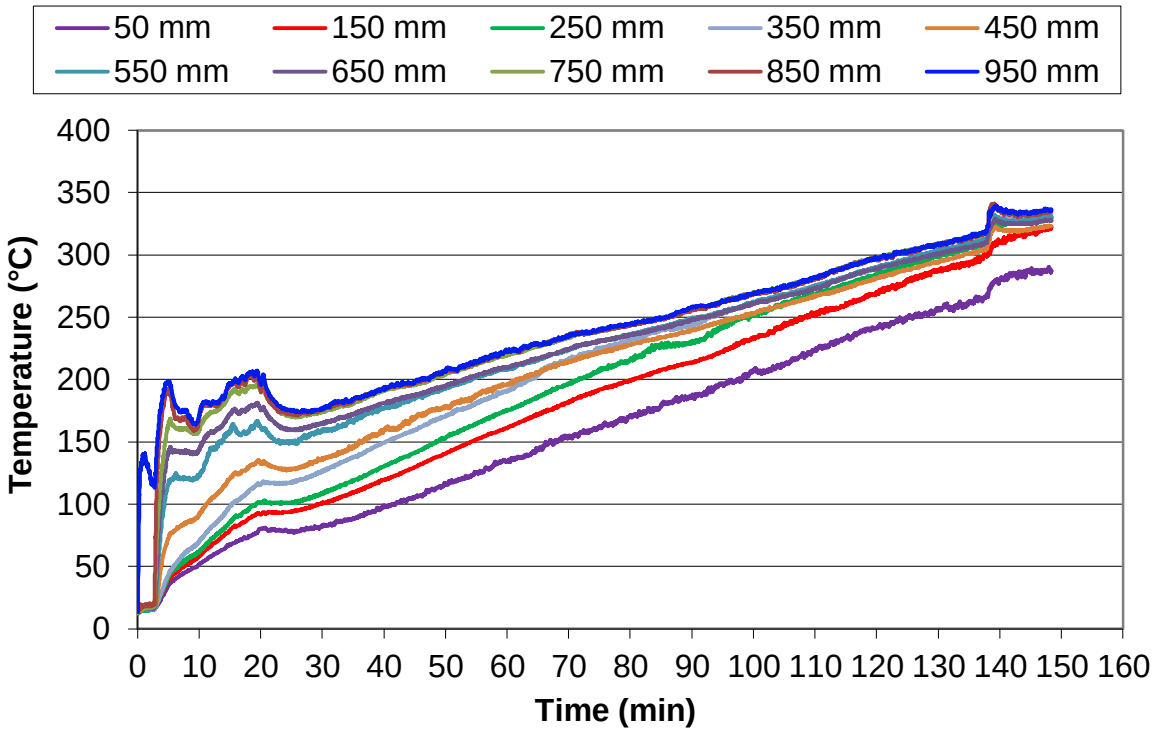


**Figure C.5: Temperature histories for experiment 10-F-50 at the front of the compartment**

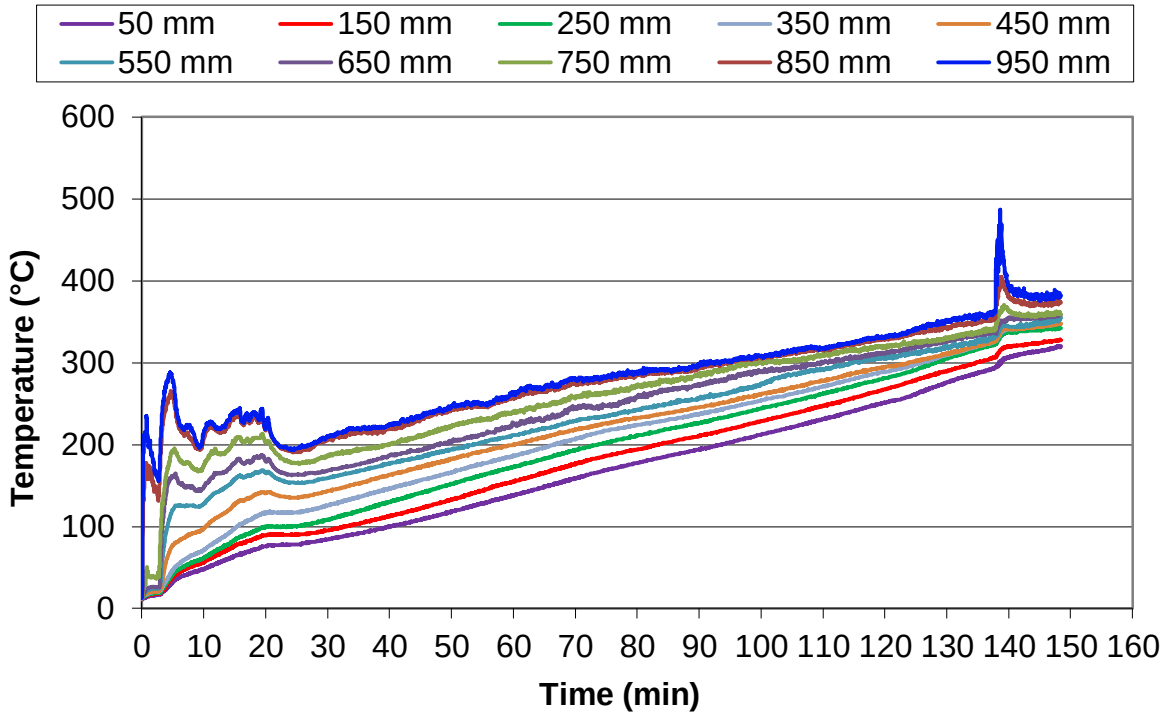


**Figure C.6: Temperature histories for experiment 10-F-50 at the rear of the compartment**

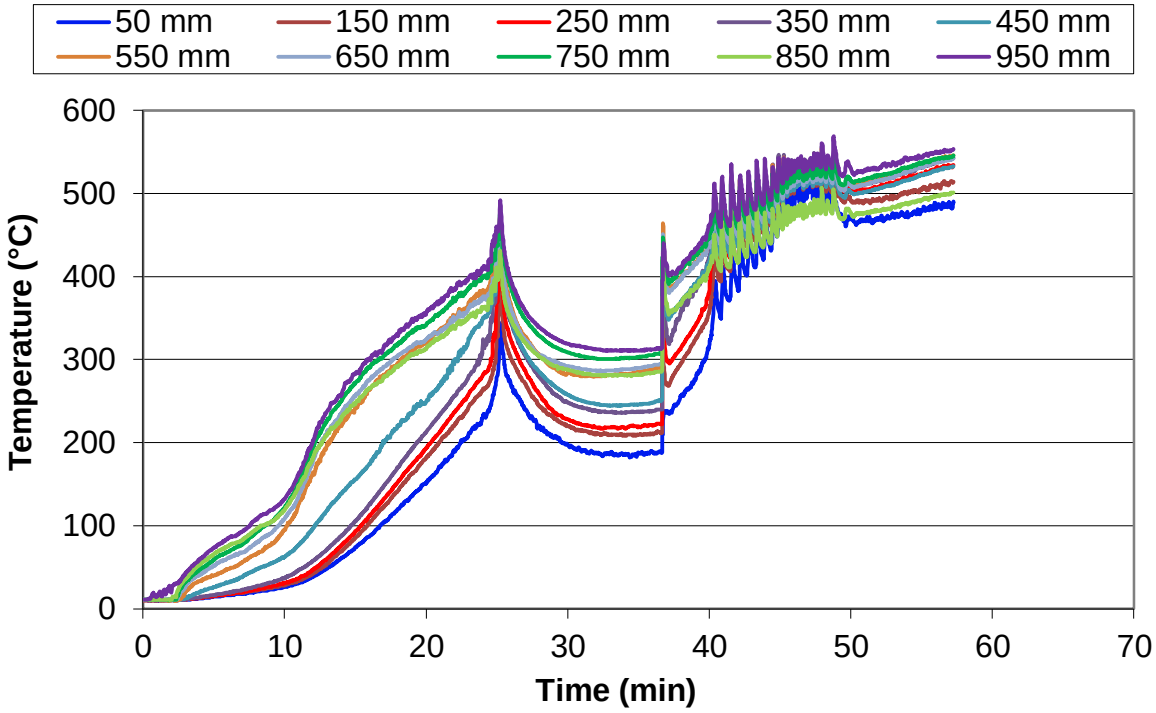


**Figure C.7: Temperature histories for experiment 10-M-100 at the front of the compartment**

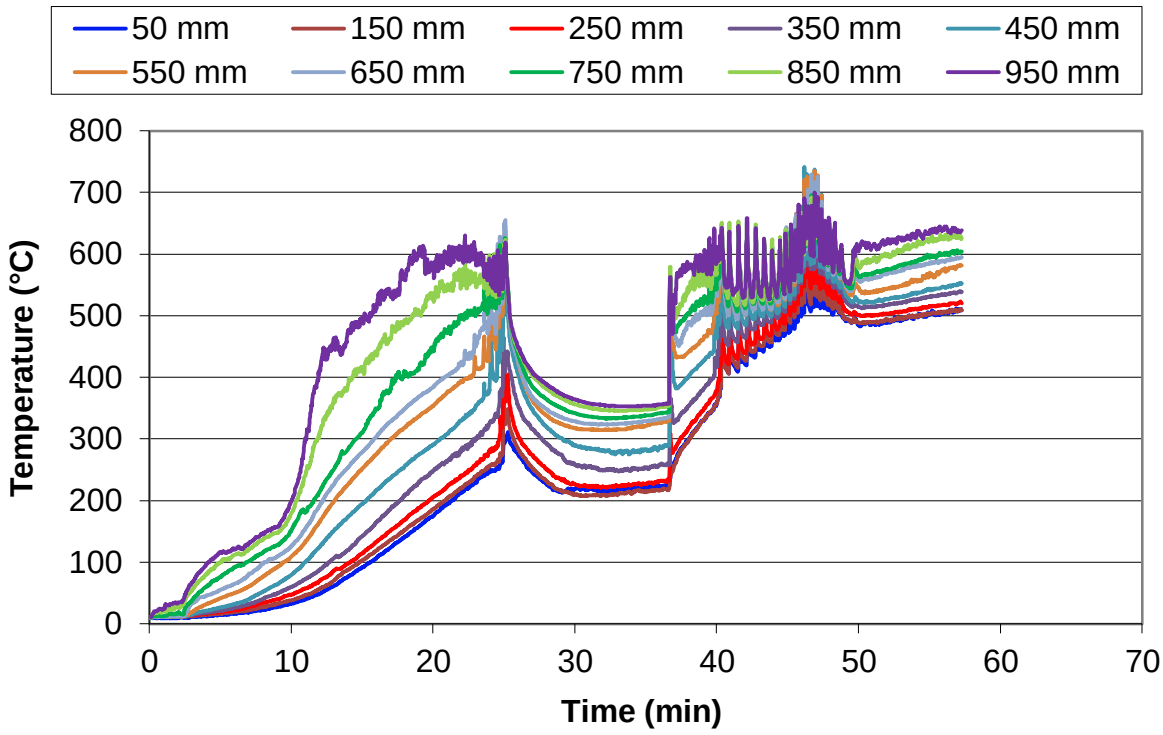


**Figure C.8: Temperature histories for experiment 10-M-100 at the rear of the compartment**

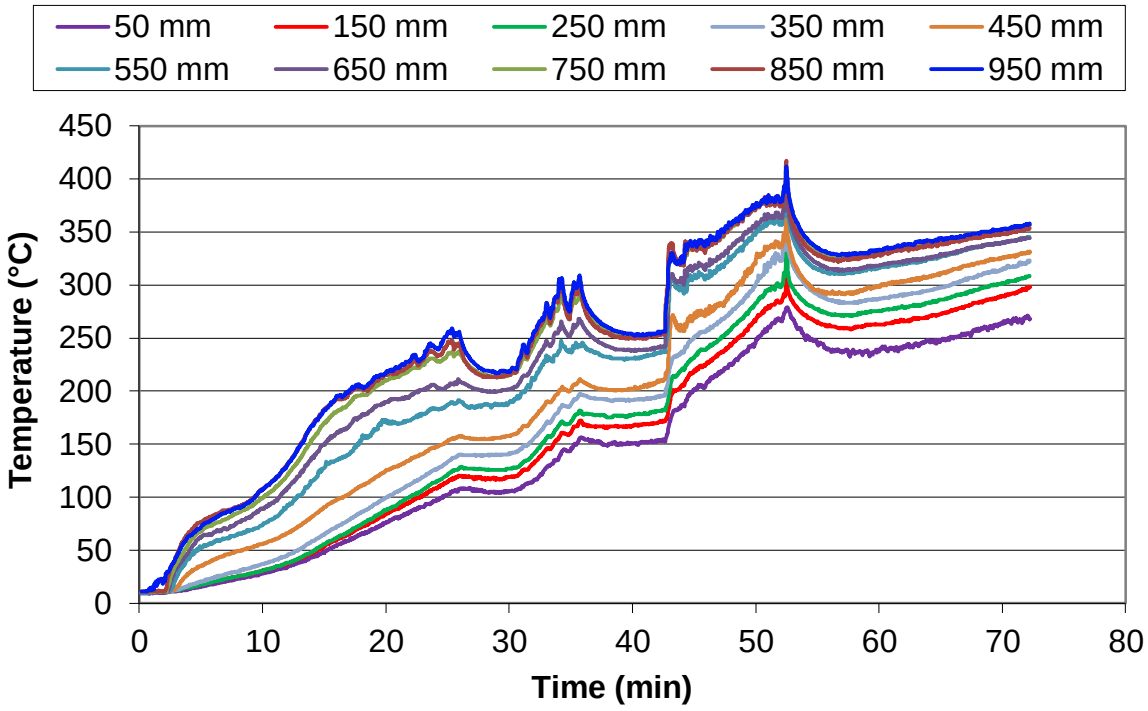


**Figure C.9: Temperature histories for experiment 10-M-71 at the front of the compartment**

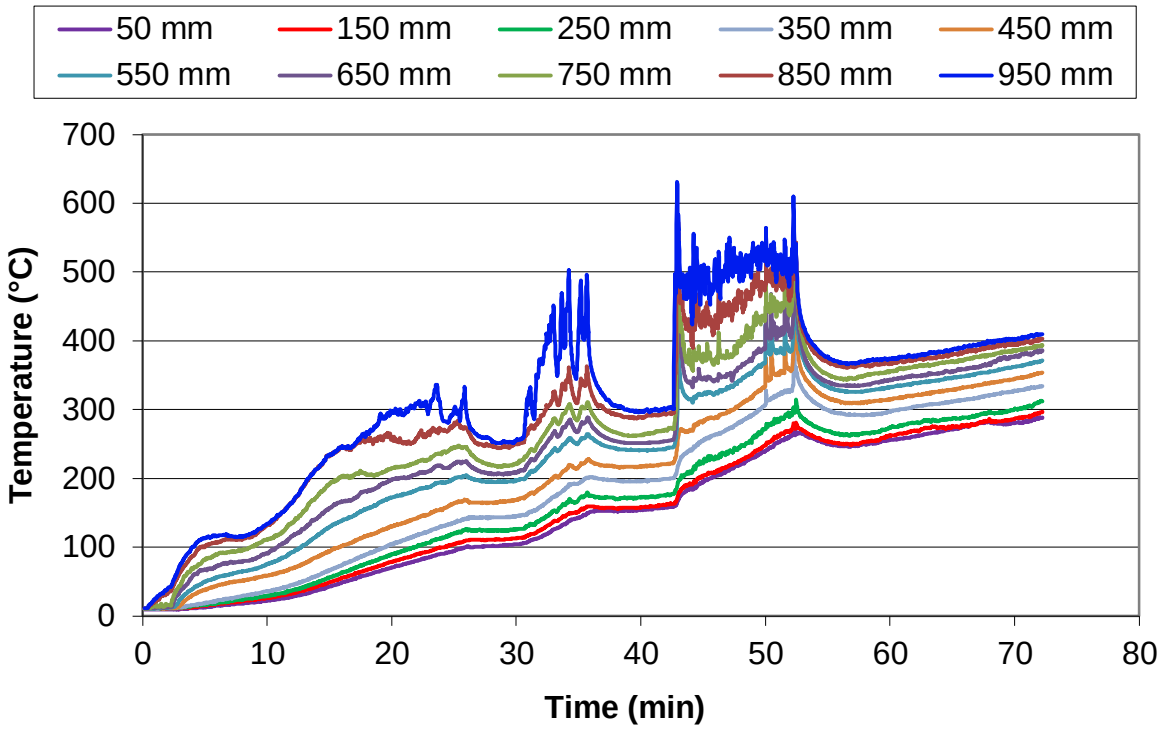


**Figure C.10: Temperature histories for experiment 10-M-71 at the rear of the compartment**

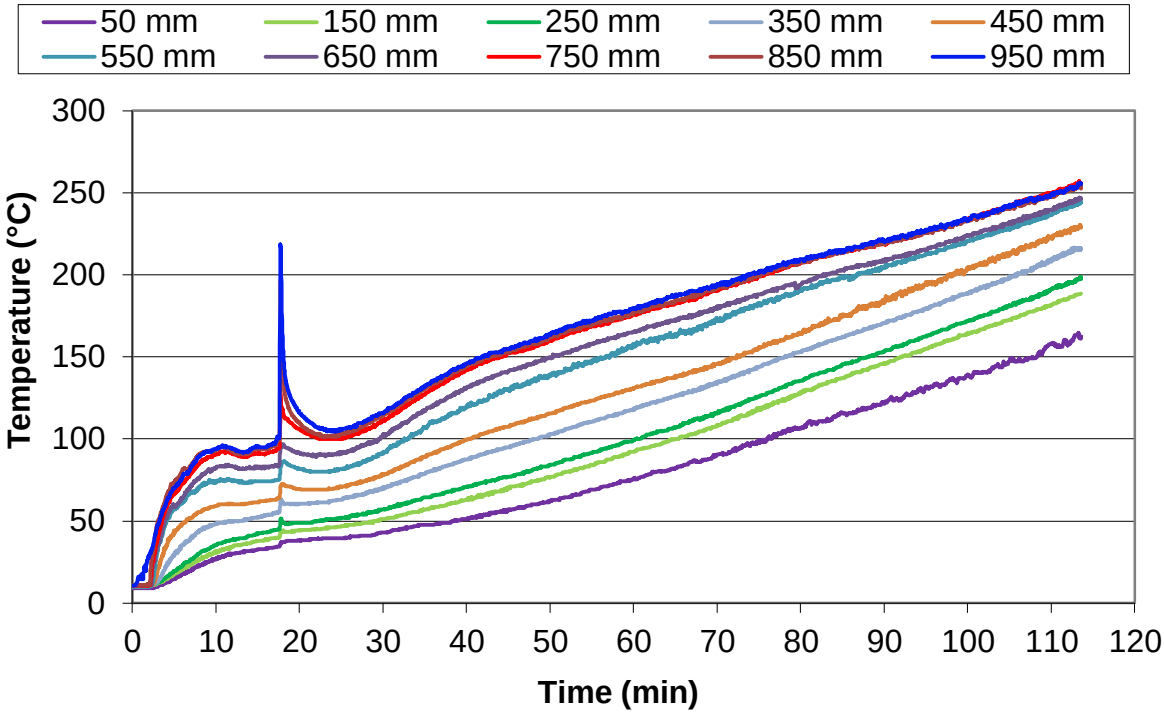


**Figure C.11: Temperature histories for experiment 10-M-50 at the front of the compartment**

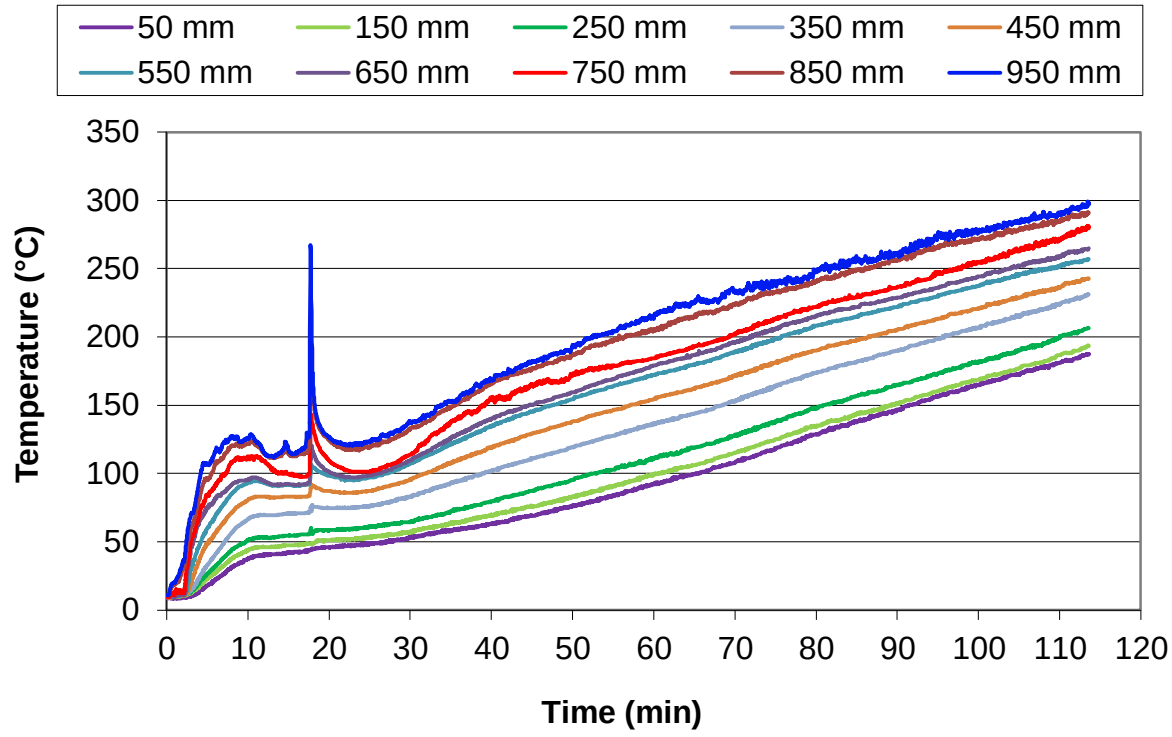


**Figure C.12: Temperature histories for experiment 10-M-50 at the rear of the compartment**

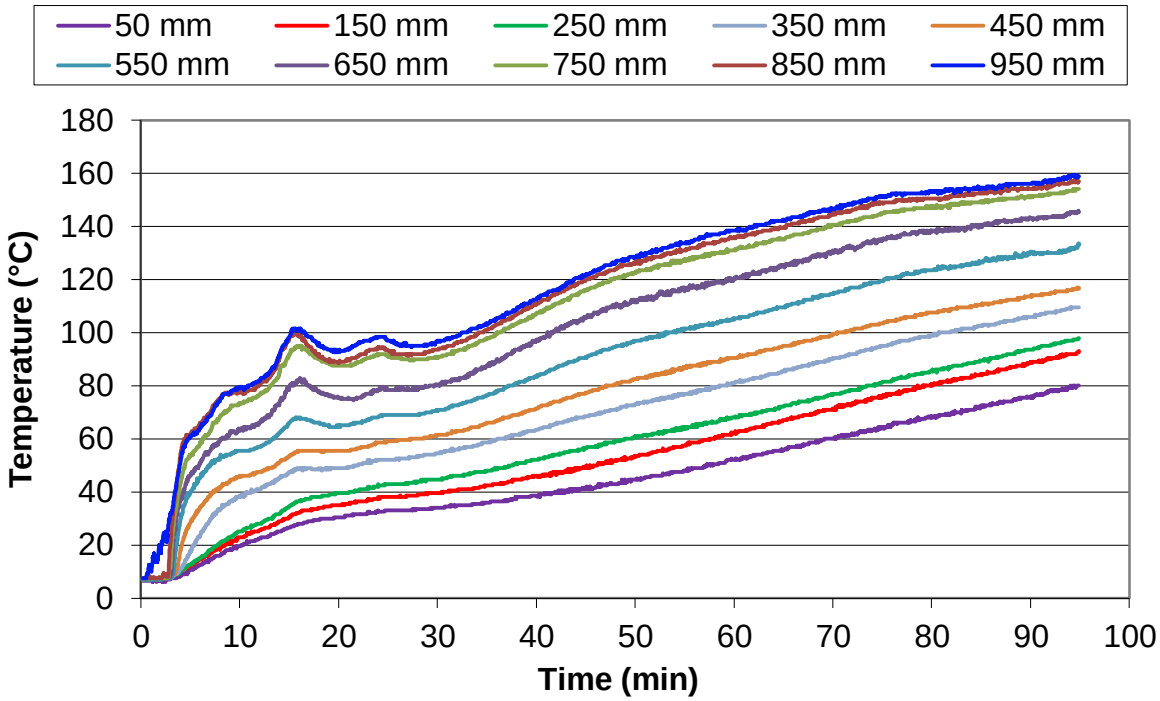


**Figure C.13: Temperature histories for experiment 10-M-36 at the front of the compartment**

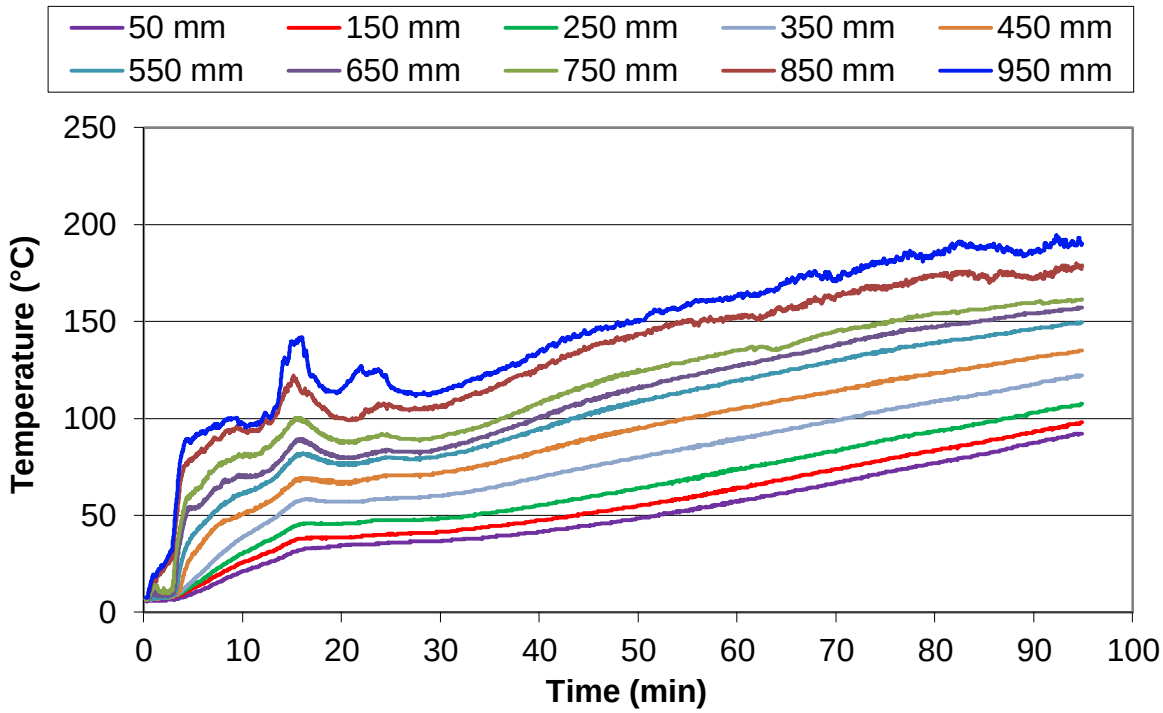


**Figure C.14: Temperature histories for experiment 10-M-36 at the rear of the compartment**

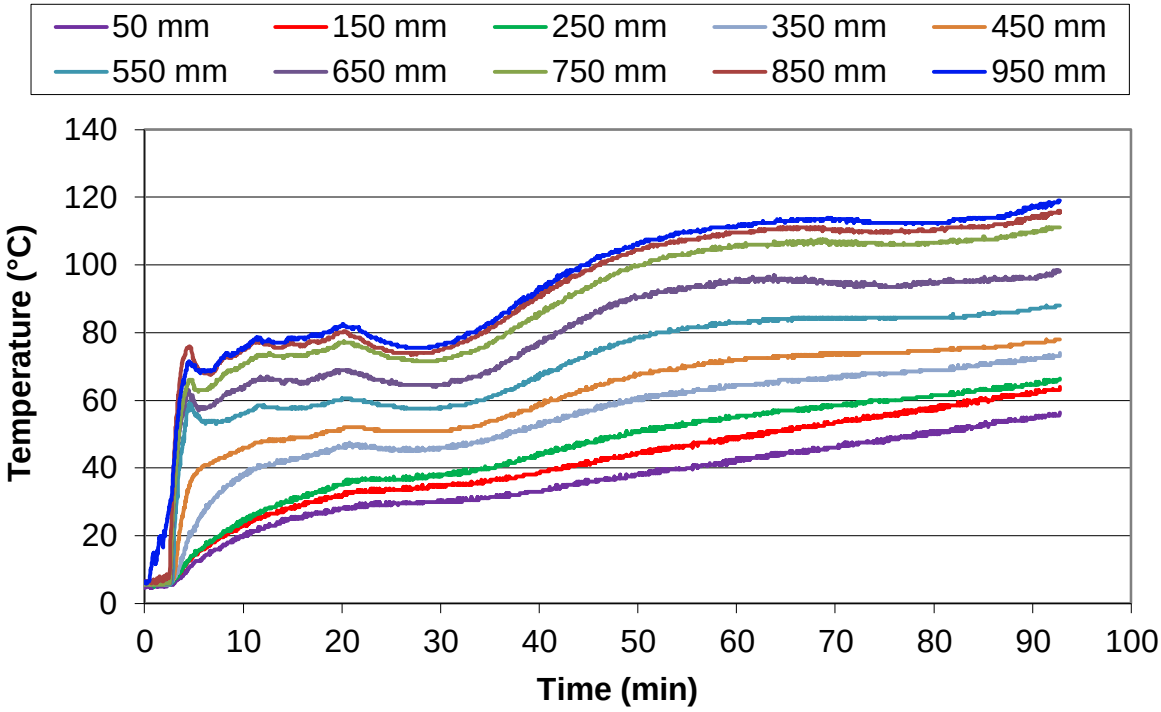


**Figure C.15: Temperature histories for experiment 10-M-25 at the front of the compartment**

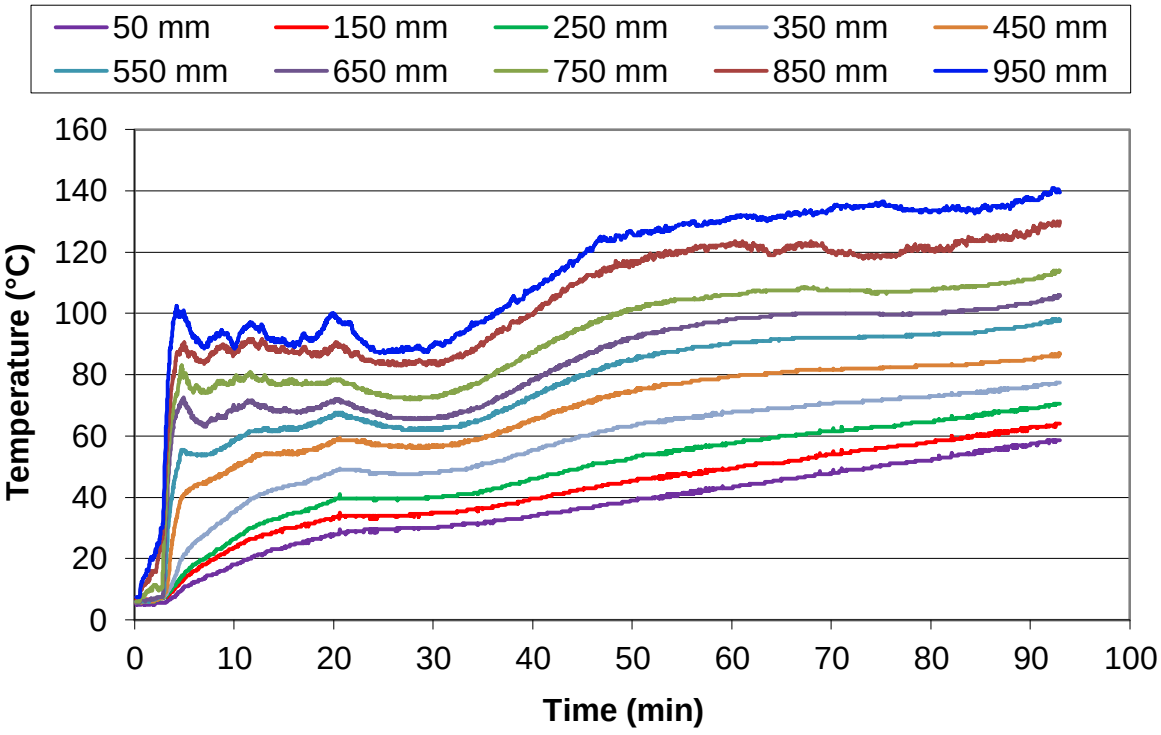


**Figure C.16: Temperature histories for experiment 10-M-25 at the rear of the compartment**

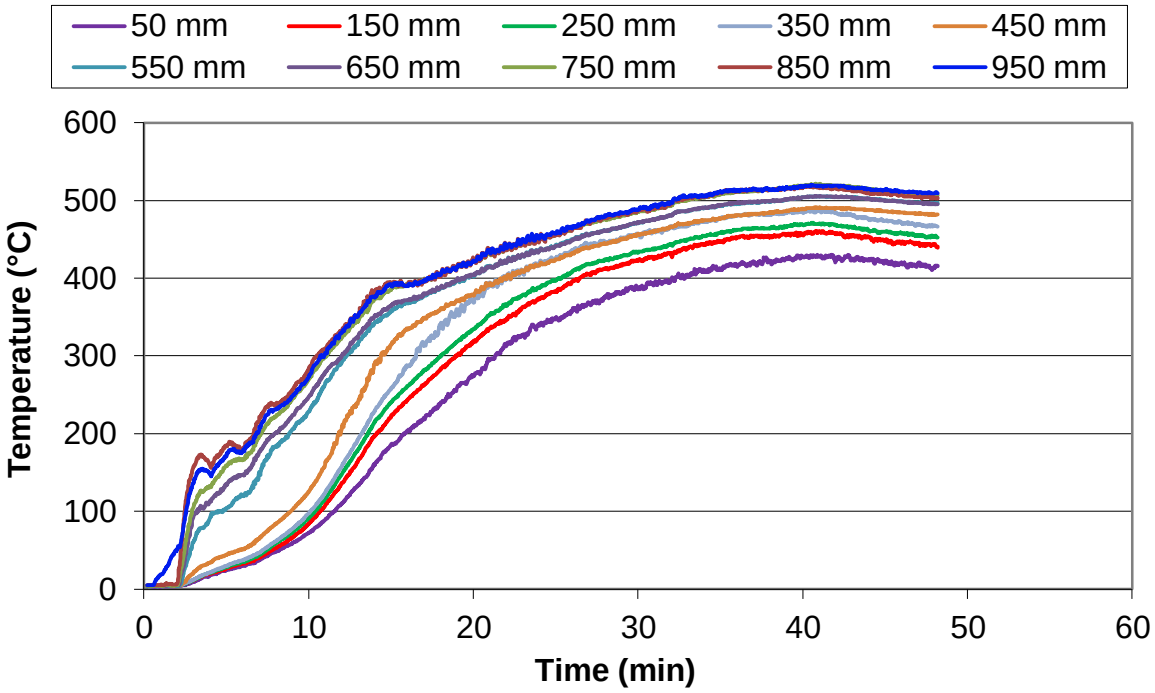


**Figure C.17: Temperature histories for experiment 5-M-100 at the front of the compartment**

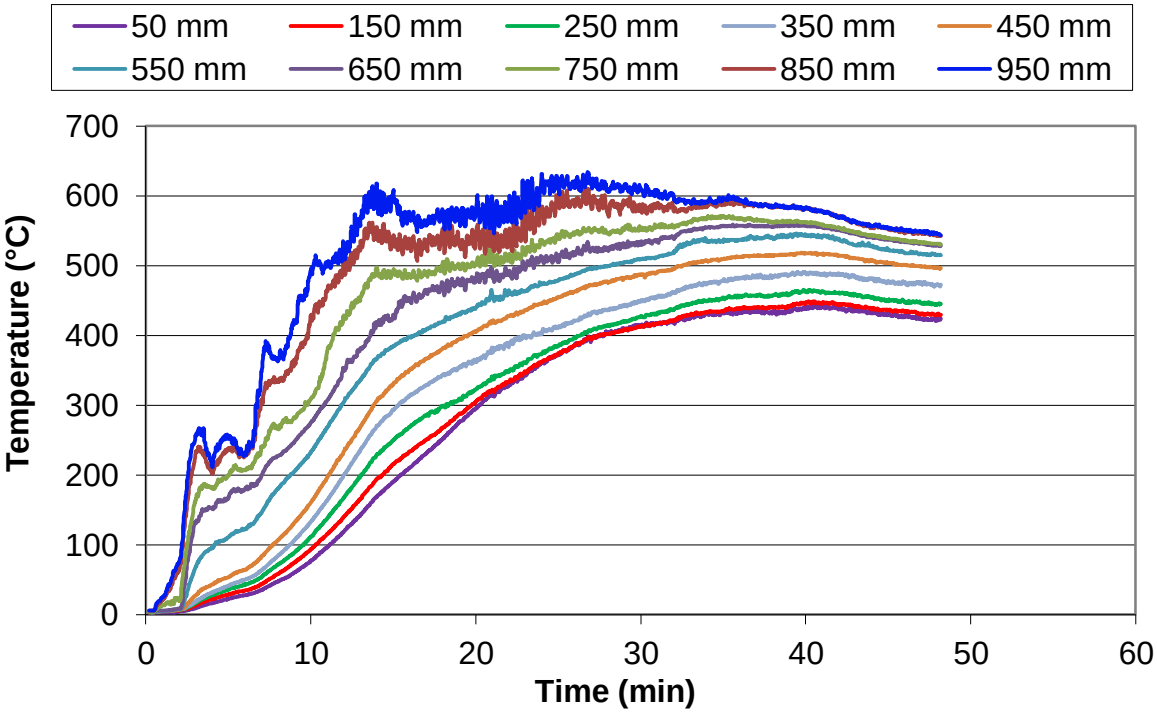


**Figure C.18: Temperature histories for experiment 5-M-100 at the rear of the compartment**

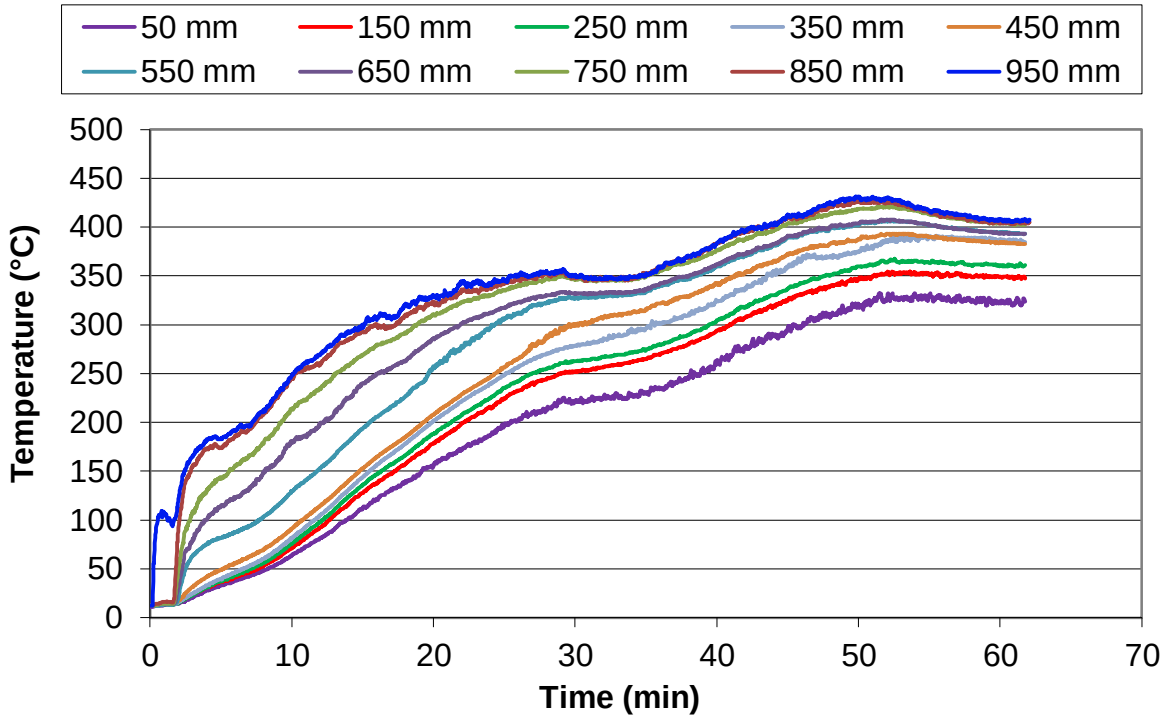


**Figure C.19: Temperature histories for experiment 5-M-71 at the front of the compartment**

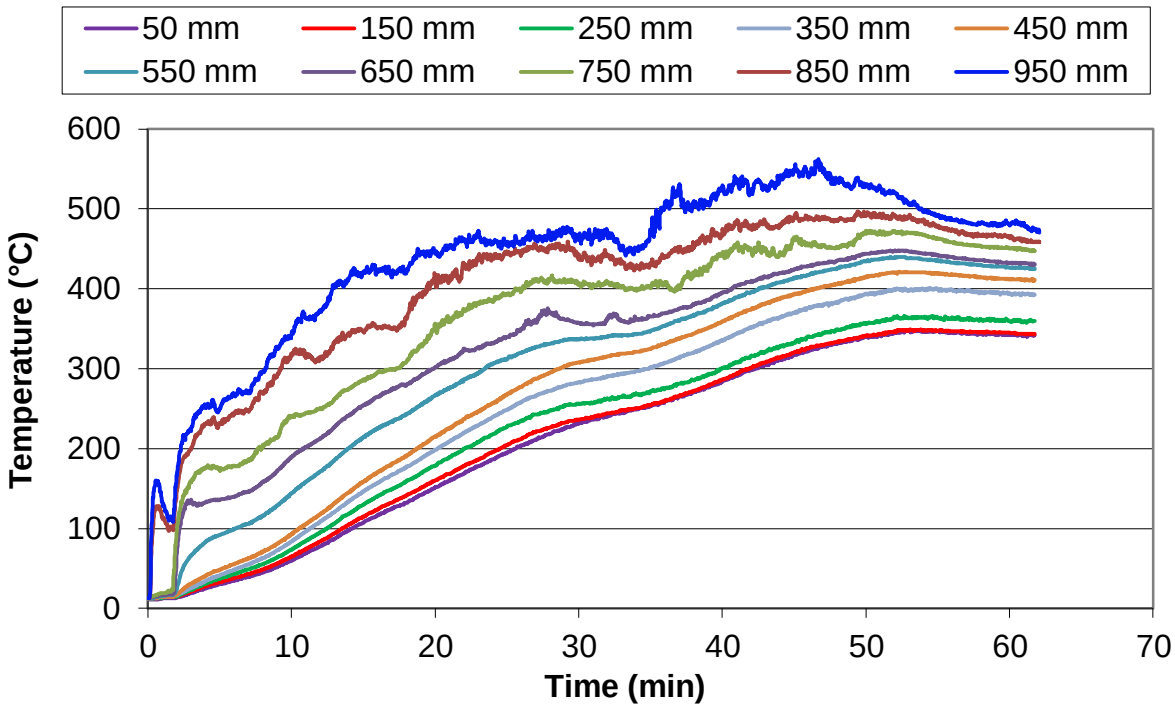


**Figure C.20: Temperature histories for experiment 5-M-71 at the rear of the compartment**

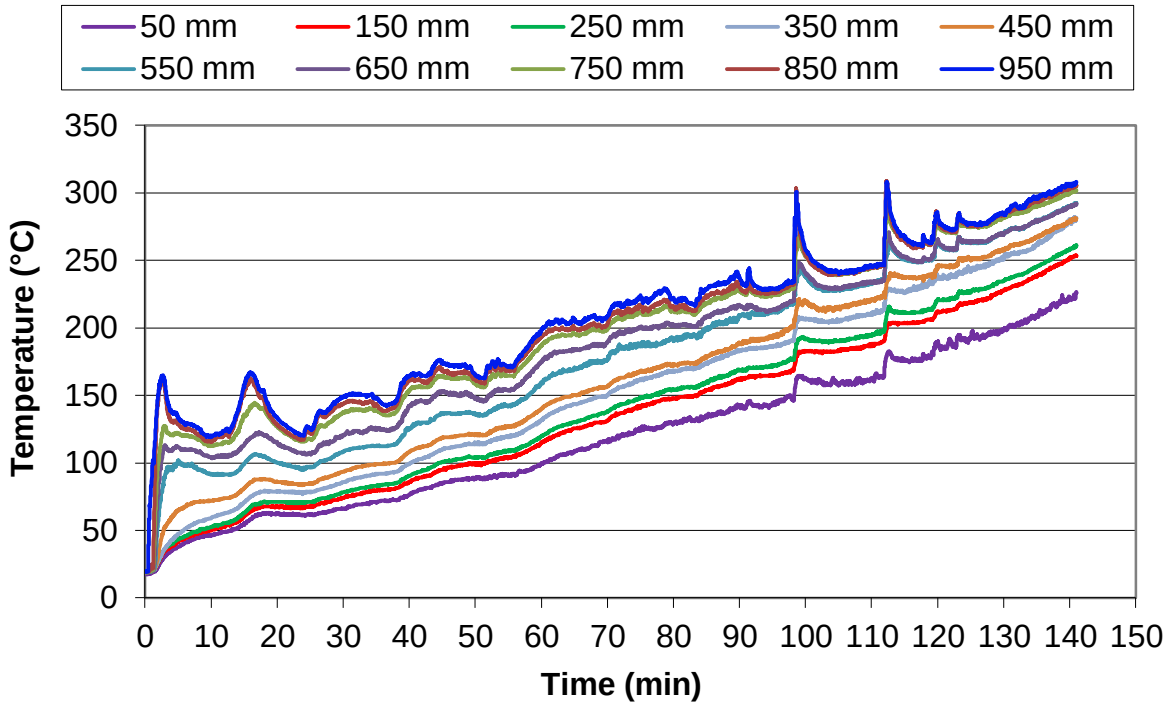


**Figure C.21: Temperature histories for experiment 5-M-50 at the front of the compartment**

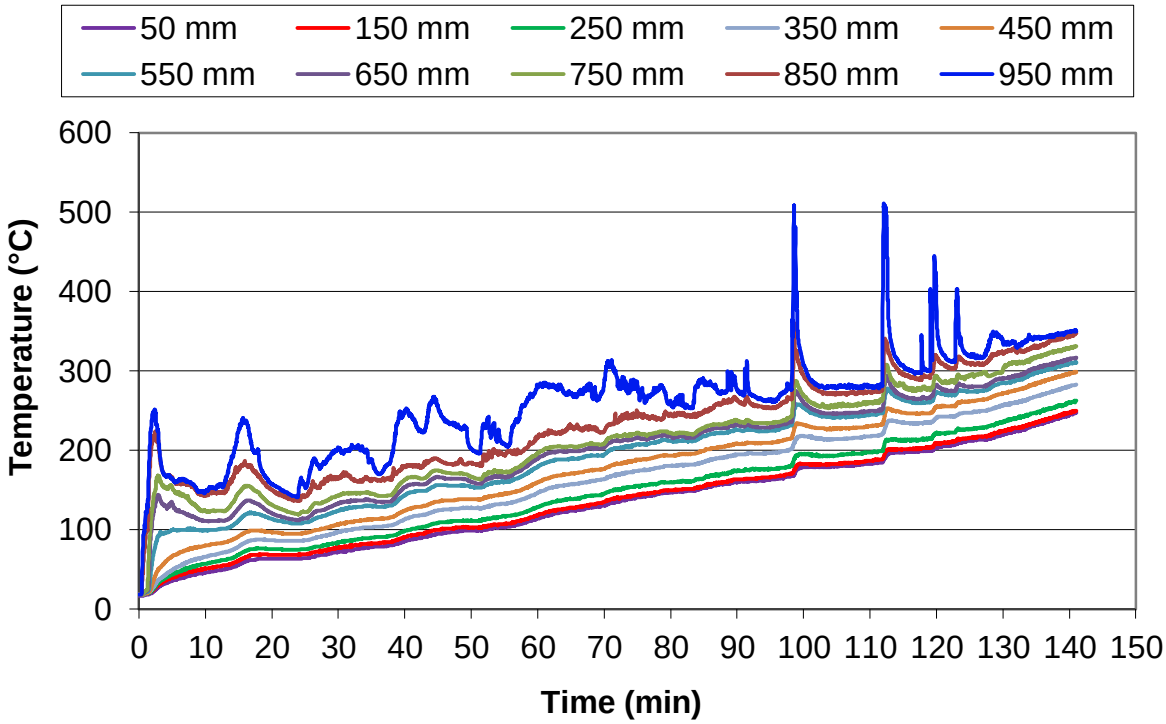


**Figure C.22: Temperature histories for experiment 5-M-50 at the rear of the compartment**

# Appendix D Final Experiments Data

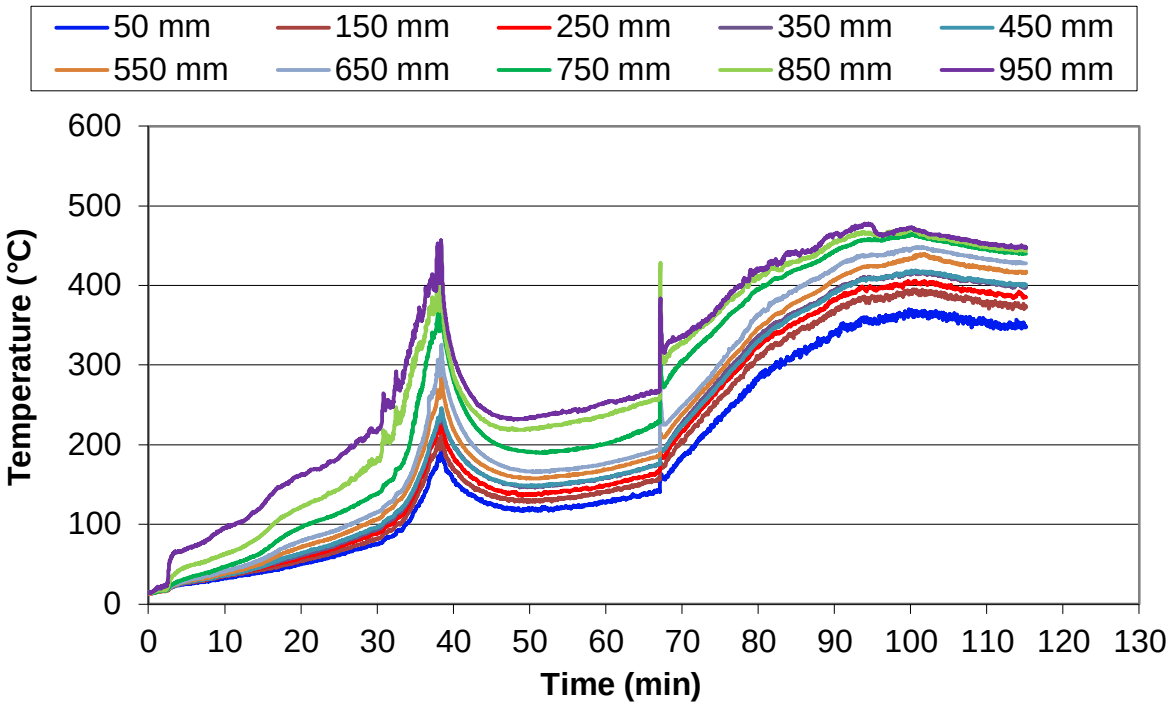


**Figure D.1: Temperature histories for experiment 10-C-100 at the front of the compartment**

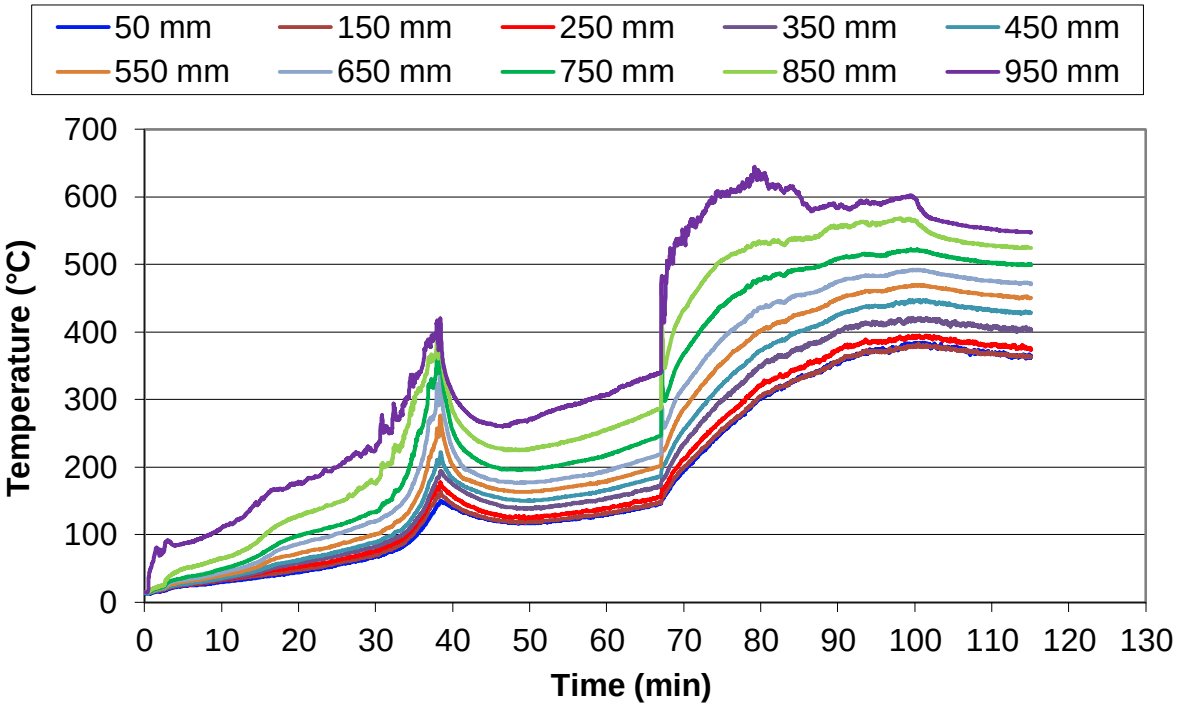


**Figure D.2: Temperature histories for experiment 10-C-100 at the rear of the compartment**

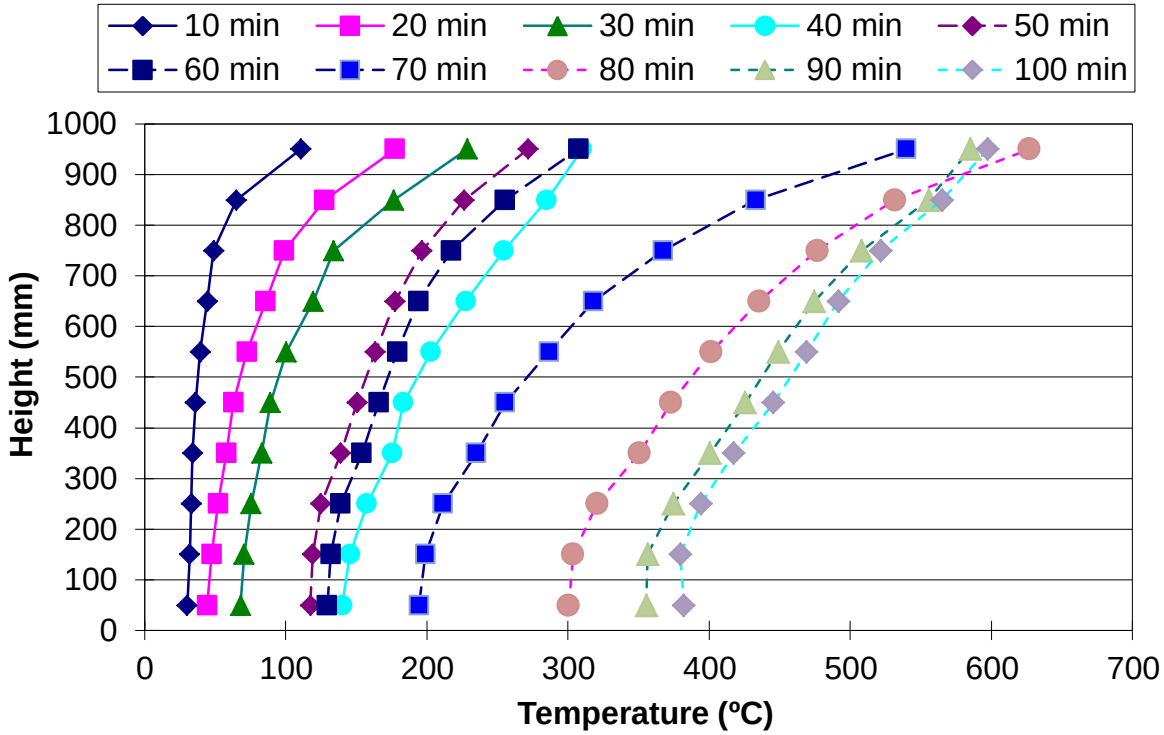


**Figure D.3: Temperature profile constructed from the rear thermocouple tree for experiment 10-C-100**

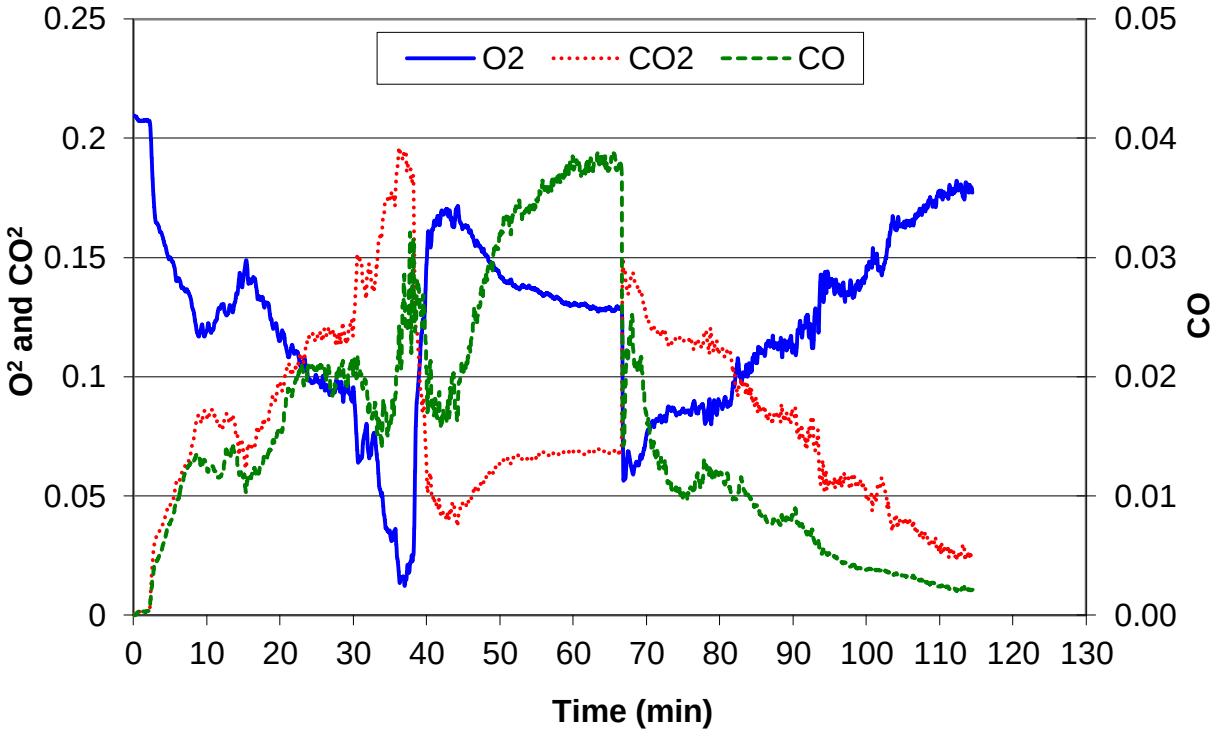


**Figure D.4: $O_2$, $CO_2$ and CO molar concentrations for experiment 10-C-100**

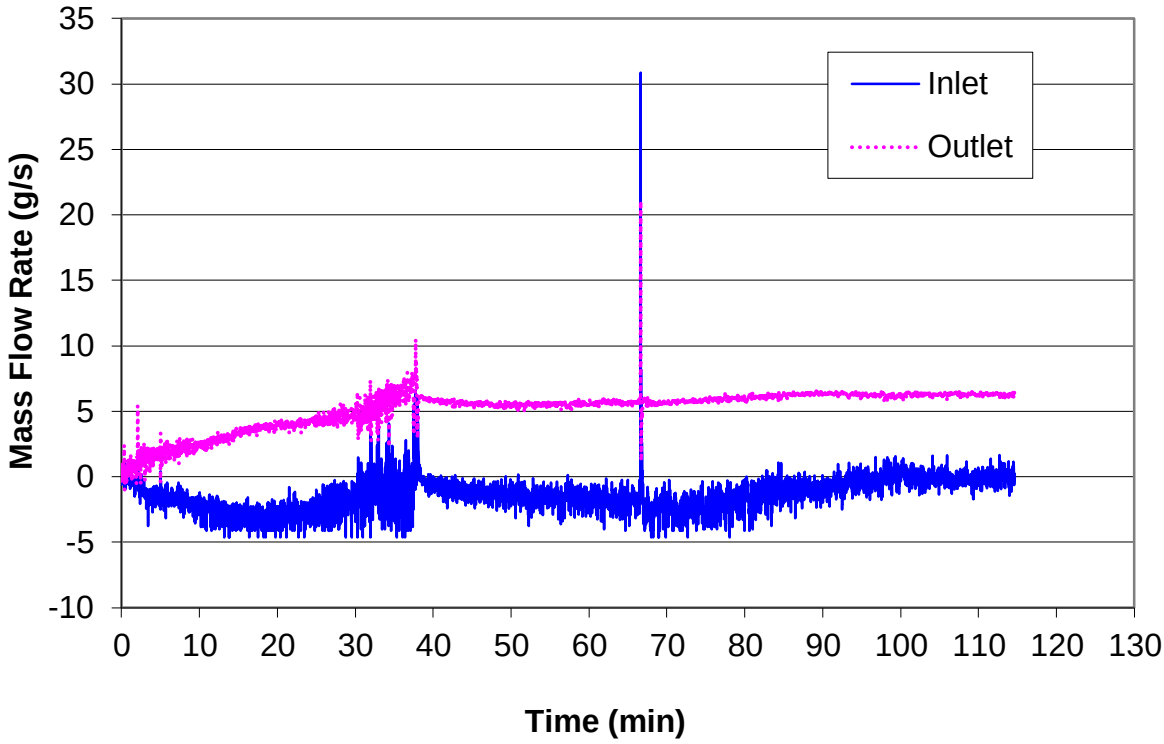


**Figure D.5: Mass flow rate through both opening vents for experiment 10-C-100**

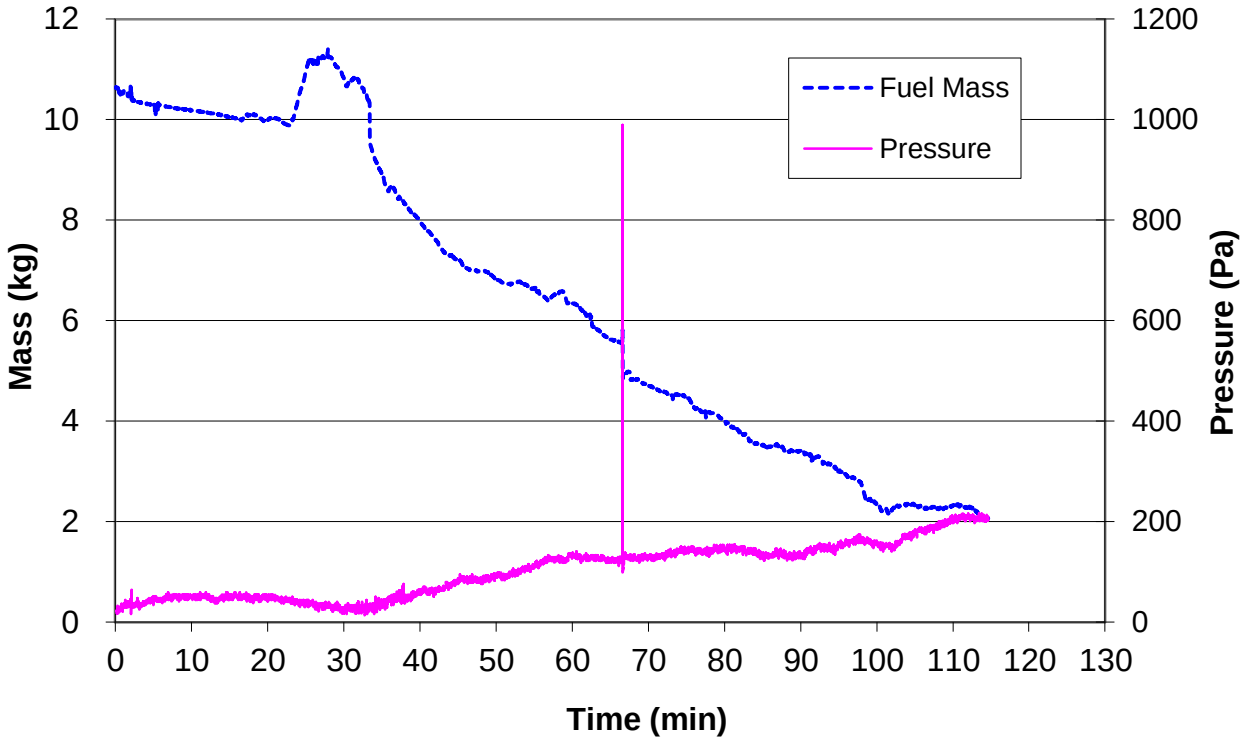


**Figure D.6: Mass loss history and pressure history for experiment 10-C-100**

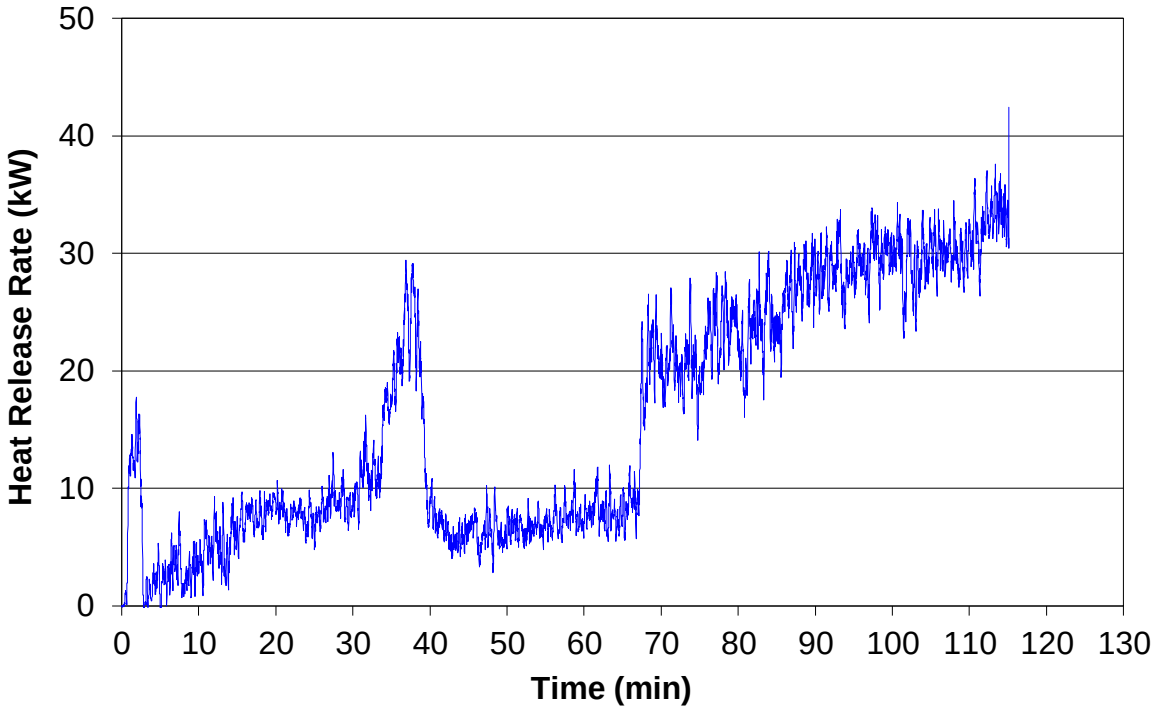


**Figure D.7: Heat release rate history for experiment 10-C-100 with a 10-point moving average**

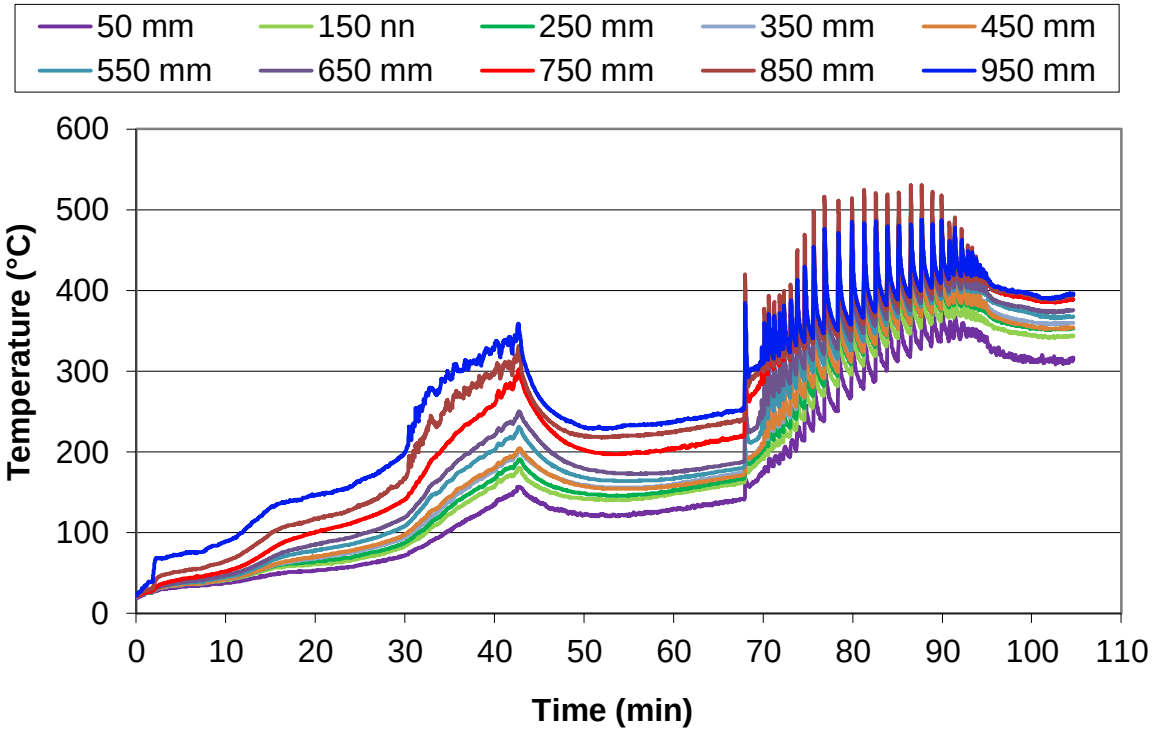


**Figure D.8: Temperature histories for experiment 10-C-71 at the front of the compartment**

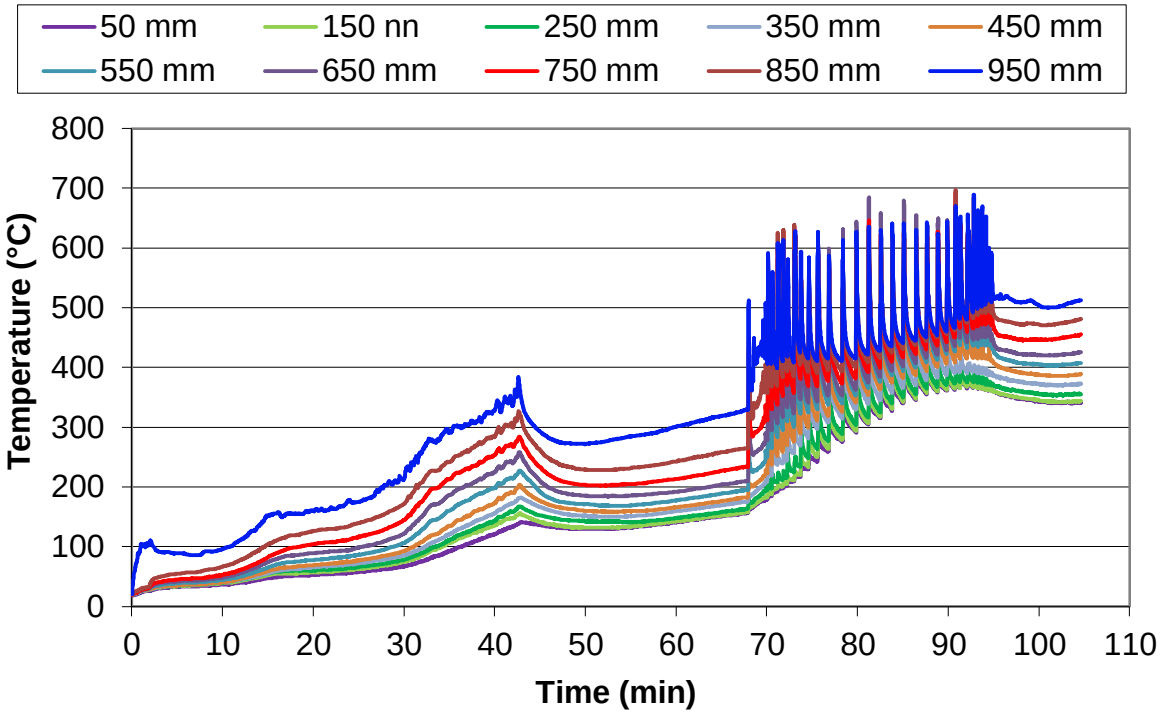


**Figure D.9: Temperature histories for experiment 10-C-71 at the rear of the compartment**

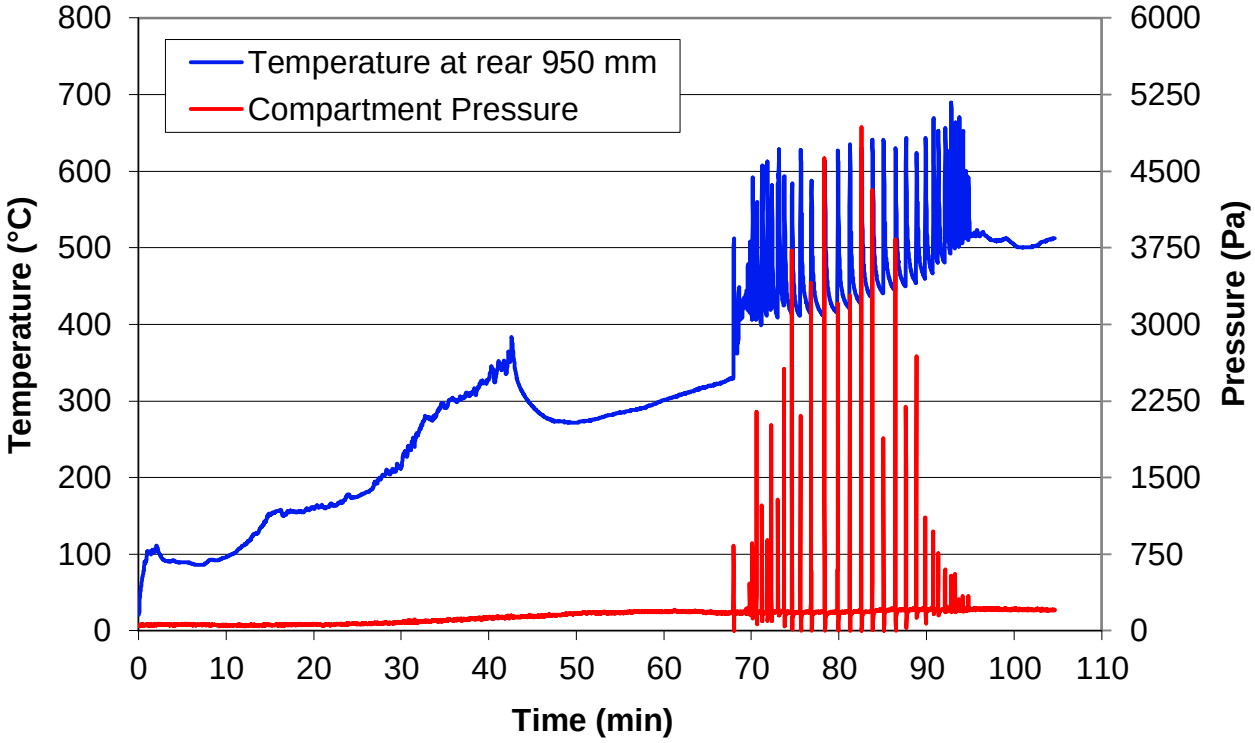


**Figure D.10: The compartment pressure and the temperature history compiled from the top rear thermocouple for experiment 10-C-71**

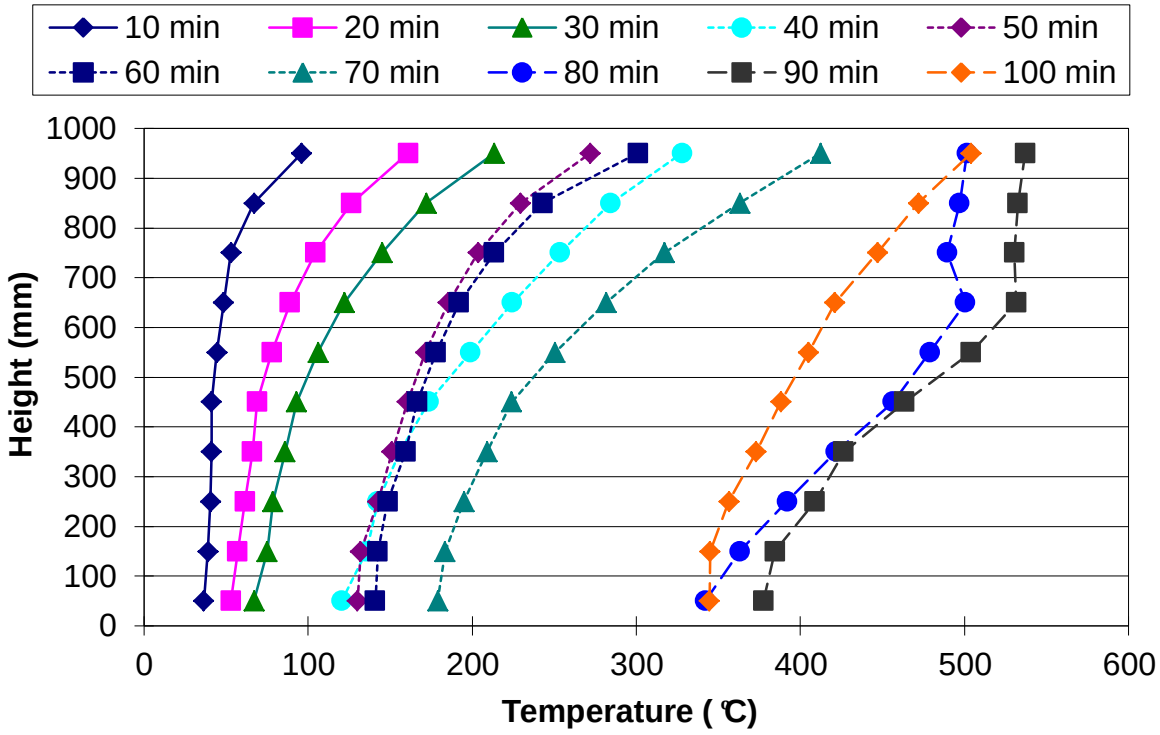


**Figure D.11: Temperature profile constructed from the rear thermocouple tree for experiment 10-C-71**

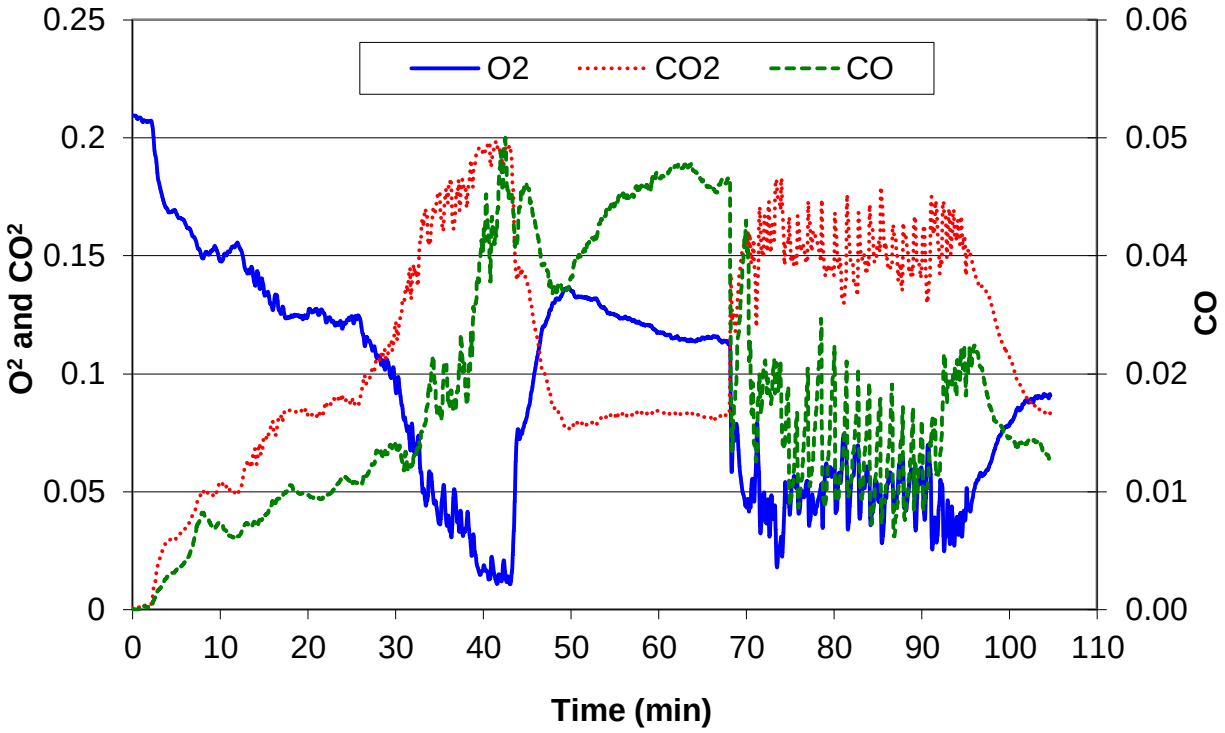


**Figure D.12: $O_2$, $CO_2$ and CO molar concentrations for experiment 10-C-71**

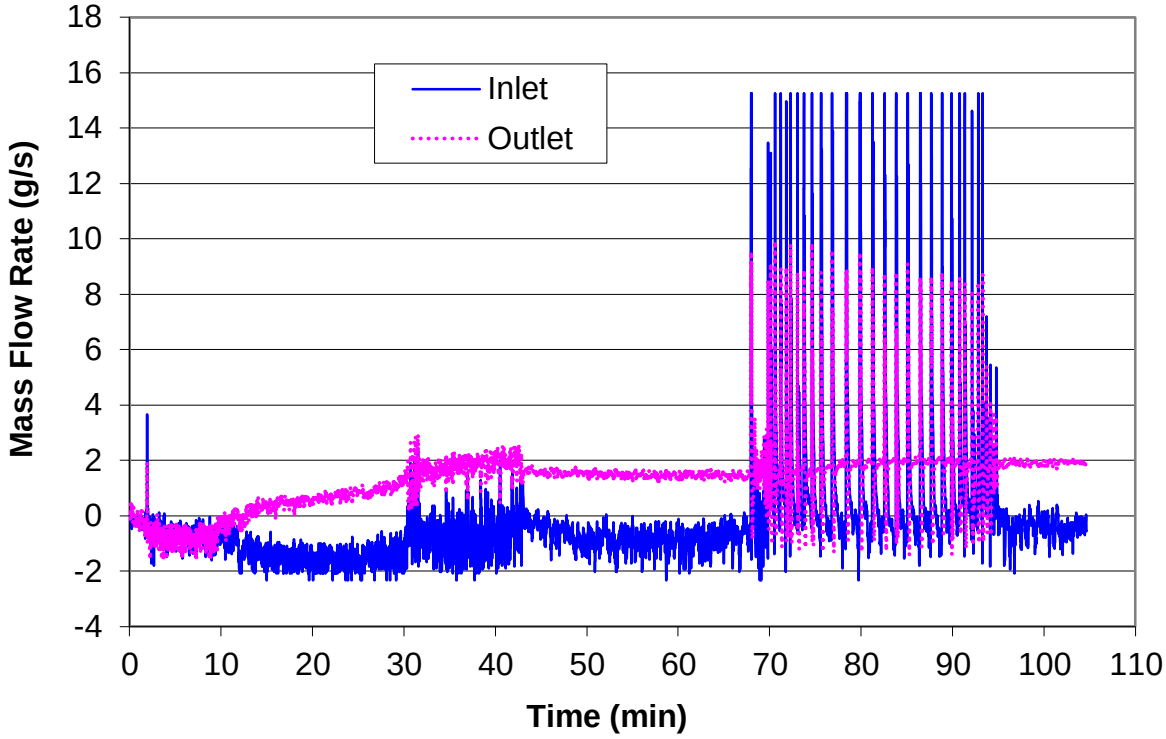


**Figure D.13: Mass flow rate through both opening vents for experiment 10-C-71**

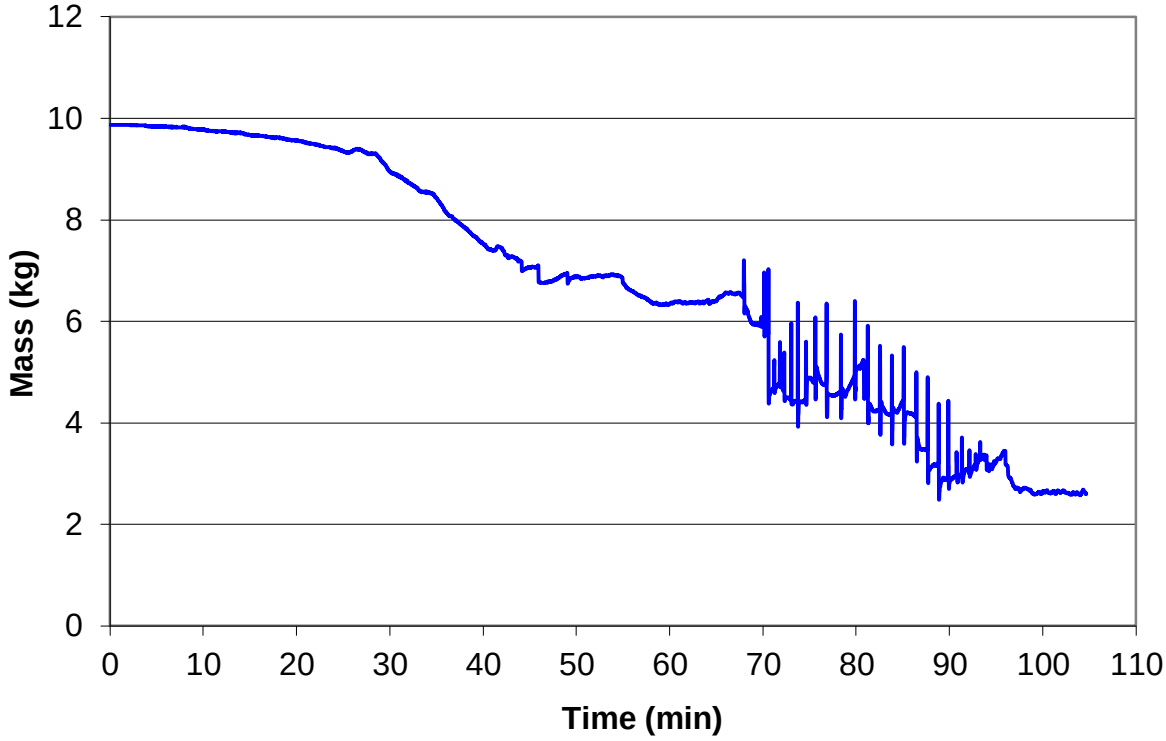


**Figure D.14: Mass loss history for experiment 10-C-71**

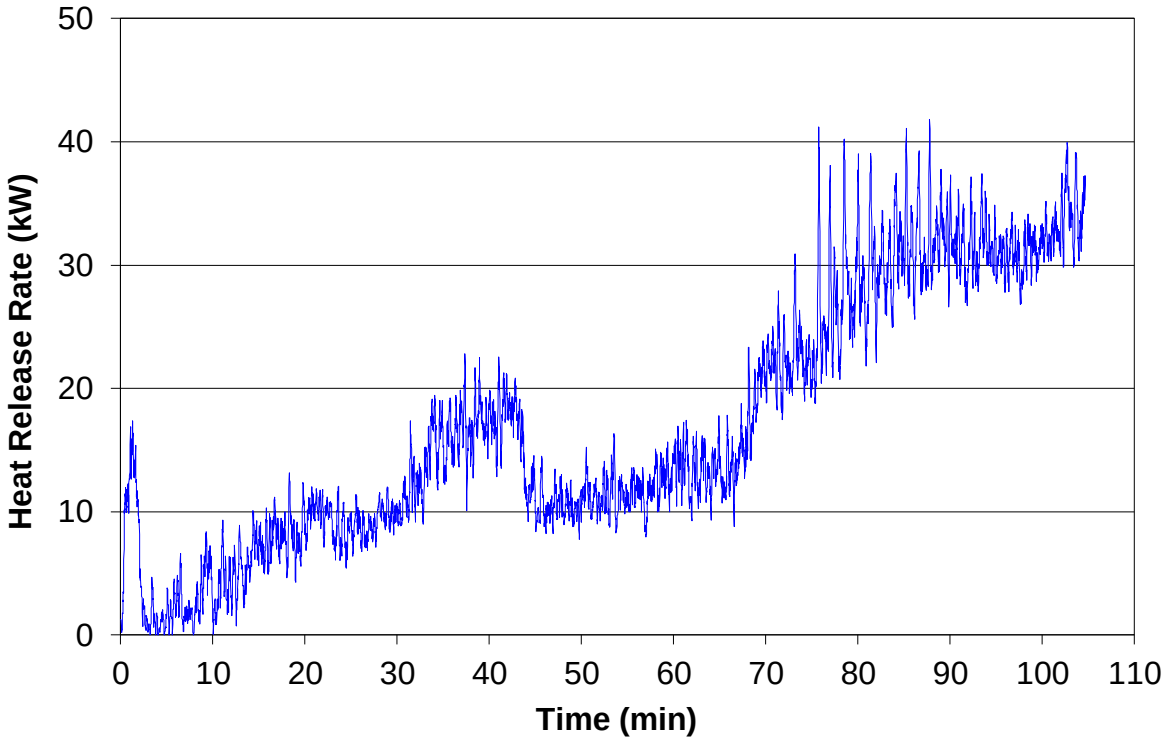


**Figure D.15: Heat release rate history for experiment 10-C-71 with a 10-point moving average**

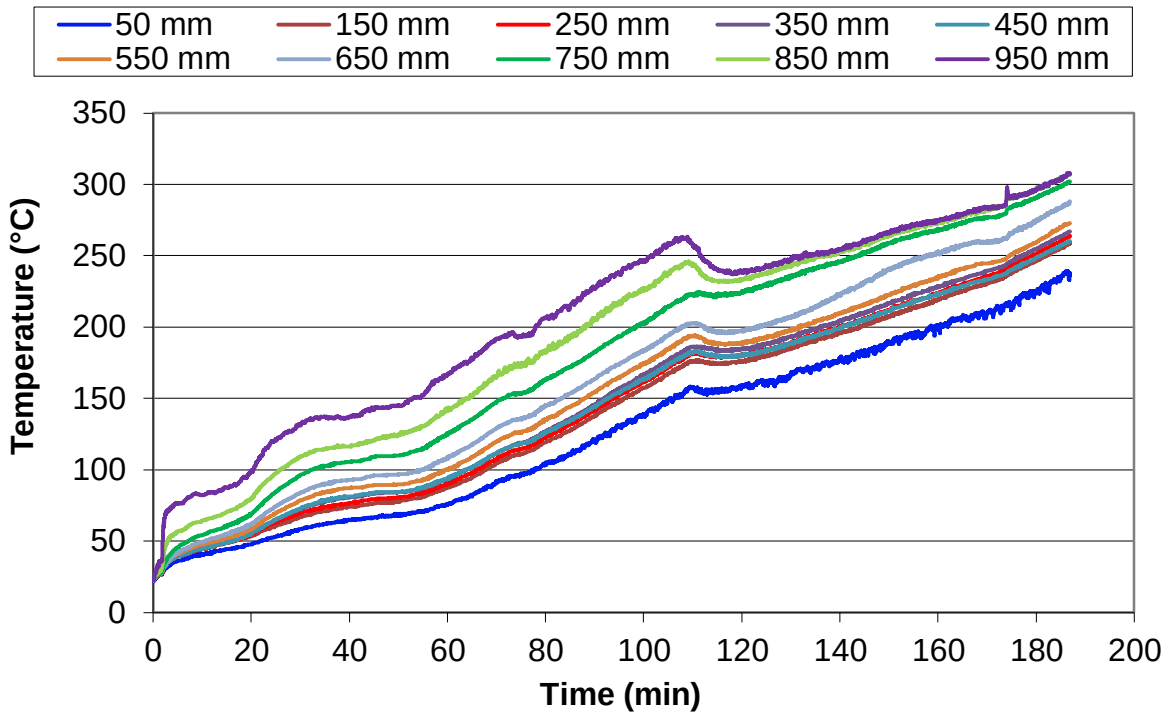


**Figure D.16: Temperature histories for experiment 10-C-50 at the front of the compartment**

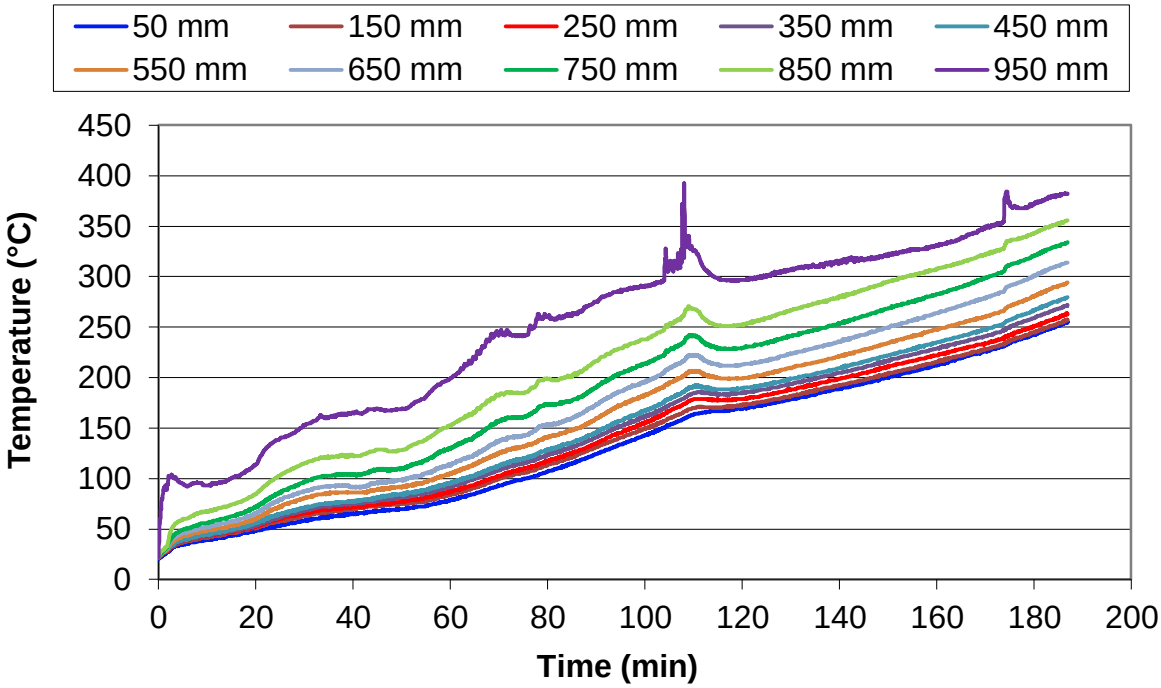


**Figure D.17: Temperature histories for experiment 10-C-50 at the rear of the compartment**

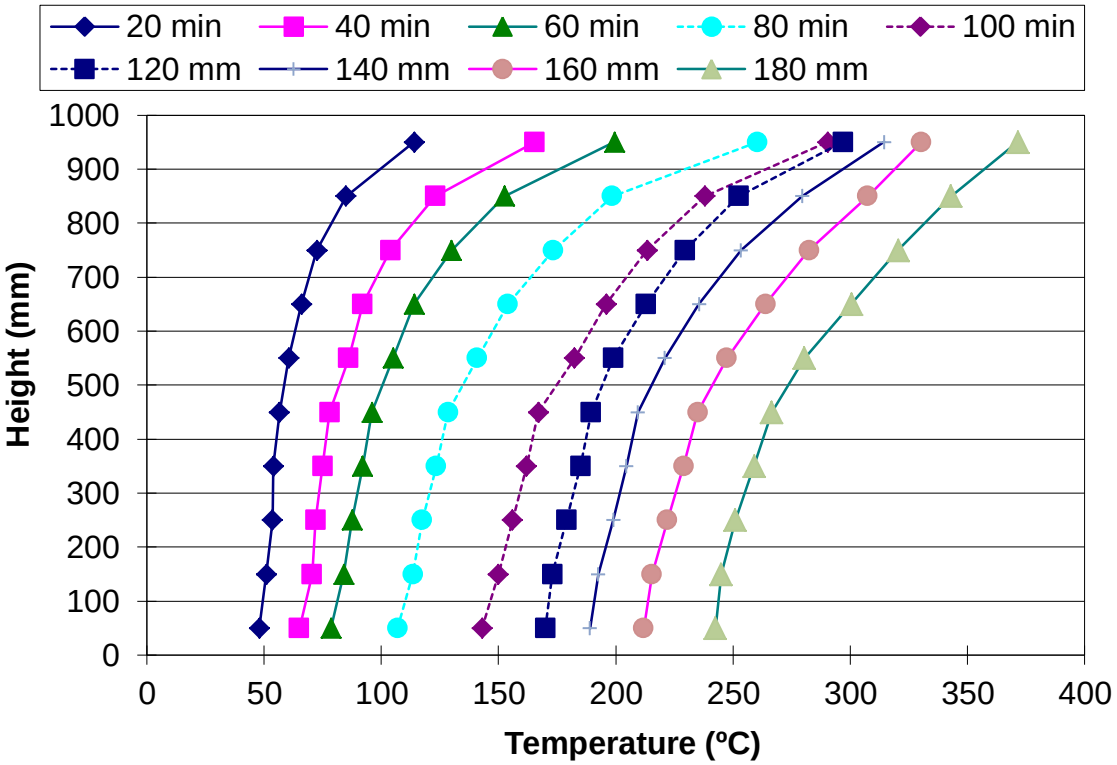


**Figure D.18: Temperature profile constructed from the rear thermocouple tree for experiment 10-C-50**

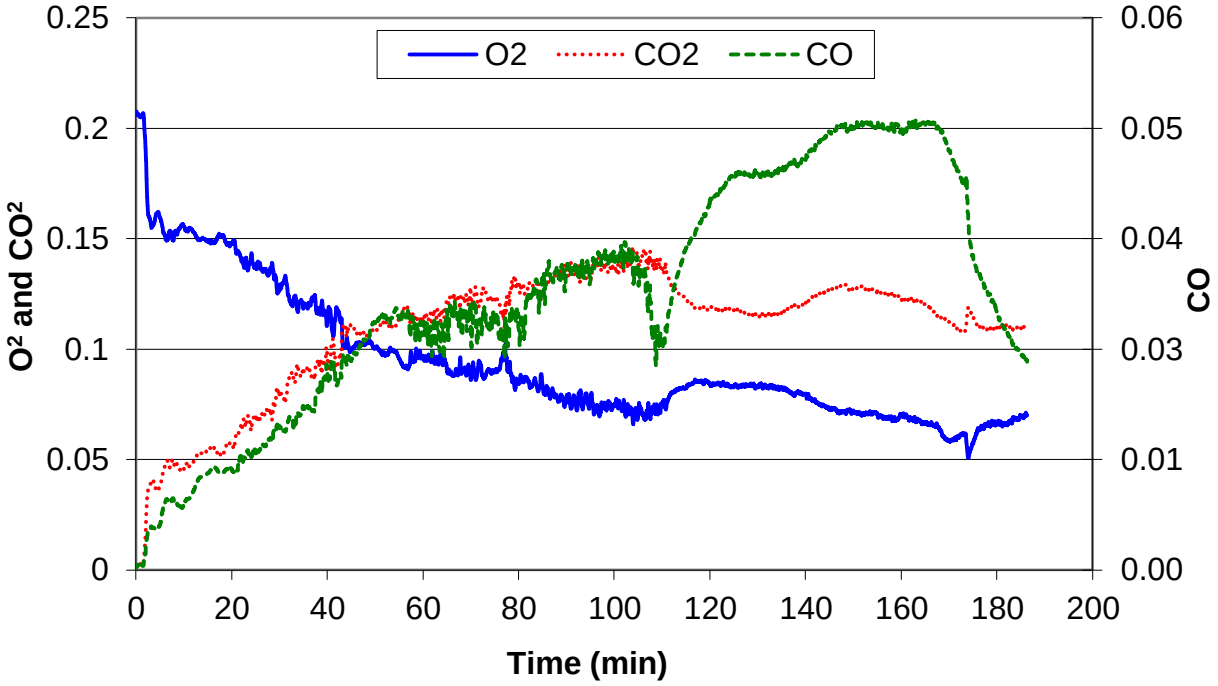


**Figure D.19: $O_2$, $CO_2$ and CO molar concentrations for experiment 10-C-50**

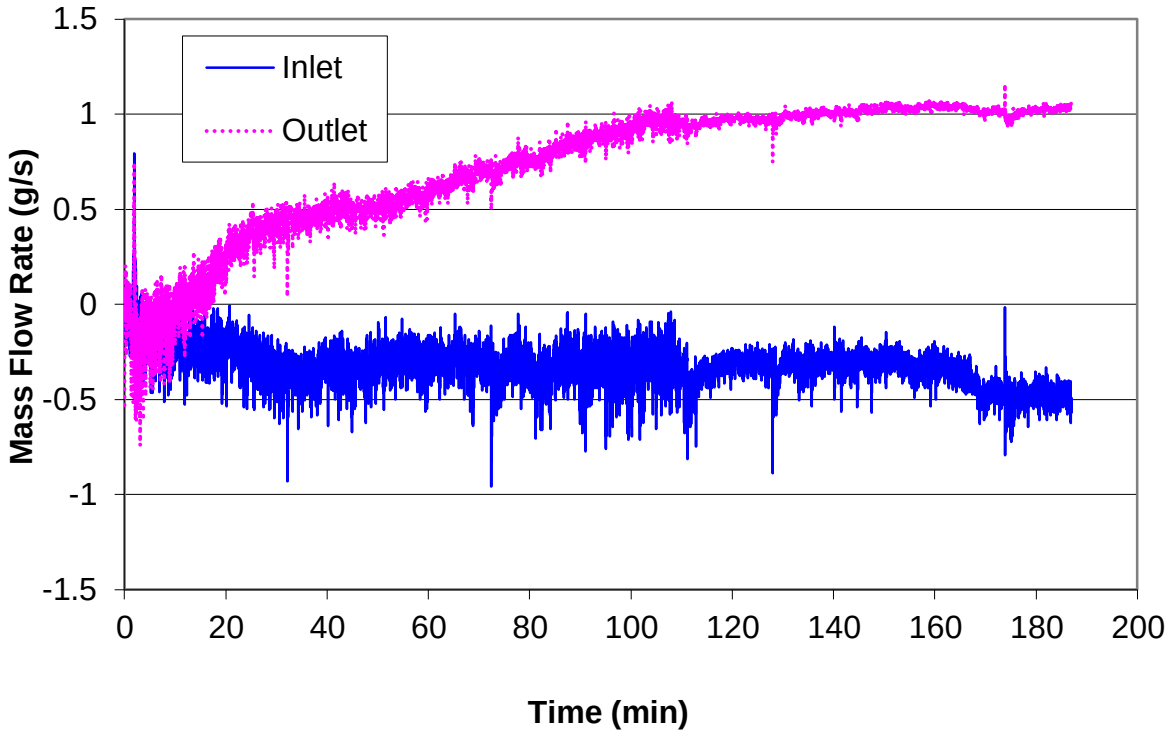


**Figure D.20: Mass flow rate through both opening vents for experiment 10-C-50**

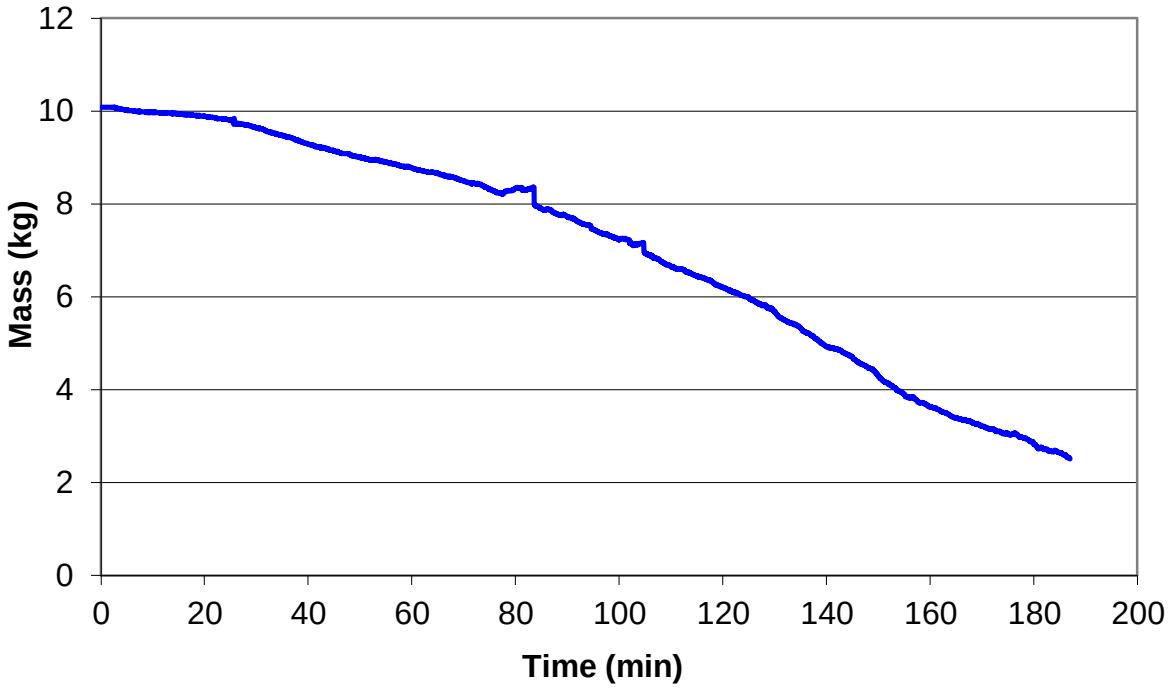


**Figure D.21: Mass loss history for experiment 10-C-50**

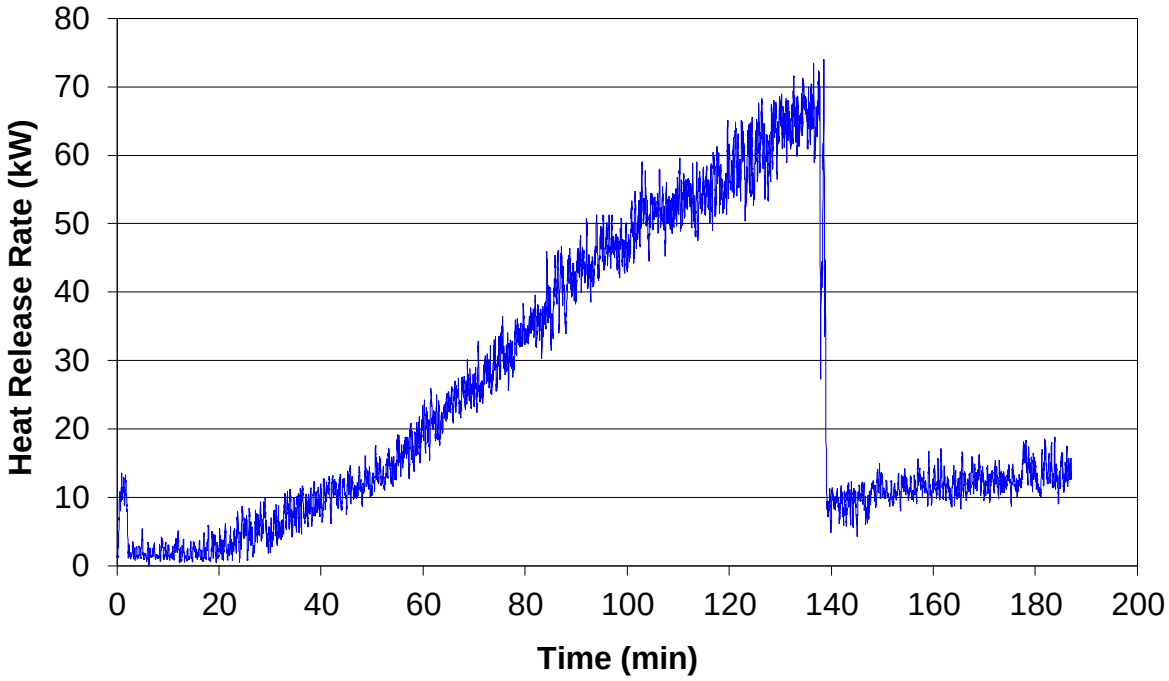


**Figure D.22: Heat release rate history for experiment 10-C-50 with a 10-point moving average**

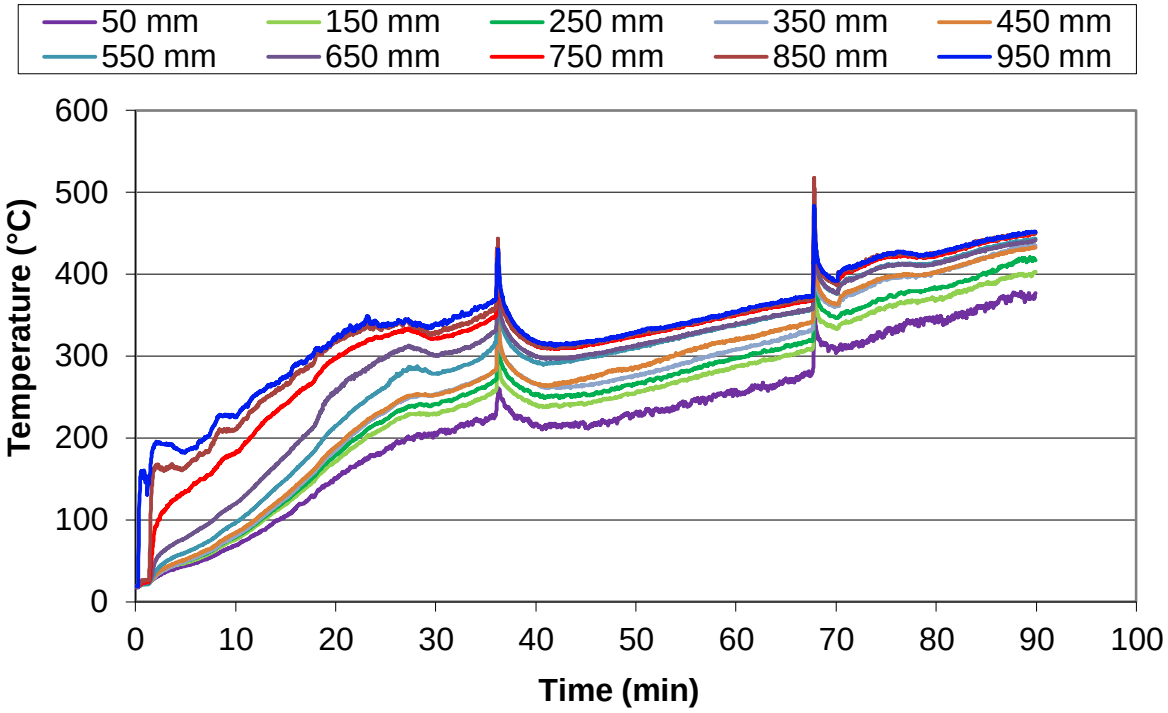


**Figure D.23: Temperature histories for experiment 10-M-71 at the front of the compartment**

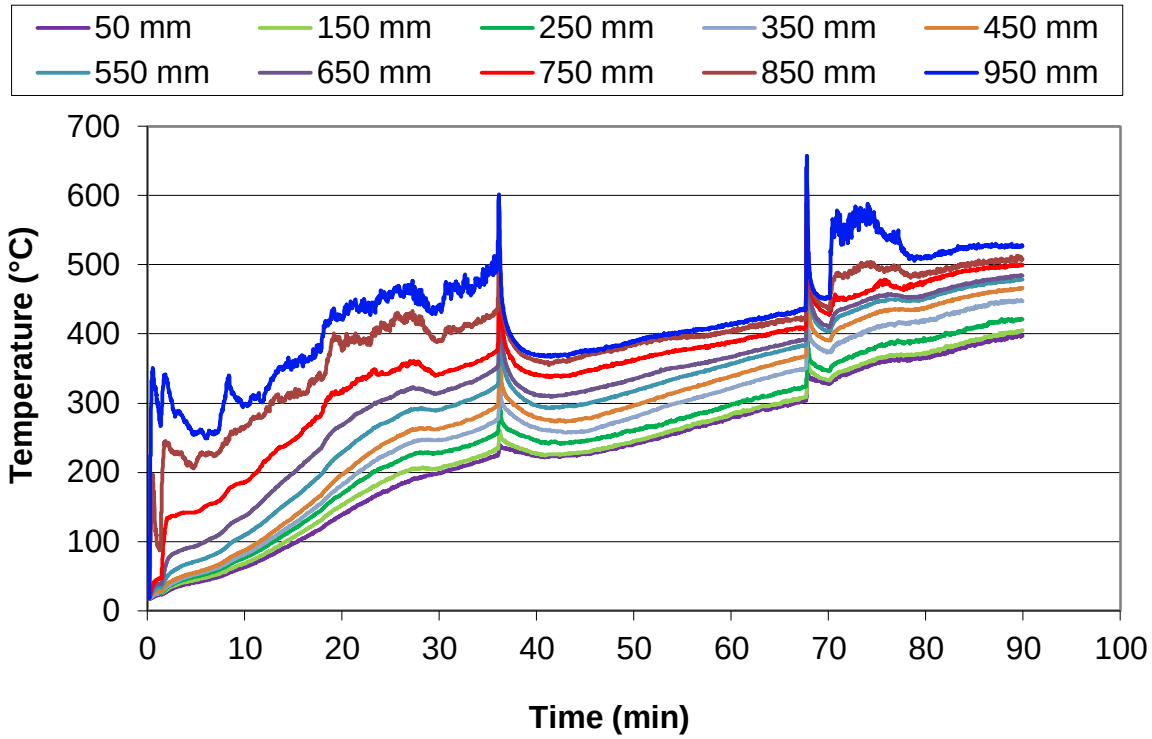


**Figure D.24: Temperature histories for experiment 10-M-71 at the rear of the compartment**

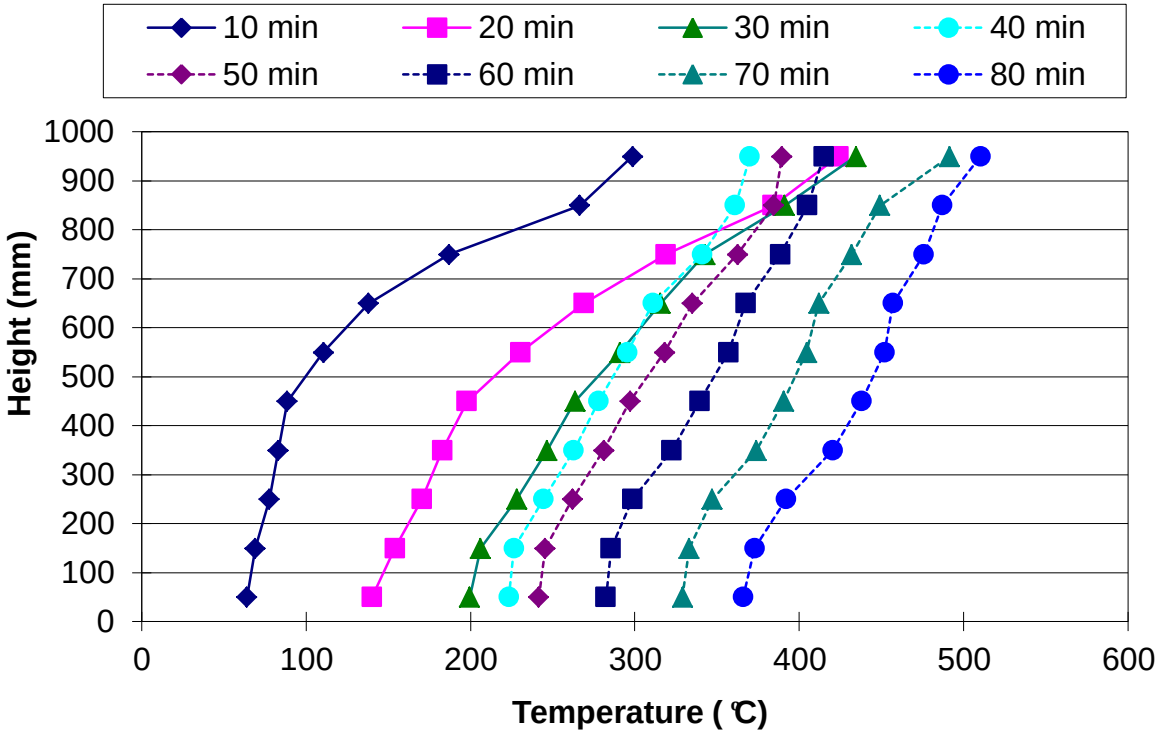


**Figure D.25: Temperature profile constructed from the rear thermocouple tree for experiment 10-M-71**

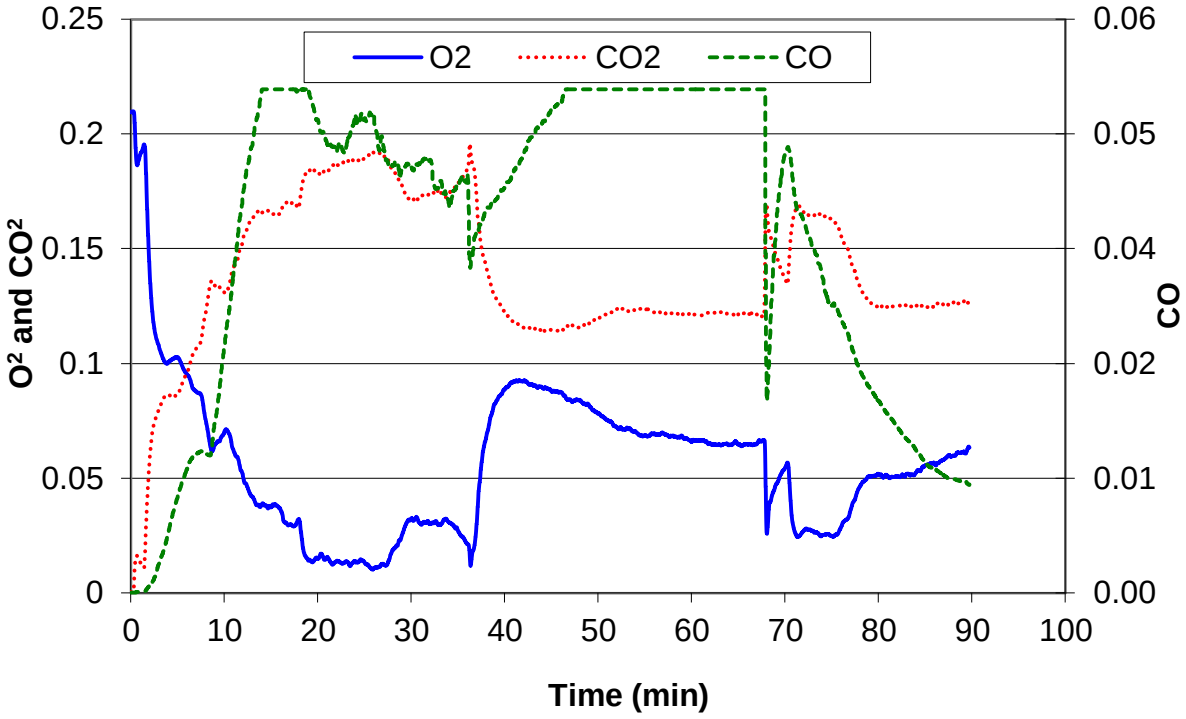


**Figure D.26: $O_2$, $CO_2$ and CO molar concentrations for experiment 10-M-71**

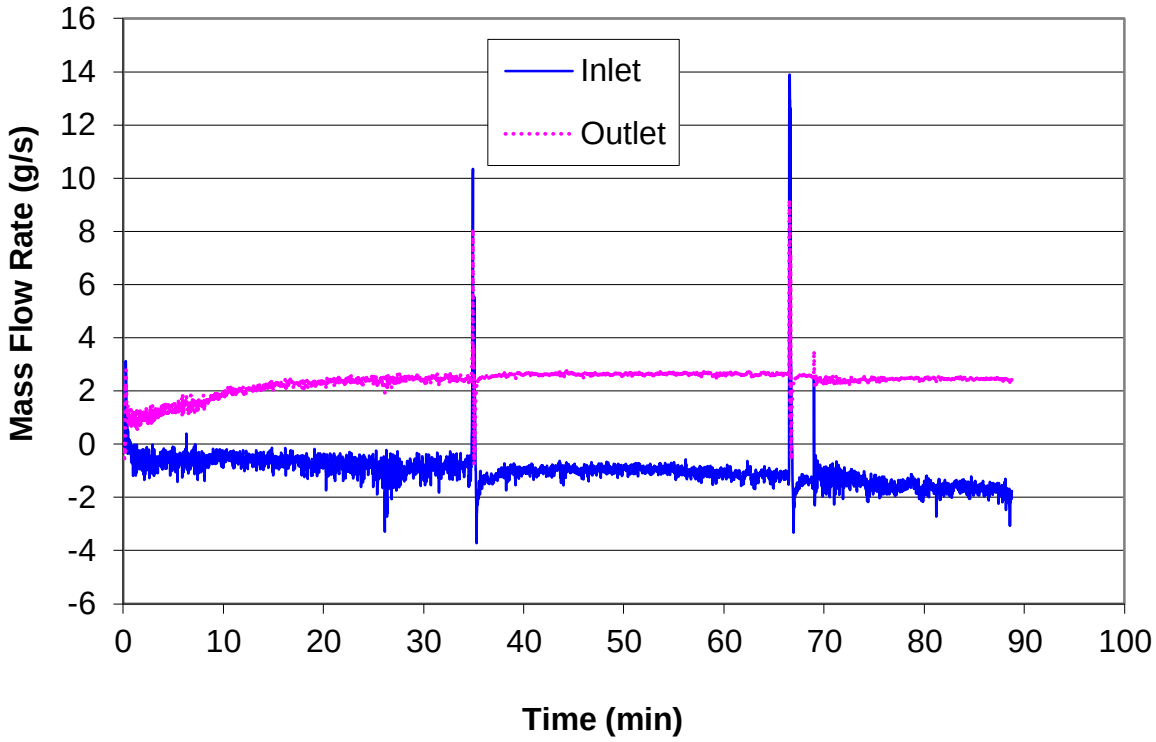


**Figure D.27: Mass flow rate through both opening vents for experiment 10-M-71**

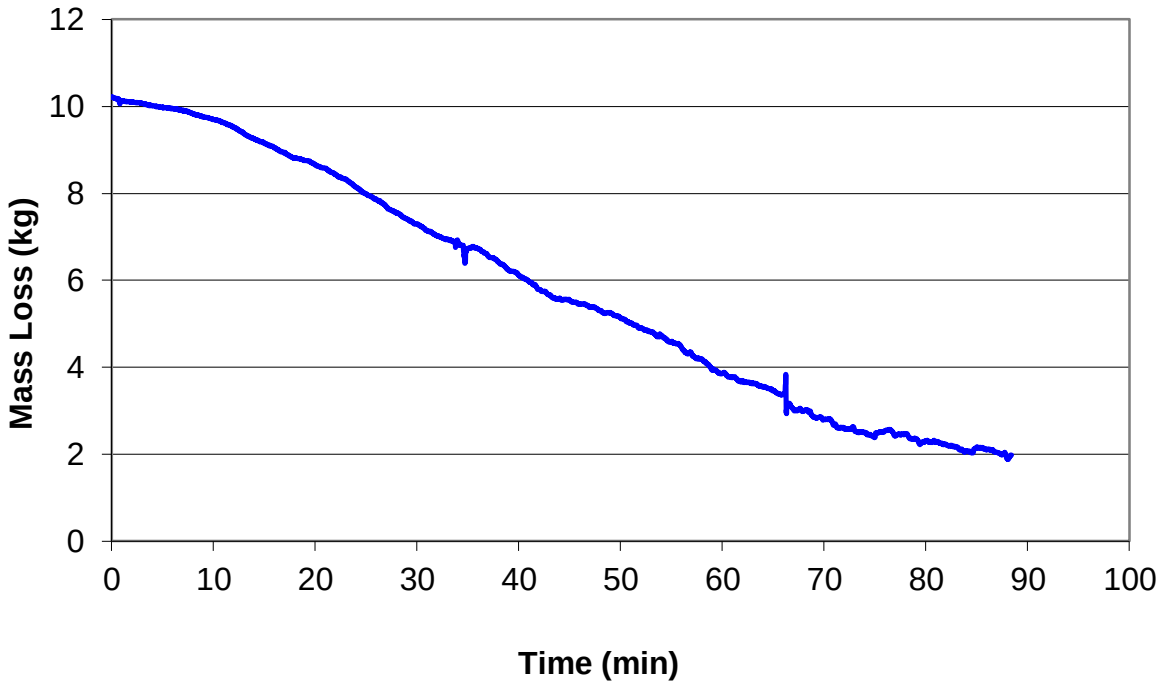


**Figure D.28: Mass loss history for experiment 10-M-71**

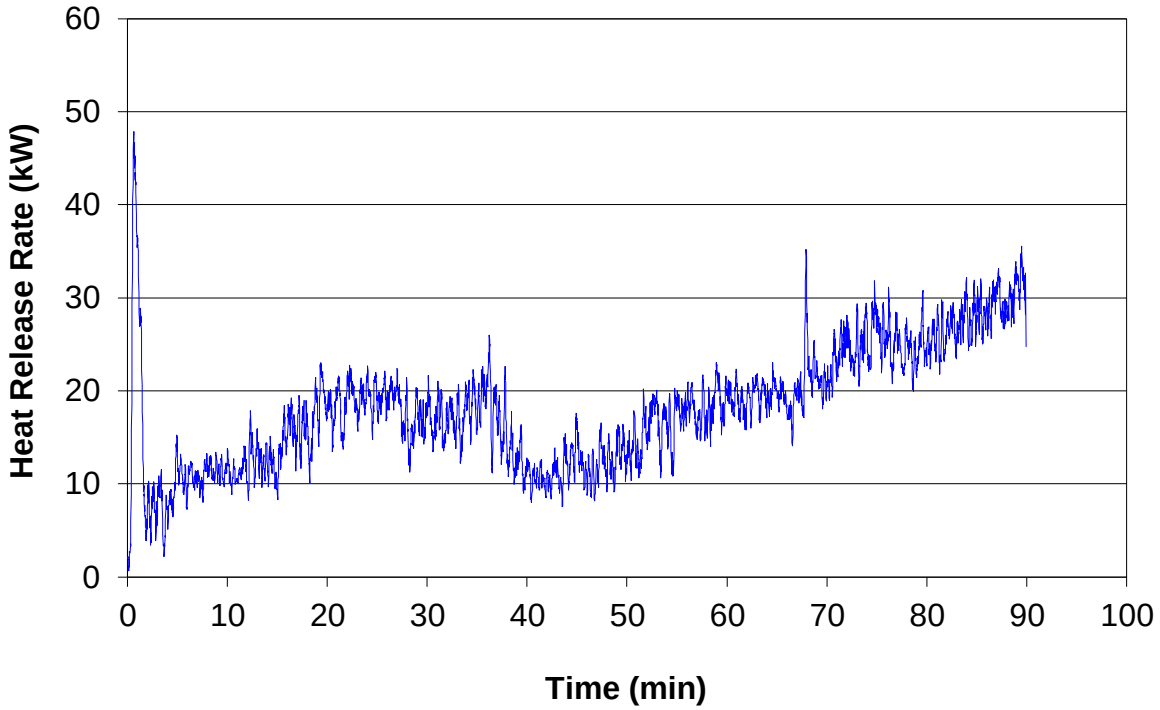


**Figure D.29: Heat release rate history for experiment 10-M-71 with a 10-point moving average**

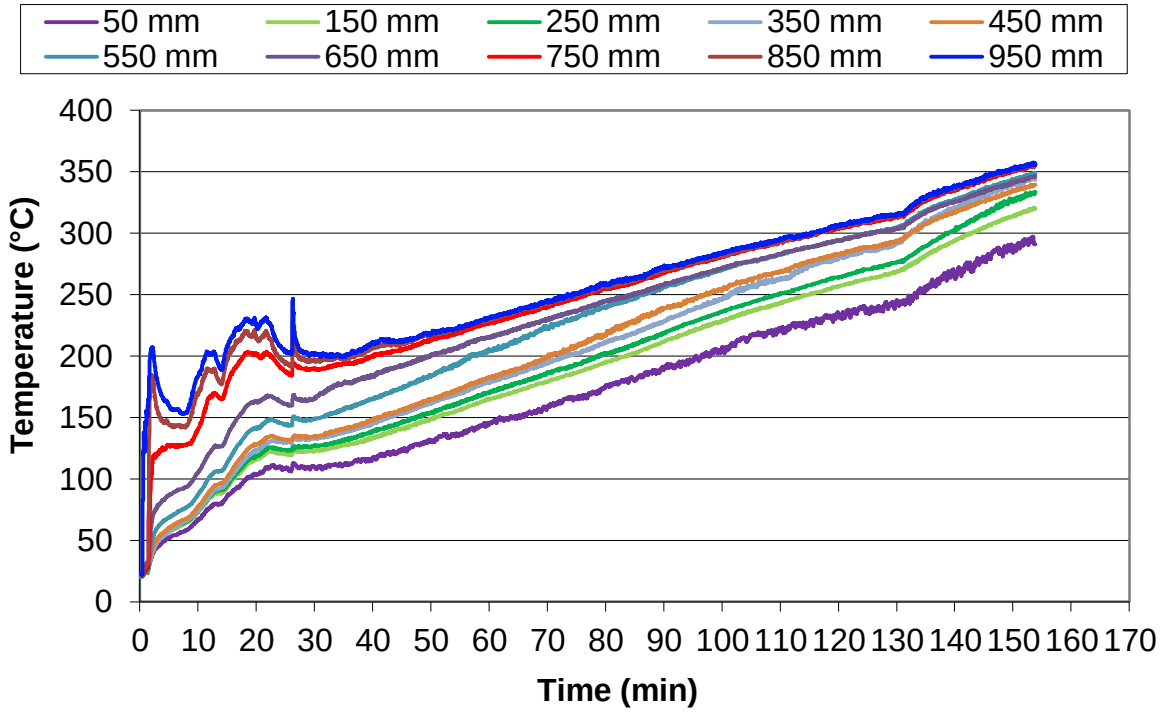


**Figure D.30: Temperature histories for experiment 10-M-50 at the front of the compartment**

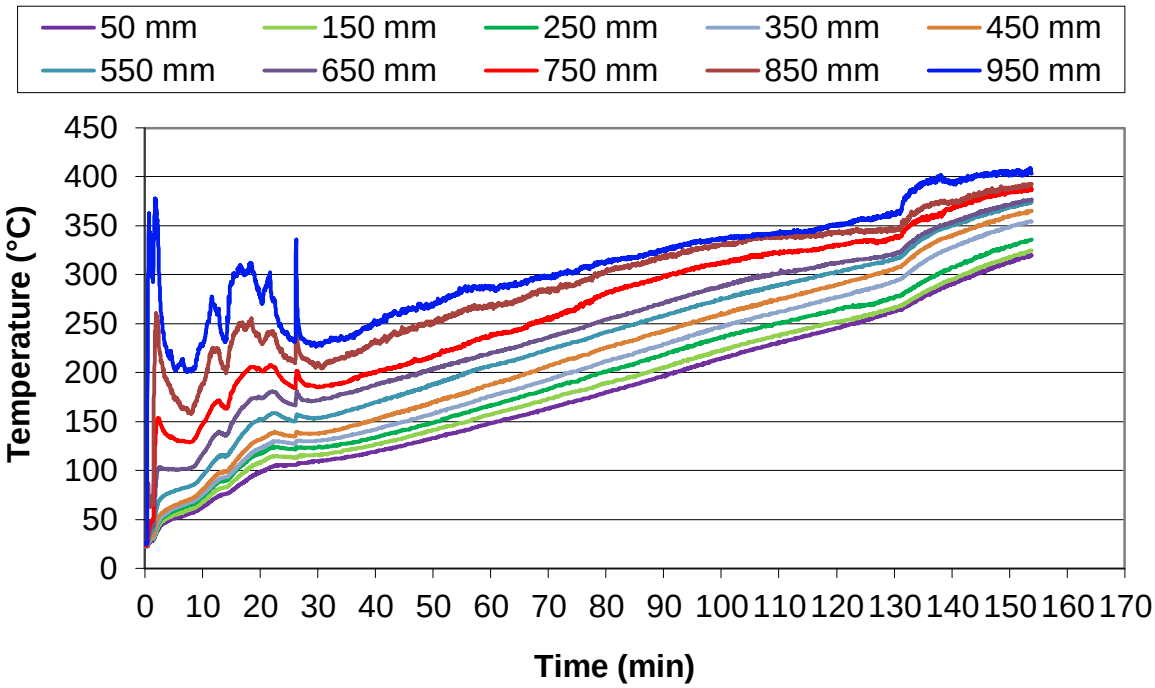


**Figure D.31: Temperature histories for experiment 10-M-50 at the rear of the compartment**

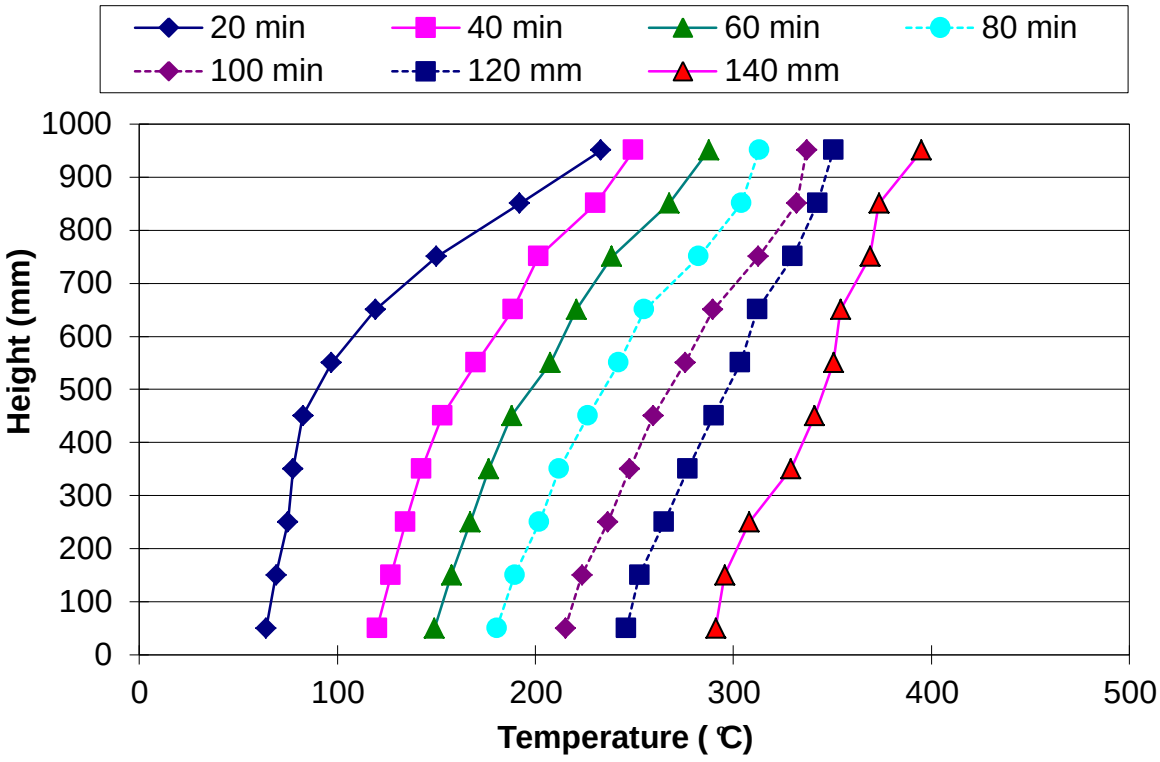


**Figure D.32: Temperature profile constructed from the rear thermocouple tree for experiment 10-M-50**

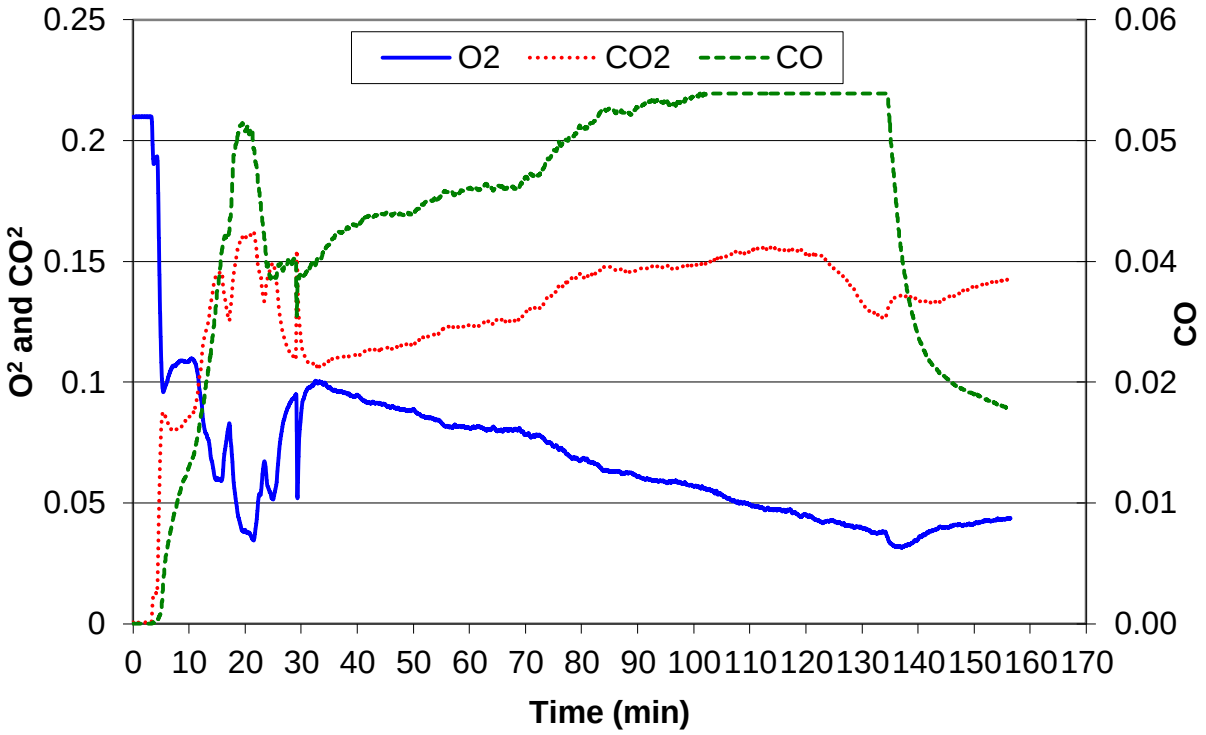


**Figure D.33: $O_2$, $CO_2$ and CO molar concentrations for experiment 10-M-50**

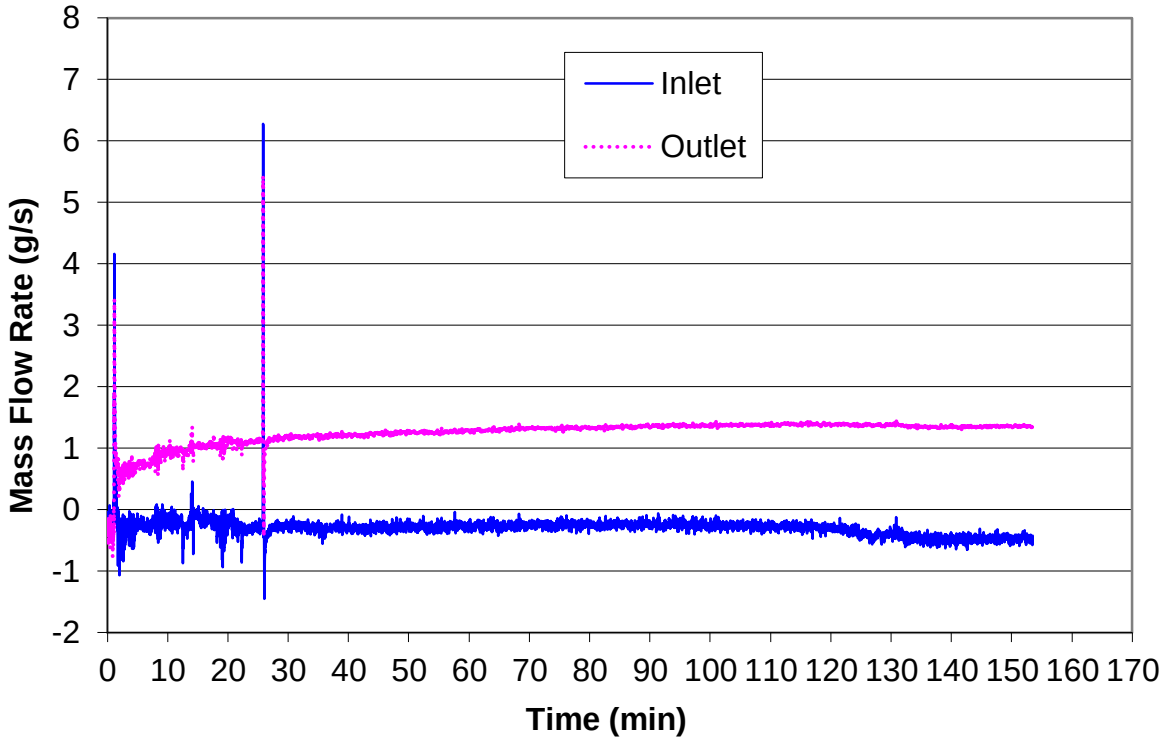


**Figure D.34: Mass flow rate through both opening vents for experiment 10-M-50**

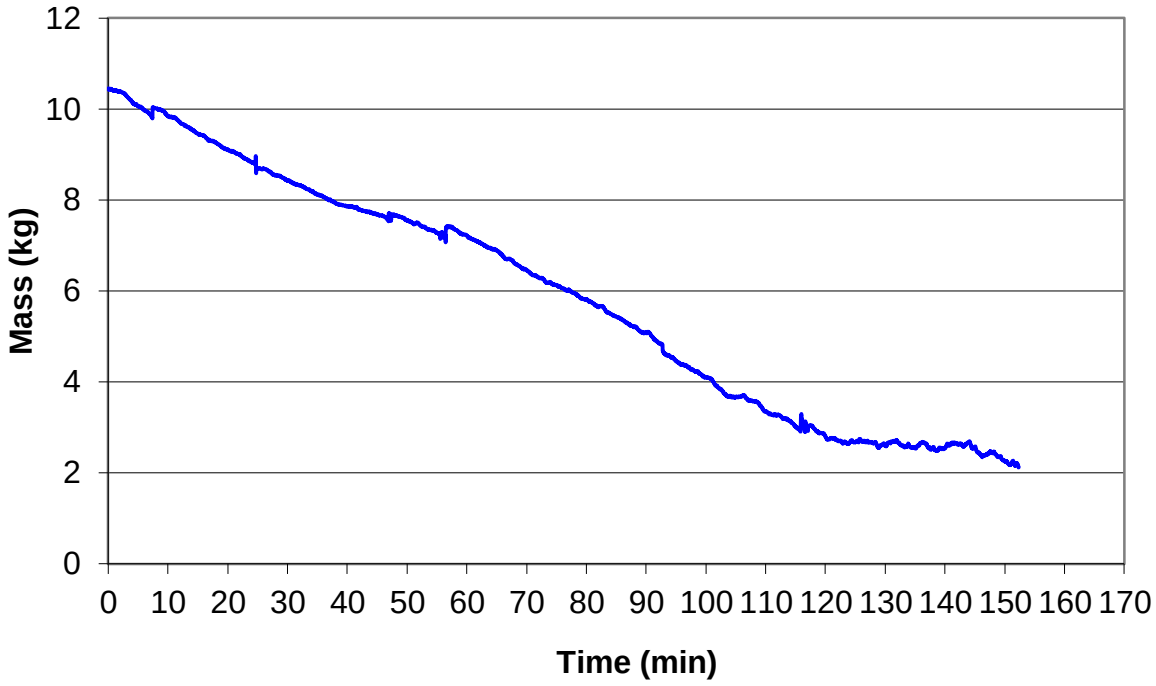


**Figure D.35: Mass loss history for experiment 10-M-50**

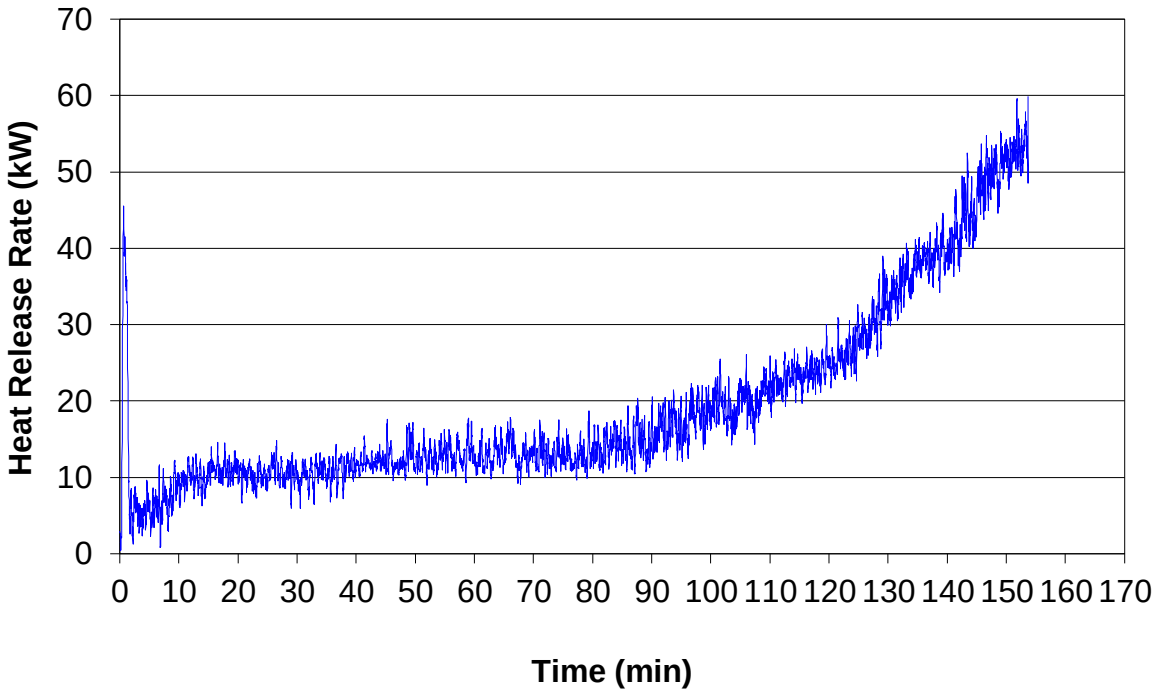


**Figure D.36: Heat release rate history for experiment 10-M-50 with a 10-point moving average**

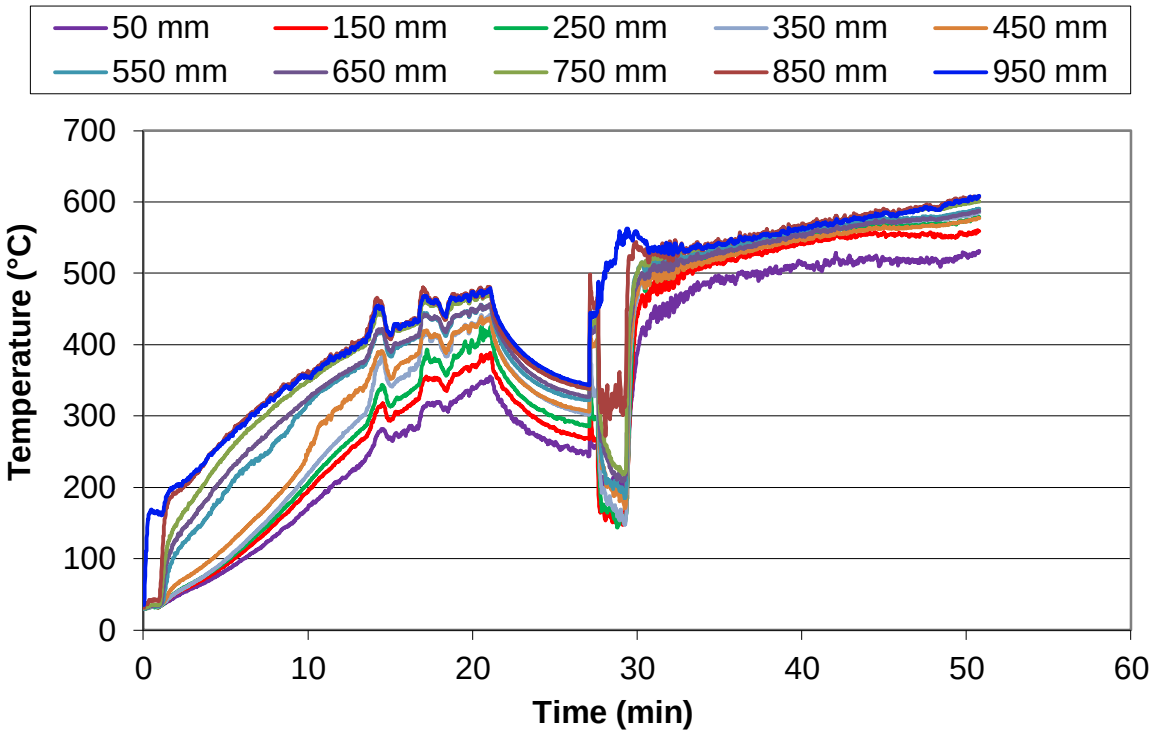


**Figure D.37: Temperature histories for experiment 10-F-100 at the front of the compartment**

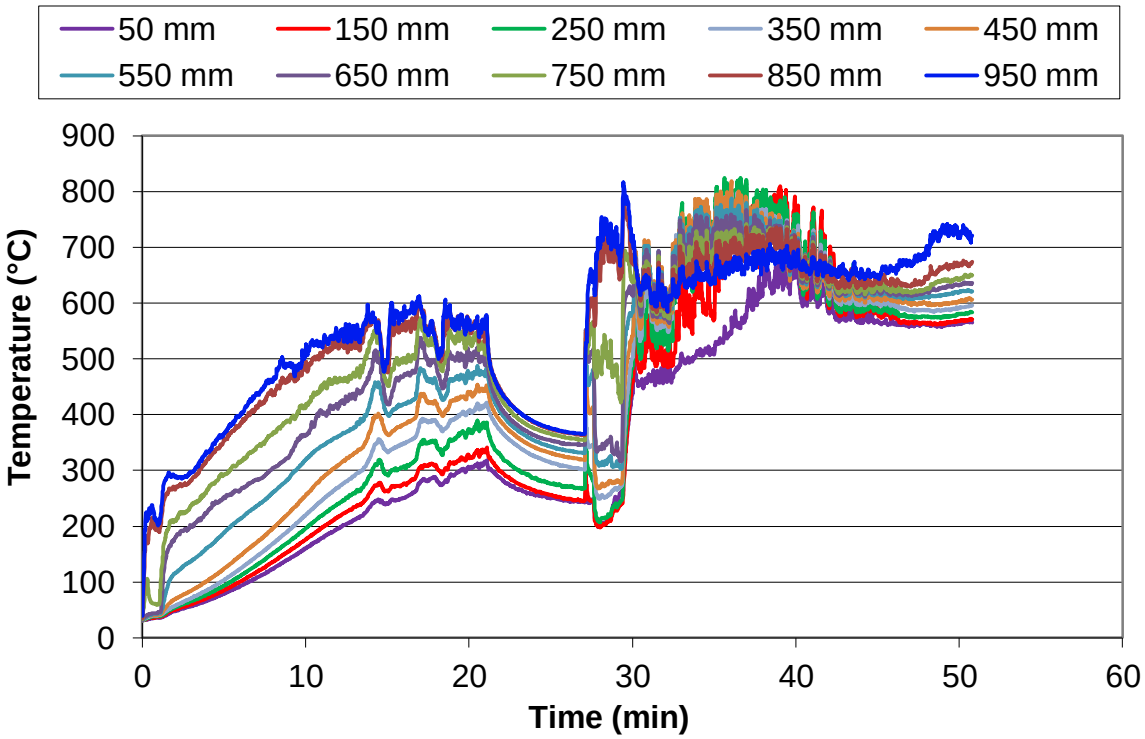


**Figure D.38: Temperature histories for experiment 10-F-100 at the rear of the compartment**

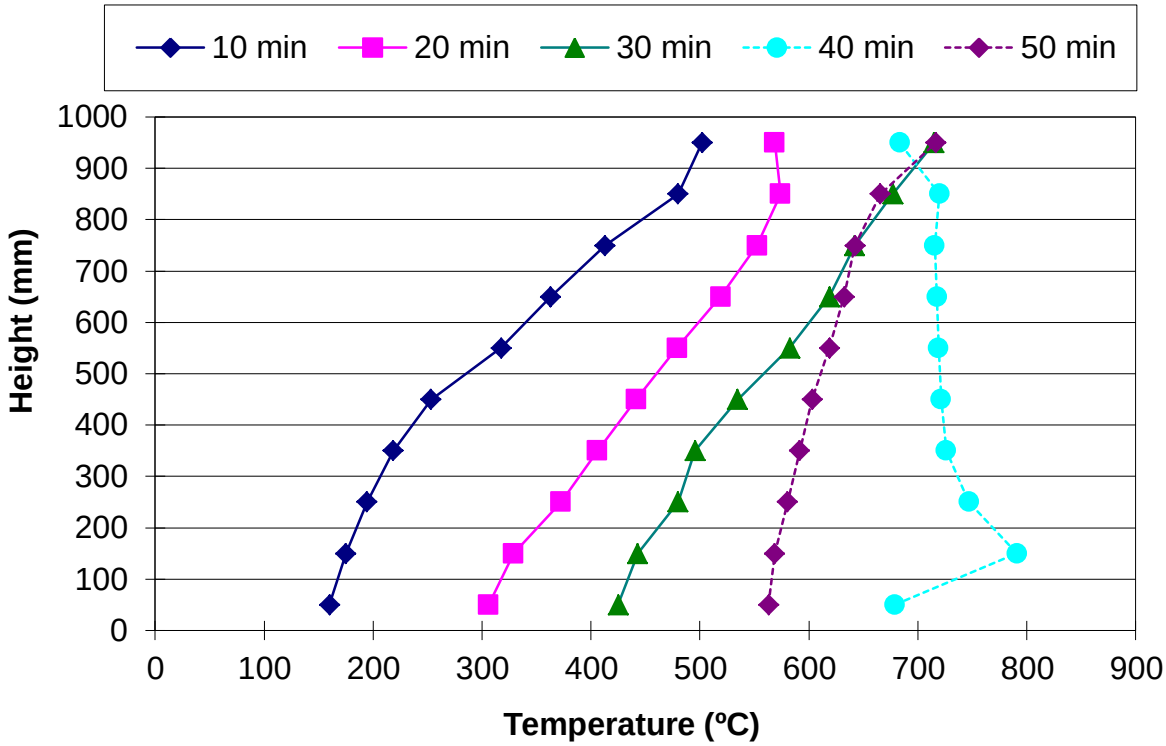


**Figure D.39: Temperature profile constructed from the rear thermocouple tree for experiment 10-F-100**

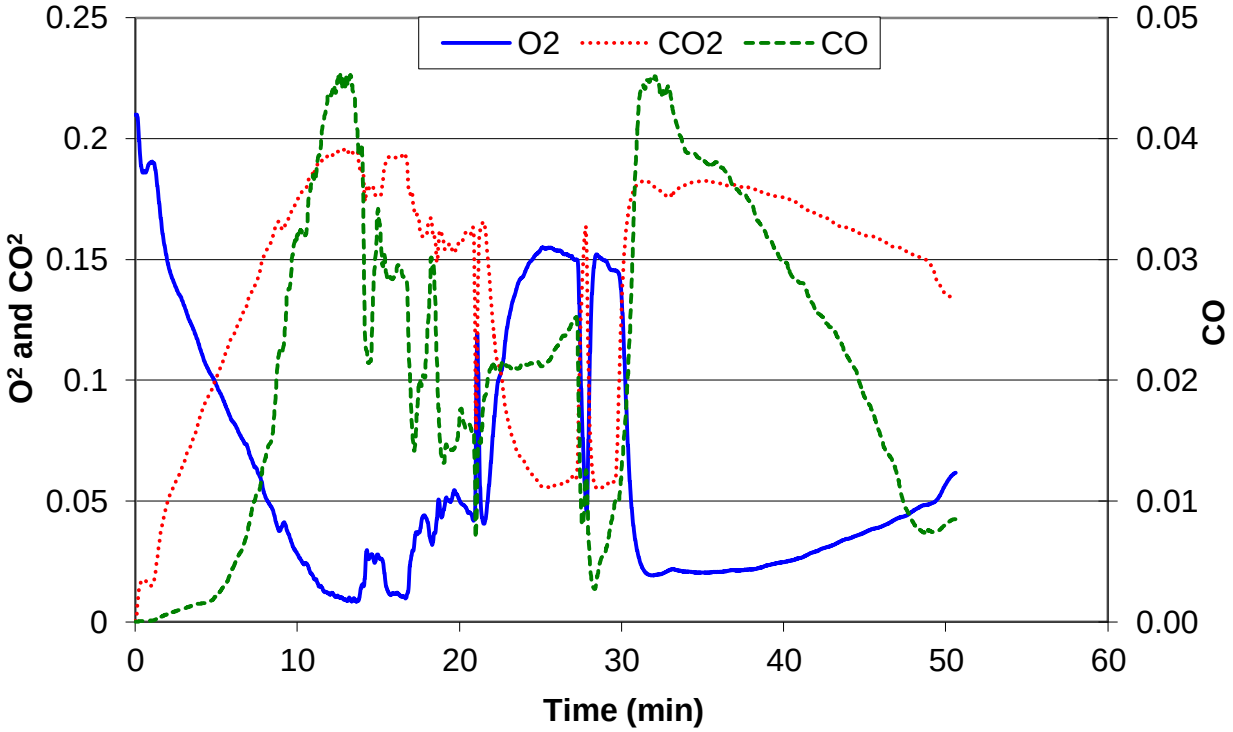


**Figure D.40: $O_2$, $CO_2$ and CO molar concentrations for experiment 10-F-100**

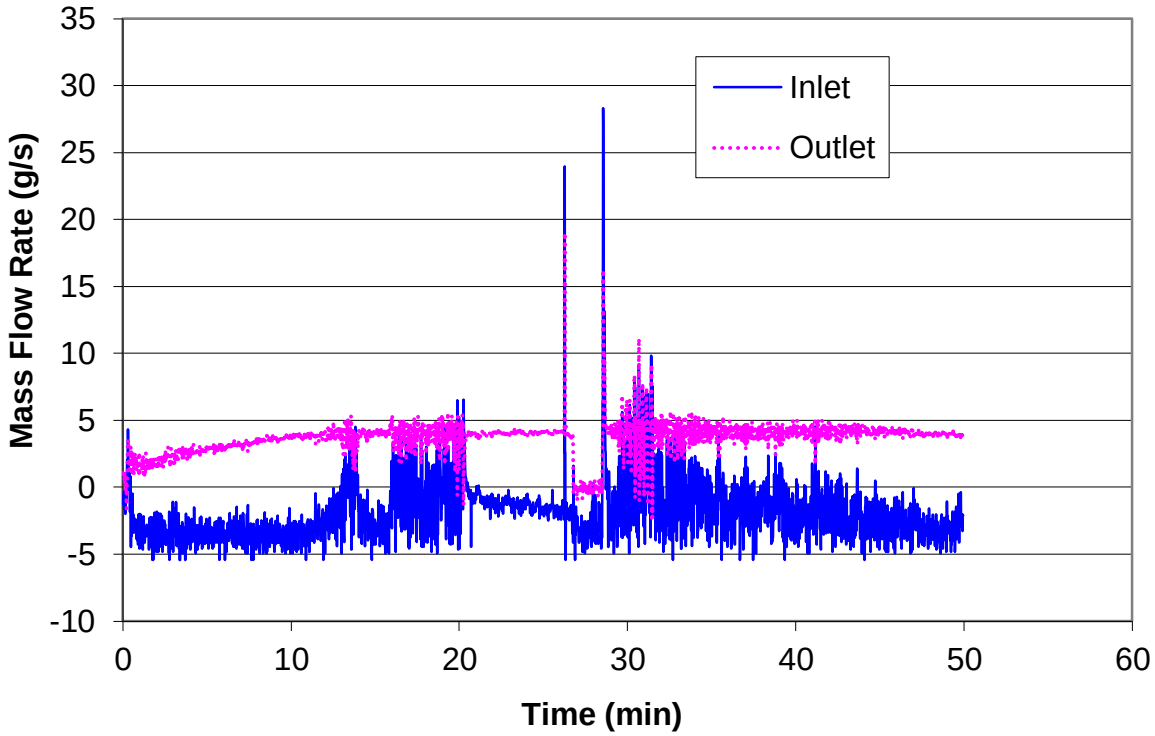


**Figure D.41: Mass flow rate through both opening vents for experiment 10-F-100**

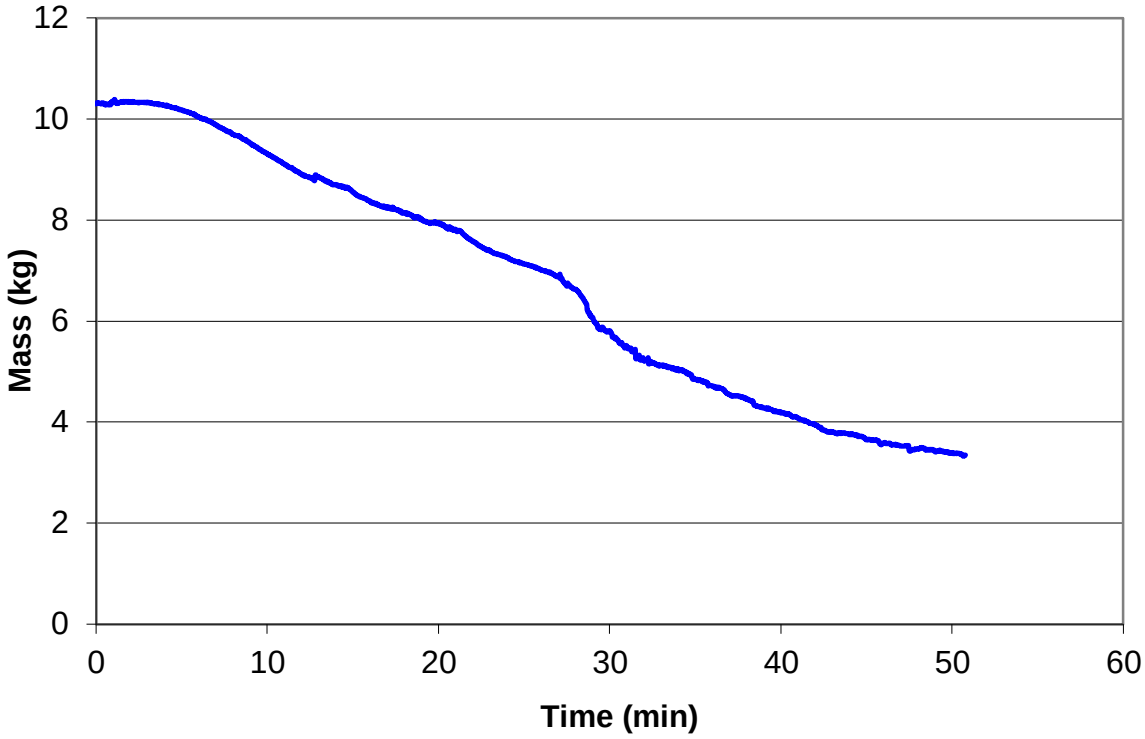


**Figure D.42: Mass loss history for experiment 10-F-100**

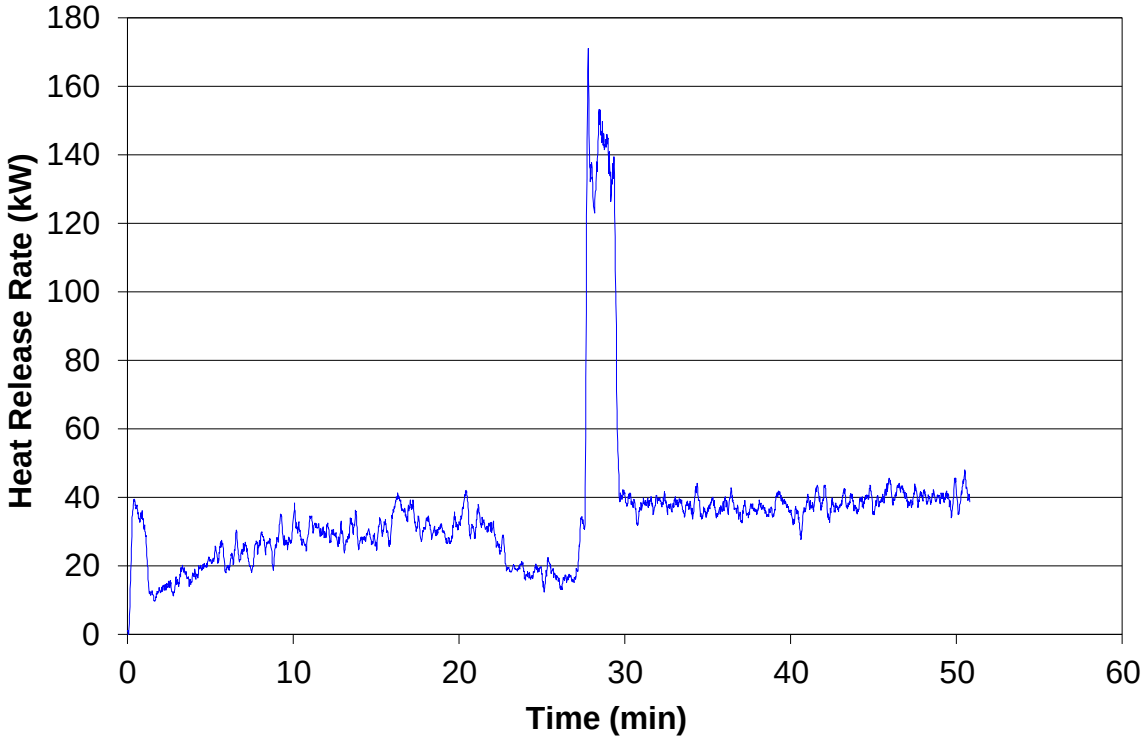


**Figure D.43: Heat release rate history for experiment 10-F-100 with a 10-point moving average (The large increase at 28 minutes is caused by the pressure relief panel being blown out)**

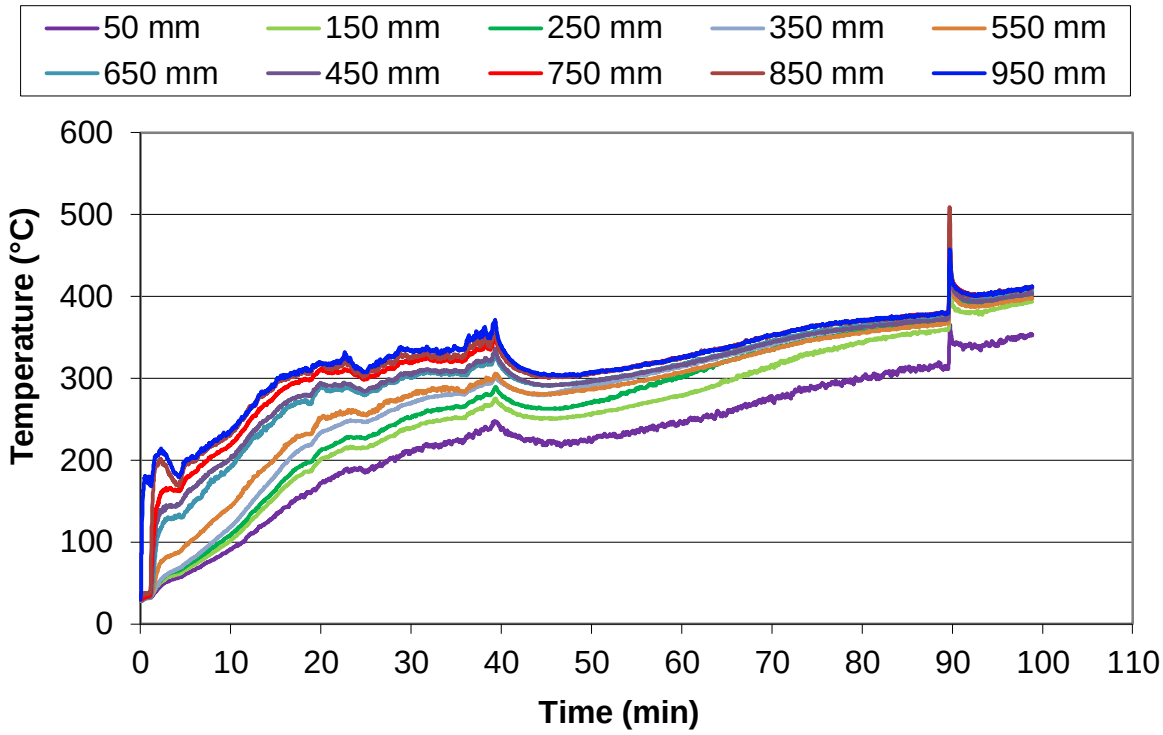


**Figure D.44: Temperature histories for experiment 10-F-71 at the front of the compartment**

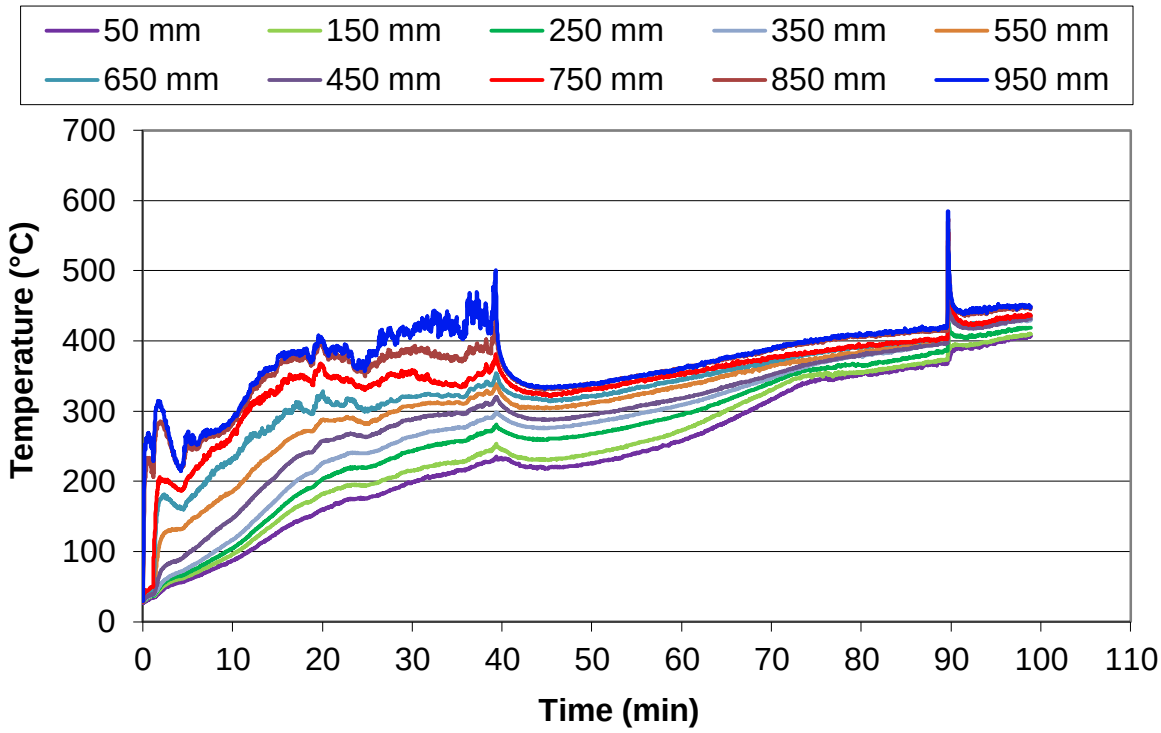


**Figure D.45: Temperature histories for experiment 10-F-71 at the rear of the compartment**

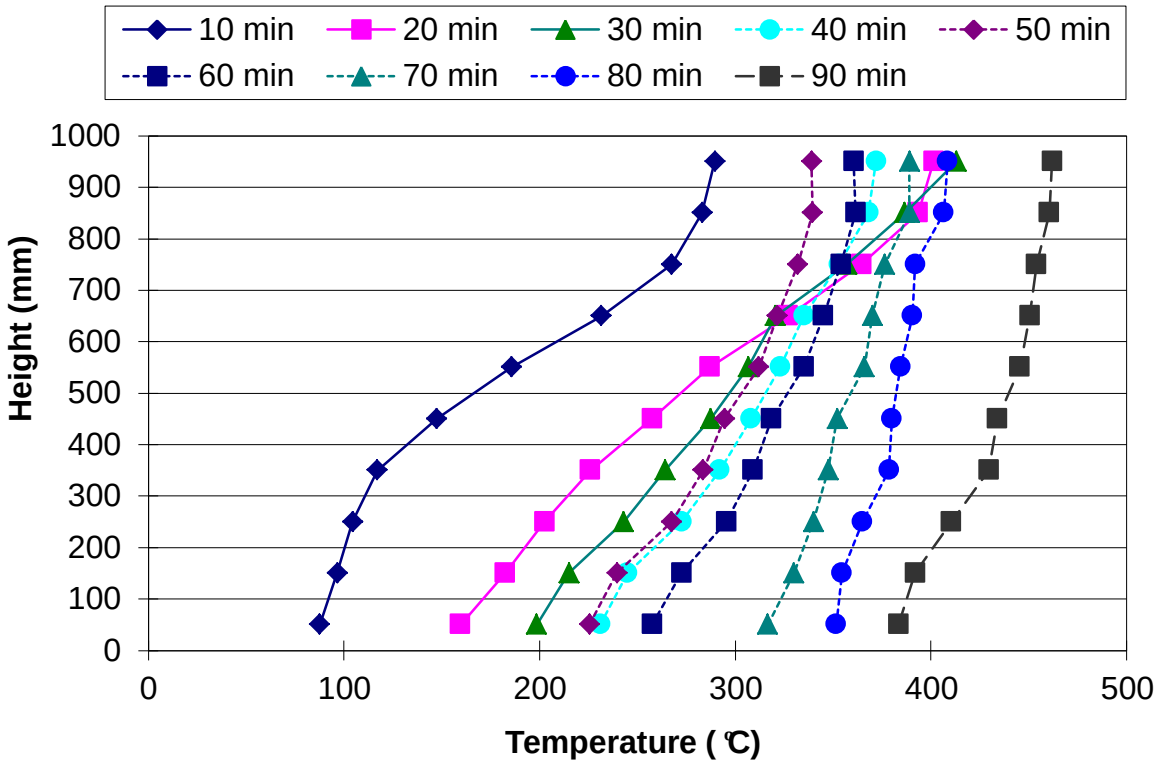


**Figure D.46: Temperature profile constructed from the rear thermocouple tree for experiment 10-F-71**

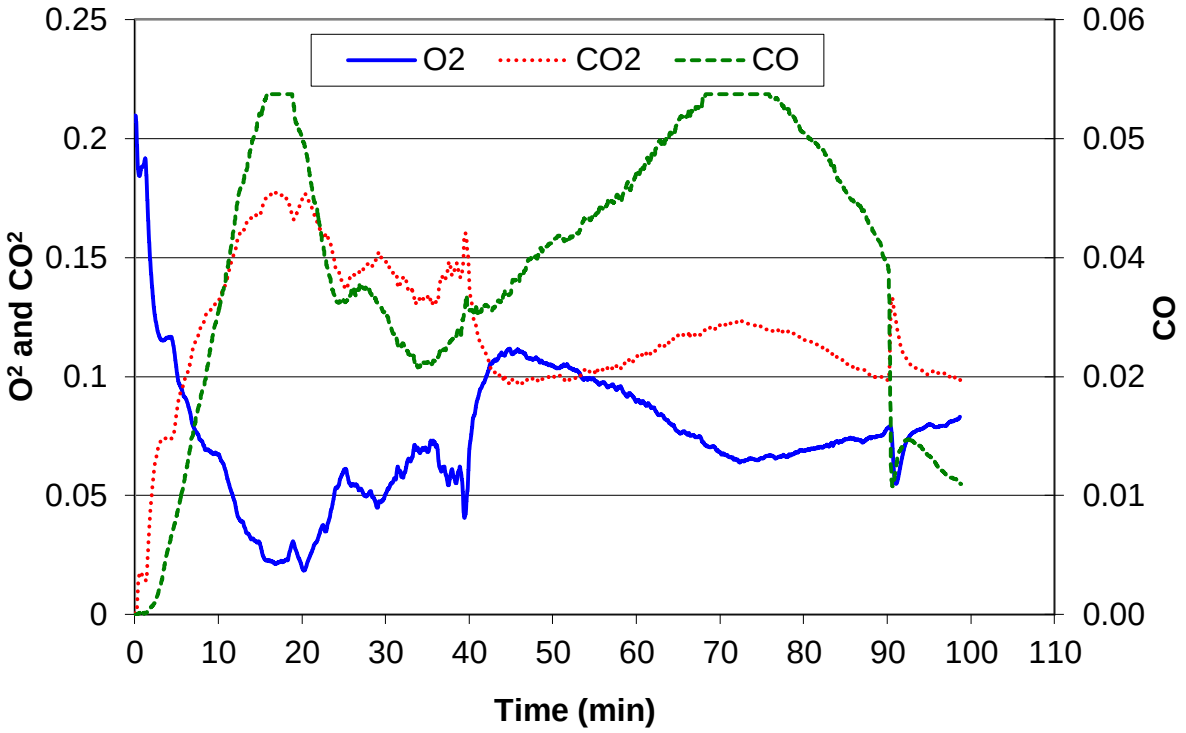


**Figure D.47: $O_2$, $CO_2$ and CO molar concentrations for experiment 10-F-71**

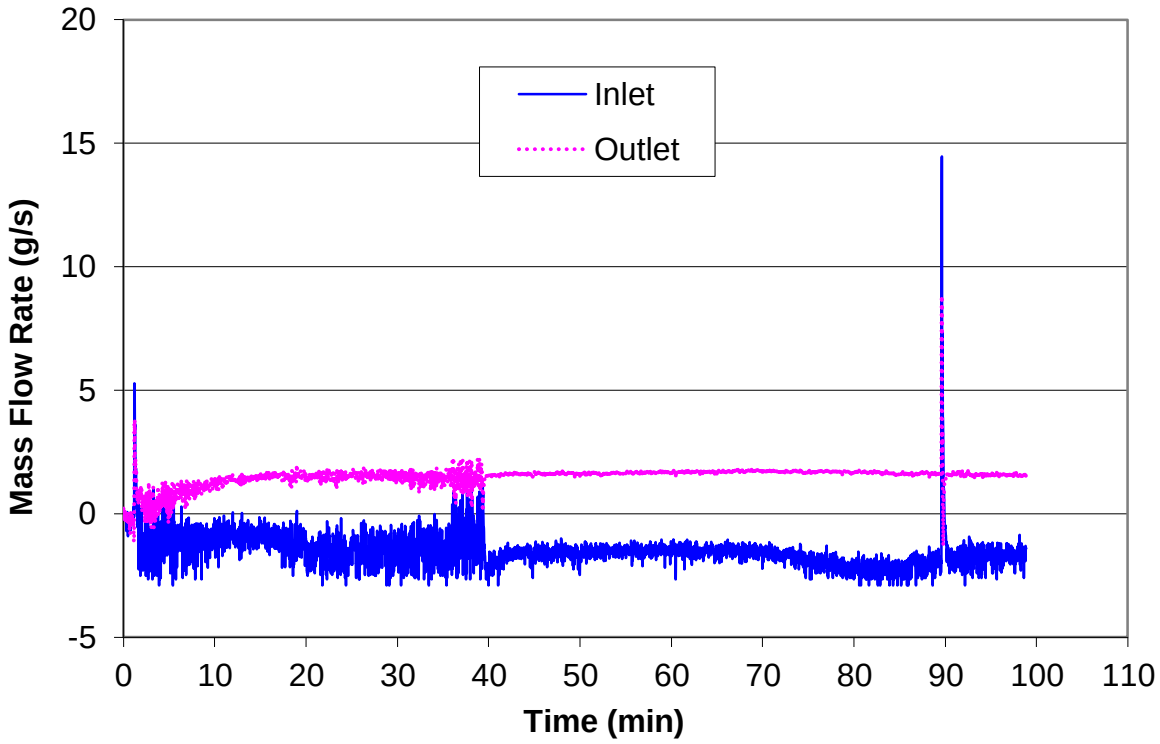


**Figure D.48: Mass flow rate through both opening vents for experiment 10-F-71**

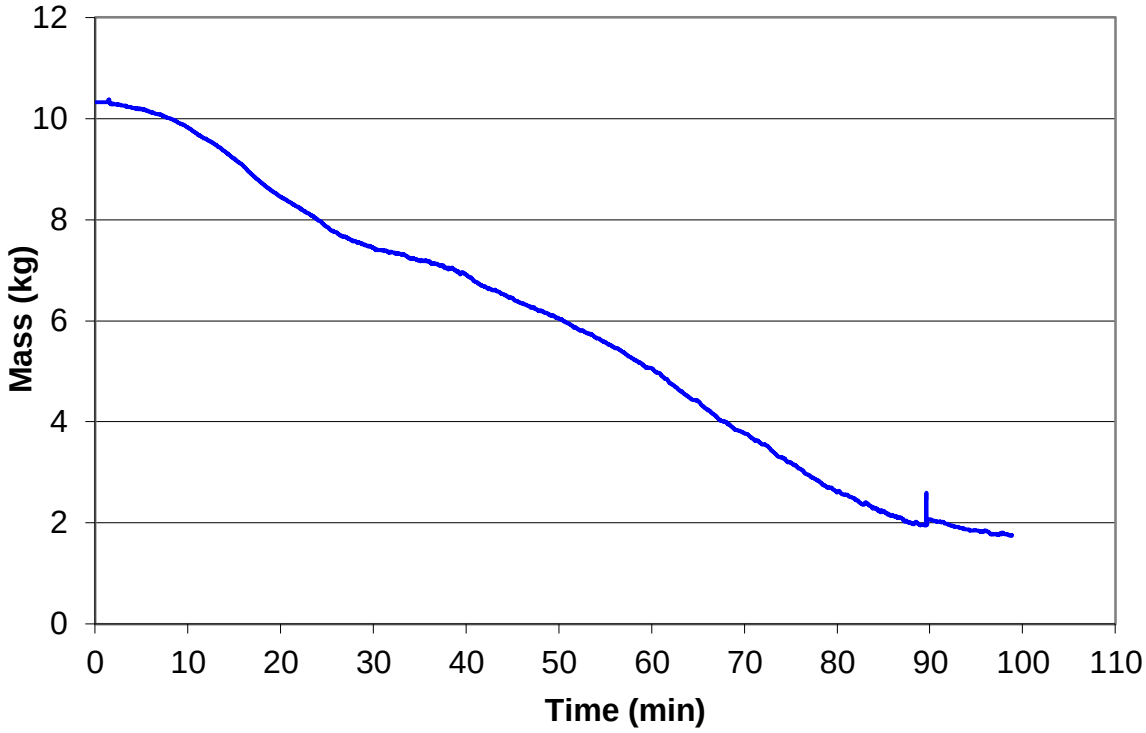


**Figure D.49: Mass loss history for experiment 10-F-71**

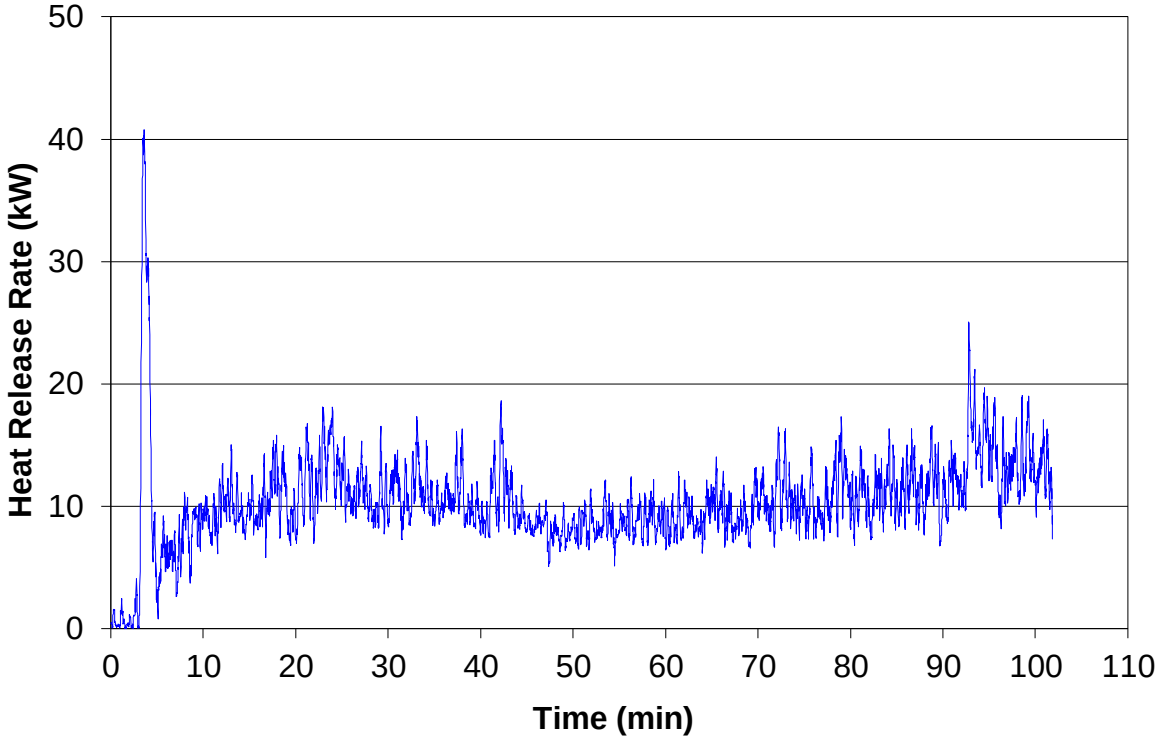


**Figure D.50: Heat release rate history for experiment 10-F-71 with a 10-point moving average**

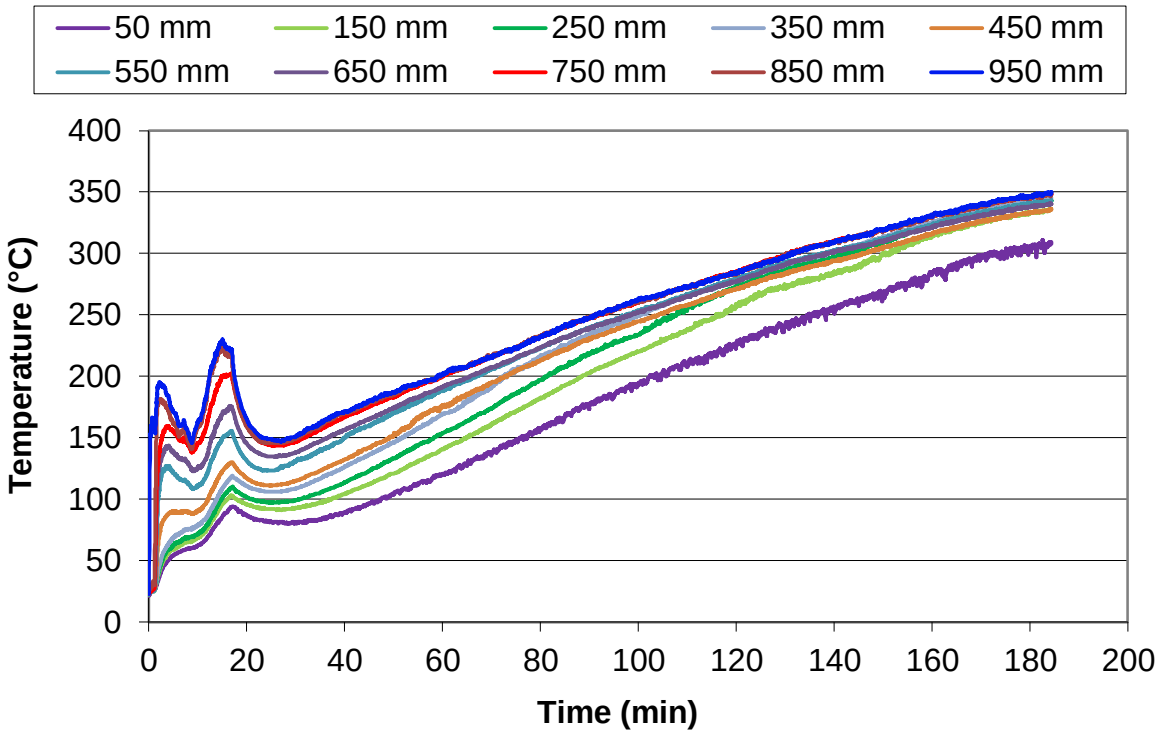


**Figure D.51: Temperature histories for experiment 10-F-50 at the front of the compartment**

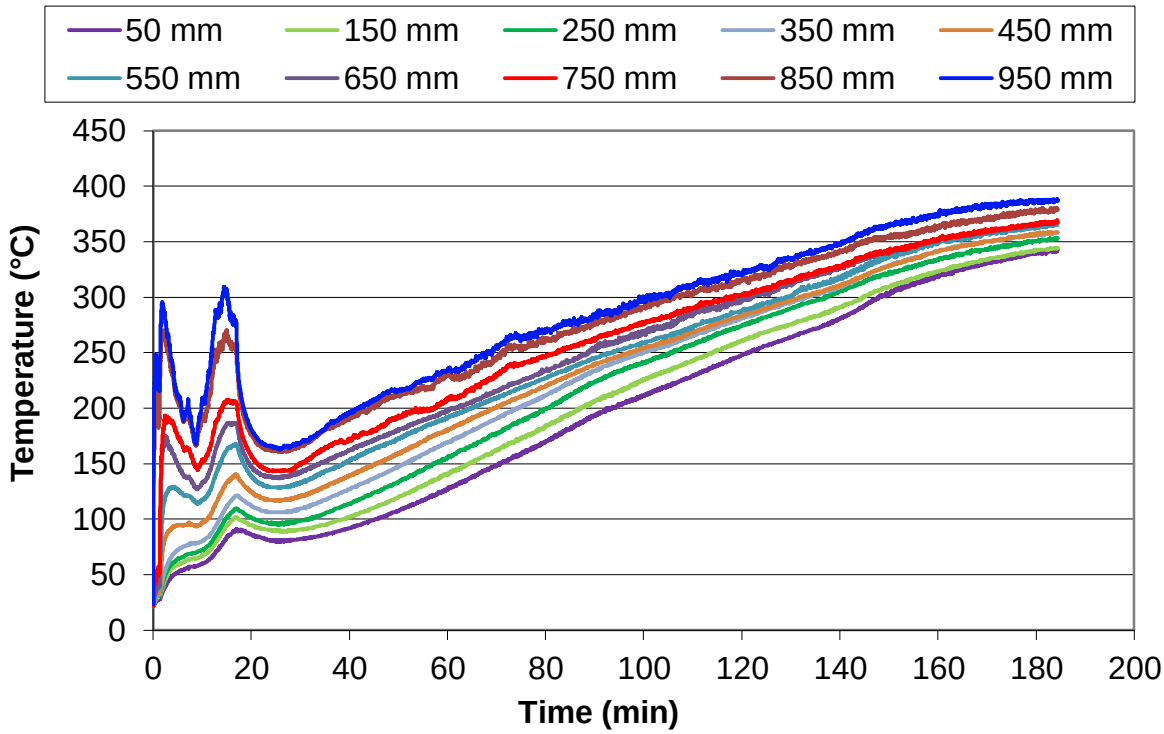


**Figure D.52: Temperature histories for experiment 10-F-50 at the rear of the compartment**

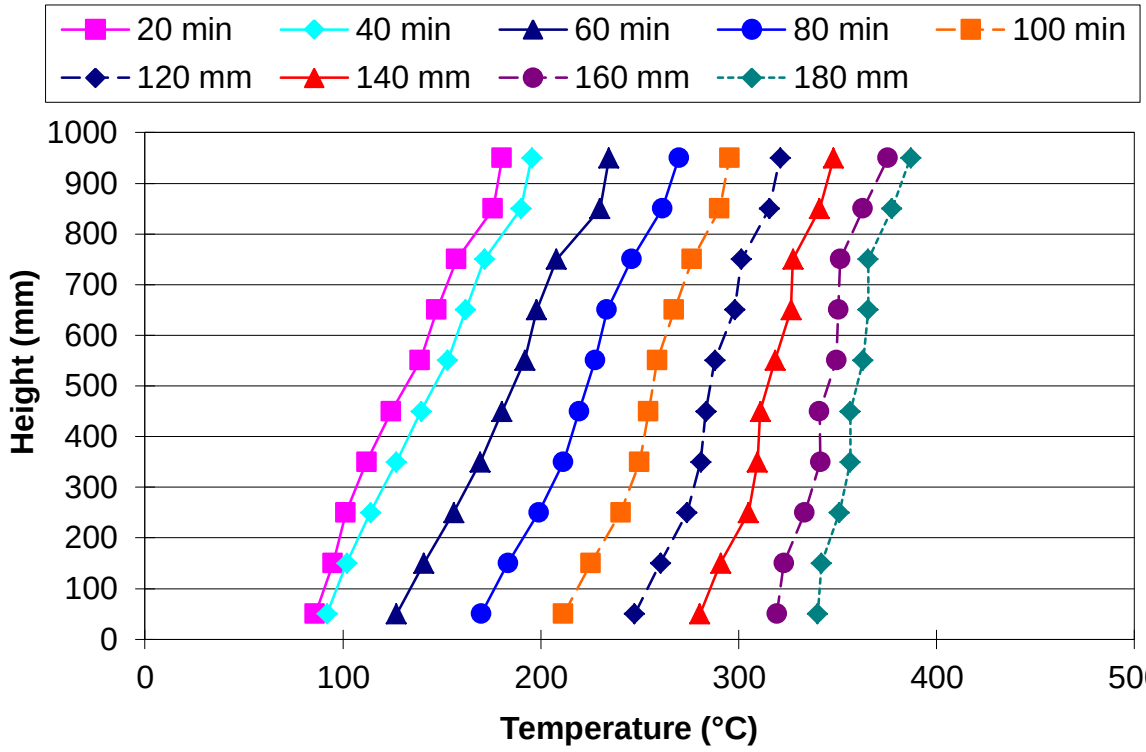


**Figure D.53: Temperature profile constructed from the rear thermocouple tree for experiment 10-F-50**

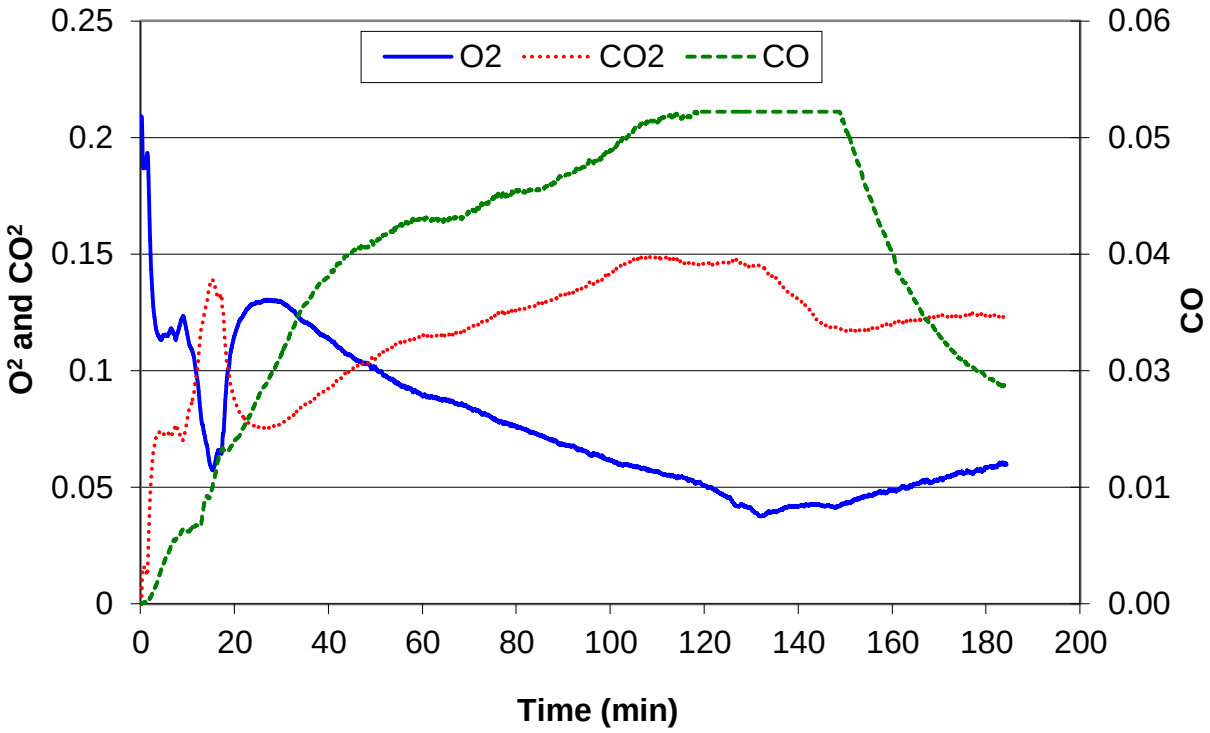


**Figure D.54: $O_2$, $CO_2$ and CO molar concentrations for experiment 10-F-50**

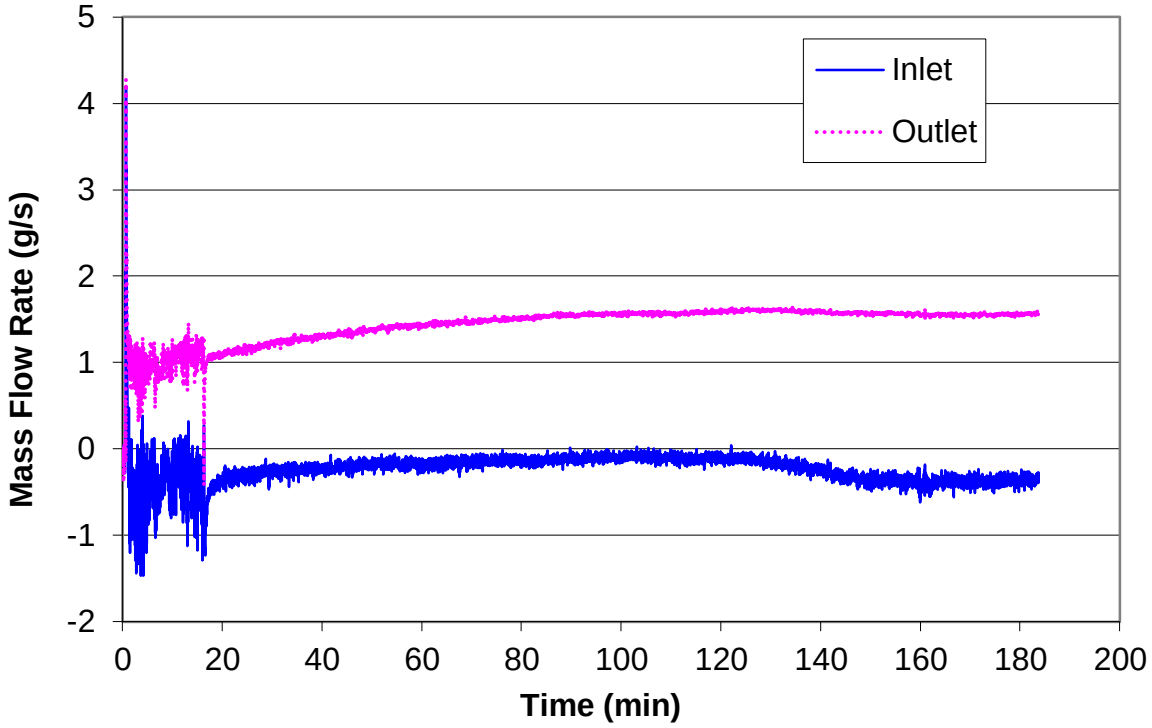


**Figure D.55: Mass flow rate through both opening vents for experiment 10-F-50**

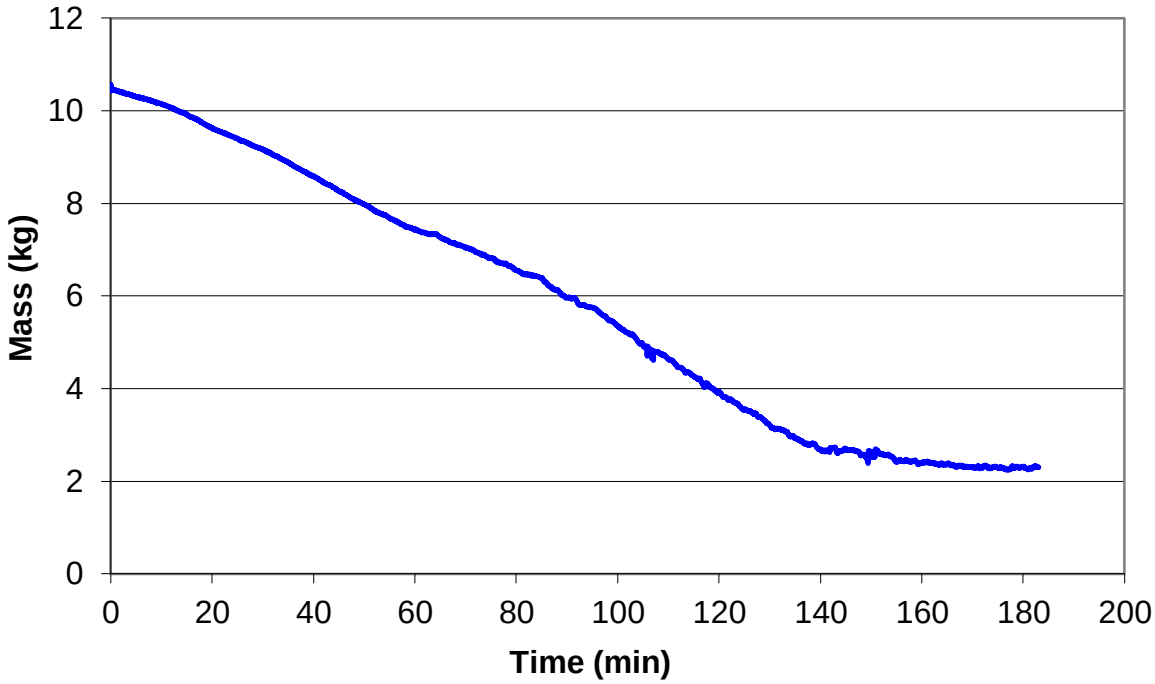


**Figure D.56: Mass loss history for experiment 10-F-50**

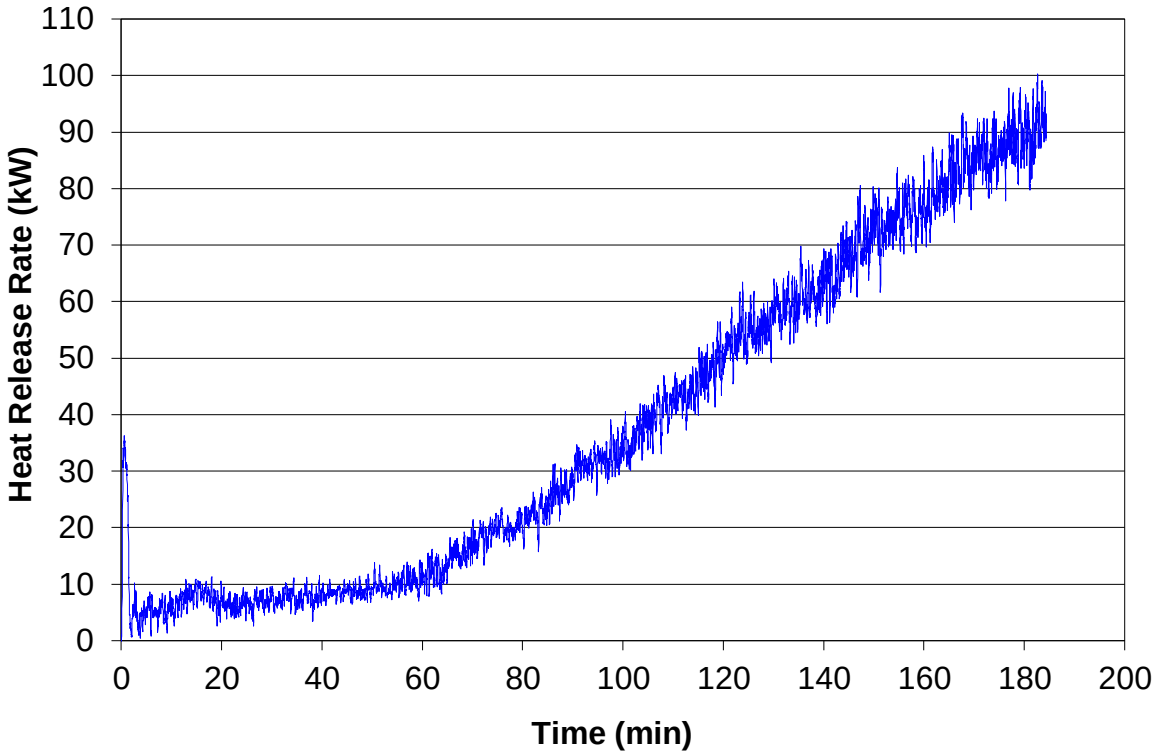


**Figure D.57: Heat release rate history for experiment 10-F-50 with a 10-point moving averageh**